AN ABSTRACT OF THE THESIS OF

Bryndís Brandsdóttir for the degree of Master of Science in Geophysics presented on October 3, 1986.

Title: Precise Measurements of Coda Buildup and Decay Rates of Western Pacific P, P_0 and S_0 Phases and their Relevance to Lithospheric Scattering.

Redacted for Privacy

Abstract approved: _____
William H. Menke

Empirical functions were used to fit band-passed P, P_0, and S_0 coda envelopes of 93 earthquakes. The data sets consisted of earthquake data from the western and northwestern Pacific recorded by arrays of several stations and included both hydrophone and geophone recordings on analog and digital instruments. Prior to the fitting each earthquake was band-passed into six frequency bands, each an octave wide, with a total range in frequency from 0.8 - 50 Hz. The falloff rate was measured individually for each band. These analytical results were then compared to predictions of theoretical models.

The study showed that P, P_0, and S_0 average falloff rates vary systematically with frequency, where the lowest frequencies most commonly have the minimum falloff rates and the middle frequencies have the maximum falloff rates. The variation in falloff between earthquakes is large, with the trends only becoming apparent upon averaging many measurements. A strong increase in falloff rates at about 3 Hz may be associated with a decrease in the amount of scatterers with scale lengths of about one half the wavelength of a 3 Hz compressional wave, which is about 1.3 km.

Falloff rates were seen to decrease with epicentral range. The falloff rates of the Northwest Pacific Basin data set, with an epicentral range of 8 - 21° are 20 - 30% higher than those of the Wake data set that has an epicentral range of 20 - 35°. The fact that both the data sets have raypaths through the Cretaceous and Jurassic Northwest Pacific lithosphere indicates that the difference in observed falloff rates may be due to increased scattering with length of propagation path. The scattering that produces the coda is thus not concentrated in the source region but distributed along the propagation path.

Falloff rates were seen to decrease with increasing age of crust. The P_o and S_o falloff rates at 10 Hz are about 50% lower for the Pacific Northwest Basin than for the Philippine Sea. The difference may be due to the different average age of the lithosphere in these two geographical areas. The Pacific Northwest Basin crust is of Cretaceous and Jurassic age whereas the Philippine crust is of Tertiary age. Average apparent P_o velocities recorded by the Northwest Pacific Basin and Wake arrays are higher than recorded from the Philippine Sea. Oceanic crust thickens with age, and presuming that thinner (younger) crust has less heterogeneities than thicker (more hydrothermally altered?) crust we can explain the higher falloff values in the Philippine Sea as due to fewer heterogeneities and less scattering.

Earthquakes with 100 - 300 km deep hypocenters have systematically lower Po falloff values than shallow (< 100 km deep) earthquakes. The effect is seen in outer trench/inner trench EQs recorded by the Wake array, where the inner trench (deeper) EQs have lower falloff values than the outer (shallower) EQs. This difference indicates that significant scattering is occuring within (or near) the deeply buried part of the subducting plate. There is some indication (though it is not statistically significant because of uncertainties in the earthquake location) that rays that travel obliquely up (or along) the slap have lower falloff than those that travel straight up (or through) the slab.

Significant difference was found in average falloff rates of P_o versus S_o between falloff measurements made on geophone data and hydrophone data. The P_o/S_o falloff ratio for the geophone data is 1.7 - 2.0 which is consistent with the rate of falloff being dominated by frictional attenuation. The P_o/S_o falloff ratio for the

hydrophone data is 0.8 - 1.1, a factor of two lower than for the geophone measurements. As the geophone and hydrophone data have similar apparent velocities the difference in their falloff ratios cannot be ascribed to a different quality factor ratios. The difference is most likely due to conversion of shear waves at or below the sea floor.

The average falloff rates are inversely related to the quality factor (Q) where $\gamma = 2\pi f/Q$. At 10 Hz our falloff rates give Q = 1250 which is a reasonable number for a compressional wave quality factor in rock. However the fact that the falloff rates are fairly consistent in the frequency range 5 - 30 Hz but vary with propagation distance suggest that attenuation cannot be the only phenomenon determining the decay of the coda. Other factors, such as reverberations in the water column, may play an important part in the coda formation as well.

A systematic variation in the position of the maximum of the coda with frequency was observed for the Philippine Sea events. The peak in the low-frequency (0.8 - 3.1 Hz) coda occured 60 - 100 s after the peak of the high-frequency (50 - 100 Hz) coda. This 'reverse-dispersion' may be due to a correlation between attenuation and velocity in the lithosphere where the low-frequency coda will then contain mostly crustal rays, which have propagated at lower speeds.

Precise Measurements of Coda Buildup and Decay Rates of Western Pacific P, P_o and S_o Phases and their Relevance to Lithospheric Scattering.

by

Bryndís Brandsdóttir

A THESIS
submitted to
Oregon State University

in partial fulfillment of
the requirements for the
degree of

Master of Science

Completed October 3, 1986
Commencement June 1987

APPROVED:

Redacted for Privacy

Assistant Professor of Geophysics in charge of major

Redacted for Privacy

Dean of College of Oceanography

Redacted for Privacy

Dean of Graduate School

Date thesis is presented October 3, 1986

Typed by Bryndís Brandsdóttir

ACKNOWLEDGEMENTS

This thesis is a result of a joyful, although sometimes frustrating, cooperation between a theoretical seismologist (W. H. Menke) and an observational seismologist (author) who, before this study, had never considered looking past the first arrival of P and S phases. So I would like to thank my major professor, William H. Menke, for teaching me how to look 'beond the observational world' and do a little math. My other professors Dale Bibee and Martin Fisk I thank good reviews.

The data used in this study was generously supplied by L. D. Bibee (OSU), N. Frazer, C. McCreery, and D. Walker (HIG).

To my fellow students, may you have a good time now and good Vitas in the future whether at OSU or in Florida, New Orleans, The Netherlands, France, Mexico, Taiwan, and Kópavogur.

I thank Sarah Hoffman and Dallas Abbott for editing this thesis.

This research was supported by the National Science Foundation under grant No. OCE - 8417959.

TABLE OF CONTENTS

LIST OF FIGURES

PRECISE MEASUREMENTS OF CODA BUILDUP AND DECAY RATES OF WESTERN PACIFIC P, P_0 AND S_0 PHASES AND THEIR RELEVANCE TO LITHOSPHERIC SCATTERING

INTRODUCTION:

Since their identification by Linehan (1940), P_0 and S_0 phases (also called high-frequency and long-range P_n and S_n phases) have intrigued seismologists studying the propagation of waves through the oceanic lithosphere. The main characteristics of P_0 and S_0 phases (o for oceanic) are their relatively high frequency, their efficient transmission, the typically gradual buildup, and the long duration of their coda (Figures 1, 2, 3, and 4). The P amplitudes are generally smaller than P_0 amplitudes (Figures 3 and 4). However, some earthquakes (EQs) have smaller P_0 than P amplitudes (Figure 5) or no visible P_0 and S_0 phases (Figure 6). The same relationship applies to P_0 versus S_0 amplitude ratios. S_0 phases have been observed which have amplitudes larger than P_0 phases (Figures 1, 2, and 3) as well as those having equal or smaller amplitudes than P_0 phases. These different amplitude ratios have been attributed to regional effects (Fedotov, 1963; Oliver and Isacks, 1967; Molnar and Oliver, 1969; Mitronovas et al., 1969; Walker, 1977a) where P_0 and especially S_0 energy is absorbed in areas of high attenuation, such as at plate boundaries or hot spots. They could also be related to source excitation effects where the source mechanism generates no shear waves. Furthermore, hydrophone data are likely to have higher P_0/S_0 amplitude ratios than geophone data from the same events (Figures 1, 2, 3, 4, and 5) because shear waves do not couple well to the compressional waves recorded by hydrophones.

One of the reasons why P_0 and S_0 have been of interest to seismologists is that they may be able to provide some information about the structure of the oceanic crust and upper mantle. Other available data, such as marine refraction surveys, are

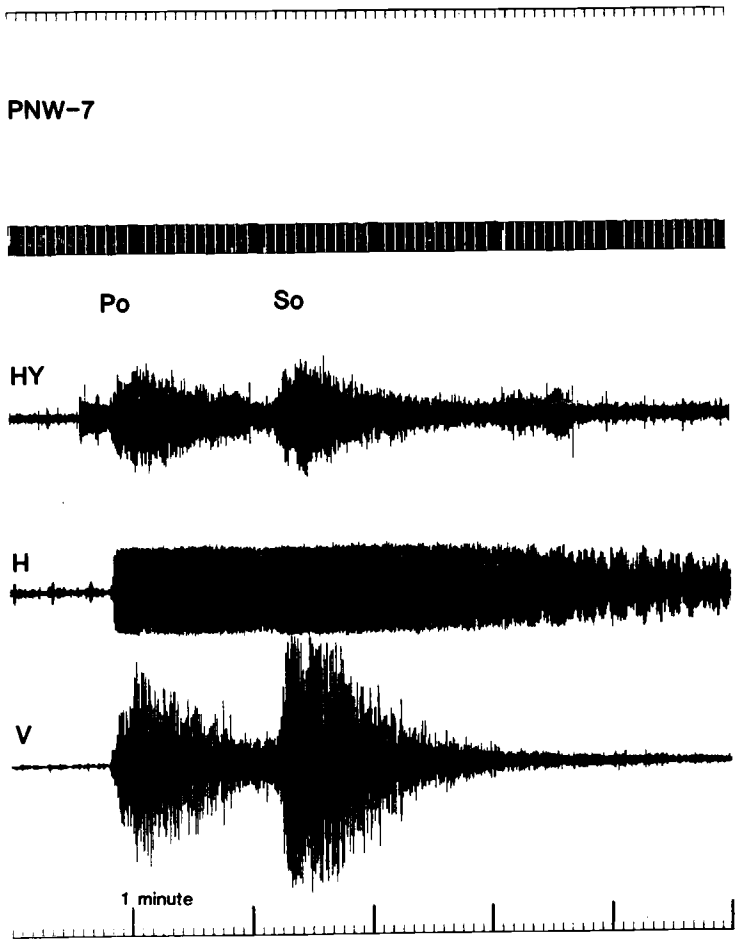

Figure 1. Typical Po/So seismograms of a Kuril trench earthquake (EQ 7) recorded by an instrument in the Pacific Northwest Basin (distance 8°). The three channels shown are the hydrophone (HY, top), horizontal geophone (H, middle) and vertical geophone (V, bottom). Note that the H component is clipped, that is, the signal is too strong for the instrument to record. The HY channel has noise arriving just before the onset of the P_O phase and 2 minutes after the onset of the S_O phase. The onset of each phase is labeled on the seismogram.

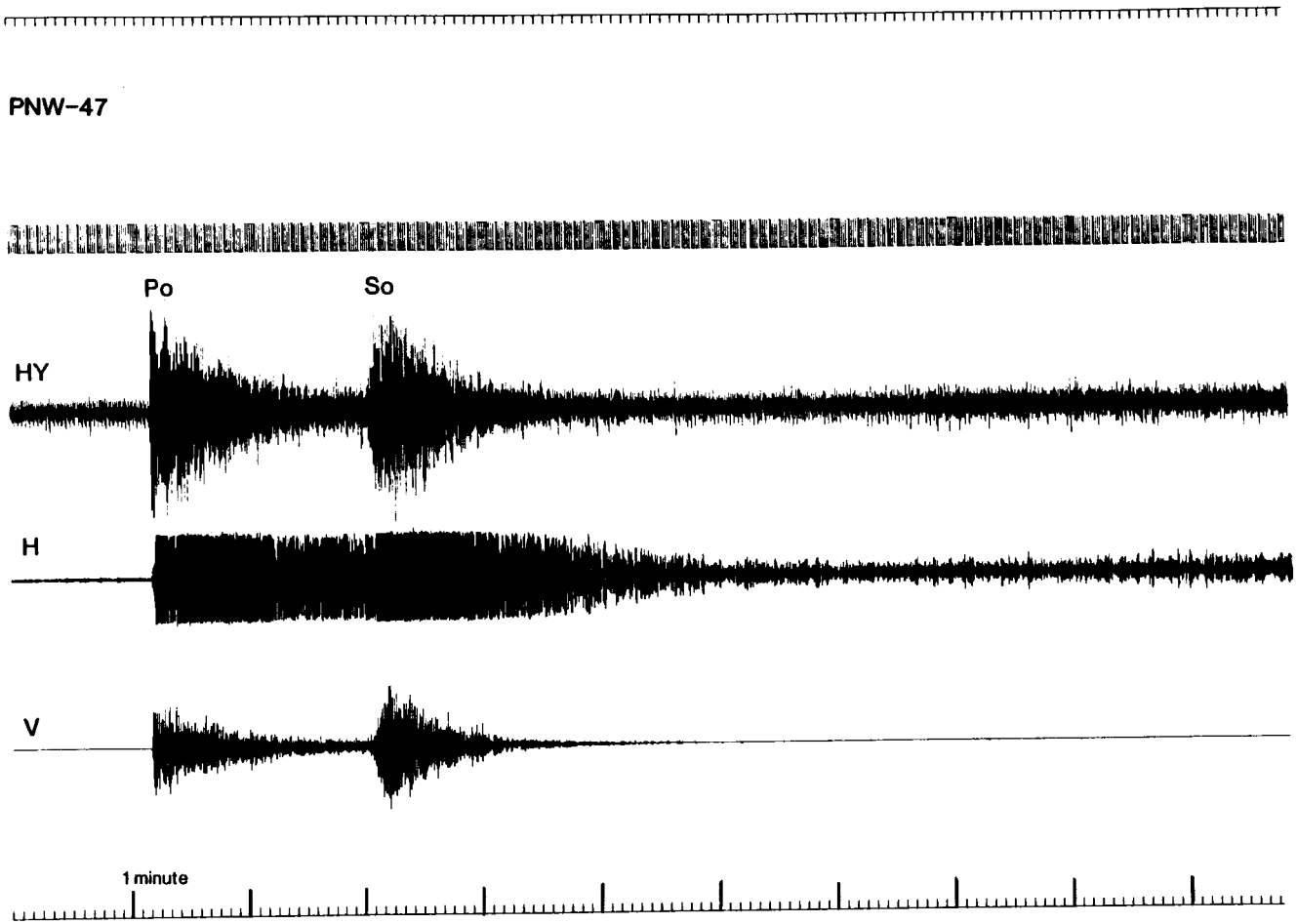

Figure 2. Po/So seismogram of a Kamchatka earthquake (EQ 47) recorded by an instrument in the Pacific Northwest Basin (distance 11°). This Figure has the same format as Figure 1.

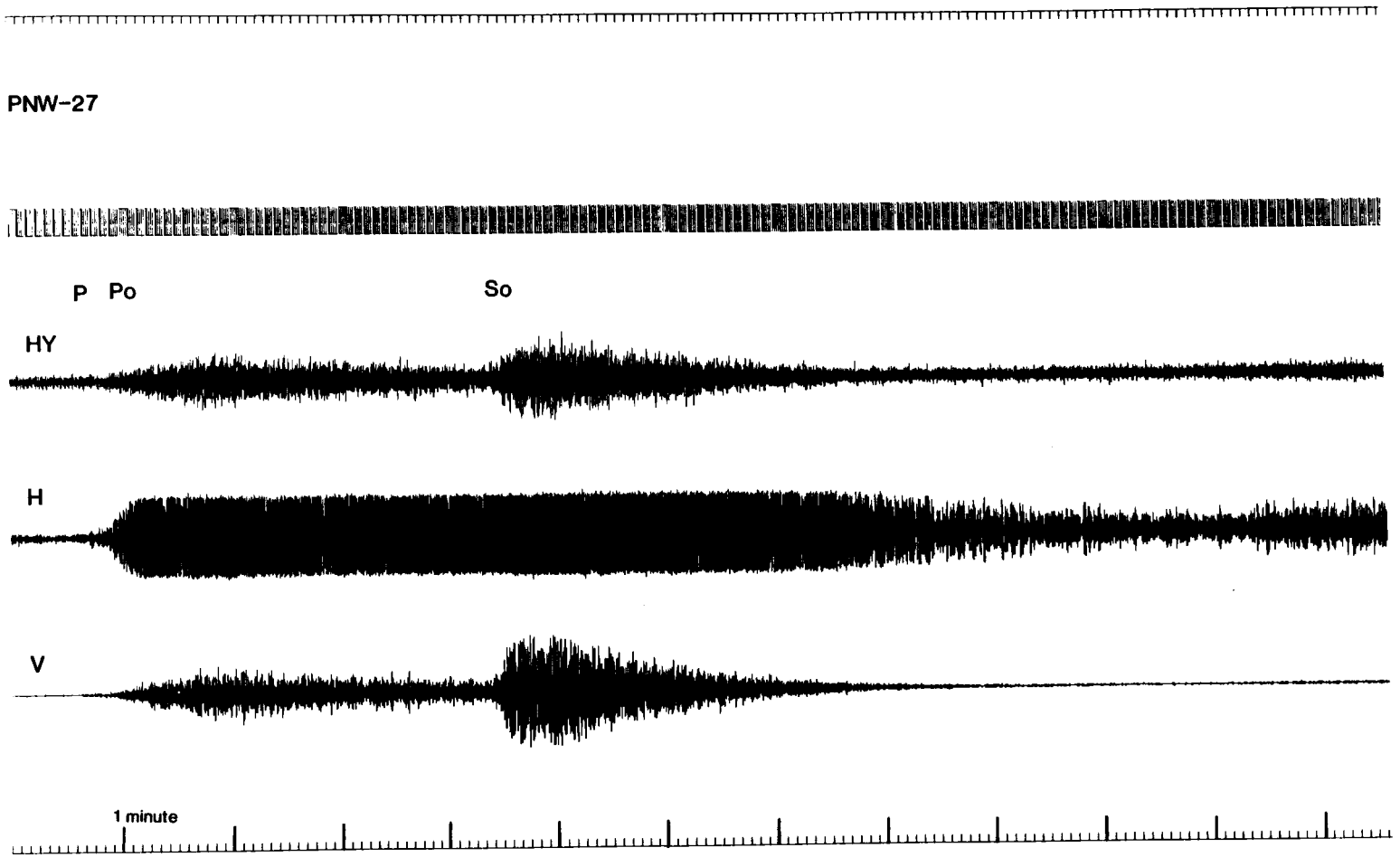

Figure 3. Po/So seismogram of an Izu trench earthquake (EQ 27) recorded by an instrument in the Pacific Northwest Basin (distance 21°). This Figure has the same format as Figure 1.

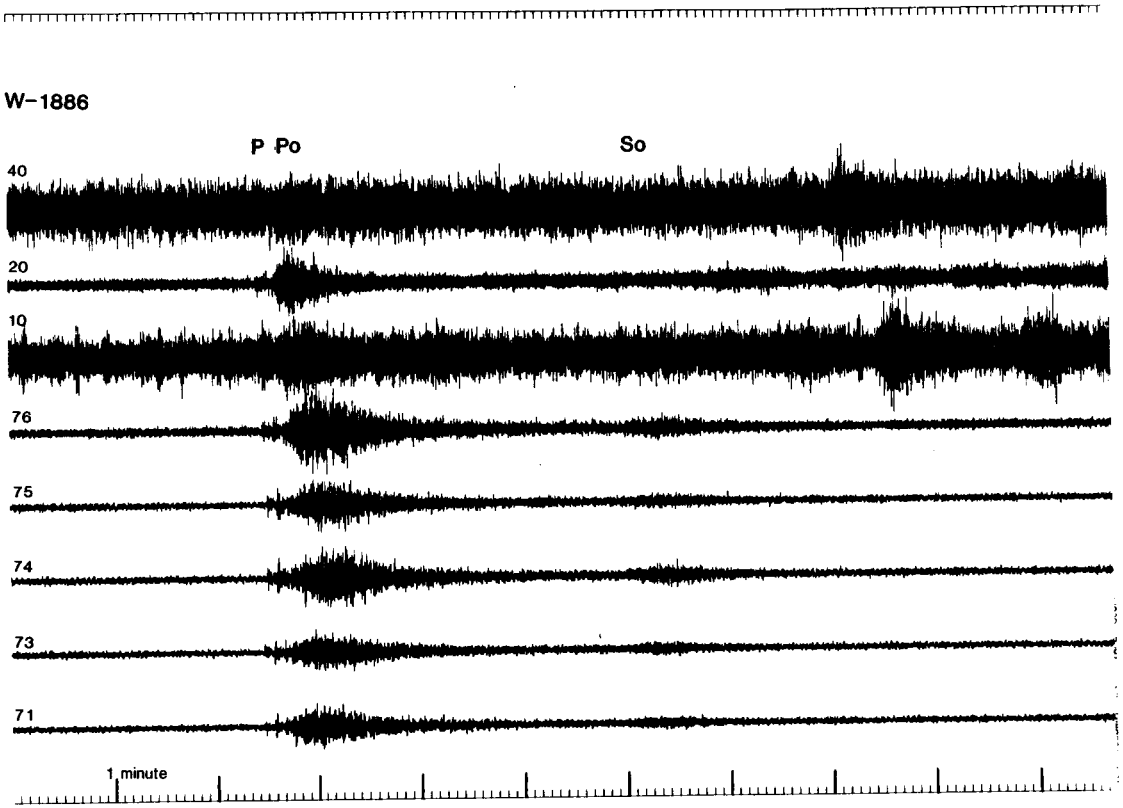

Figure 4. P_o/S_o seismogram of the Mussau trench earthquake (EQ 1886) recorded by the Wake hydrophone array. Numbers on the left at the beginning of each signal are the hydrophone identification number. Hydrophones 10, 11, 20, 21 and 40 are located in the SOFAR channel, 71-76 near the ocean bottom. The onset of each phase is labeled on the seismogram. Note the amplitude ratio between the P, P_o, and the S_o phases, both the P and S_o phase amplitudes are smaller than the P_o amplitude.

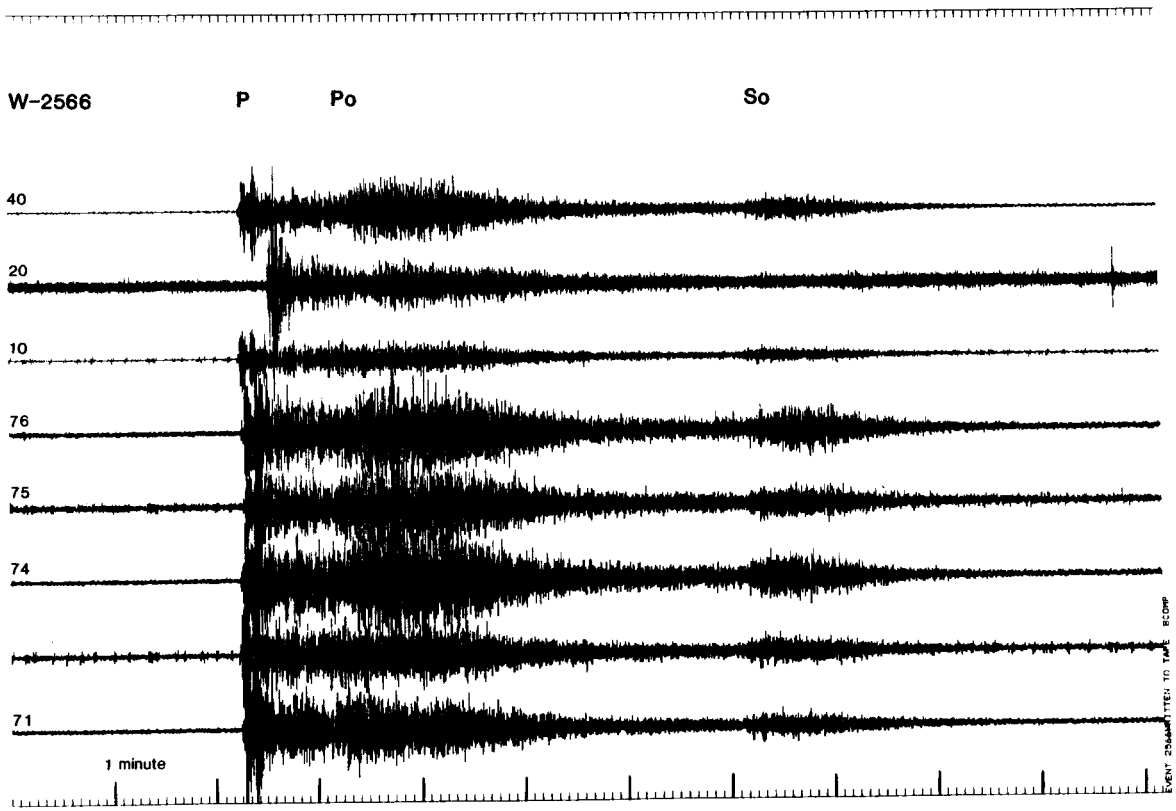

Figure 5. P_o/S_o seismogram of a Sea of Okhotsk earthquake (EQ 2566) recorded by the Wake hydrophone array. This Figure has the same format as Figure 4. Here, the P phase amplitude is larger than that of the P_o phase.

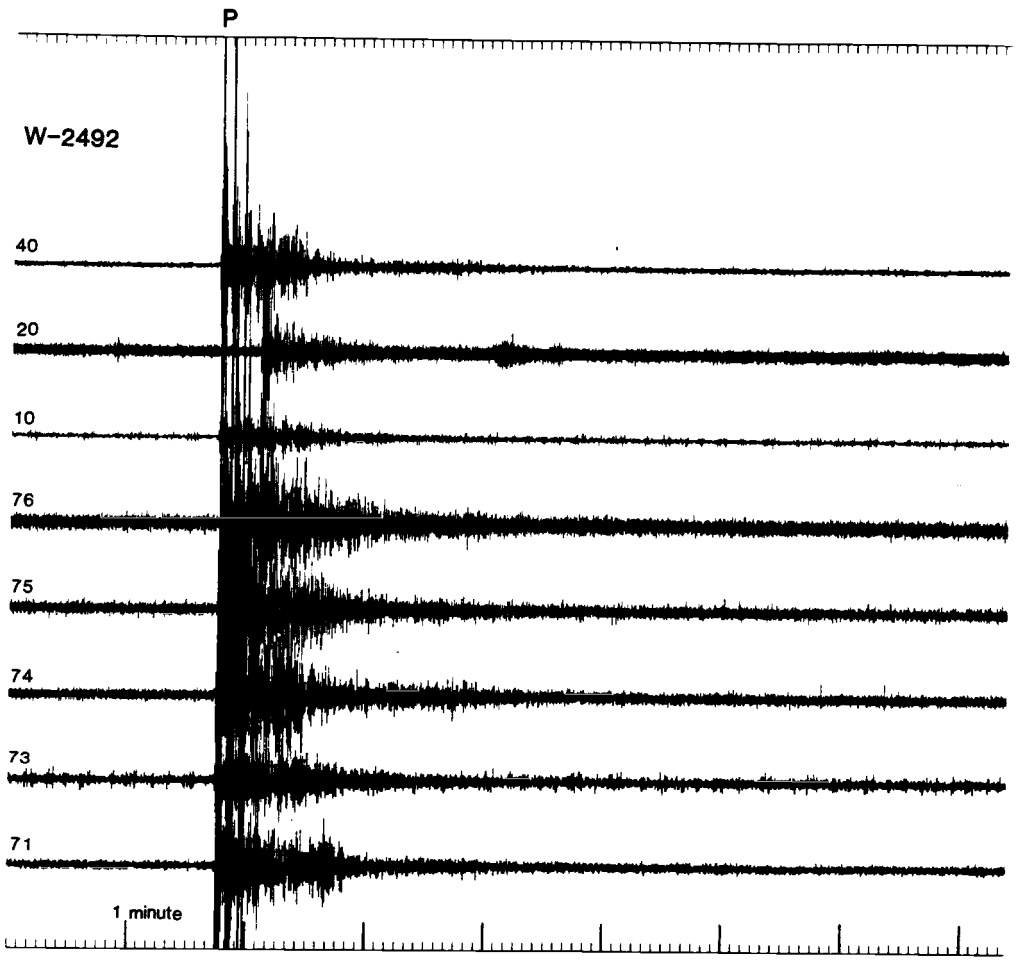

Figure 6. P_O/S_O seismogram of another Sea of Okhotsk earthquake (EQ 2492) recorded by the Wake hydrophone array. This Figure has the same format as Figure 4. No Po and S_O phases are visible.

restricted to very shallow (<10 km) depths or, in the case of surface wave dispersion data, to very large scale features (>50 km wavelength). P_o and S_o, being high frequency phases, may be able to constrain kilometer scale features.

An important characteristic of the P_o and S_o phases is the unusually long duration of their coda compared to other body wave phases. Their coda can be several minutes long (hundreds of oscillations), and most often the P_o coda extends into the S_o coda even at large epicentral distances (> 20 degrees). The coda most frequently has a gradual buildup to a maximum amplitude that may last for several up to tens of seconds (Figures 1 to 5). The P_o and S_o coda amplitudes have been observed to vary with frequency (Asada and Shimamura, 1976; Ouchi, 1981; Menke and Chen, 1984; Butler, 1985; Novelo-Casanova and Butler, 1986). Walker et al. (1983) concluded from composite spectra that the P wave amplitudes decrease faster with frequency than the P_o wave amplitudes and that the S_o phases decreased slightly faster than the P_o phases. However, due to large deviations between different earthquake spectra, the differences between P_o and S_o spectral falloffs observed in the composite spectra are highly questionable.

Currently available quantitative data on P_o and S_o phases are limited to phase velocities of the onset of the coda and primitive spectral analyses (Press and Ewing, 1955; Shurbet, 1962; Herrin and Taggart, 1962; Walker, 1965; Båth, 1966; Fedotov, 1968; Molnar and Oliver, 1969; Walker and Sutton, 1971; Sutton and Walker, 1972; Hart and Press, 1973; Huestis et al., 1973; Asada and Shimamura, 1976; Walker, 1977 a; Stephens and Isacks, 1977; Mantovani, 1977; Walker et al., 1978; Sutton et al., 1978; Talandier and Bouchon, 1979; McCreery, 1981; Ouchi, 1981; Walker et al., 1983; Ouchi, 1983). Most of these studies were done on small data sets (see upper part of Table 1) using single station observations and regression analyses on X/T observations from different stations (where X is a range measured along a great circle on the earth's surface and T is the travel time). Single station observations on apparent phase velocities (X/T) cannot be compared primarily because of the different tectonic settings for different raypaths. Anisotropies, observed in nonarray experiments (Talandier and Bouchon, 1977), are caused by heterogeneities in the oceanic and upper mantle structure of different regions. Array measurements

OBSERVER	YEAR	NO OF EQ	RANGE	AGE	Po RANGE	TYP Po	NO OF EQ	RANGE	AGE	So RANGE	TYP So	STUDY AREA
Press&E.	1955	3	69-79		7.98-8.24		15	52-125		4.34-4.63	4.58	various areas
Shurbet	1962	10	13-30		7.7-8.2	7.8	10	13-30		4.2-4.7	4.5	Bermuda
Herrin&T.	1962				7.6-8.3							USA
Shurbet	1964	5			8.07-8.34		5			4.55-4.63		Bermuda
Walker	1965	24	17-32			8.1	28	17-32			4.65	Pacific
Båth	1966	5	31.5-35.1		8.21-8.31	8.26	33	21.6-41.4		4.66-4.78	4.72	Russia
Oliver & I.	1967					8.4					4.75	Tonga
Fedotov	1968				8.13-8.25						4.57	Kamchatka
Molnar&O.	1969						60	6-35		4.64-4.68	4.66	various areas
Walker&S.	1971	62	0-30		8.25-8.31	8.28	40	0-30		4.75-4.83	4.79	N - Pacific
Sutton&W.	1972						4	7.6-20.6		4.74-4.80	4.77	Pacific
Hart&Press	1973			0-50 m.y.			>130	1-27	0-50 m.y.	4.70-4.72	4.71	N - Atlantic
Hart&Press	1973			> 50 m.y.				1-27	>150 m.y	4.56-4.60	4.58	N - Atlantic
Huestis&al.	1973						30	8-27		4.69-4.75	4.72	India
Huestis&al.	1973						20	14-34		4.75-4.87		W - Australia
Stephens&I.	1977							35-40			4.7	
Walker	1977a	45	8-30	60-130 m.y.	8.38-8.66	8.52		8-30	60-130 m.y.	4.63-4.77	4.7	NW - Pacific
Walker	1977a	45	8-30	>130 m.y	8.28-8.38	8.33		8-30	>130 m.y	4.74-4.80	4.77	NW - Pacific
Talandier&B.	1977		3-16		7.92-7.98	7.95		3-16				C&S - Pacific
Walker	1981		>30		7.90-8.12	8.01		>30		4.64-4.72		

OBSERVER	YEAR	NO OF EQ	RANGE	AGE	Po RANGE	TYP Po	NO OF EQ	RANGE	AGE	So RANGE	TYP So	STUDY AREA
McCreery	1981	14	4-13	< 30 m.y.	7.23-7.47	7.35						Cocos Plate
Ouchi	1983	4	9-18		8.1-8.3							Japan
Butler	1985	11	17-35	150 m.y.	7.91-7.96	7.96	10	17-35	150	4.53-4.61	4.57	NW - Pacific

(shown in lower part of Table 1) have been made by McCreery (1981), Ouchi (1983), and Butler (1985). Unfortunately, these array studies were also done on small data sets so their results are limited to small areas and are sometimes highly questionable (Ouchi, 1983; Butler, 1985). No systematic polarization studies on P_o and S_o phases are available, but authors have commented on their chaotic particle motion (Båth, 1966).

P_o and S_o phase velocities have been found to depend on: 1) tectonic setting and epicentral depth (Fedotov, 1963; Oliver and Isacks, 1967; Utsu and Okada, 1968; Molnar and Oliver, 1969; Mitronovas et al., 1969; Huestis et al., 1973; Walker, 1977 a; Talandier and Bouchon, 1979; McCreery, 1981); 2) range interval (Fedotov, 1968; Walker and Sutton, 1971; Sutton and Walker, 1972; Walker 1977 a,b); and 3) lithospheric age and cooling (Hart and Press, 1973; Asada and Shimamura, 1976; Walker, 1977 a; McCreery, 1981; Black and Braile, 1982). P_o and S_o phase velocities have been used as constraints on petrological models of the upper mantle (Hart and Press, 1973; Fuchs and Schulz, 1976).

The large amplitudes of P_o and S_o phases as well as their nearly range-independent phase velocity and low attenuation have prompted past investigators to conclude that they are guided waves. The type, location, and shape of their waveguide are not clearly defined or understood. Several modes of propagation have been proposed; for example:

1) Transmission by whispering gallery propagation in the mantle by multiple grazing reflections from the MOHO discontinuity (Press and Ewing, 1955; Menke and Richards, 1980) (Figure 7, top);

2) Transmission in a layer of increasing velocity directly below the MOHO and above the LVZ (Shurbet, 1964; Stephens and Isacks, 1977);

3) Transmission through a minimum velocity channel (LVZ) slightly below the MOHO (Shurbet, 1962; Walker, 1965; Sutton and Walker, 1972) (Figure 7, bottom).

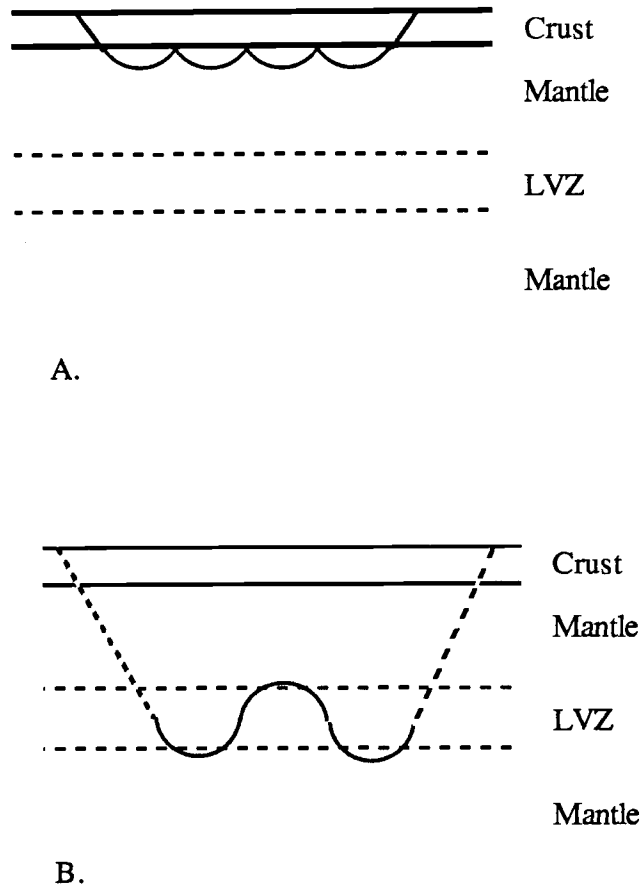

Figure 7. Two models for the proposed propagation paths of P_o and S_o.
A) Propagation by whispering gallery modes at the crust-mantle boundary.
B) Propagation through a mantle low-velocity zone.

In addition, the following questions have been debated:

1. Is there more than one waveguide involved (Molnar and Oliver, 1969; Mantovani et al., 1977; Walker, 1977a, b)?
2. Is the high frequency nature of P_o and S_o phases a result of the tunneling of low frequency waves by thin high velocity layers in the lower lithosphere (Fuchs and Schulz, 1976; Ouchi, 1981)?
3. Perhaps the waveguide is not present, and the coda is simply created by reverberations in a very simple lithospheric structure (Gettrust and Frasier, 1981; Sereno and Orcutt, 1985)?
4. How do the crust, sediments, and water column affect the coda production? Are reverberations in those layers important in building the coda (Gettrust and Frasier, 1981; Sereno and Orcutt, 1985)?
5. Are the scatterers that cause the coda layers in the crust (Gettrust and Frasier, 1981; Sereno and Orcutt, 1985) or random irregularities in the crust or mantle (Menke and Richards, 1983; Sato, 1984)?

One reason that these questions have not yet been definitely answered is that, although the P_o and S_o phases have received considerable attention from seismologists, very little quantitative data has been published. The models that have been attempted lack good data against which they can be tested. The lack of data is due largely to the fact that digital signal analyses are required to understand this phase, and until recently, most recordings of it were analog paper records.

The fact that P_o and S_o are composed of reverberating coda has made them very difficult to study. It has proven impossible to model the waves in a 'wiggle-by-wiggle' way that is commonly done today with simpler, long period seismograms. An alternative is to model the coda statistically, that is, to match only the gross shape of the coda. Recent work on other kinds of coda-dominated waves (notably local EQs), when combined with theoretical models of coda generation, have demonstrated that this technique can produce interesting results (Toksöz et al., 1974;

Aki and Chouet, 1975; Menke and Richards, 1980; Gettrust and Frazer, 1981; Richards and Menke, 1983; Menke and Richards, 1983; Menke and Chen, 1984; Sato, 1984; Sereno and Orcutt, 1985). The approach is to recognize that the coda is a product of two competing phenomena in the earth: Scattering of waves from heterogeneities in the earth, which tends to lengthen the travel time of the waves and produce long coda, and: Attenuation of waves by frictional absorption which tends to preferentially absorb waves, that have travelled an extra distance, and reduce the coda. Both scattering and attenuation are known to be frequency dependent phenomena. The amount of scattering is controlled by the amount of heterogeneities in the earths structure at scale lengths comparable to the wavelength of the seismic waves. Attenuation often causes waves to loose energy at a rate proportional to $\exp(-2\pi f t/Q)$ where f is frequency, t, travel time, and Q, the quality factor. Thus by measuring the shape of the coda in different frequency bands it may be possible to recover information about the scale length of heterogeneities in the earth and about the magnitude of the attenuation. Both of these parameters are of considerable geophysical interest, since they may be related to the type of lithospheric formation and its current thermal state.

Aki and Chouet (1975) studying shear wave coda of local EQs demonstrated that they could recover both the attenuation and degree of heterogeneity along their raypaths. However, their work was greatly simplified by the geometry of local EQs where the overall seismic structure is simple, the raypaths of the waves forming the coda short, and largely known. This is not the case with P_o and S_o phases so we cannot hope to apply Aki and Chouet's (1975) simple formulas to the coda falloff measurements made in this study. Instead, our approach will be more ad hoc. We use empirically chosen functions to describe the shape of the coda, functions that do not have much theoretical justification except that they vary with frequency and contain a term that exponentially decays with time as is suggested by the attenuation rule. It is our expectation that, when compared to similar measurements derived from synthetic P_o and S_o seismograms (for instance, those of Gettrust and Frazer, 1981; Sato, 1984; Sereno and Orcutt, 1985), our measurements will help constrain the lithospheric structures that form the P_o/S_o 'waveguide'.

The purpose of this study is to quantitatively describe the shape of the coda for different frequency bands by fitting empirical functions to the coda envelope in each band, using a large (~100) EQ data set recorded on hydrophones and geophones in the NW - Pacific (Figure 8). These analytical results can then be compared to the predictions of theoretical models. Furthermore any variations in coda falloff values can be related to variables such as epicentral range, tectonic setting, age of the crust, depth of focus, and apparent raypaths. The data consist of EQs from the western and northwestern Pacific recorded by arrays of several stations and includes both hydrophone and geophone recordings on analog and digital instruments. This study concentrates on the P_0 and S_0 coda, and especially on its decay rate, because the coda is very sensitive to the type of scatterers, to their size and shape, and because measurements of coda buildup and decay are independent of the response of the recording instrument and of the seismic source (Aki and Chouet, 1975). We therefore can use existing data, some of which is only poorly calibrated, to make high quality measurements of the properties of the coda.

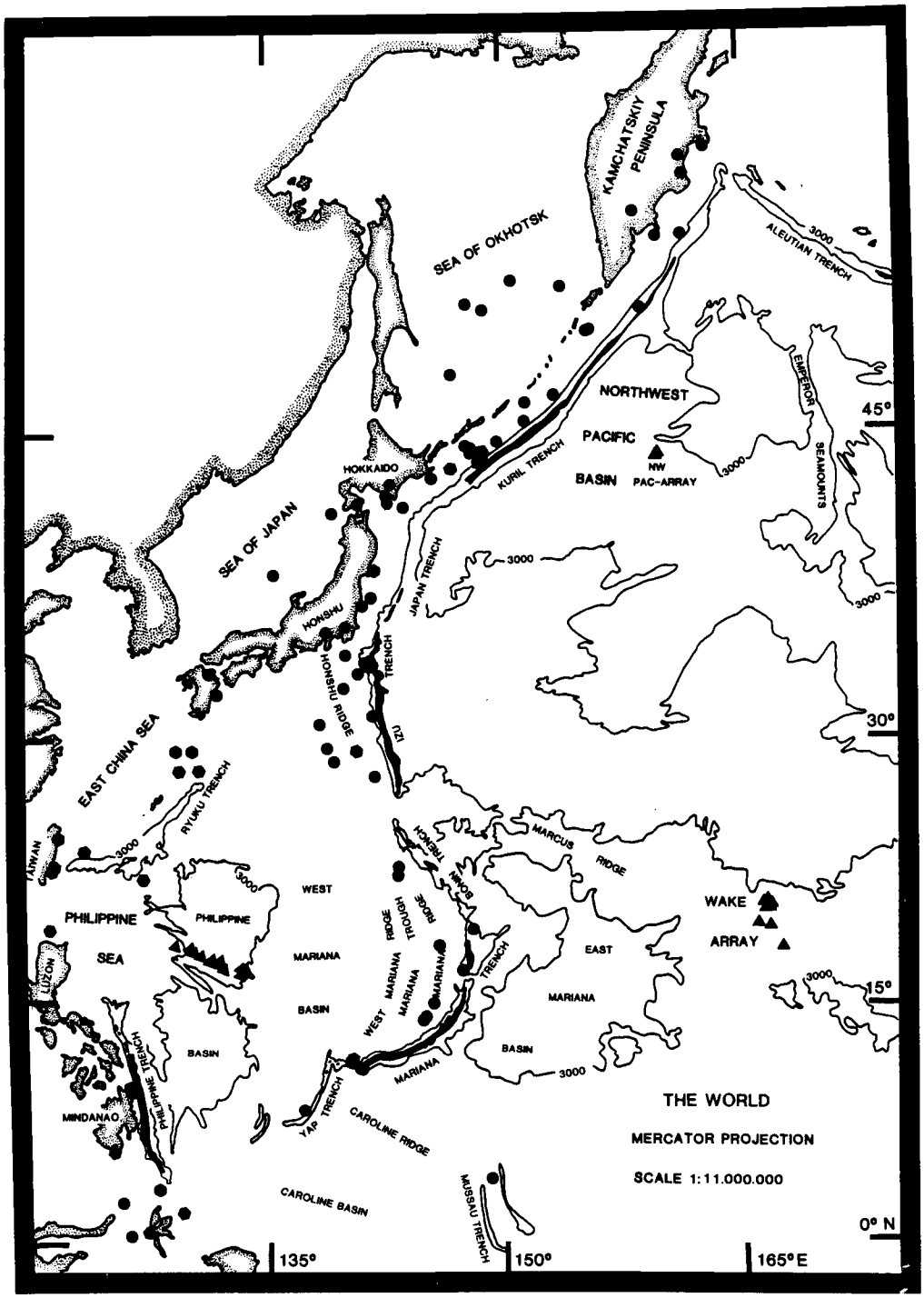

Figure 8. Location map of all earthquakes (circles and hexagons) and the three recording arrays (triangles) used in this study. Each array operated during different time intervals. Earthquakes denoted by circles were recorded by the Wake hydrophones; those denoted by hexagons were recorded on the OSU OBSs.

DATA ACQUISITION:

The data sets:

Three data sets were used in this study. Two sets were recorded by OSU ocean bottom seismometers (OBS) during an experiment in the Philippine Sea in February and March, 1981, and during the Deep Sea Drilling Project (DSDP) Leg 88 in the Northwest Pacific Basin in September, 1982. The OSU data sets were made available to this study by L. D. Bibee. The third data set contained 106 selected EQs recorded by the Wake hydrophone array from September, 1982, to January, 1985. The Wake data were made available by N. Frazer, C. McCreery, and D. Walker at the Hawaii Institute of Geophysics (HIG). The EQ locations were obtained from the Preliminary Determination of Epicenters-Earthquake Data Report (PDE-EDR) monthly reports. They are listed in Appendix 1. The PDE-EDR locations are sufficiently accurate to be used in this study because the size of our geometrical array is very large compared to hypocentral location errors.

The OSU OBS experiments:

The Philippine Sea data were recorded in a three phase experiment during February and March, 1981. The experiment was conducted by Oregon State University in cooperation with the Scripps Institute of Geophysics and Planetary Physics (IGPP). The objective of this project was to determine compressional and shear wave velocities as well as attenuation at depth in the Philippine Sea (Goodman, 1983). During the first phase of this experiment, seven ocean bottom seismometers were deployed in a line, about 500 km in length, striking NW - SE in the West Philippine Basin (Figures 8 and 9). Due to inoperative satellite navigation, only five OBSs (stations A, B, D, E, and G) were recovered at the end of the first phase. During the second phase, data were collected by three instruments, stations AA, BB, and EE (Figure 9). In the third phase, five OBSs were deployed, and four were recovered (stations BBB, DDD, EEE, and FFF). The Philippine Sea stations have a location error of about 500 m. For further description of the Philippine Sea refraction

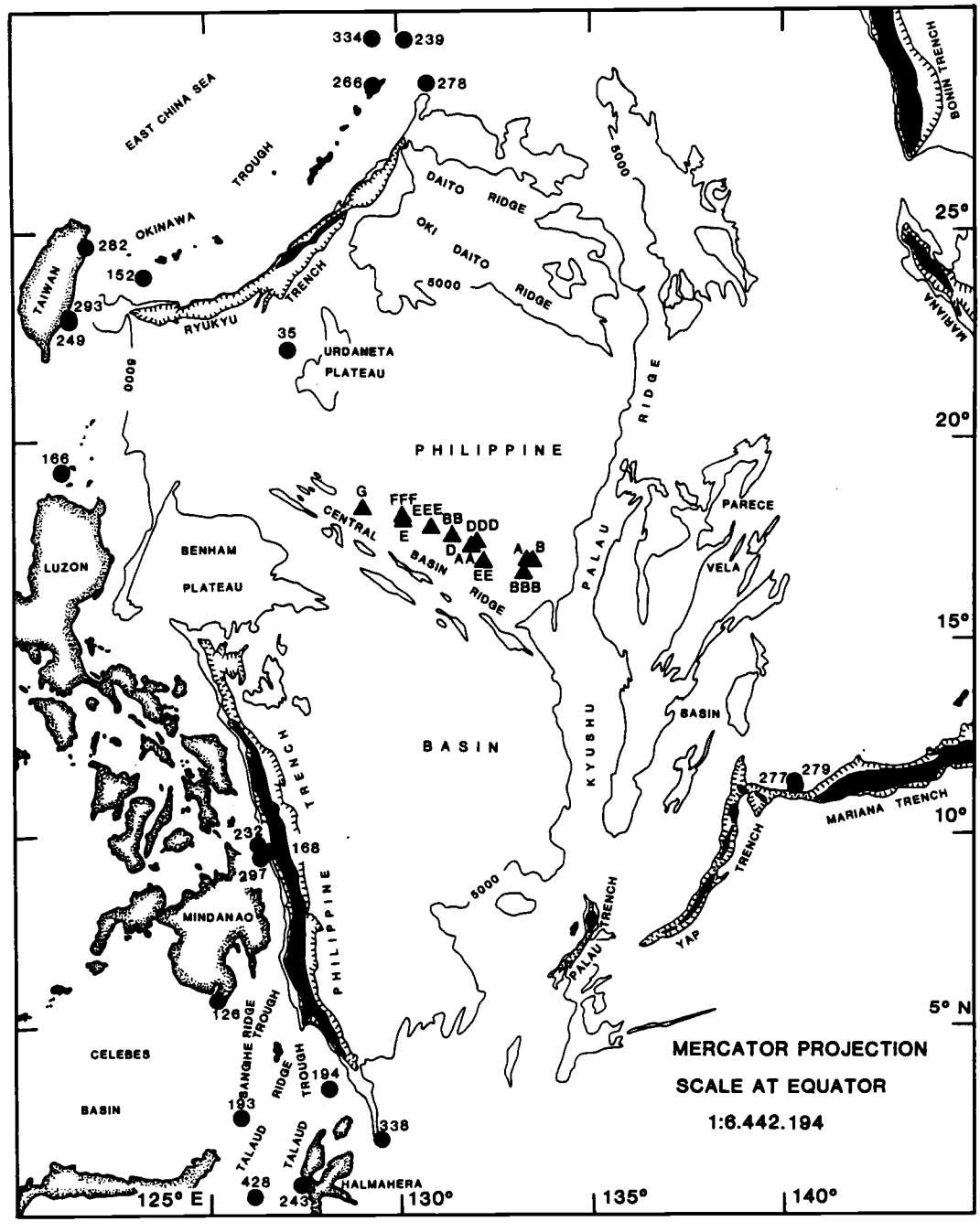

Figure 9. Location map for the Philippine Sea data set. Earthquakes (circles) and stations (triangles) are numbered and further described in Appendix 1.

survey, the reader is referred to Goodman (1983).

The second data set was recorded in September, 1982, during DSDP Leg 88, in the NW Pacific Basin, near 160°W and 44°N, using two OSU OBSs and a digital ocean sub-bottom seismometer (OSS) developed by Hawaii Institute of Geophysics (HIG). Figures 8 and 10 show the location of the NW Pacific Basin array. The location error for each station is about 250 m. Only data from the two OSU OBSs, were used in this study. One of the objectives of the NW Pacific Basin project was to obtain information on the crustal structure of the 110 m.y. old crust in the Northwest Pacific Basin. For further description of the project the reader is referred to Bée, (1984).

The OSU analog OBS:

The OSU ocean bottom seismometer is a four-channel, analog instrument consisting of horizontal and vertical geophones with a natural frequency of 3 Hz and of a pressure-compensated hydrophone with a flat frequency response between 1 and 30 Hz. The fourth data channel is the time signal. The OBS clocks are corrected by using the Universal Time Code (UTC), transmitted from stations on land. The OSU OBS frequency range is 2 - 30 Hz. After filtering, the data is converted into the digital domain at a rate of 100 samples per second, resulting in a Nyquist frequency of 50 Hz, twice that of the high frequency setting of the anti-alias filter. Signals between 2 - 25 Hz are thus fairly well recovered, with little aliasing noise from higher frequencies. The data reduction converts the raw data into the standardized ROSE format decribed by LaTraille et al. (1982).

Figure 11 shows different response curves for the OSU OBS system. The response is approximately flat from 5 - 18 Hz with a highpass slope of approximately 6 dB/octave and a lowpass slope of approximately 16 dB/octave. The 40 Hz noise is due to the recorder motor. The dynamic range of the seismometer is about 40dB, which equals approximately 1.8 units of magnitude being recorded without distortion. For further information on the OSU OBS instrumentation, refer to Goodman (1983) and Solano (1984).

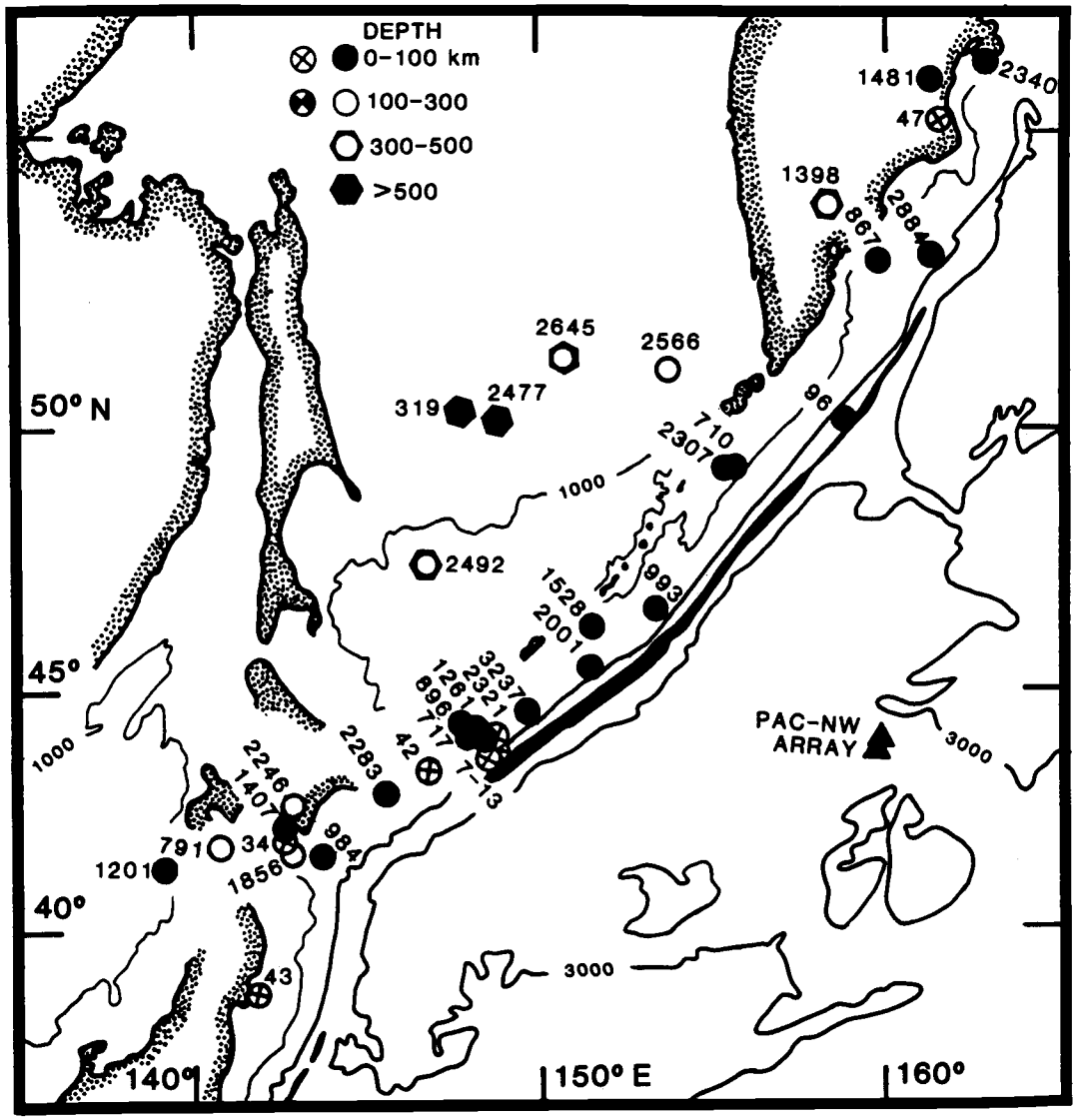

Figure 10. Location map for the Pacific Northwest Array and earthquakes recorded by that array (circles with crosses) and the Wake array (circles). Each earthquake is numbered and further decribed in Appendix 1.

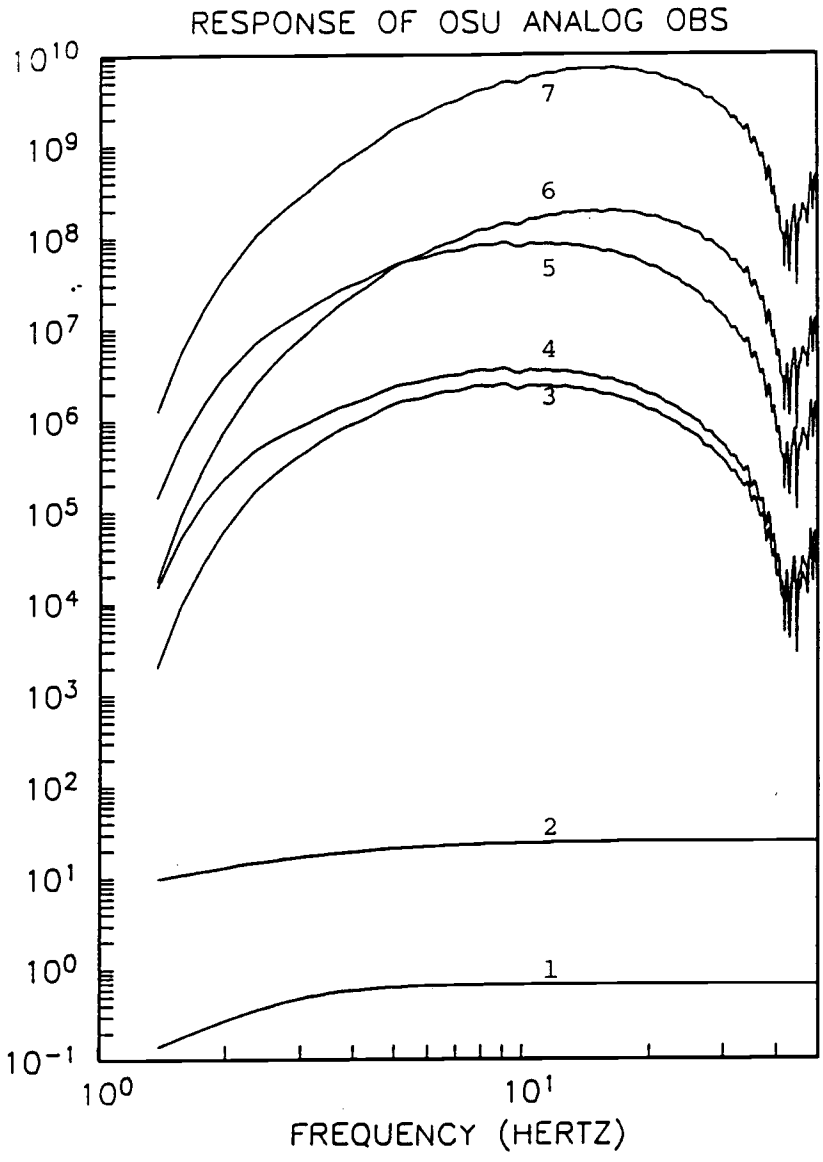

Figure 11. Adapted from Solano (1984). Frequency response of the OSU analog OBS. Curve 1) Geophone response to velocity. Curve 2) Hydrophone response to pressure. Curve 3) Electronics response. Curve 4) Geophone plus electronics response to velocity. Curve 5) Hydrophone plus electronics response to pressure. Curve 6) Geophone plus electronics response to displacement. Curve 7) Hydrophone plus electronics response to displacement.

The digital WAKE array:

In August, 1982, a continuous digital data collection system was installed on Wake island in the northwest Pacific (Figures 8 and 12) in order to record seismic signals from a nearby array of hydrophones. The array consists of six ocean bottom hydrophones (OBH) and five "doubled" sound fixing and ranging (SOFAR) channel hydrophones. Figure 13 shows the estimated response of the Wake system hydrophones. The system has a dynamic range of 96 dB, so that events ranging from at least mb = 4.0 to mb = 8.0 are recorded without distortion. For further description of the WAKE recording and processing system, the reader is referred to McCreery (no year).

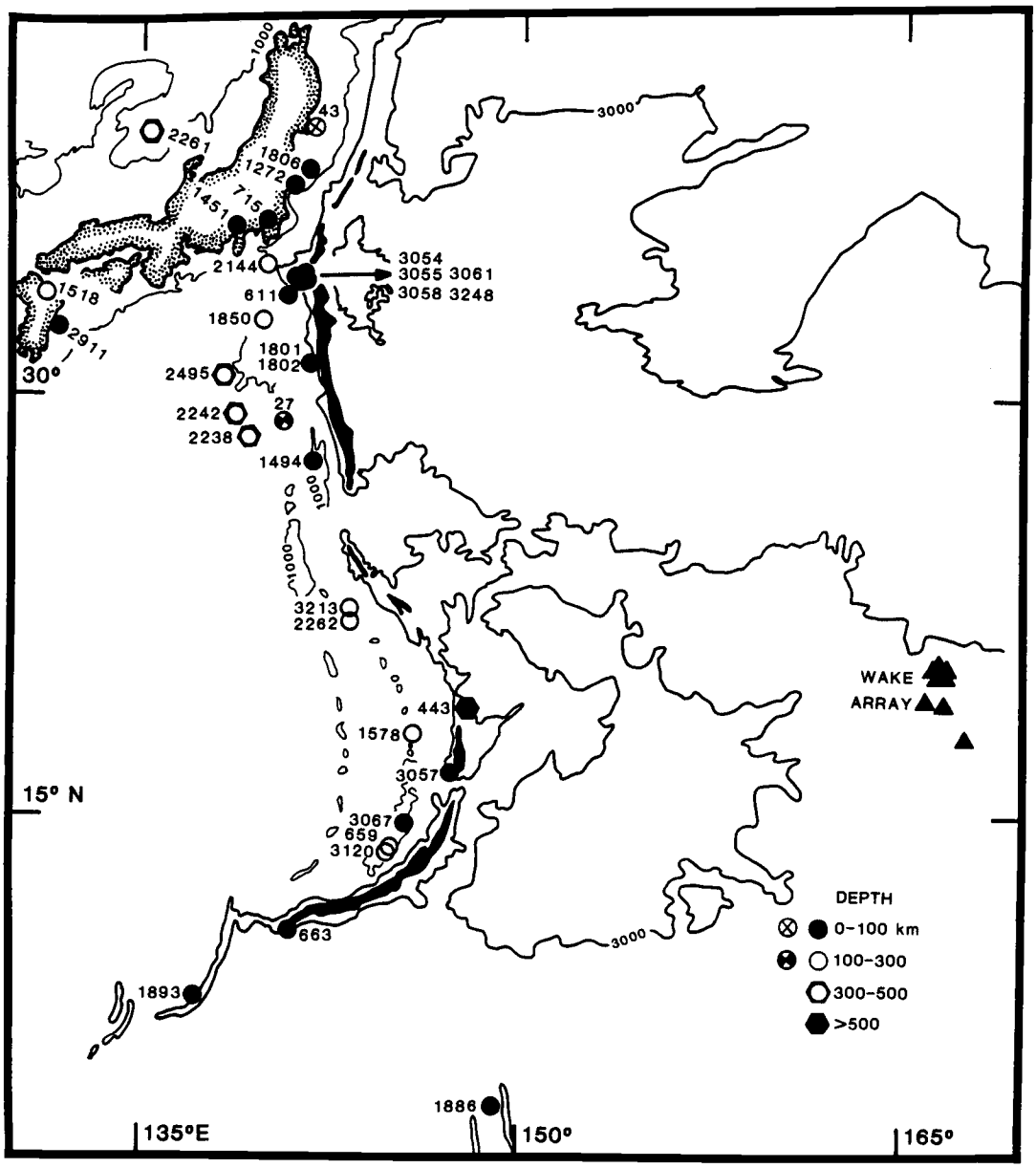

Figure 12. Location map for the southern part of the Pacific Northwest Array earthquakes (circles with crosses) and the Wake array data (circles) and stations (triangles). Each earthquake is numbered and further decribed in Appendix 1.

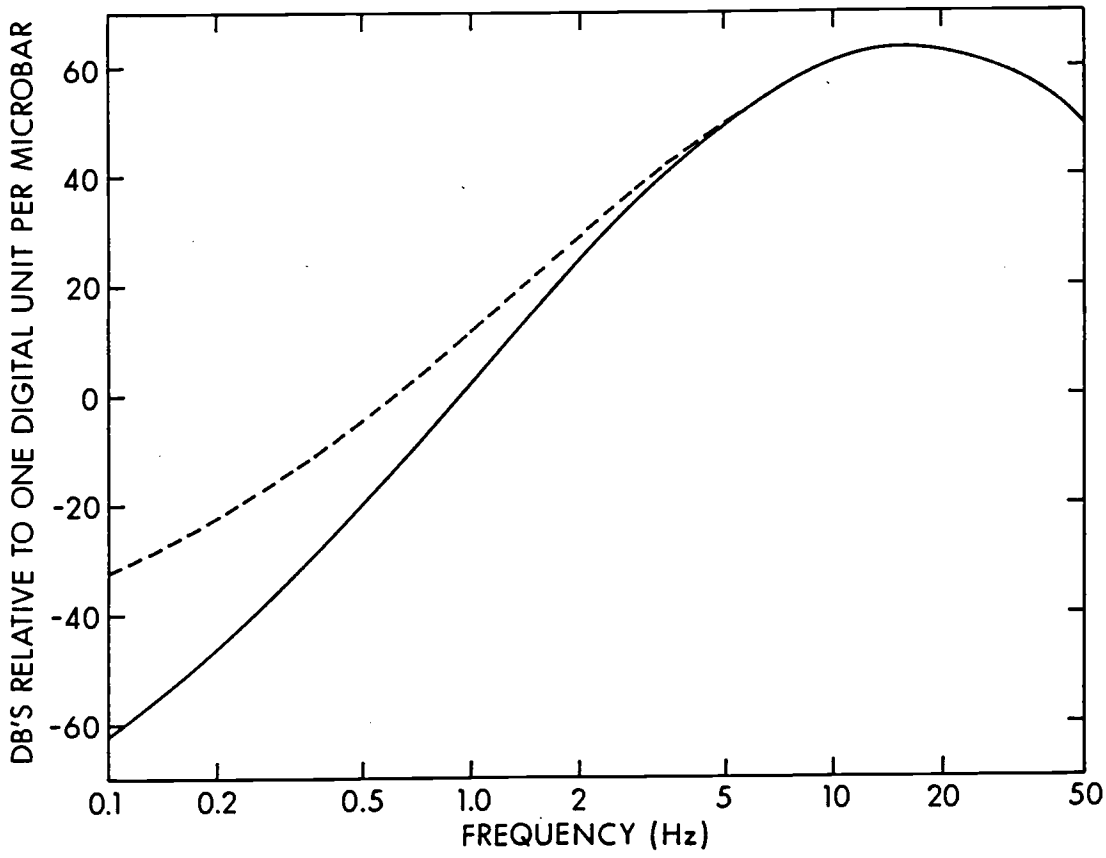

Figure 13. Response curve for the Wake hydrophone array. Pressure compensation hole closed (dashed line). Pressure compensation hole open (solid line).

DATA PROCESSING:

The purpose of this study was to fit simple empirical curves to selected phases of data in order to characterize their shape and thus evaluate their falloff rates. Each EQ was filtered into six frequency bands, and the measured falloff rates for P, P_o and S_o phases in these bands were compared for a total of 93 EQs.

Steps in Data Processing:

Step 1. Bandpassing the signal. Before bandpassing each data channel, its mean was removed, and it was padded with zeroes to a total of 65536 points. Each data channel was then bandpassed into six frequency bands using a standard Fast Fourier Transform (FFT), tapering the transform to remove unwanted frequencies, and then applying an inverse FFT. The bands were chosen to be about one octave wide, with the highest band being between 0.5 f_n and f_n, where f_n is the Nyquist frequency. We tested two filters, one based on cosine functions and the other on gaussian curves (Figure 14).

The cosine filter we use has overlapping pass-bands. Consequently, considerable energy spreads between the frequency bands of a channel, especially at the higher frequency bands where the tapers are broader (Figure 15).

The gaussian filter we use does not taper into adjacent frequency bands, since we truncate it at the edges of each octave band. We investigated several values for the variance of the gaussian filter. A higher variance creates a broader "gaussian bell" resulting in a slight increase in frequency domain amplitude which is transmitted to the bandpassed time series (Figure 16).

Our experiments indicated that the gaussian filter, with a variance chosen such that its amplitude was 0.9 at the edge of the pass-band (that is, almost a box-car), was most appropriate for our purposes.

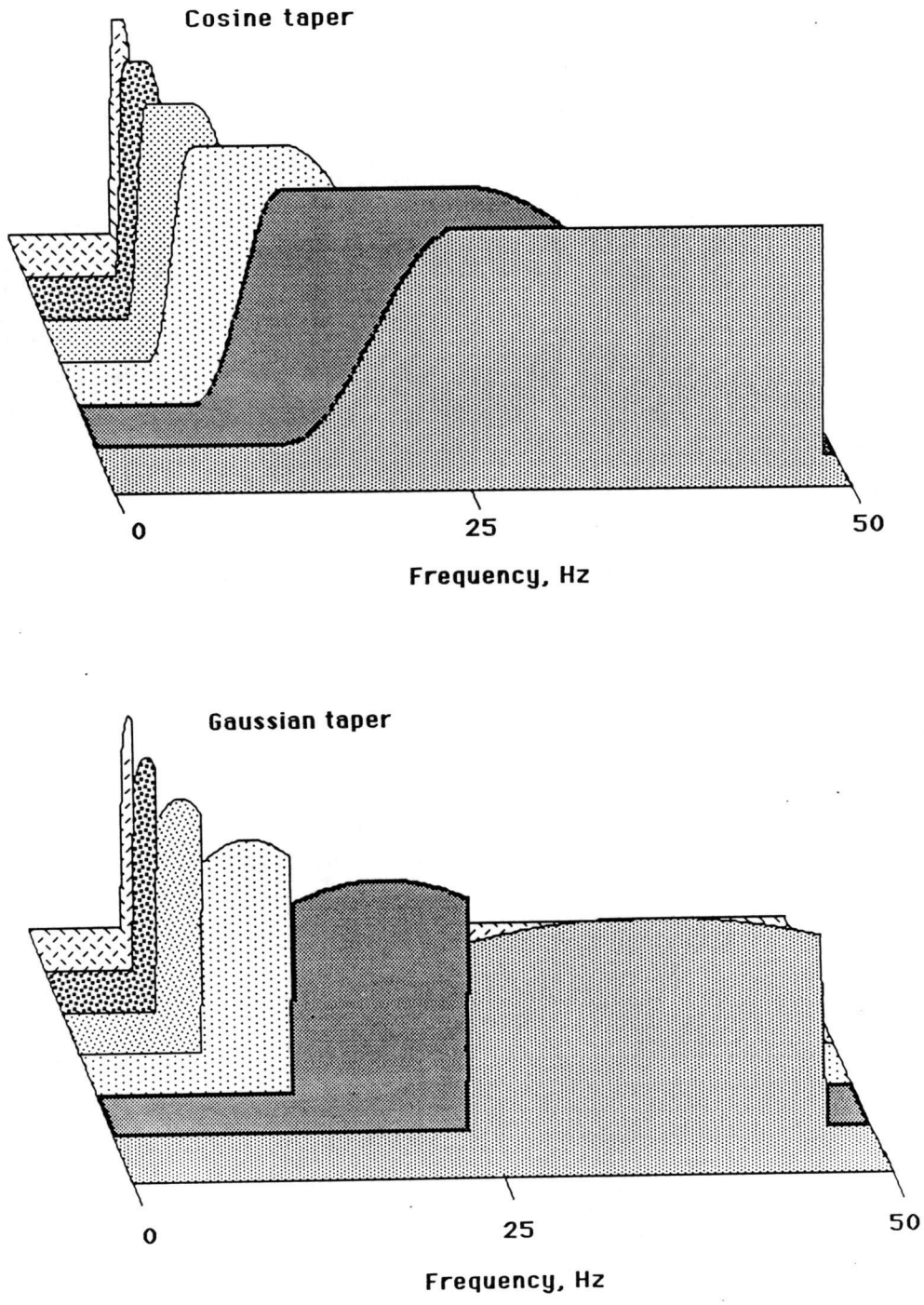

Figure 14. Frequency domain tapers used in bandpassing the P_0/S_0 seismograms. Top) Cosine taper. Bottom) Gaussian Taper. After initial experimentation, the Gaussian taper was exclusively used to compute falloff values.

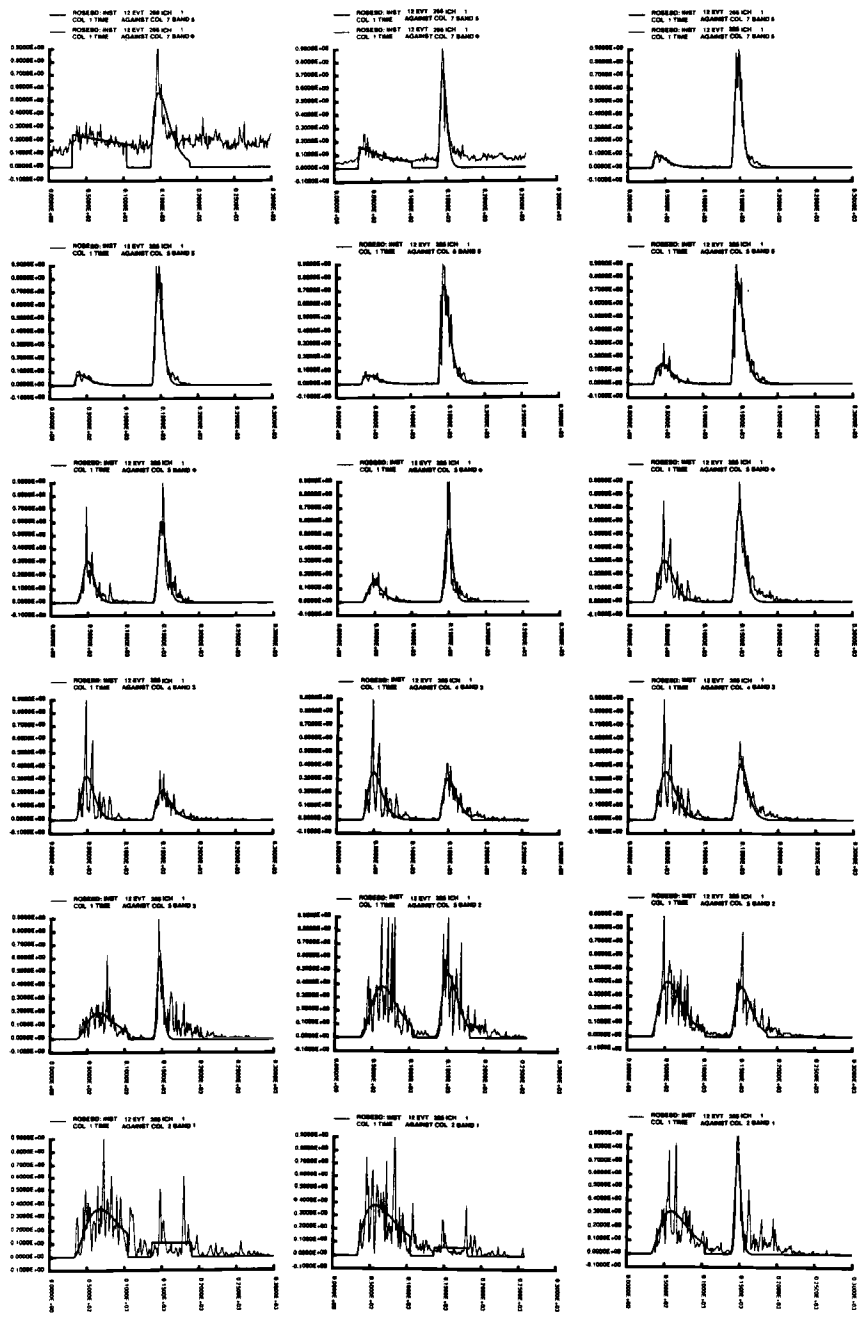

Figure 15. Comparison of cosine and gaussian bandpass filtered and rectified seismograms. The different rows are different octave-widepass bands, with the highest frequency (25-50 Hz) at the top, and the lowest (0.78-1.56 Hz) at the bottom. Right column, Gaussian filtered seismogram with a cutoff value 0.1. Middle column, Gaussian filtered seismogram with a cutoff value 0.9. Left column, Cosine filtered seismogram. Higher Gaussian cutoff values give better signal-to noice ratios for the bandpassed data. Note that the cosine taper spreads energy from adjacent bands into the filtered band. This is best seen in the highest and lowest frequency bands.

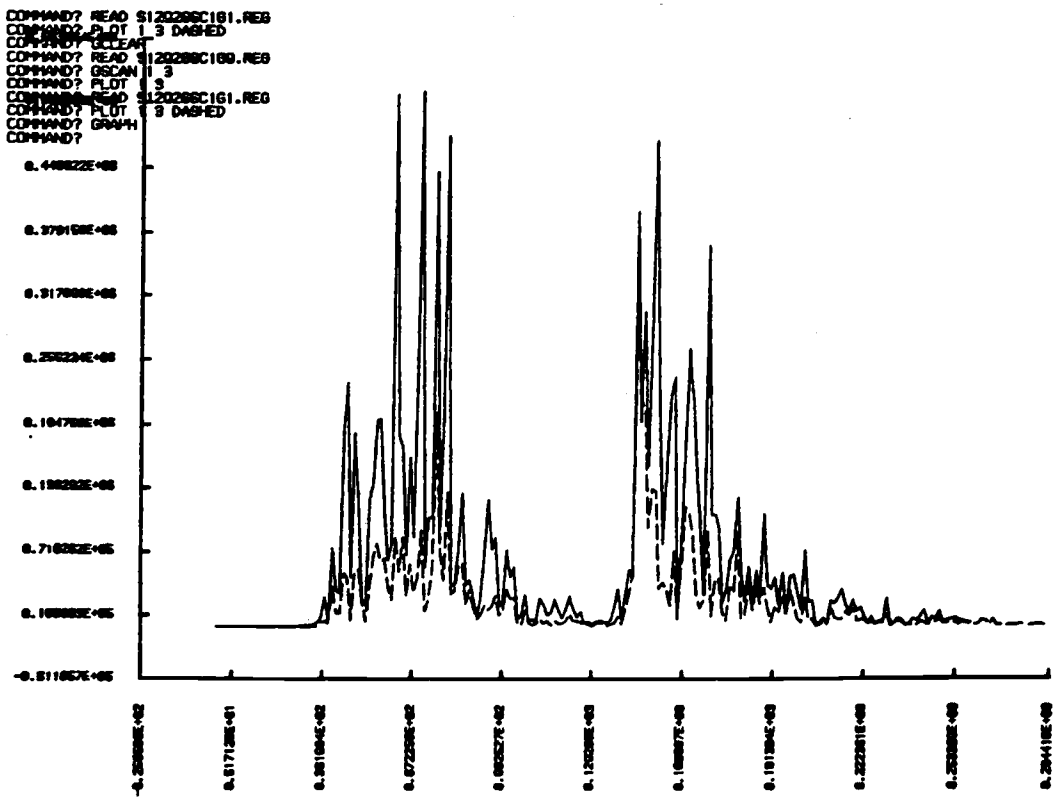

Figure 16. Comparison between two Gaussian bandpass filtered and rectified seismograms, with two different cutoffs of the Gaussian, 0.1 (dashed) and 0.9 (solid). Note that the 0.9 cutoff gives a higher amplitude signal, but that the shapes of the envelopes are similar.

Step 2. Forming Band-limited Envelopes. The band-limited time series were then squared and summed over either 128 point intervals (for the 100 Hz OSU data) or 102.4 point intervals (for the 80 Hz Wake data). This created six band-limited envelopes, each an octave wide, in the frequency range 0.78 - 50 Hz. (OSU) and 0.62 - 40 Hz. (Wake), with a sampling interval of 1.28 seconds. The shape of the band-limited envelope is a measure of the energy in the various bands.

The summation has the effect of smoothing out small time scale (that is <1.28s) variations in the envelope. However, we have made careful tests that demonstrate that the bandpassing and summing process does not affect any of the features on scales greater than 1.28 seconds. In particular, the smoothing does not effect the decay rate of the envelopes (Figure 17). The Wake version of the bandpassing program (WAKEROSEBD) is listed in Appendix 2.

Step 3. Fitting an empirical function to the band-limited envelope.
The band-limited envelope data were windowed (parts of the data were selected) by hand-picking the desired phases on a high-resolution graphics terminal. The windowed data were then fitted using a modified version of the Poisson distribution. The Poisson distribution is a discrete distribution on the integers of n:

$$P_n = e^{-\beta}(\beta^n/n!) \qquad n = 0, 1, 2, \cdots\cdots \qquad (1)$$

where β is a fixed positive number called the parameter of the Poisson distribution. In our analyses,

$$\beta = \gamma t$$

where t is the time after the beginning of the phase and γ is a positive constant hereafter called the falloff. Figure 18 shows the Poisson distribution for n = 0, 1, 2, 3, and 4. As n increases the distribution becomes longer-tailed. We modify this distribution

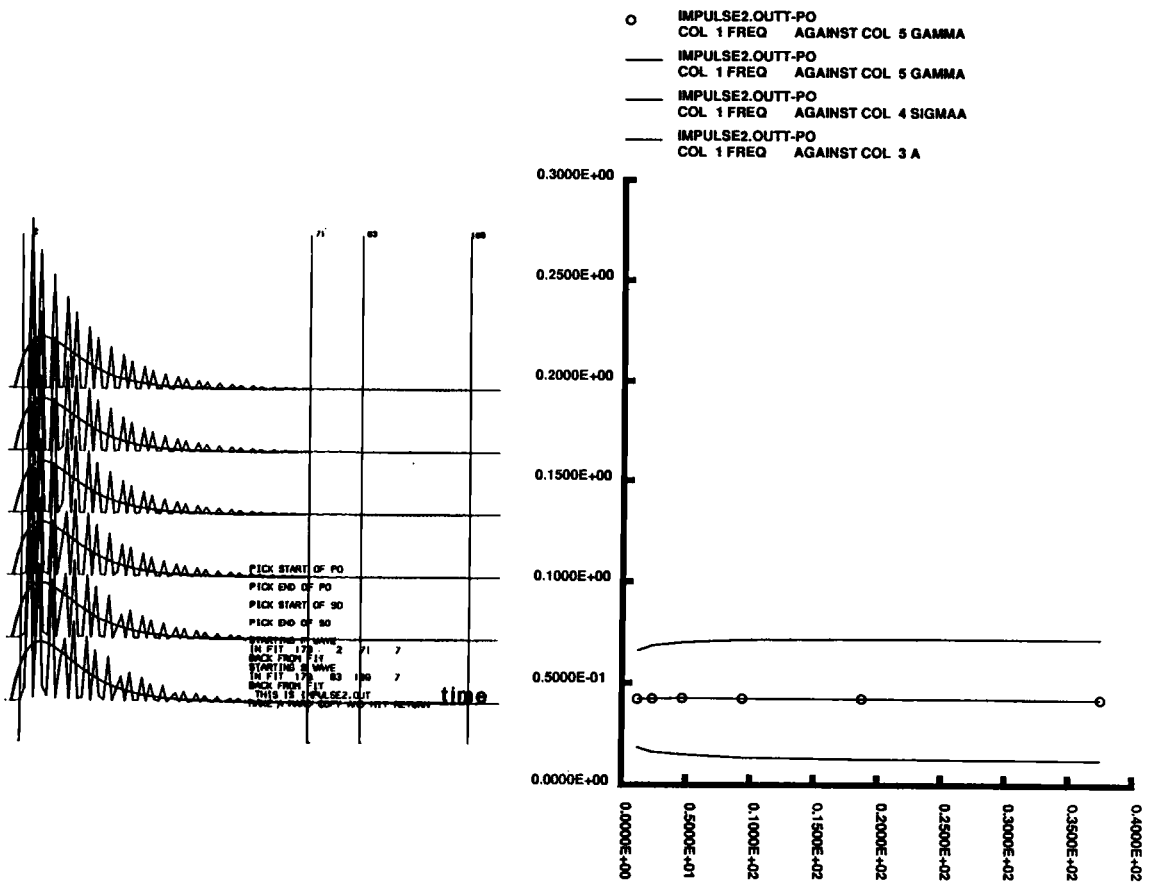

Figure 17. Test of the bandpassing and fitting algorithms. Left) Bandpassed and rectified seismograms, where the original function consisted of a set of exponentially decaying spikes. Right) Falloff as function of frequency (circles) and 1σ error bars. Note that the falloff is constant with frequency.

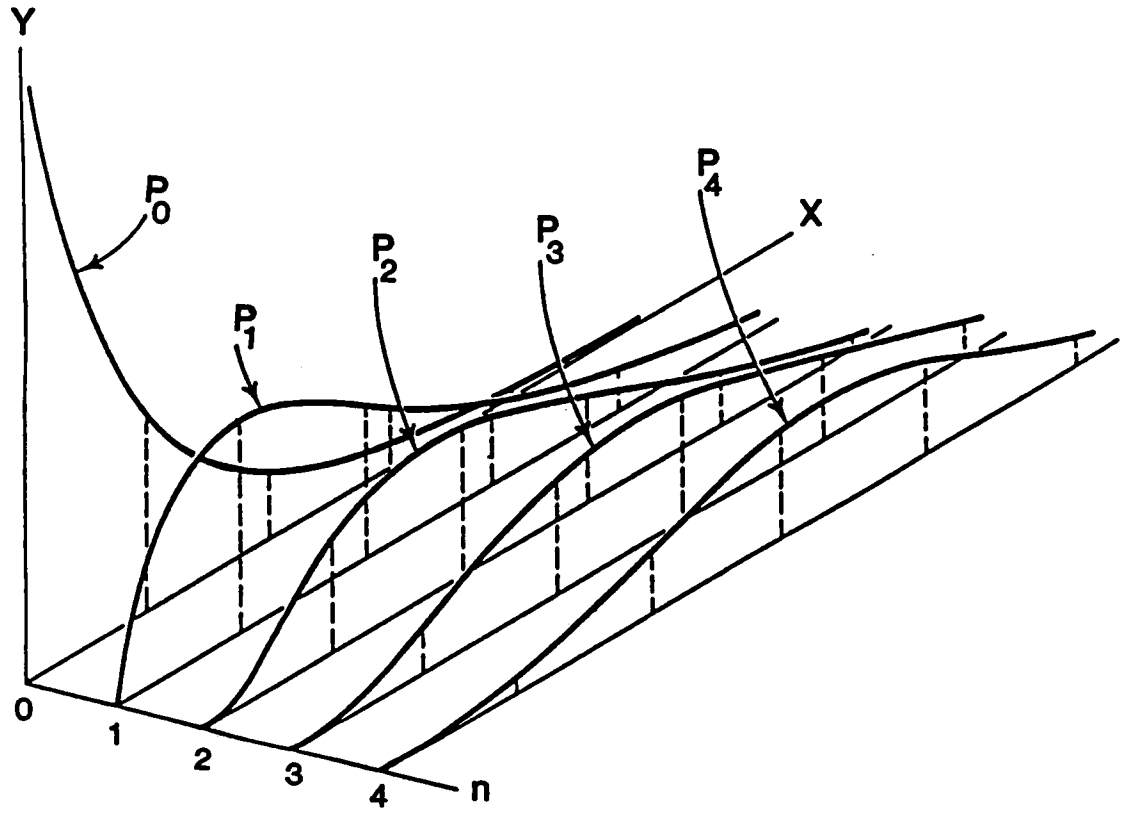

Figure 18. The Poisson distribution, $P_n(x)$, used to fit the P_O and S_O bandpassed and rectified seismograms.

slightly by requiring that it have area, A. Because:

$$\int_0^\infty e^{-\gamma t} t^n \, dt = \Gamma(n+1) / \gamma^{n+1} = n! / \gamma^{n+1} \qquad n = 0, 1, 2,....$$

the normalized formula is:

$$P_n(\gamma,t) = A \gamma^{n+1} t^n \, e^{-\gamma t} / n! \qquad (2)$$

This formula is a reasonable one because its shape changes for each n, and by fitting various n's of the formula to the data, one can iteratively approximate the shape of each phase envelope. We do not claim that the true shape of the coda falloff is a Poisson distribution, only that the distribution is a reasonably good approximation to the shape of the coda envelopes. The fitting process used a combination of a nonlinear least squares procedure for the parameters, A and γ (Menke, 1984), and an exhaustive search for the best parameter, n. In other words, different A's and γ's were determined for n = 0,1,2,3..., with those values which minimized the error being chosen as the best fitting ones. The fitting program (WAKEFALLOFF) for the Wake data is listed in Appendix 2. The area, A, is un-normalized in that we have not tried to remove source/receiver effects. As an result, A becomes useless, except when comparing ratios between several phases in same band.

We also estimated the standard error for the parameters A and γ. The least-squares fitting subroutine estimates the variance (σ_d^2) of the bandlimited envelopes timeseries, d_i, as;

$$\sigma_d^2 = \Sigma (d - d^{pre})^2 / (N - 2)$$

where d is the observed data, d^{pre} the predicted data, and the summation takes place over the N samples in the portion of the band-limited envelope being fitted.

We then define the normal equation matrix:

$$[G^T G] = \begin{bmatrix} \Sigma\,(\partial P/\partial A)^2 & \Sigma\,(\partial P/\partial \gamma)\,(\partial P/\partial A) \\ \Sigma\,(\partial P/\partial \gamma)\,(\partial P/\partial A) & \Sigma\,(\partial P/\partial \gamma)^2 \end{bmatrix} = \begin{bmatrix} A & B \\ C & D \end{bmatrix}$$

The standard error in the area, A, and the falloff, γ, are given by the following equations,

$$\sigma_A = \sigma_d\,[\,A\,/(AD - BC)]^{1/2} \text{ and}$$

$$\sigma_\gamma = \sigma_d\,[\,D\,/(AD - BC)]^{1/2}$$

The time interval of the fit for each EQ was determined by handpicking the beginning and end of each phase. The same interval was then used to fit all spectral envelopes of that particular EQ. The phase interval had to be handpicked due to variations in apparent phase velocities (X/T) in the data. The handpicking subroutine also calculated the apparent velocity of each pick. Averaging (over 1.28 s intervals) of the data increases the error in calculated apparent velocities. This error decreases with increased travel time (T) and is therefore larger (0.2 - 0.3 s) for the P_o phases than for the S_o phases (0.1 - 0.2 s). In comparing theoretical fits to the data, one observes that most often the fit integral is equal to 90% or more of the data function integral (A). To be used in the final data processing, the fits had to include at least 90% of the data envelope and had to be satisfactory in the eye of the analyser; in other words, had to follow the eye-fitted falloff of the data reasonably well. We observed that signal-to-noise ratios varied greatly for different EQs and also between different instruments recording the same EQ. The best signal-to-noise ratios are in the two middle frequencies for all instruments, i.e. at 2.5 - 10 Hz for the Wake data and at 3 - 12.5 for the OSU OBS data. Noise in the highest frequencies is often generated by explosive devices, such as airguns and sparkers, operated in the vicinity of the instruments during their time of recording. High frequency noise is also generated by the biggest inhabitants of the recording area, the great whales. Often the "whale pulses" alternate between the two highest frequencies, 10 - 20 Hz and 20 - 40 Hz.

The noise in the two lowest frequency bands of the spectra is primarily caused by seafloor microseismic activity. Recent studies on seafloor microseismicity by Webb and Cox (1986) show close agreement between the theory of microseismic generation and observations of changing wind wave field, where changes in wind energy are directly related to the magnitude of the noise level in the lowest frequency bands. The horizontal component of the seafloor noise has significiantly higher noise level than the vertical component (Figures 1, 2, and 3). To compensate for this, the horizontal OBS geophone has a lower magnification than the vertical OBS geophone. Still, most of the recorded horizontal phases are clipped. The clipping is caused by a signal too strong for the instrument to record. Why the amplitude of the signal recorded on the horizontal component is many times greater than of the signal recorded on the vertical component is not clearly understood. It could be caused by coupling and orientation differences, with respect to the seafloor, between the two components.

TECTONIC SETTING OF THE PHILIPPINE SEA:

The Philippine Sea is one of several western Pacific marginal seas, some of the others being the Sea of Okhotsk, the Sea of Japan and the East China Sea (Figure 8). Marginal seas are isolated ocean basins found at the margins between continents and major ocean basins. Numerous seismic studies have revealed crustal and mantle velocities similar to that of the major oceans. Three hypotheses on the origin of marginal seas have been developed. One suggests that marginal basins represent older oceanic crust trapped as a result of the initiation of intraplate subduction or from the relative motion of trench boundaries (Uyeda and Ben-Avraham, 1972). Alternative models for explaining the structural history of marginal sea basins propose that they are formed by extension behind an island arc (Karig, 1971) or by retreating subduction where the Philippine plate's eastern trench system has progressively migrated over the subducting Pacific plate (Kanamori, 1977).

The Philippine plate is juxtaposed between the Asian continent and the NW Pacific (Figure 8). The plate is bordered by active trenches and is composed of several distinctly defined basins. The Philippine Basin (Figures 8 and 9) is considered to be the largest and deepest marginal basin in the world, and compared to ocean floor of similar age (early Eocene), it is anomalously deep by as much as 1000 m. This anomaly may in part be an isostatic response to crustal and/or upper mantle anomalies (Goodman, 1983). The NW - SE trending Central Basin ridge divides the Philippine Basin. The N - S trending Kyushu - Palau ridge separates the Philippine Basin from the Parece - Vela Basin. Goodman (1983), in a detailed refraction study on the crustal and upper mantle structure in the Philippine Basin, found the oceanic layer (layer 3) in the basin to be abnormally thin by about 2000 m, compared to average crustal thicknesses. The crust was shown to be thinner in the eastern part of the basin. Typical upper mantle velocities (at 4 km depth) were found to be around 8 km/s. Crustal thinning towards the east is believed to be consistent with the Kyushu - Palau ridge being a remnant transform fault connecting the Central Basin ridge with the subducted Kula - Pacific ridge, as proposed in the model of Uyeda and Ben-Avraham

(Goodman, 1983). The presence of symmetric magnetic anomalies having strikes roughly parallel to the Central Basin ridge (Louden, 1976) also supports this model, but N - NE spreading is not in agreement with the retreating subduction model.

Katsumata and Sykes (1969) studied the seismicity of the Philippine plate boundary. They found that the western boundaries of the plate from the Philippines to Japan and the Mariana trenches, are fairly well defined whereas the southern boundaries have shallower and more diffuse seismic zones. They did not detect any events from the Kyushu - Palau ridge, from the Central Basin ridge, or from the rest of the Philippine plate. Seismic cross-sections of the Izu, Bonin, and Mariana trenches have been used to delineate the dip, vertical extension, and subduction mechanism of the Pacific slab (Katsumata and Sykes, 1969; Samowitz and Forsyth, 1981; Roecker, 1985; Creager and Jordan, 1986). According to the Plate-Tectonic map of the Circum-Pacific Region (1981), maximum EQ focal depths are 200 - 300 km along the eastern border of the Philippine plate (Molocca Sea - Phillippine trench - Taiwan - Ryukyu trenches). On the western border, focal depths greater than 600 km are observed along the Izu, Bonin, and Mariana trenches south to about 15°N. South of 15°N, the seismic zone extends only to 200 km depth and becomes progressively shallower towards the Yap trench. Seismicity in the Yap and Palau trenches is low, and focal depths are less than 70 km.

PHILIPPINE SEA P_0 AND S_0 FALLOFF MEASUREMENTS:

Figure 9 shows the location of EQs recorded by the Philippine array during the refraction survey in 1981. The EQs and their measured falloff rates are listed in Appendix 3A. The dataset consists of 21 EQs which all occur in the shallow seismic regions of the Philippine plate (< 200 km depth). One EQ (35) has an intraplate epicenter just south of the Ryukyu trench. The epicentral distance of these EQs ranges from 5 to 18 degrees. Plots of apparent P_0 and S_0 velocities (X/T) versus distance for the vertical (Figure 19) and horizontal (Figure 20) components indicate average P_0 and S_0 velocities of 8.06 ± 0.04 km/s and 4.69 ± 0.02 km/s, respectively. The P_0 apparent velocities (APVELs) range from 7.6 to 8.6 km/s, whereas the S_0 APVELs have a smaller range from 4.4 to 5.0 km/s. This smaller range is most likely due to increasing accuracy in APVEL calculations with increasing timespan on the seismogram. Because of higher noise amplitude on the horizontal component, fewer APVEL measurements could be made on that component, but they show a similar velocity range. Frequently, the vertical component of a given EQ has a slightly higher APVEL than the horizontal component (see Appendix 3A). Plotting APVEL versus depth (Figure 21) shows a cluster of EQs at 33 km depth having a total P_0 velocity span from 7.6 to 8.6 km/s. As hypocenter location is often hindered by unsufficient station coverage in the epicentral area of an EQ, a normal depth of 33 km is chosen for the EQ location. The Phillippine EQs that have a normal depth of 33 km have greater hypocentral errors, resulting in greater inaccuracies in their APVEL determinations. EQs 35 and 152, which have an epicentral distance of less than 9 degrees, have higher APVELs, up to 8.6 km/s, whereas EQs 194, 338, 428, 232, 166, and 239 have lower than average APVEL on one or more stations. Only EQ 35 has a normalized depth at 33 km. Apart from these EQs, APVEL measurements give fairly constant P_0 and S_0 phase velocities both with range and depth to 160 km for the Philippine plate.

Falloff values for the Philippine data set showed considerable variations for individual EQs both within the same band and between different frequency bands. Average falloff values on the vertical component for the Philippine Sea show little

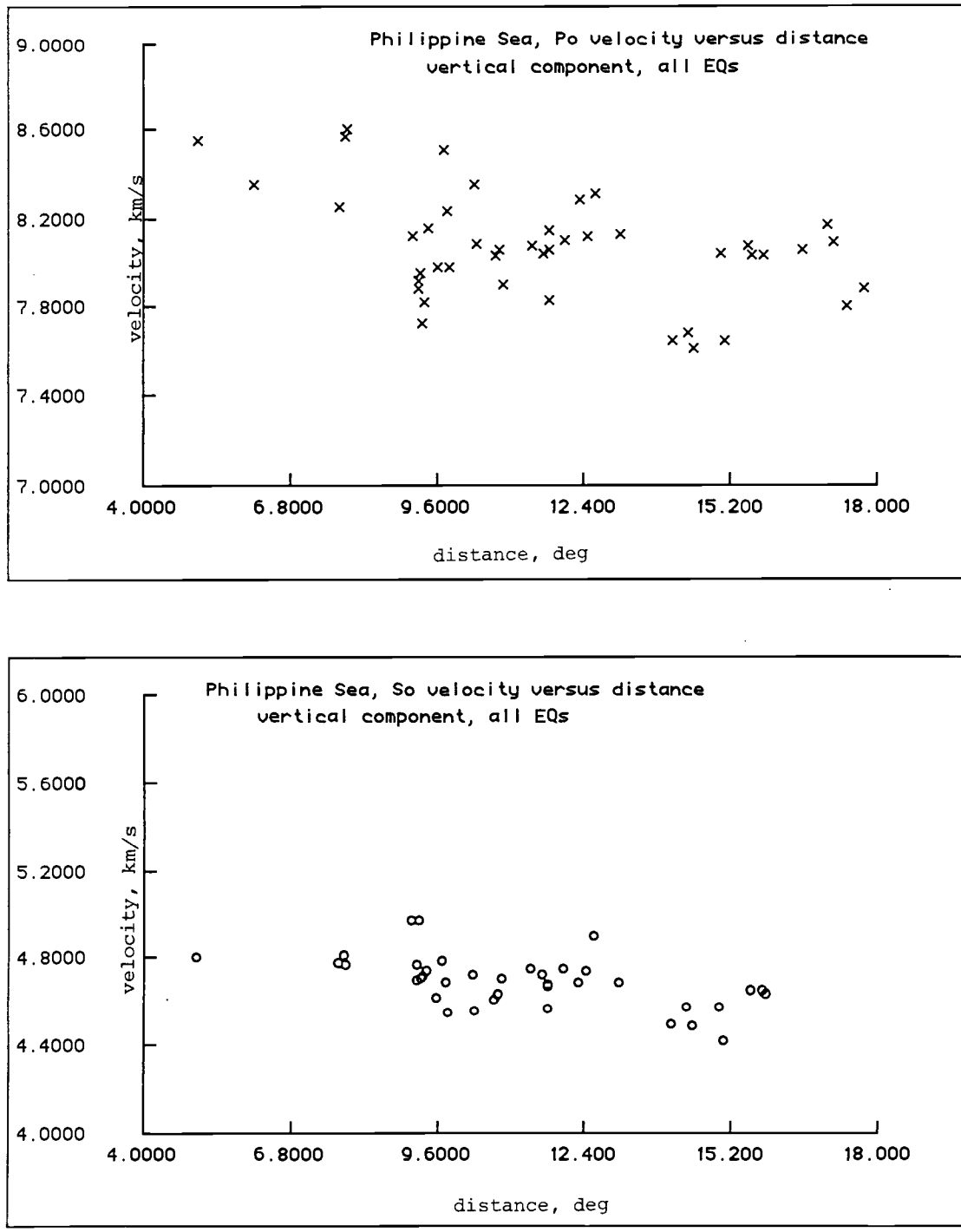

Figure 19. Apparent velocity of P_o and S_o onset versus distance for the vertical component of the Philippine Sea data set. Top) P_o phase. Bottom) S_o phase.

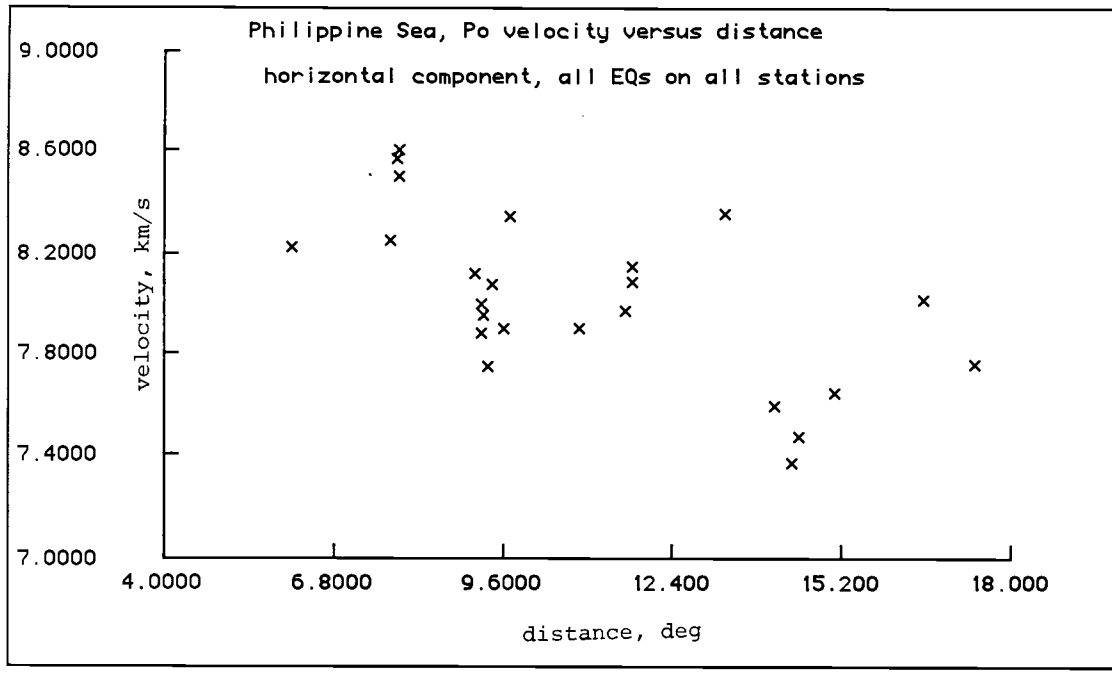

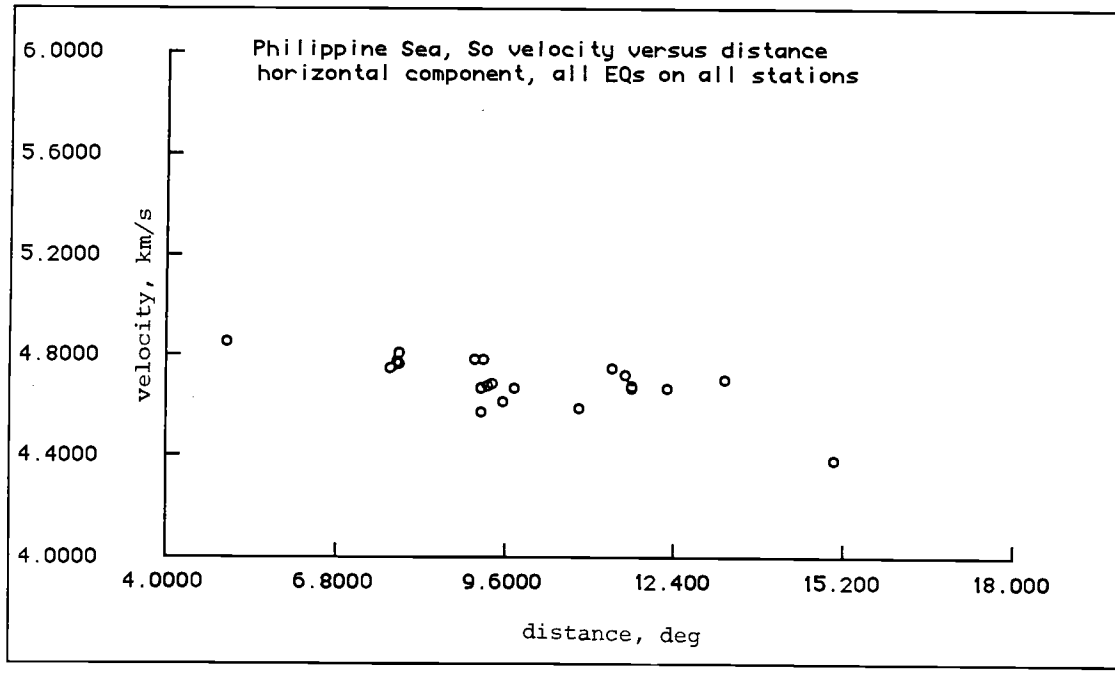

Figure 20. Apparent velocity of P_o and S_o onset versus distance for the horizontal component of the Philippine Sea data set. Top) P_o phase. Bottom) S_o phase.

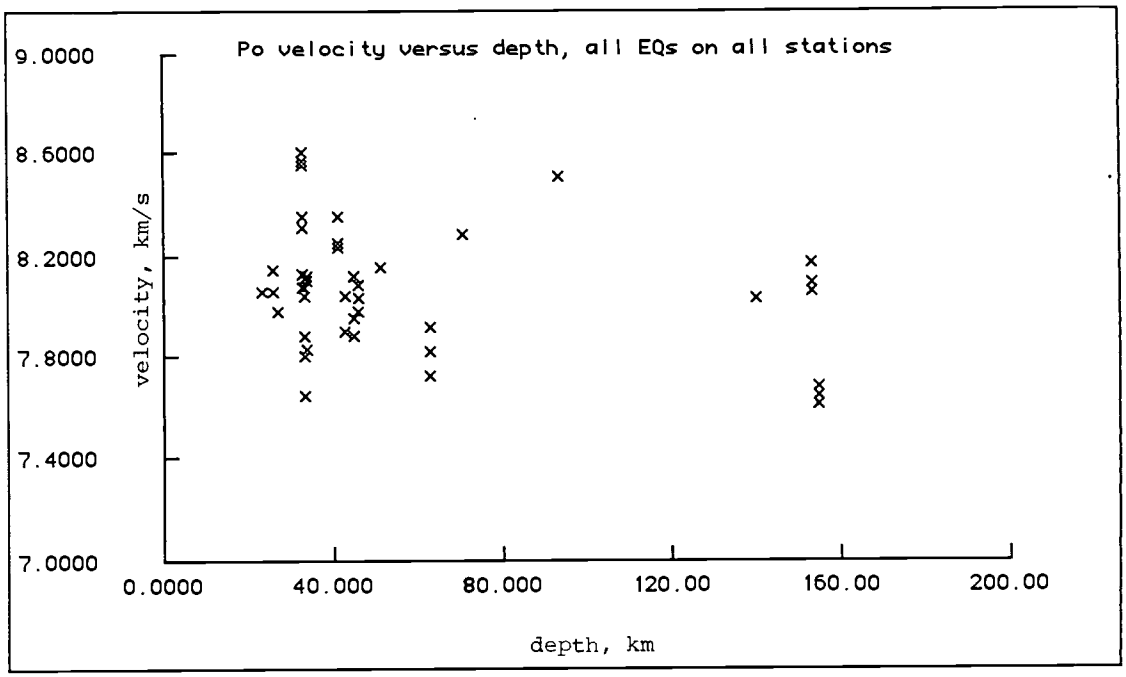

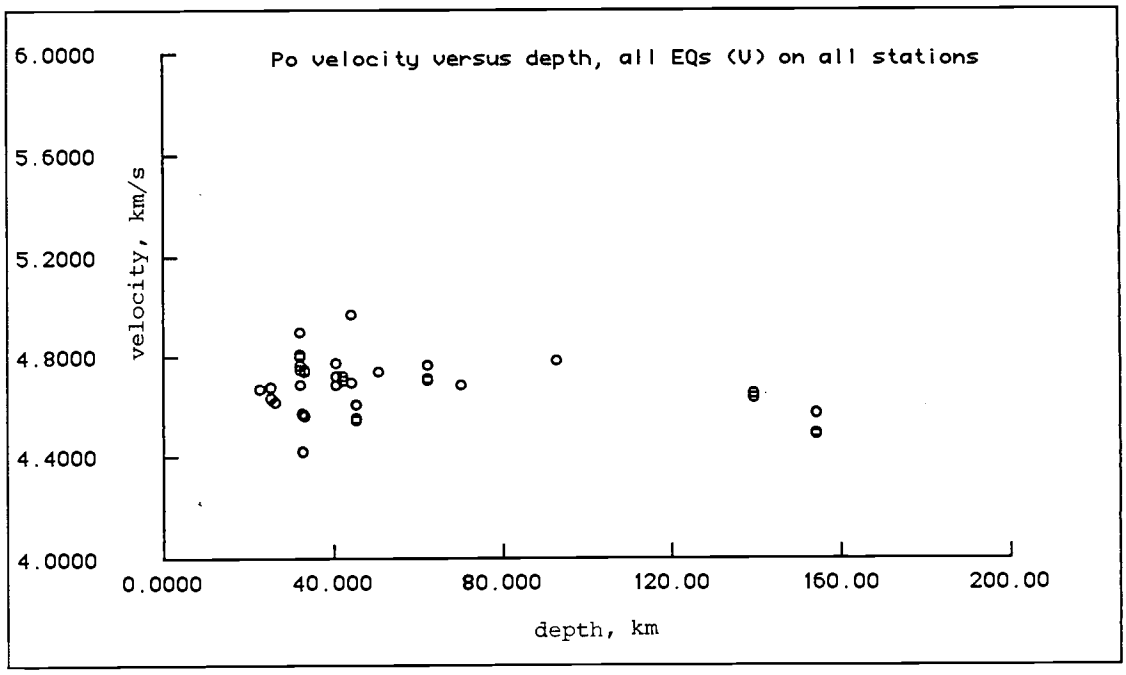

Figure 21. Apparent velocity of P_O and S_O onset versus earthquake depth for the Philippine Sea data set. Top) P_O. Bottom) S_O.

variation between different frequency bands (Figure 22). It is much smaller than the falloff variation within the same band. Although the averaging smears out individual characteristics, we see that the average falloffs are significiantly lower in the two lowest frequency bands. The average falloff for the S_0 phase is considerably higher than for the P_0 phase especially in the lowest two bands. Comparing average P_0 and S_0 falloffs indicates that the S_0 decay rate is twice the rate of the P_0 decay. This effect could also be due to the fact that many EQs completely lack low frequency S_0 energy. An overall effect is, that whereas P_0 falloff values seem to decrease with increasing frequency, S_0 falloffs remain fairly constant. In the bandpassed data, S_0 phases have more peaked coda shape but P_0 phases have more gradually shaped coda in the highest bands.

A typical P, P_0, and S_0 falloff curve with standard error bars is shown in Figure 23. The P_0 falloff (shown for EQ 297) is low in the lowest two bands, highest in the middle bands, and slowly decreases in the two highest bands. As mentioned earlier the individual EQ falloff pattern shows greater deviations between frequency bands than is seen in the average pattern. The individual pattern is governed by regional effects at the EQ source and along each raypath, as different frequencies are scattered and attenuated by different structures. The effect of depth can be seen by comparing two EQs (277 and 279) located in the same area at different depths. Band-passed and squared seismograms and their theoretical fits are shown in Figure 24. EQ 277 has a focal depth of 27 km and a smaller-than-average APVEL (7.9 - 8.0 km/s (P_0) and 4.6 km/s (S_0)), whereas EQ 279 has a focal depth of 93 km and higher-than-average APVEL (8.3 - 8.5 km/s and 4.8 km/s). The P_0/S_0 amplitude ratio is much higher for 279, as hardly any S_0 phase is associated with the deeper EQ, while the shallower EQ has some S_0 energy in all bands. Comparing the same bands shows that both EQs have similar buildup rates, but the lower frequency bands have a more gradual P_0 phase buildup than the higher bands. As a result, the maximum amplitude of the P_0 phase (reflecting the group velocity) shows a dispersion effect where the group velocity increases with increasing frequency. Most of the Philippine Sea EQs exhibit this dispersion effect. Figure 25 shows a plot of absolute falloff values versus frequency for the vertical P_0 and S_0 phases of EQs 277 and 279. The

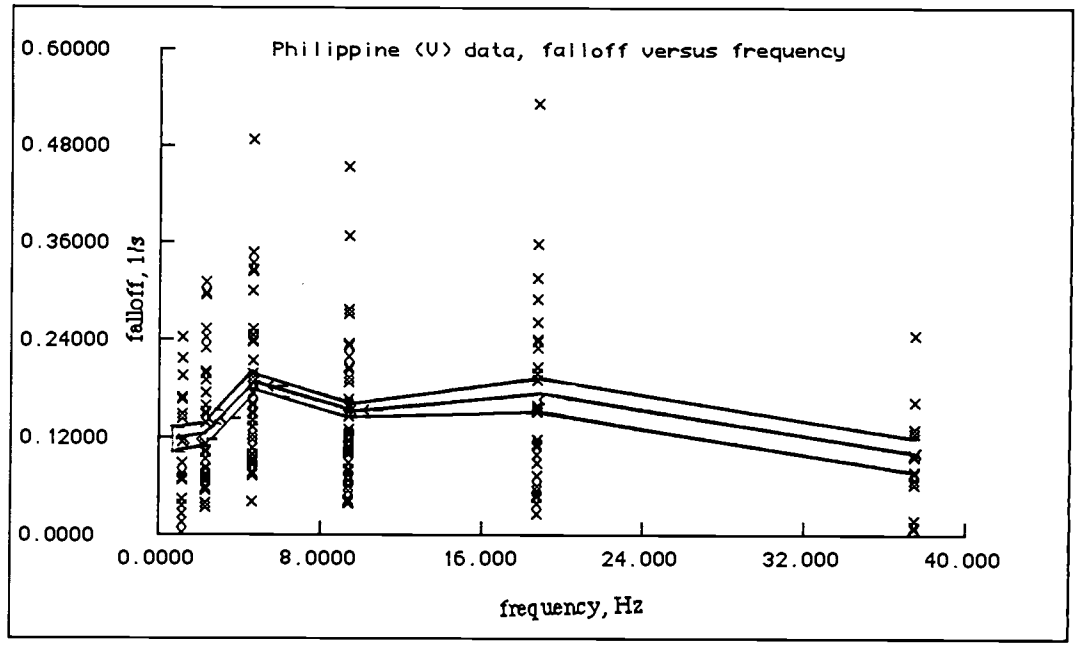

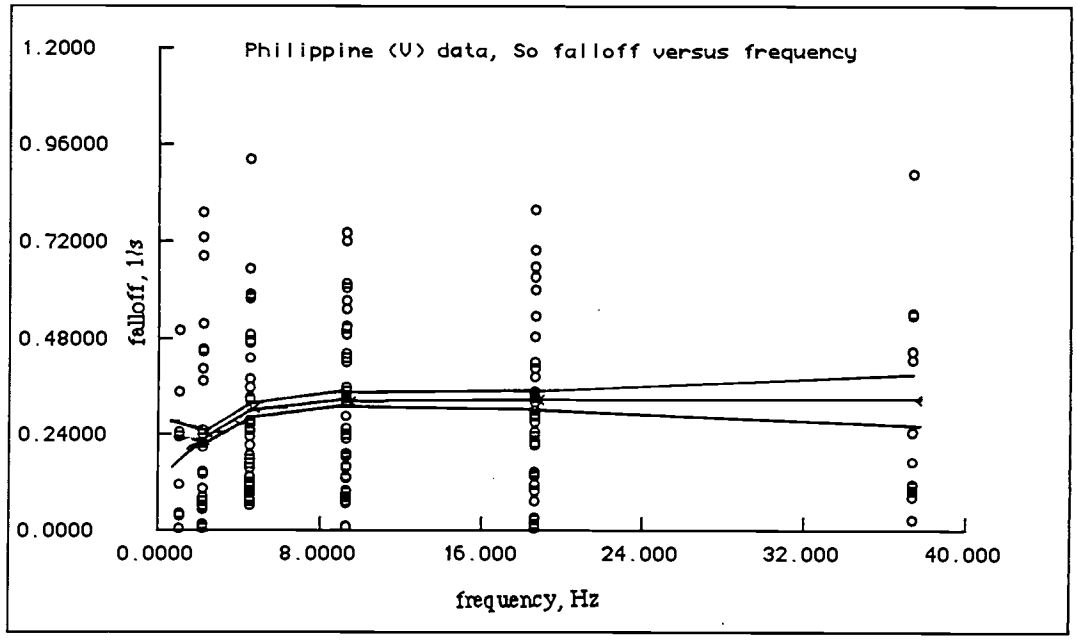

Figure 22. Falloff rate of the P_0 and S_0 bandpasses and rectified seismograms as a function of frequency. Top) P_0 measurements (crosses), mean (middle solid line) and 1σ standard errors of the mean (outer lines). Bottom) S_0 measurements (crosses), mean (middle solid line), and 1σ standard errors of the mean (outer lines). Note the large scatter in values. Nevertheless a trend is detectable, with the falloff of the lowest frequencies being the lowest.

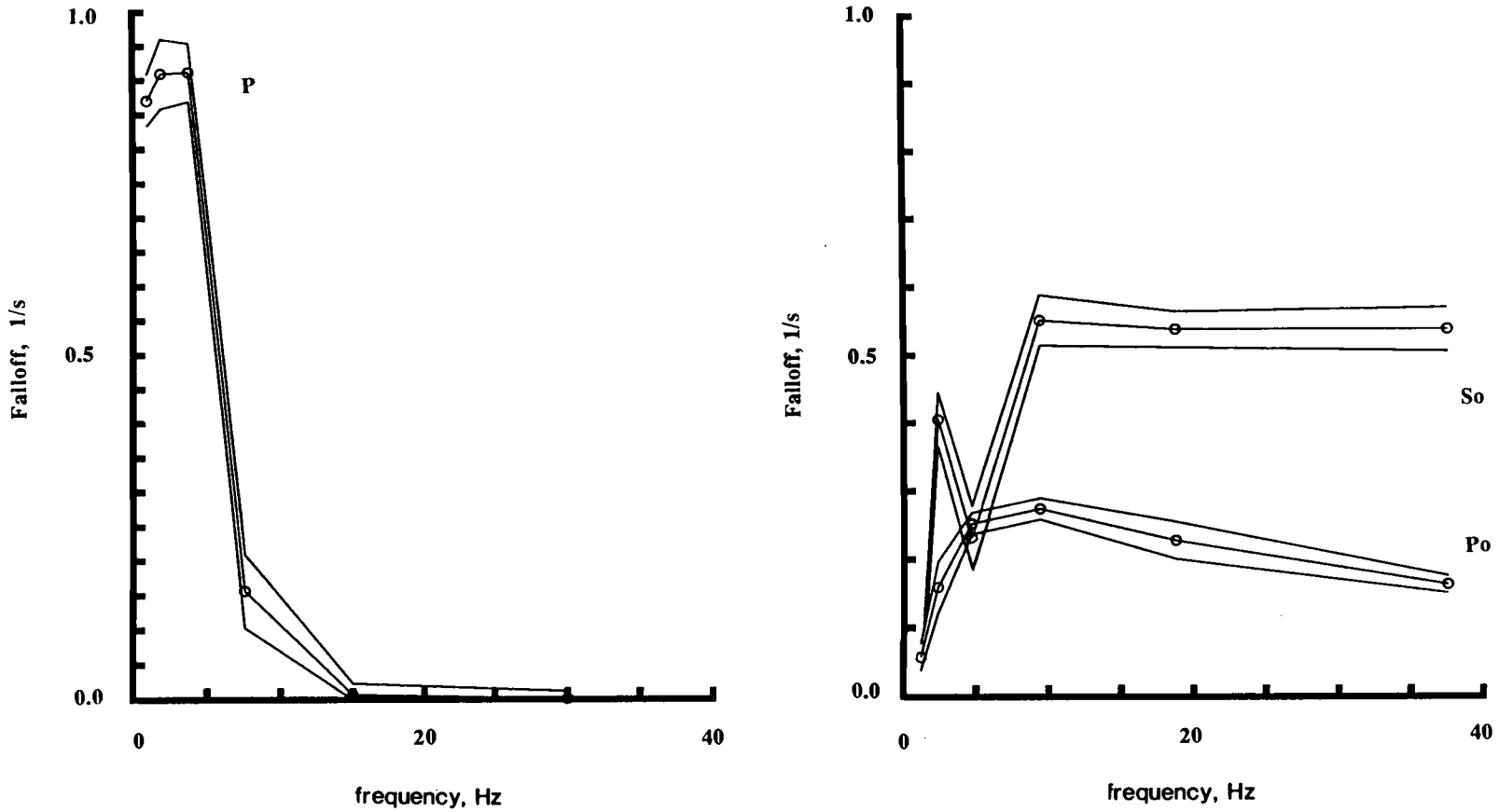

Figure 23. Falloff rate as a function of frequency for typical P, P_o, and S_o waves.

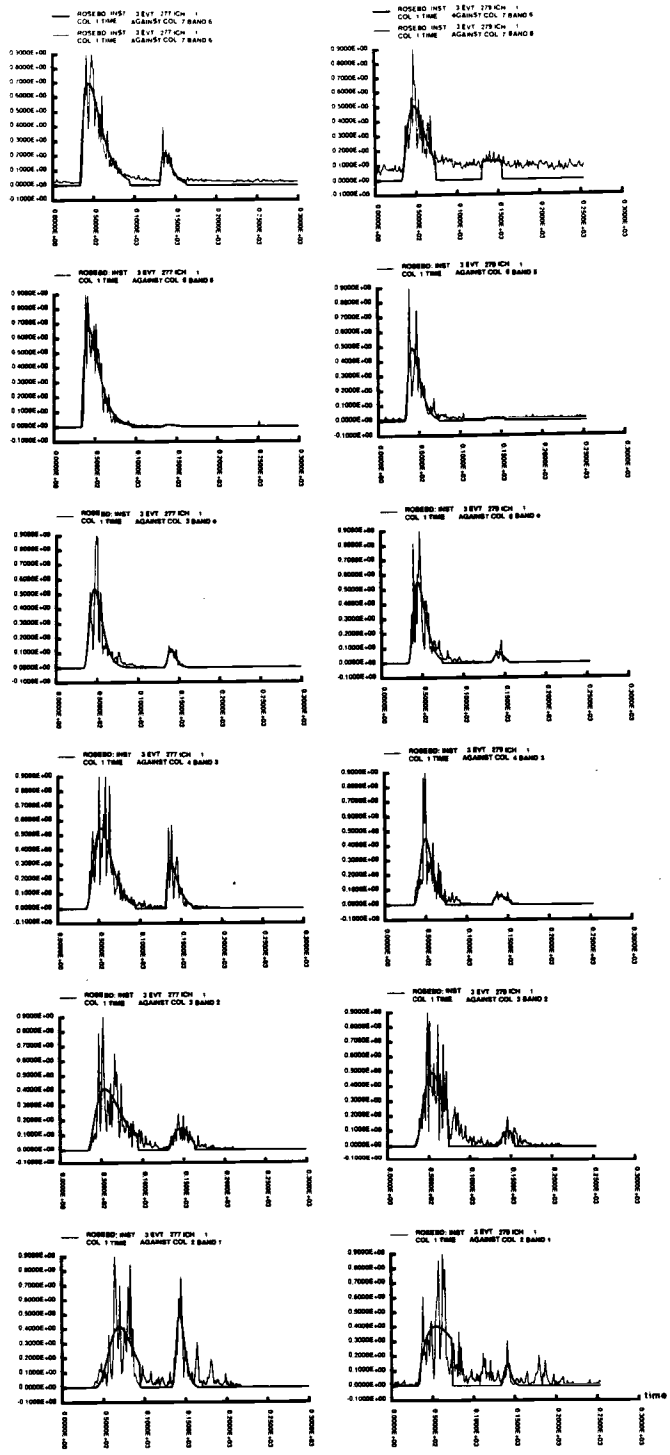

Figure 24. Bandpassed and rectified seismograms for two earthquakes with similar locations but different depths. The figure has the same format as Figure 15. Left) EQ 277 with a depth of 27 km. Right) EQ 279 with a depth of 93 km. Note that the S_o phase is more prominent in the shallower earthquake.

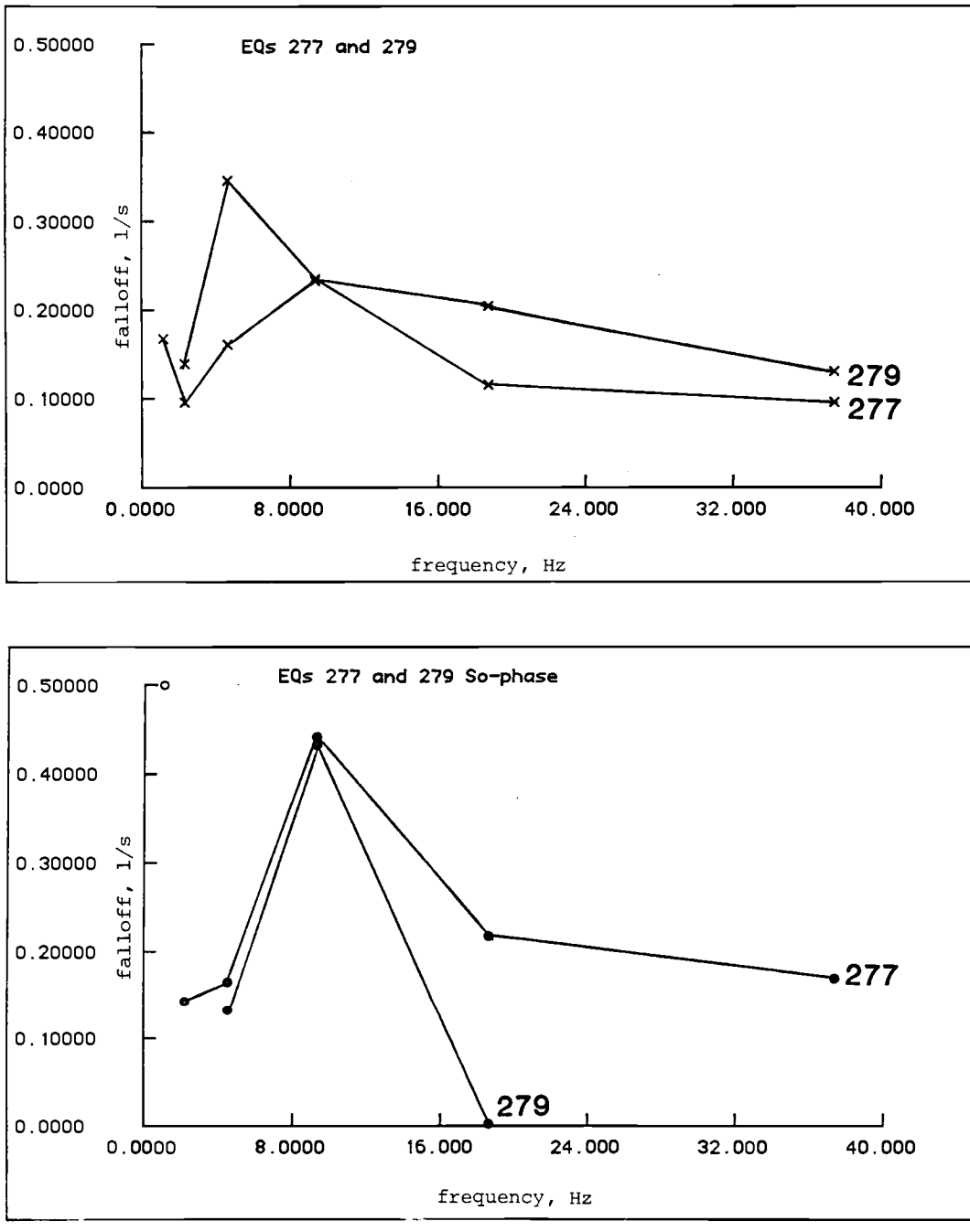

Figure 25. Falloff as a function of frequency for the two earthquakes in Figure 24. Top) P_o phase. Bottom) S_o phase.

P_0 falloff values are similar for both EQs except in band 3 (2.5 - 5Hz) where the shallower EQ has significiantly more energy and lower falloff. Comparing the S_0 falloffs, the shallower EQ has some energy in the lowest band (0.6 - 1.2Hz) and in the two highest bands (>10Hz), whereas the deeper EQ has no detectable S_0 energy in these bands.

Both the horizontal (H) and hydrophone (HY) components have considerably lower signal-to-noise ratios than the vertical (V). Their signal-to-noise ratios are best in the two middle frequency bands. Where measureable, V, H and HY falloff rates have similar trends.

South Mindanao - Molucca Sea region:

The Molucca Sea is situated at the junction of the Eurasian, Indian - Australian, Pacific, and Philippine plates. Figure 26 (adapted from Hamilton, 1979) shows a map of the tectonic features of this area along with the seismic profile of Hatherton and Dickinson (1969). Tectonic features in the area strike roughly N - S and consist of alternating ridges and troughs (Figures 9 and 26). A seismic profile (Figure 26) compiled by Hatherton and Dickinson (1969) revealed two oppositely dipping seismic zones, interpreted to represent the subduction of two slabs, one towards NW and one towards SE (Figure 27). The slabs subduct beneath the Sangihe (W) and Halmahera (E) volcanic arcs (ridges) and connect in the Molucca Sea. A tectonic model (Figure 27) by Silver and Moore (1978) shows the Molucca Sea to be a collision complex between the two slabs. The convexly-facing Sangihe and Halmahera volcanic arcs are separated by about 250 km at their closest points. Recent focal solution studies from EQs in the upper part of subducting slabs show normal faulting, indicating the existence of extensional forces in the upper part of the slab. These focal solutions and the fact that the Molucca slabs are subducting in opposite directions suggests that the overlying region must be extensional rather than collisional. Figure 28 presents a tectonic model of the Molluca Sea which incorporates extension rather than collision. The following facts support this model:

1) The south end of the Philippine slab subducting underneath the eastern border of

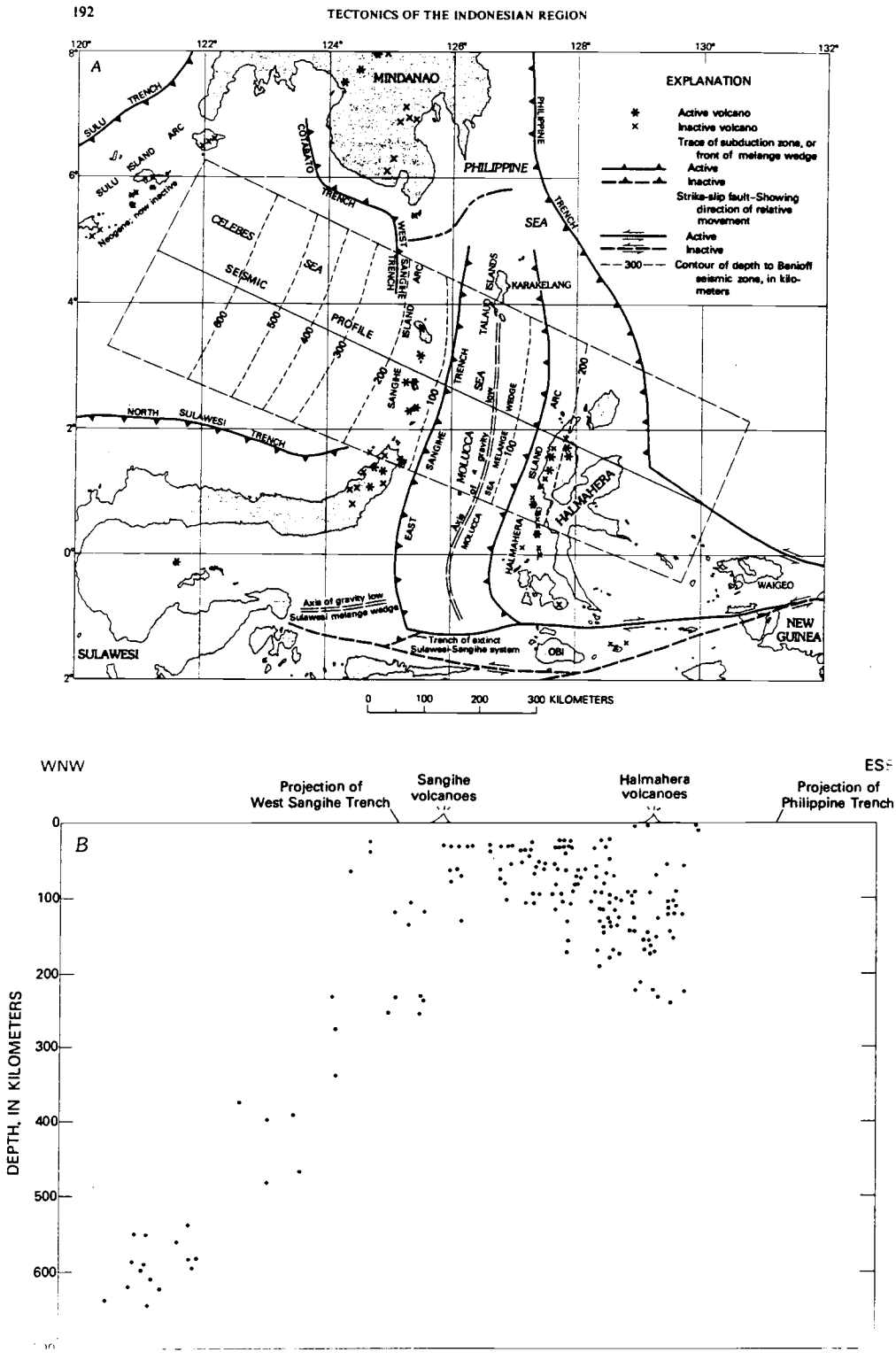

Figure 26. Top) Tectonic map of the Molucca Sea region, adapted from Hamilton (1979). Bottom) The seismic profile by Hatherton and Dickinson (1969).

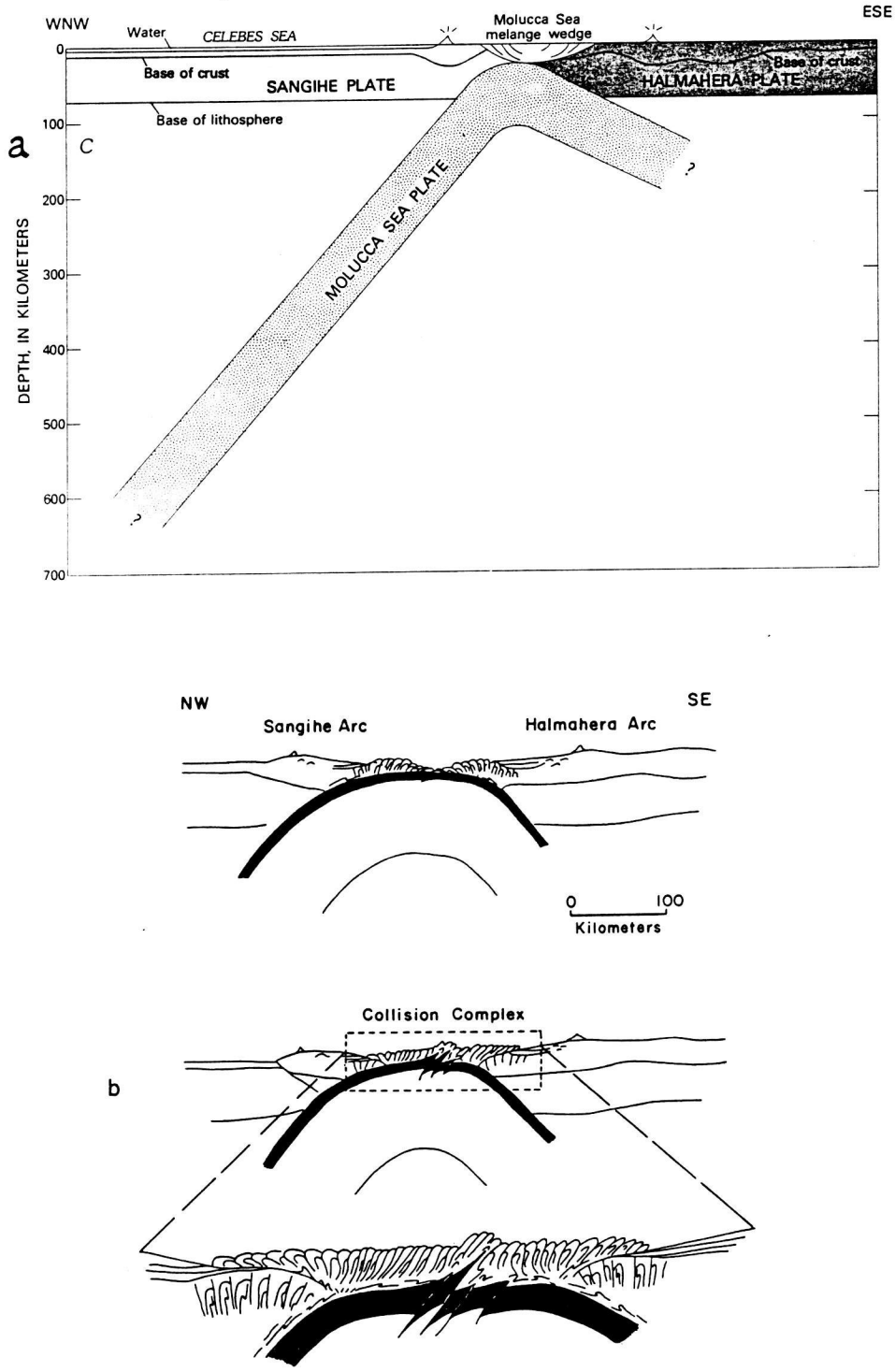

Figure 27. Tectonic models of the Molucca Sea region. Top) Hatherton and Dickinson (1969) interpretation of the seismic data. Bottom) Model of Silver and Moore (1978).

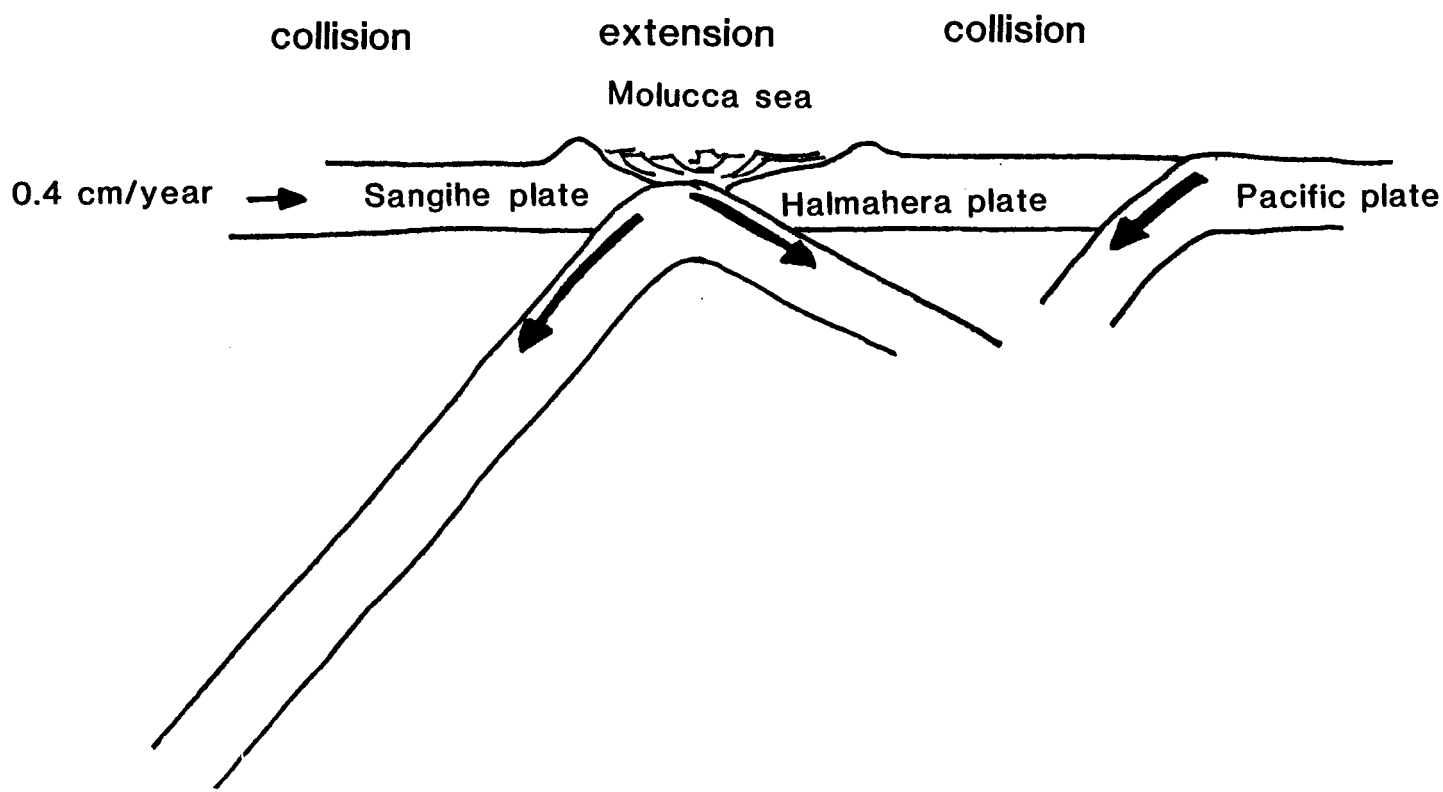

Figure 28. The tectonic model of the Molucca Sea region proposed in this study.

the Halmahera plate is not very active. This can be interpreted to indicate that the thrust (convergence) from the Pacific plate in that area is small.

2) The absolute eastward motion of the Eurasian plate in the Celebes Sea is very small, 0.4 cm/year, also indicating a slow convergance from the Eurasian plate.

3) No recent island arc traces are obvious on each concave side of the Sangihe and Halmahera island arcs indicating that if those island arcs are colliding, their rate of converging is very slow.

4) The Molucca Sea is underlain by an extremely large gravity low indicating missing crustal volumes resulting from extension. This is incompatible with compression which would increase crustal volume in the area. The tectonic model in Figure 28 shows the Molucca Sea as an extensional area of a unique kind, a kind of a passive rift valley.

Six EQs were recorded with epicenters in the South Mindanao - Molucca Sea region (Figure 9, EQs 126, 193, 194, 243, 338, and 428; at depths 230, 140, 155, 153, 34, and 34 km, respectively). Figures 29 and 30 show bandpassed and squared seismograms along with theoretical fits for those EQs recorded on stations EE (126, 193, 194, and 243) and DDD (338 and 428). All these EQs have either abnormally small or no S_o phases, making measured S_o falloff values inaccurate. Two of these EQs (126, depth 230 km, and 193, depth 140 km) have epicenters in the Sangihe arc and two (194, depth 155 km, and 243, depth 153 km) have epicenters in the Halmahera arc. Unfortunately, event 126 occurred during a period of high microseismic activity so no reliable falloff measurements could be made on that EQ. EQ 193 has a partly split P_o phase. This effect is not visible on the other EQs in the Molucca Sea. All EQs in this area show the same dispersion effect as the Mariana EQs where the higher frequencies peak early while the lower frequencies are more spread out. This dispersion effect occurs on all three components of an EQ (Figure 31) and is most likely caused by different frequencies having a different modes of propagation in the lithosphere. The Molucca sea EQs have P_o APVELs ranging from 7.6 to 8.2 km/s. APVELs for EQs 338, 194, and 428 are markedly lower than those of 193 and 243 (Figure 19, see Appendix 3). The lower velocities of EQs 338 and 428 can possibly be explained by their shallow origin, but this is not the case for EQ 194,

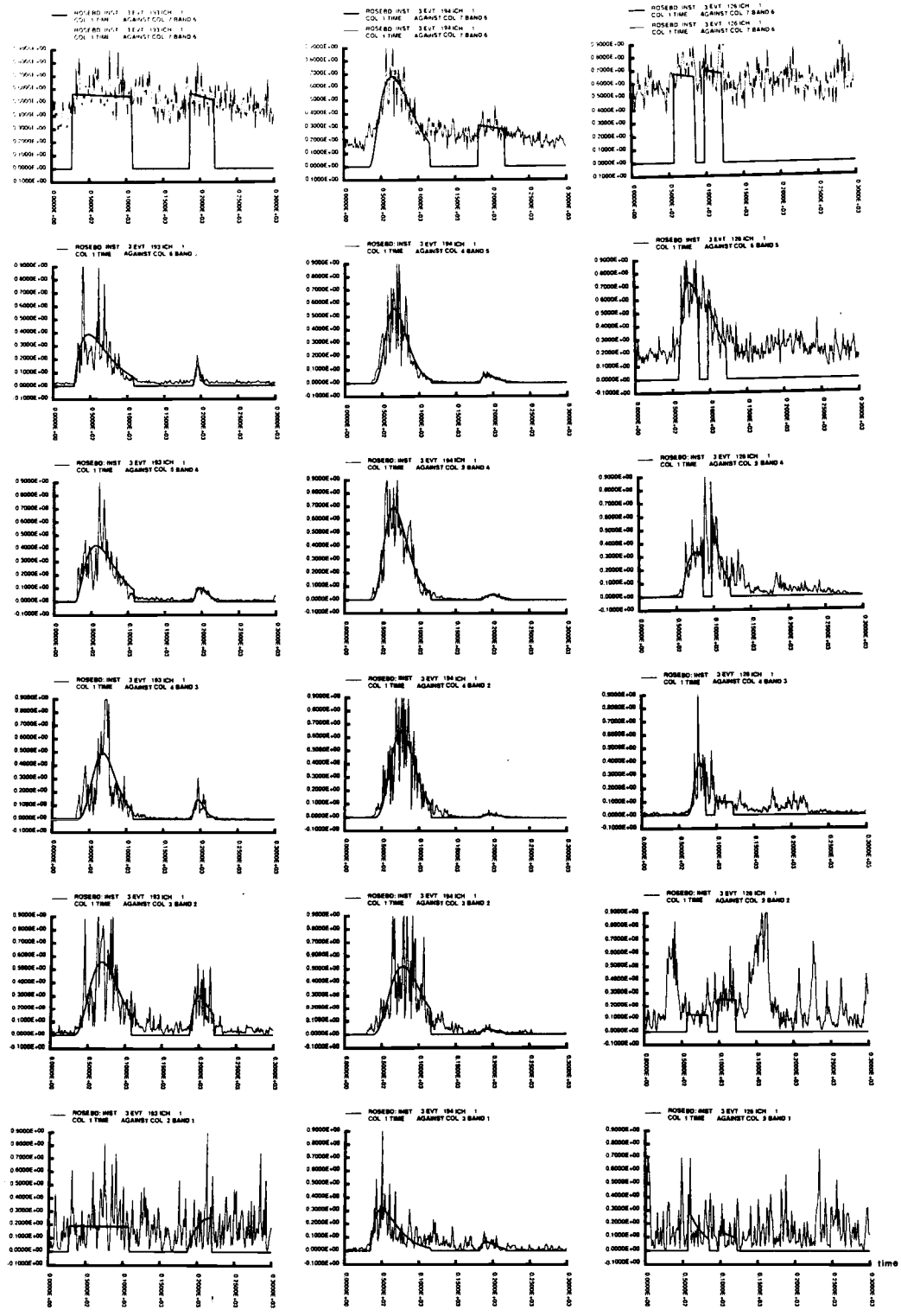

Figure 29. Bandpassed and rectified seismograms for three Molucca Sea earthquakes. The figure has the same format as Figure 15. Left) EQ 193. Middle) EQ 194. Right) EQ 126.

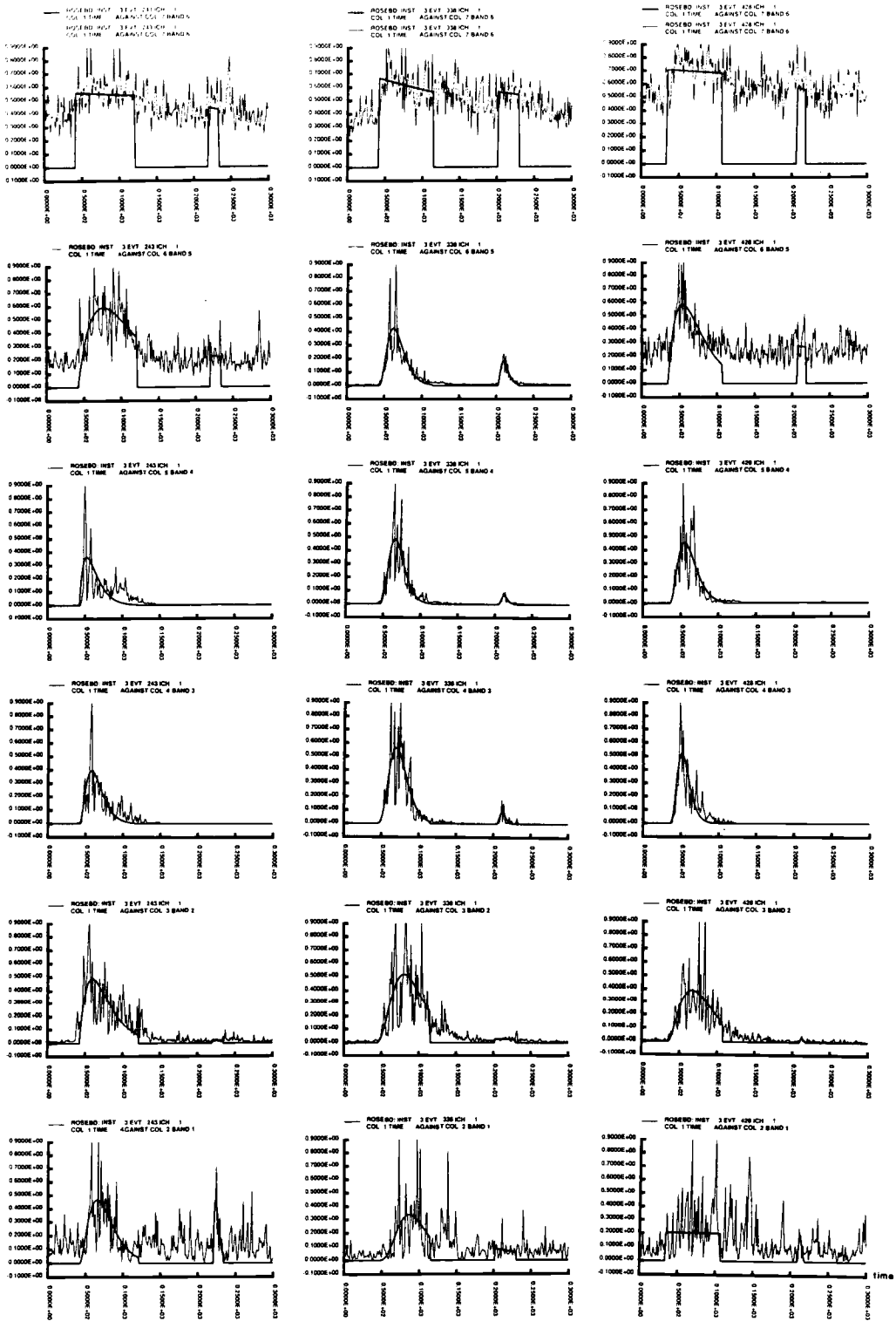

Figure 30. Bandpassed and rectified seismograms for three Molucca Sea earthquakes. The figure has the same format as Figure 15. Left) EQ 243. Middle) EQ 338. Right) EQ 428.

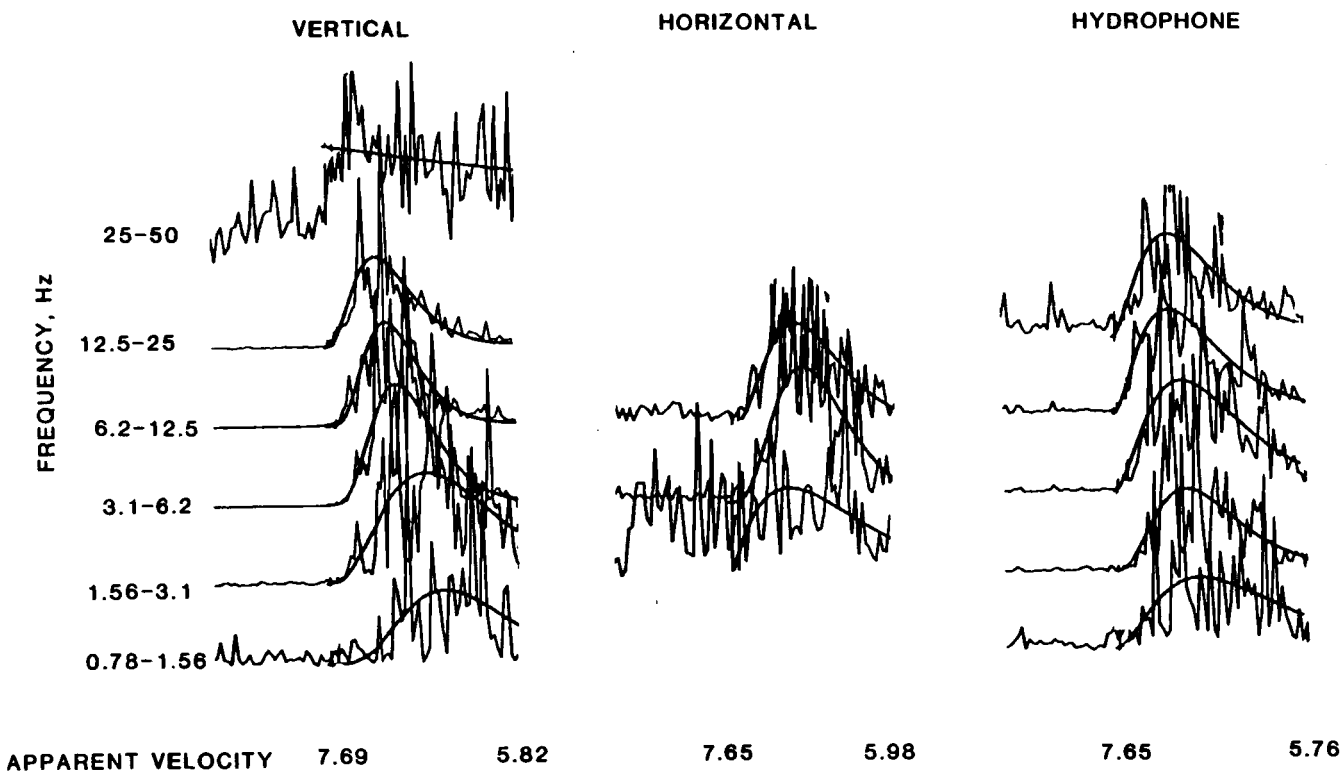

Figure 31. Example of dispersion in P_o coda from Philippine Sea EQs (here shown for EQ 338). Note that the coda maximum occurs later in the lower frequencies of the bandpassed and rectified seismograms. This effect is visible in all three components, vertical (left), horizontal (middle), and hydrophone (right).

which has anomalously low P_0 velocity both with respect to distance and depth. Figure 32 shows recorded P_0 falloffs of the Molucca Sea EQs (EQs 193, 194, and 243) on instruments 3 (station EE), 12 (BB), and 14 (AA). Each EQ exhibits the same falloff pattern on all three stations, which indicates that their coda generation is not dominated by near-receiver structures, or that the structure of the crust-upper-mantle in the receiver region is fairly homogeneous. Comparing the falloff pattern for individual EQs, EQ 194 has higher falloff rates (decays more rapidly) in bands 4 and 5. Raypaths for EQs 193, 243, and 428 cross the complicated tectonic structure of the Molucca Sea. The lack of S_0 energy for all these EQs may be an indication that all their raypaths have crossed regions of high S_0 absorption, but the data are not sufficient to determine where those regions are. Also, the lack of S_0 energy could be an source excitation effect, that is, no shear phases where generated at the source.

Philippine, Taiwan and Ryukyu trenches:

Squared and bandpassed seismograms and their fits for EQs from the Philippine trench, N - Luzon, Taiwan, and Ryukyu trench are shown in Figures 33 - 36. With respect to P_0/S_0 amplitude ratios, the Philippine data set can be divided into two groups. The first group includes all EQs from the Marianas, Molucca Sea, and Philippines (Figures 24, 29,30, 33, and 34), and the second group includes the Taiwan - Ryukyu EQs (Figures 34 - 36). The Taiwan - Ryukyu EQs (249, 293, 152, 282, 266, 239, 278, and 334) all have clear S_0 phases making their P_0/S_0 amplitude ratios much lower than those for all recorded EQs from the Philippine and Mariana trenches as well as those from the Molucca Sea. This is reflected in the falloff rates. All Philippine Sea P_0 falloff values are similar but S_0 falloff values are higher in the Taiwan to Ryukyu regions (Figures 37) than in the Mariana trench - Molucca Sea - Philippine trench EQs (Figure 38). Although the southwestern part of the Okinawa trough is presently undergoing a crustal extension with normal faulting, rifting, and magmatic intrusions (Lee et al., 1980), clear S_0 phases were observed for all EQs originating in that area.

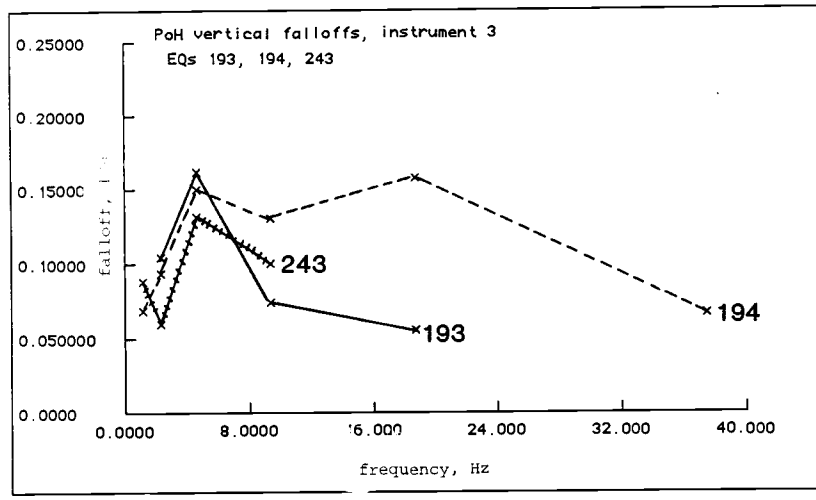

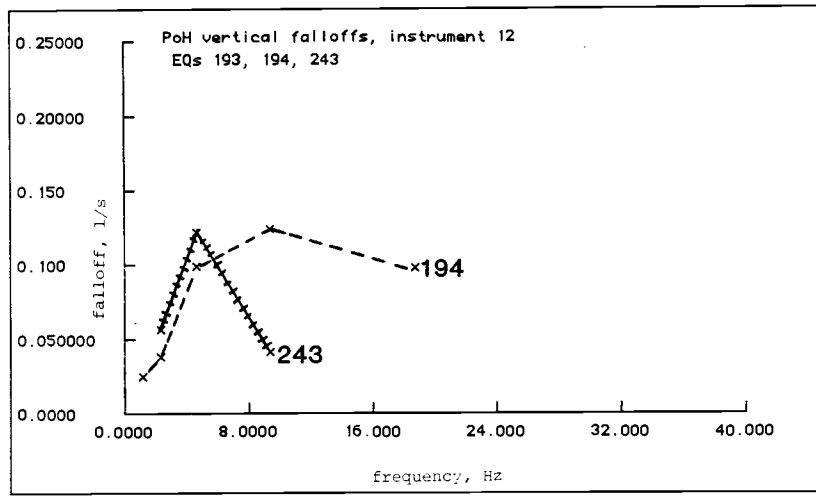

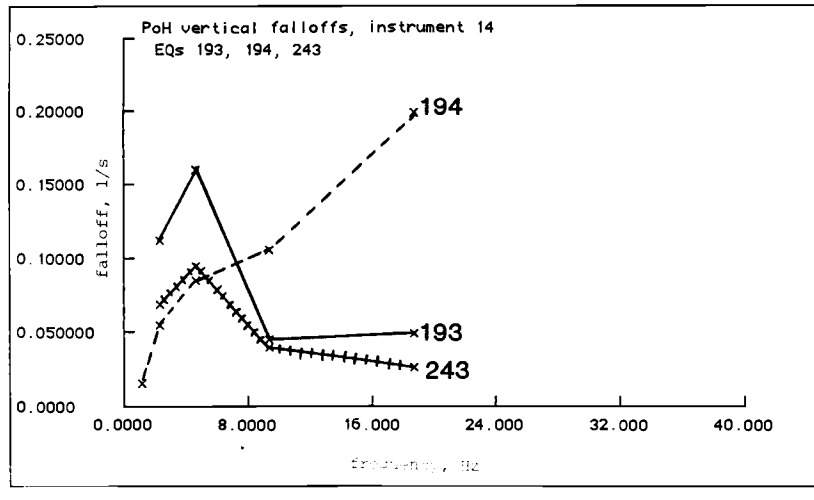

Figure 32. Falloff as a function of frequency for the three Molucca Sea earthquakes shown in Figures 29 and 30. Top) P_{oH} falloff on station EE, EQs 193, 194, and 243. Middle) P_{oH} falloff on station BB, EQs 194, and 243. Bottom) P_{oH} falloff on station AA, EQs 193, 194, and 243.

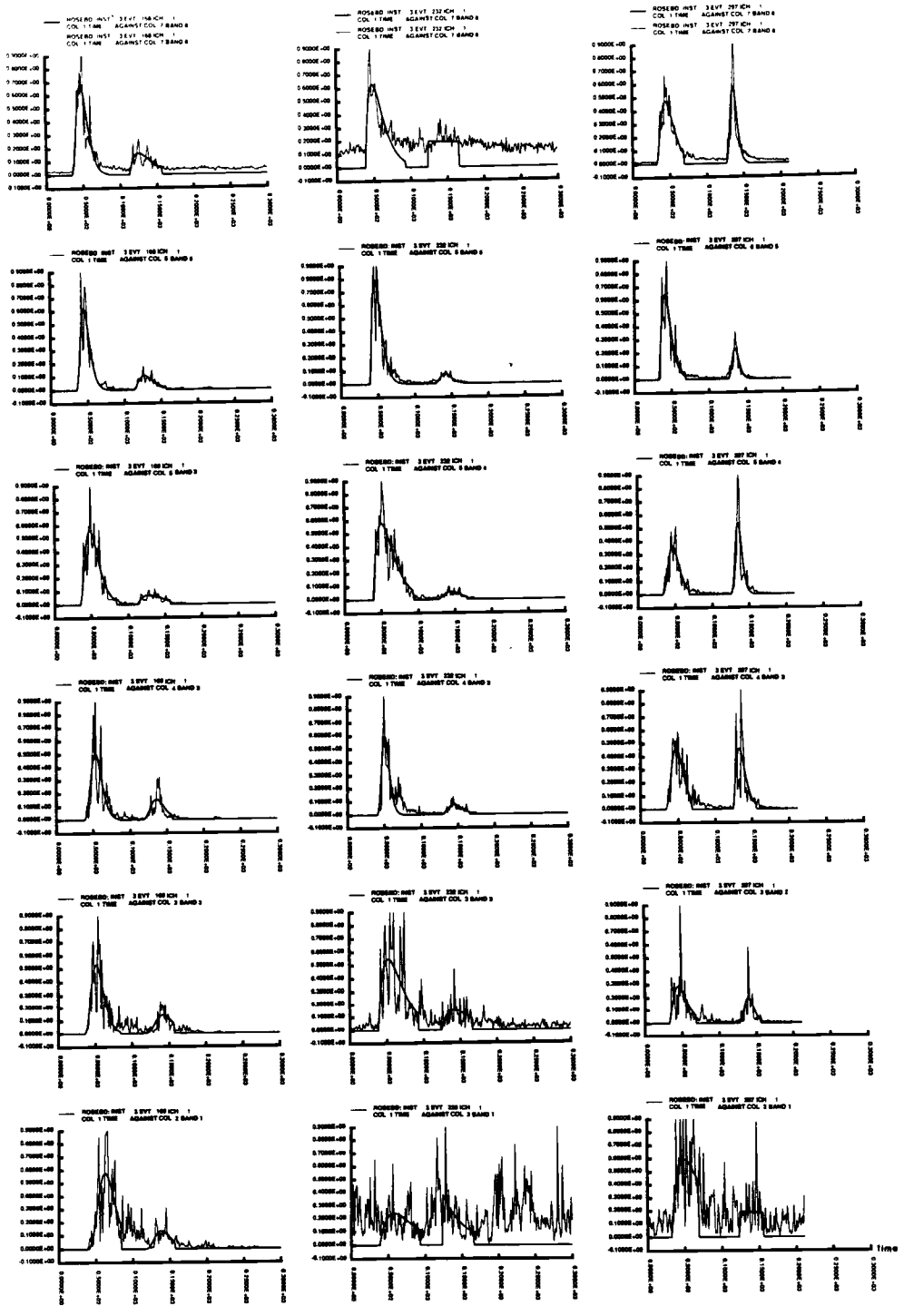

Figure 33. Bandpassed and rectified seismograms for the three Philippine trench earthquakes. The figure has the same format as Figure 15. Left) EQ 168. Middle) EQ 232. Right) EQ 297.

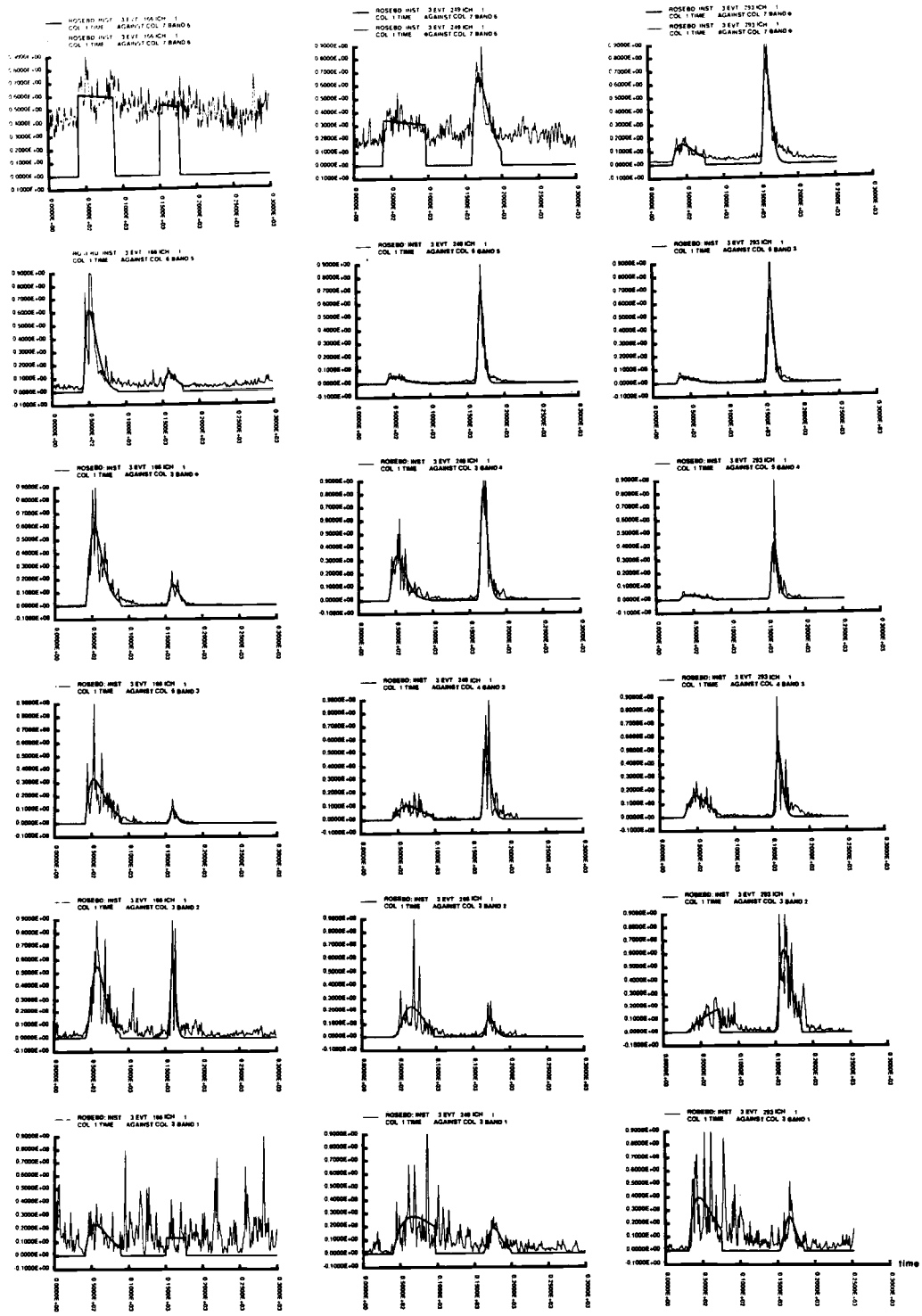

Figure 34. Bandpassed and rectified seismograms for the three Luzon-Taiwan earthquakes. The figure has the same format as Figure 15. Left) EQ 166. Middle) EQ 249. Right) EQ 293.

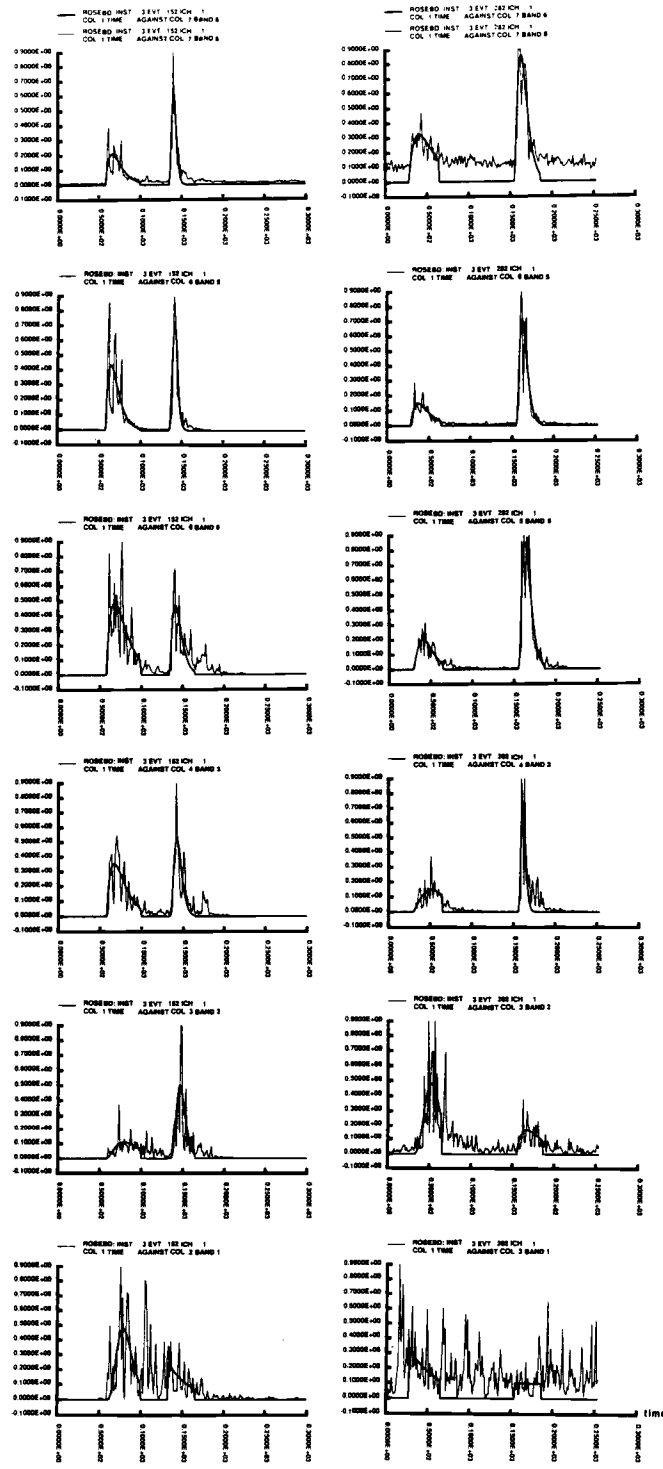

Figure 35. Bandpassed and rectified seismograms for two Taiwan - Okinawa trough earthquakes. The figure has the same format as Figure 15. Left) EQ 152. Right) EQ 282.

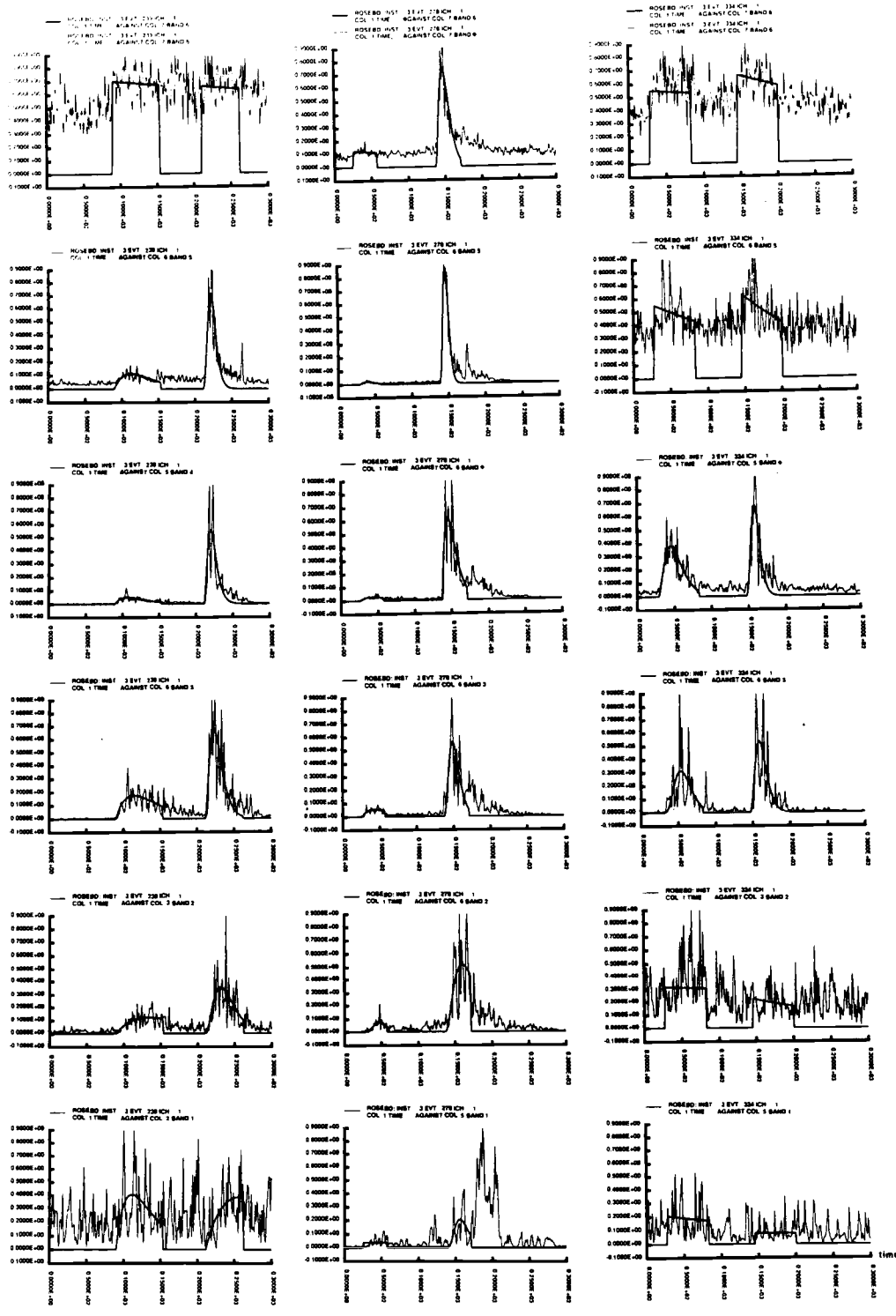

Figure 36. Bandpassed and rectified seismograms for three northeast Ryukyu trench earthquakes. The figure has the same format as Figure 15. Left) EQ 239. Middle) EQ 278. Right) EQ 334.

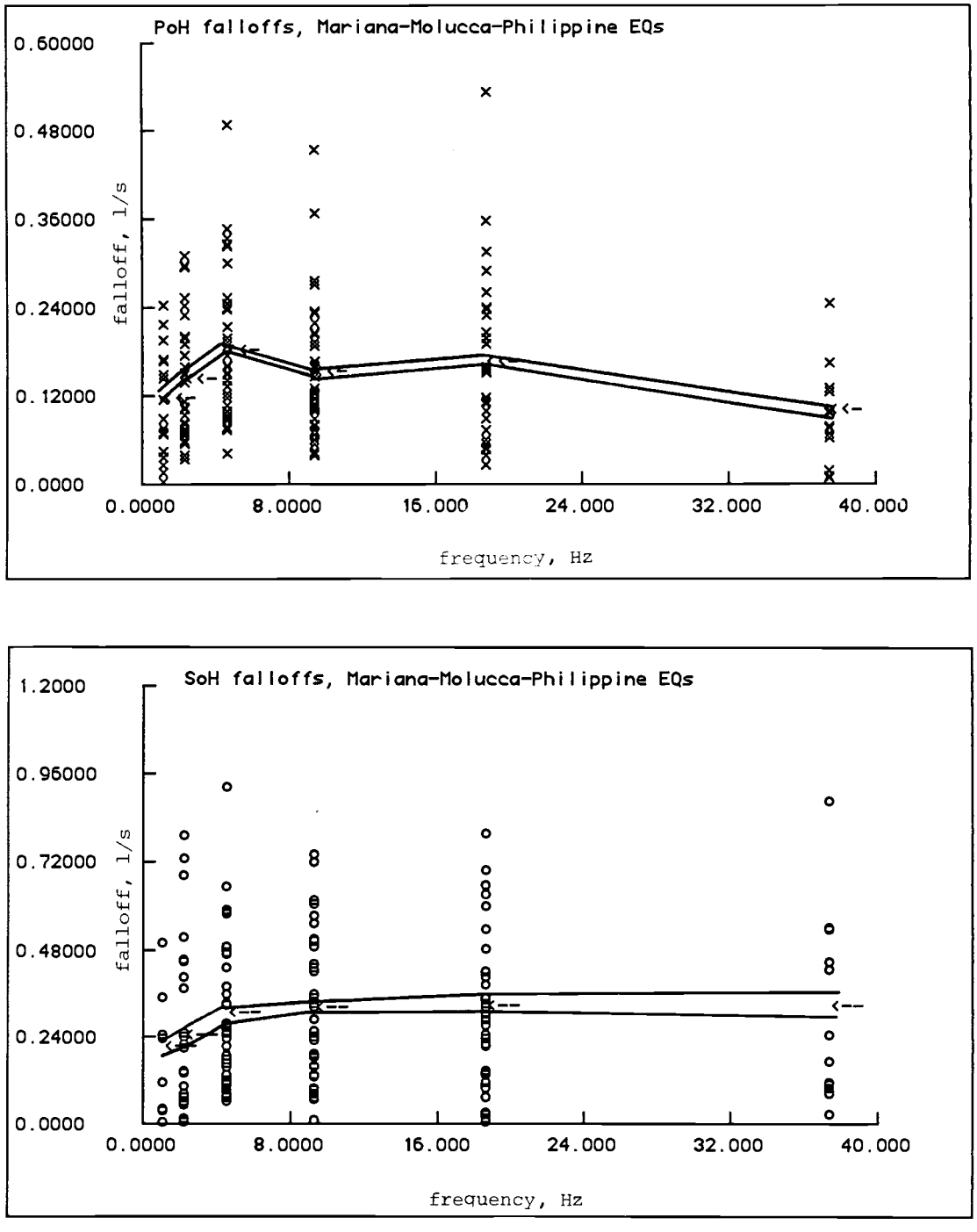

Figure 37. Falloff rate versus frequency for the Mariana, Molucca Sea and Philippine trench earthquakes recorded by the Philippine array. Top) P_0 phases (crosses). Bottom) S_0 phases (crosses). The standard error of the mean is denoted with solid lines.

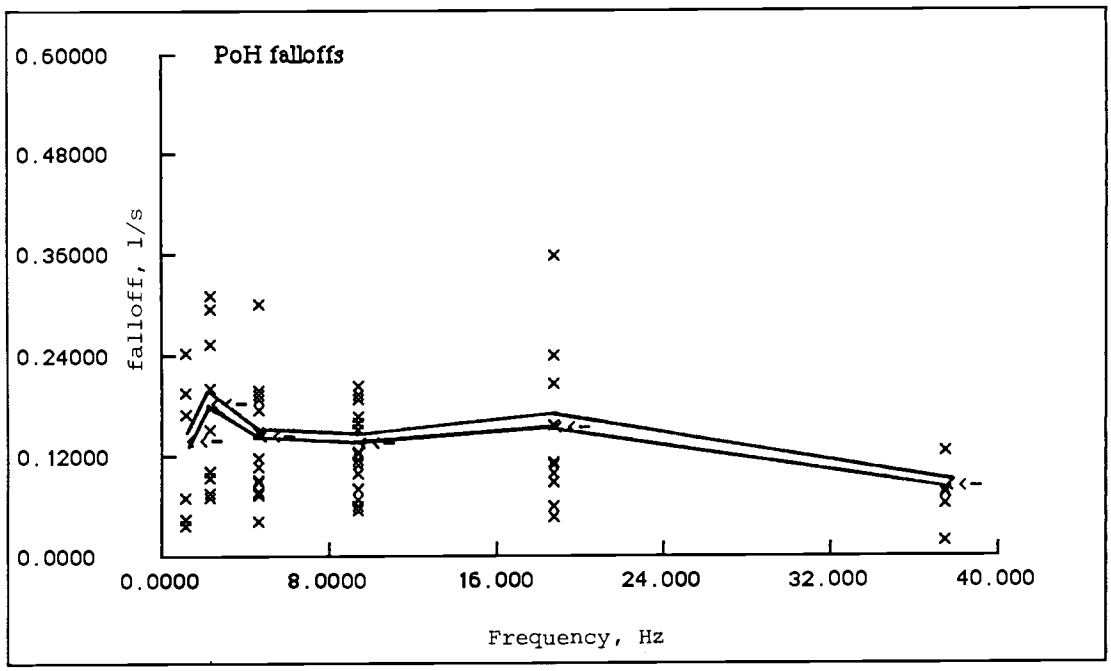

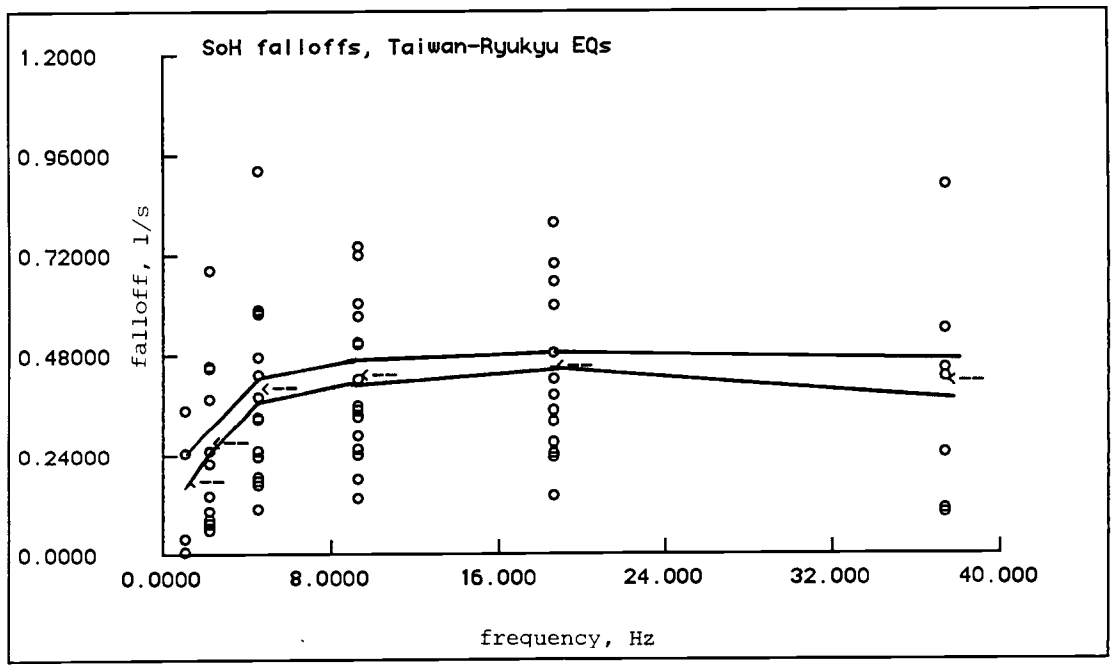

Figure 38. Falloff rate versus frequency for the Taiwan and Ryukyu trench earthquakes recorded by the Philippine array. Top) P_o phases (crosses). Bottom) S_o phases (crosses). The standard error of the mean is denoted with solid lines.

EVENTS RECORDED BY THE WAKE ARRAY:

A total of 60 EQs recorded by the digital Wake hydrophone array were used in this study. The epicenters of these EQs and their depth interval are shown in Figures 10 and 12. All of these EQs originate at convergent boundaries between the Pacific, Philippine, and Eurasian plates, northward along the Mariana trench and the Bonin, Izu, Japan, and Kuril trench system to the Kamchatka peninsula. The overall hypocentral pattern given by these EQs is consistent with the seismicity pattern of their areas, as described by Katsumata and Sykes (1969) and by the Plate-Tectonic map of the Circum-Pacific Region (1981).

The Wake array is situated in the vicinity of Wake Island on the oldest part of the Pacific plate. Seismic rays travelling from the Mariana, Bonin, and Izu trench areas have paths solely across the Jurassic platform whereas rays from the Japan and Kuril and Kamchatka trenches first cross the Cretaceous northern part of the plate before entering the Jurassic basin. The Philippine plate is Tertiary in age. Wake array raypaths thus transect older crust than the Philippine Sea raypaths.

There are large variations seen in the P, P_O, and S_O amplitude ratios of the Wake recorded EQs. Some EQs clearly exhibit all three phases (P, P_O, and S_O) while others either have an unclear P phase, consisting of a few water column reverberations or no P phase at all. Still other EQs have a clear P phase but unclear or non-existent P_O and S_O phases. All EQs which completely lack P_O and S_O phases originate at depths greater than 300 km. The reverberations seen in the P phase coda are consistent in traveltime with water column reverberations. Similar but much more diffuse reverberations can be seen in the P_O and S_O coda. Bandpassed and rectified seismograms revealed no dispersion effect like that observed for the Philippine data set, where the APVEL of the high amplitude part of the coda seemed to increase with frequency. On the other hand, the Wake data frequently exhibited an effect where a low frequency P_O phase (termed P_{OL} phase, Figure 39) was seen to arrive earlier than the higher frequency P_O phase (P_{OH}, Figure 40). The low frequency phase is most prominent in the lowest three frequency bands and hardly seen in the higher bands.

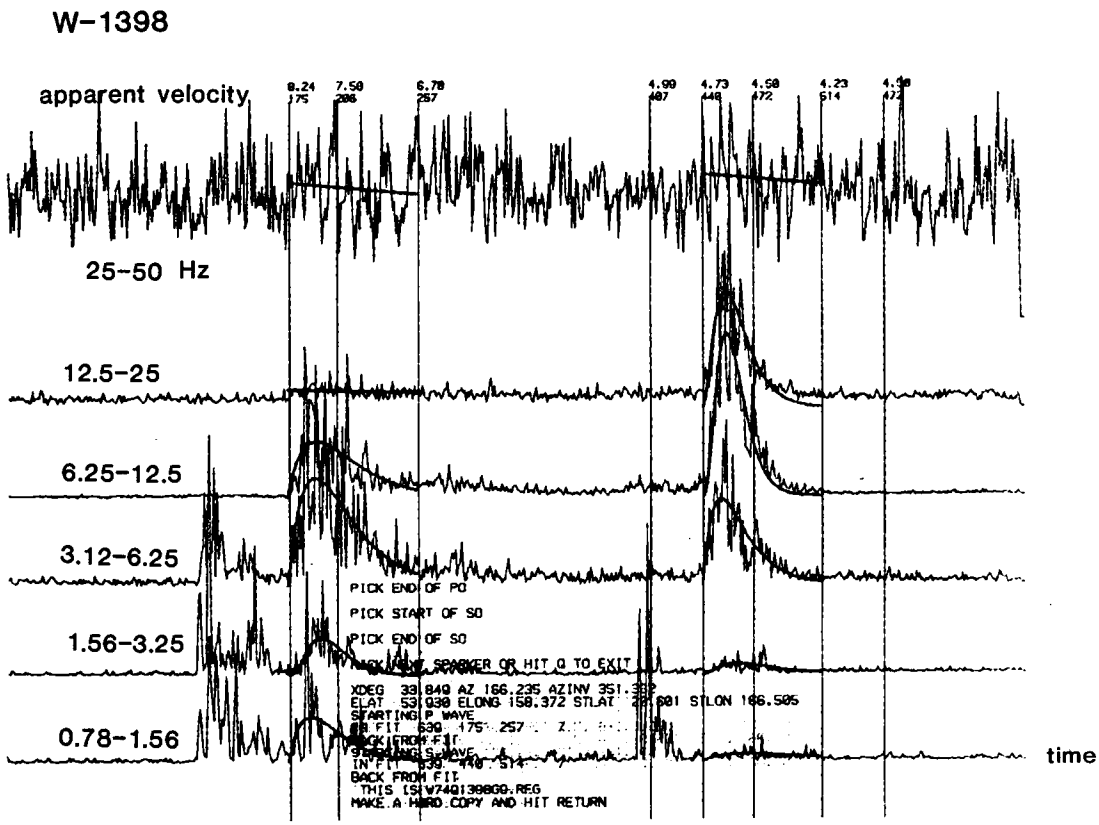

Figure 39. Bandpassed and rectified seismogram for Wake array EQ 1398. The P phase arrives about 100 seconds before the P_{oH} phase and has an apparent velocity of 9.94 km/s.

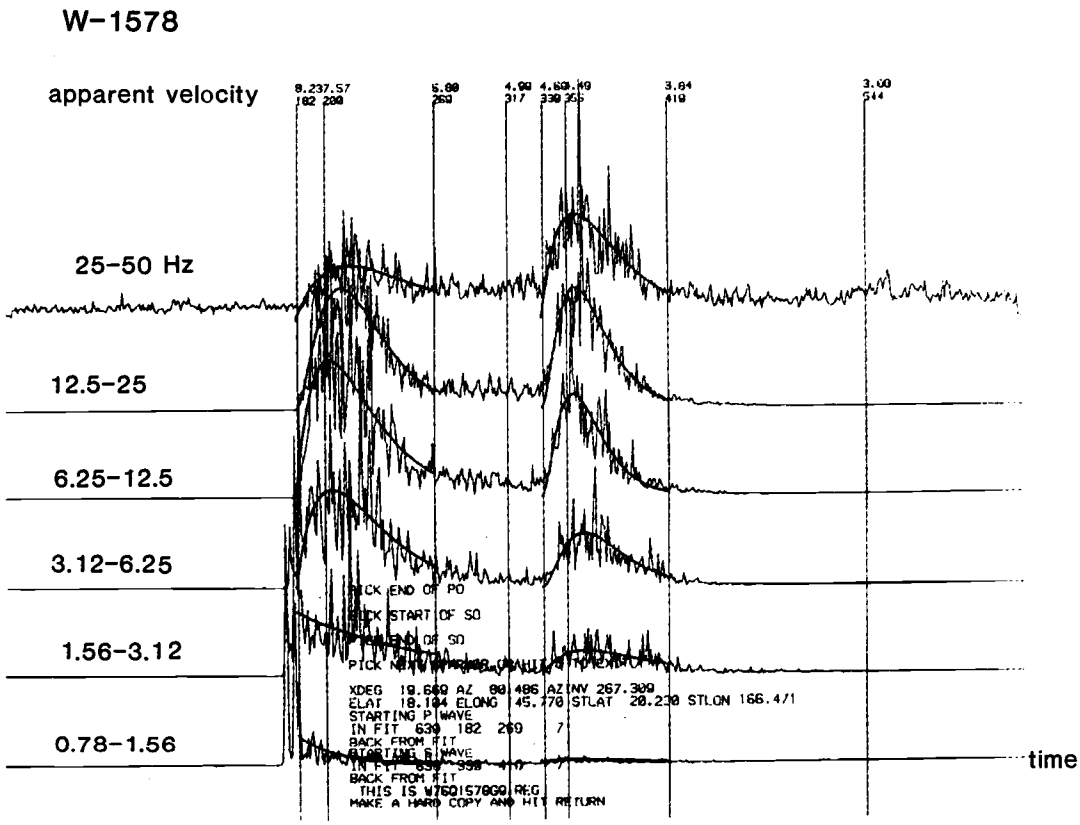

Figure 40. Bandpassed and rectified seismogram for Wake array EQ 1578.
The P_{oL} phase has an apparent velocity of about 8.7 km/s.

WAKE P, P_{oL}, P_{oH}, AND S_{oH} FALLOFF MEASUREMENTS:

Figure 41 shows apparent P, P_{oL}, P_{oH}, and S_{oH} bottom hydrophone velocities of the Wake data set plotted versus range. Each EQ was recorded by at least eight hydrophones, five sitting on the ocean bottom and 3 in the SOFAR channel. All measured SOFAR (stations 10, 11, 20, 21and 40) apparent velocities and falloffs are listed in Appendix 3. The accuracy of the SOFAR falloff measurements is significiantly reduced by attenuation and spreading properties in the water column. Therefore, they are not included in this study. Distinguishing between P and P_{oL} phases was often difficult for epicentral distances of less than 25 degrees. No successful measurements could be made on subsequent S_{oL} velocities due to their vague appearance in the coda.

Average APVELs for the Wake dataset recorded by bottom hydrophones were found to equal 8.75 ± 0.05 km/s (P_{oL} phase), 8.19 ± 0.02 km/s (P_{oH} phase), and 4.79 ± 0.02 km/s (S_{oH} phase). These average velocities are significiantly higher than those previously reported from the Philippine Sea. P_{oH} APVELs were found to range from 7.0 km/s (EQs 443 and 993) to 9.2 km/s (EQ 1886). P_{oH} and S_{oH} phases were recorded from EQs having hypocenters down to depths of 450 - 500 km (Figure 42), but those phases were too vague to produce reliable falloff measurements. The large variation in measured APVELs at depths of 20 - 30 km could be due to inaccurate hypocentral locations for those EQs. Figures 43 and 44 show average falloffs for the complete Wake dataset. The ratio of P/P_{oH} falloffs is approximately 4:1 for the three lowest frequency bands, but the falloff ratio, P_{oH}/S_{oH}, is about 1:1. The P falloff average peaks in band 3 (3.12 - 6.25 Hz) whereas both P_{oH} and S_{oH} falloffs peak in band 4 (6.25 - 12.5 Hz).

Due to the vast epicentral coverage of the Wake data, EQs their falloff analyses were divided into three main areas:

1) The Mariana, Bonin, and Izu trenches.
2) The Japan trench to 40° north.
3) The Kuril trench.

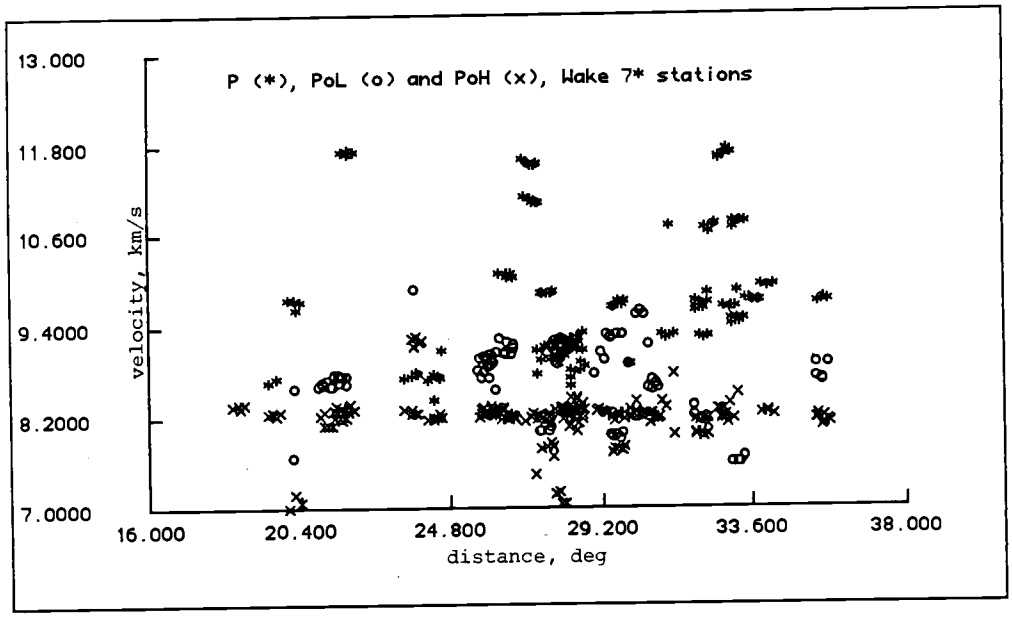

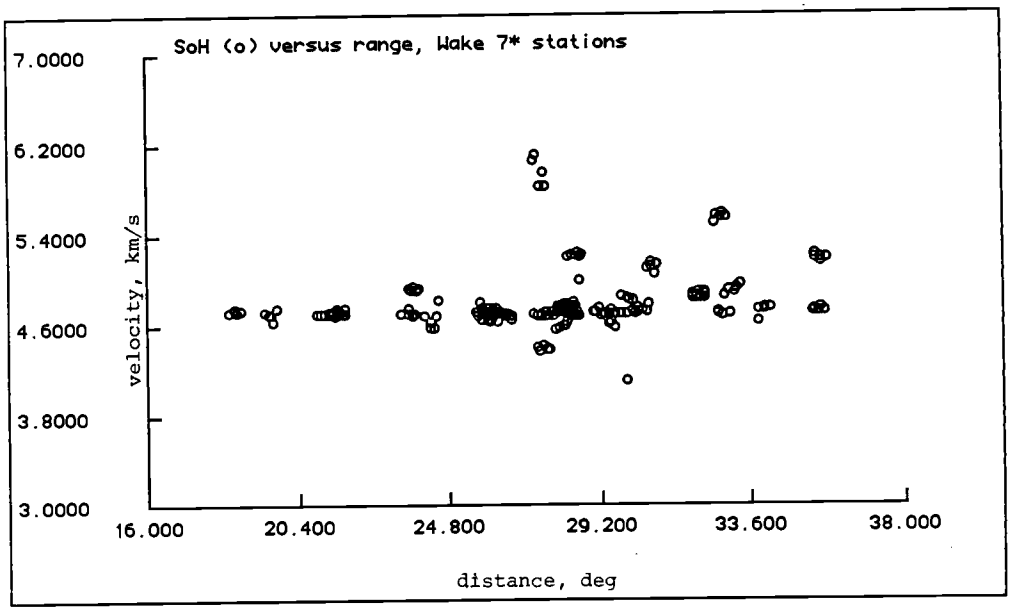

Figure 41. Apparent velocity versus range for the sea floor hydrophones of the Wake array. Top) P phases (stars), P_{oL} phases (circles), P_{oH} phases (crosses). Bottom) S_{oH} phases (circles).

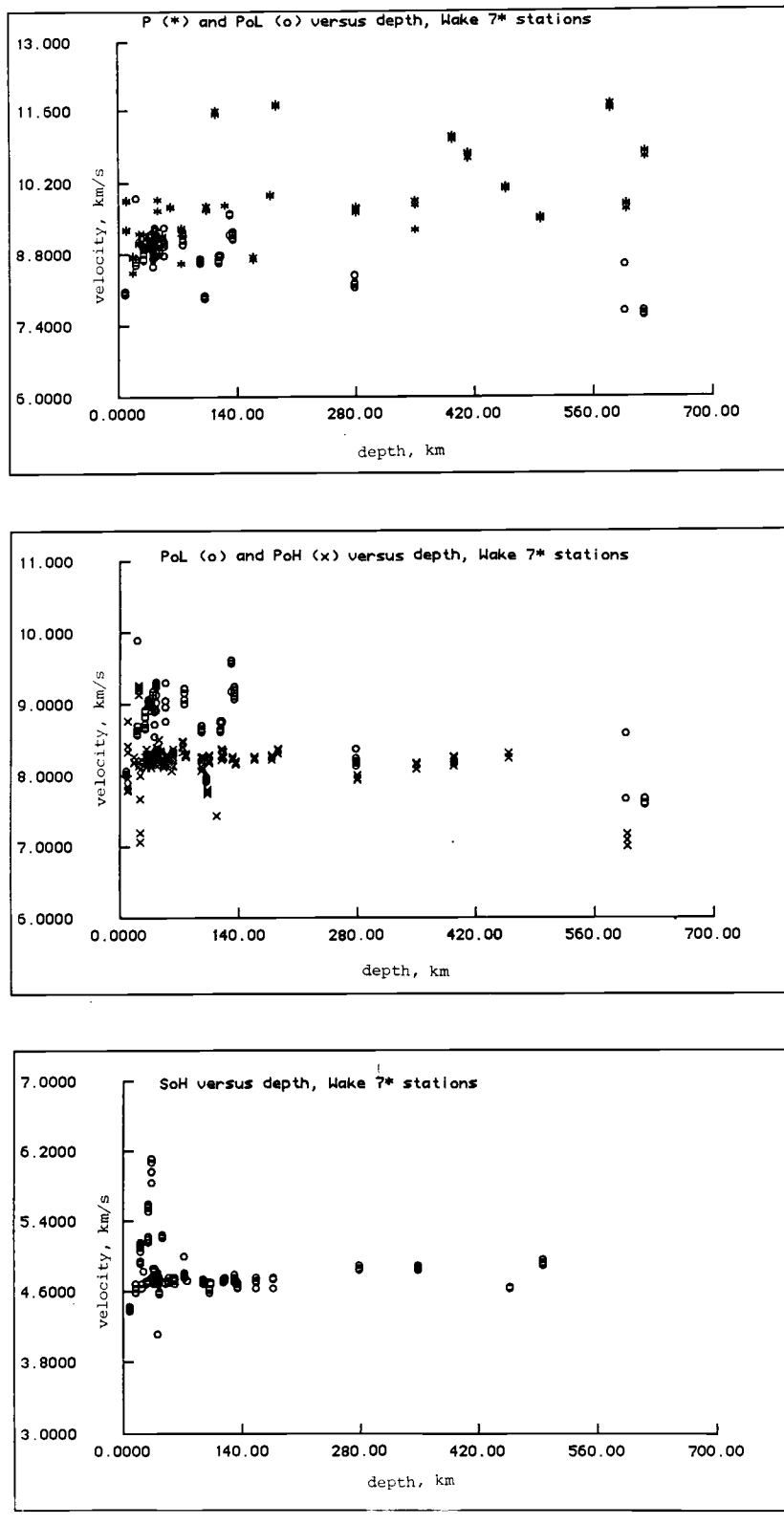

Figure 42. Apparent velocity versus depth for the sea floor hydrophones of the Wake array. Top) P phases (stars), P_{oL} phases (circles), P_{oH} phases (crosses). Bottom) S_{oH} phase (circles).

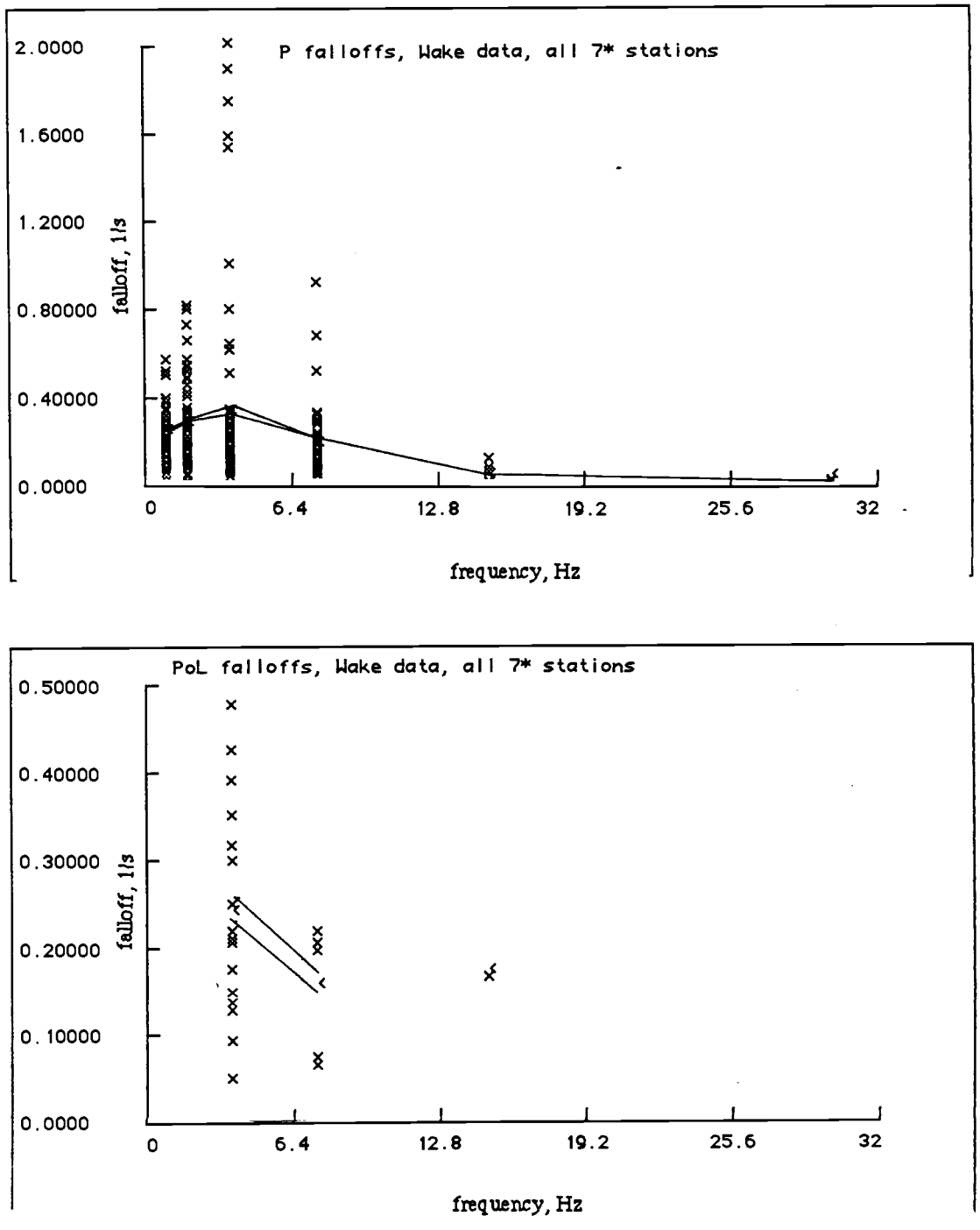

Figure 43. Falloff rate versus frequency for the sea floor hydrophones of the Wake array. Top) P phases (crosses). Bottom) P_{oL} phases (crosses). The standard error of the mean are denoted with solid lines.

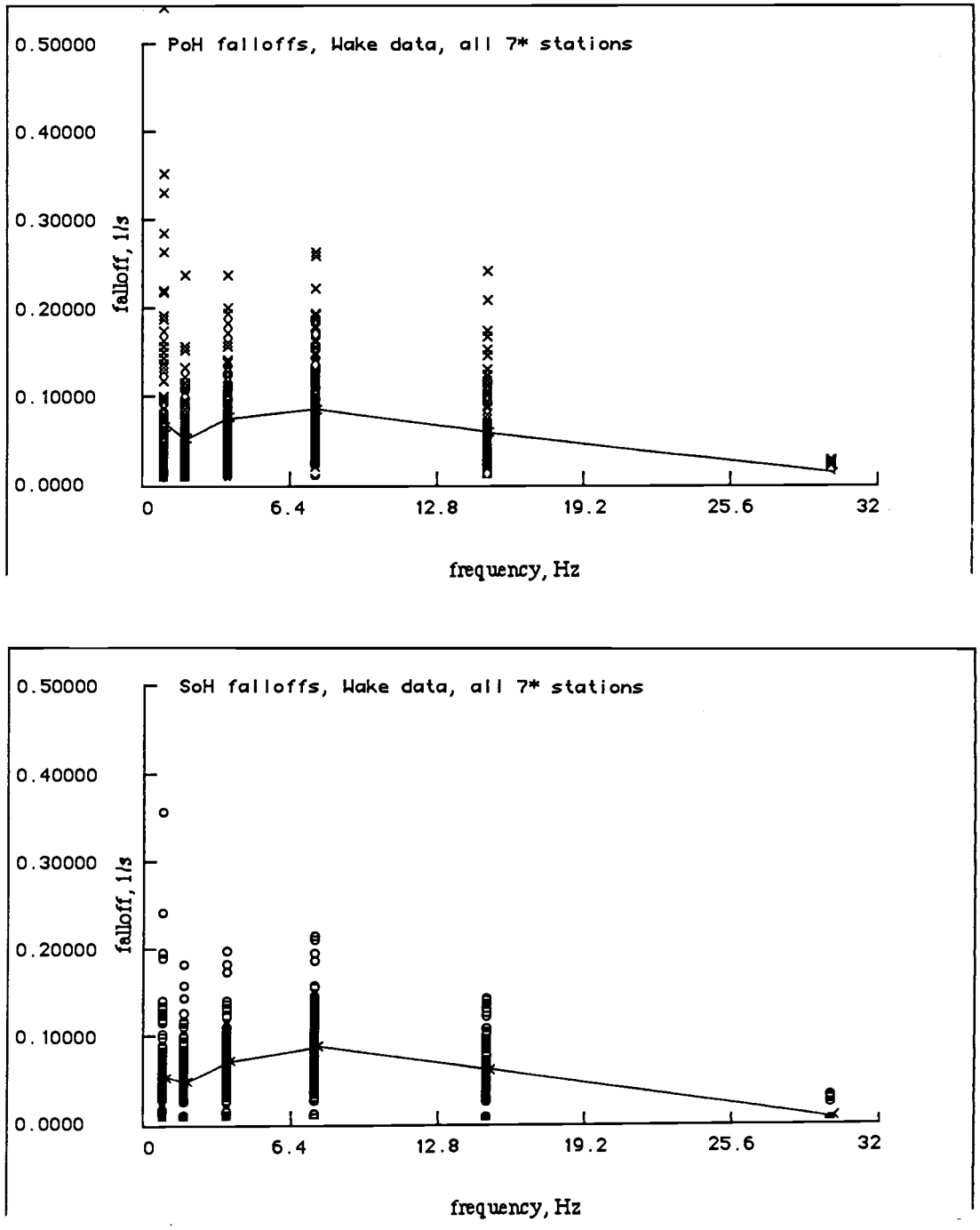

Figure 44. Falloff rate versus frequency for the sea floor hydrophones of the Wake array. Top) P_{oH} phases (crosses). Bottom) S_{oH} phases (circles). The standard error of the mean are denoted with solid lines.

Mariana, Bonin, and Izu trenches:

The Mariana and Bonin trenches data includes EQs 1893, 663, 3120, 659, 3067, 3057, 443, 1578, 2262, and 3213 along with EQ 1886 in the Mussau trench. Those eleven EQs were divided into two subsets: Inner and outer trench EQs. The inner trench EQs have a deeper origin, and their epicenters strike along the Mariana island arc. They have APVELs 8.27 ± 0.01 km/s (P_{oH}) and 4.70 ± 0.01 km/s (S_{oH}) while the outer trench EQs show more APVEL variations. Outer trench EQs 663, 3057, and 3067 have similar APVELs. EQs 443 and 1886 are the two extremes of the whole dataset with respect to APVELs. EQ 443 has an epicenter unusually far out on the convex side of the trench compared to its depth of 600 km. Its APVELs are abnormally low, 9.7 km/s (P) and 7 km/s (P_{oH}). The P_{oH} phase for EQ 443 is very vague, and it has no detectable S_{oH} phase. If it is located correctly EQ 1886 represents the other extreme, having extremely high (9.2 km/s) P_{oH} and S_{oH} (4.9 km/s) phase APVELs at Wake. Also, EQ 1893 has a high S_{oH} APVEL of about 5km/s.

P_{oH} falloff values for the outer trench EQs (Figure 45, top) are considerably higher than those for the inner trench EQs (Figure 46, top). However, their S_{oH} falloff values are similar (Figures 45 and 46, bottom). The outer trench P_{oH} falloff averages are higher than the average of the whole Wake dataset, but the inner trench P_{oH} falloff averages are lower than the total average. The S_{oH} falloff values are about the same for both the inner and outer trench falloff averages, and those values are the same as the total average. The increase in the average P_{oH} falloff value from band 2 to band 1 is caused by contamination of the P_{oH} phase by the P_{oL} phase at the lowest frequencies.

The Izu trench data covers EQs 1494, 1801, 1802, 611, 3054, 3055, 3058, 3061, and 3248 (outer trench EQs, Figure 47), and EQs 2238, 2242, 2495, 1850, and 2144 (inner trench EQs, Figure 48). The outer trench EQs have P, P_{oL}, P_{oH}, and S_{oH} average APVELs of 8.74 ± 0.04 km/s, 8.89 ± 0.03 km/s, 8.25 ± 0.01 km/s, and 4.71 ± 0.01 km/s, respectively. The P and P_{oL} are similiar because these two

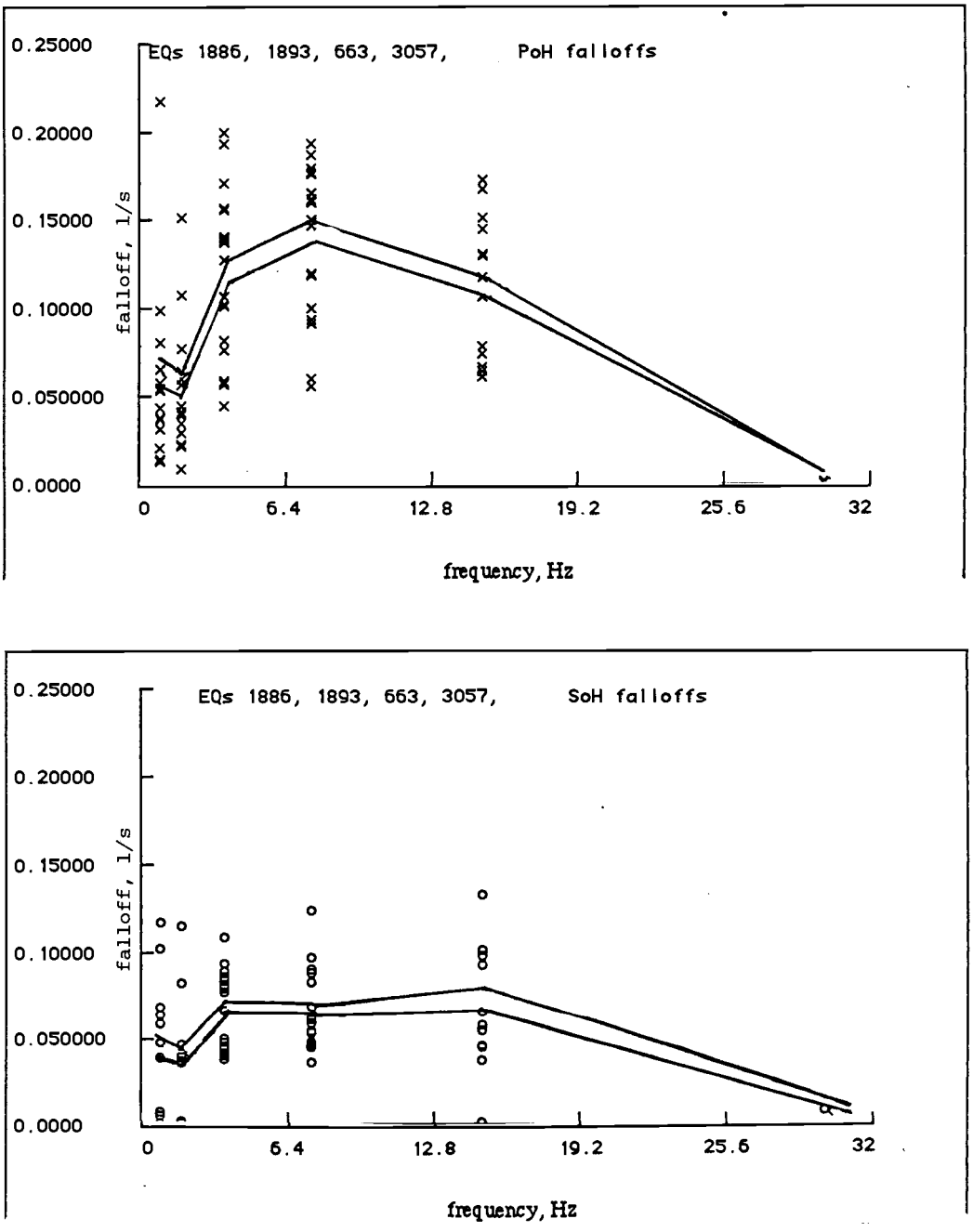

Figure 45. Falloff rate versus frequency for the sea floor hydrophones of the Wake array (outer trench Mariana earthquakes). Top) P_{oH} phases (crosses). Bottom) S_{oH} phases (circles). The standard error of the mean are denoted with solid lines.

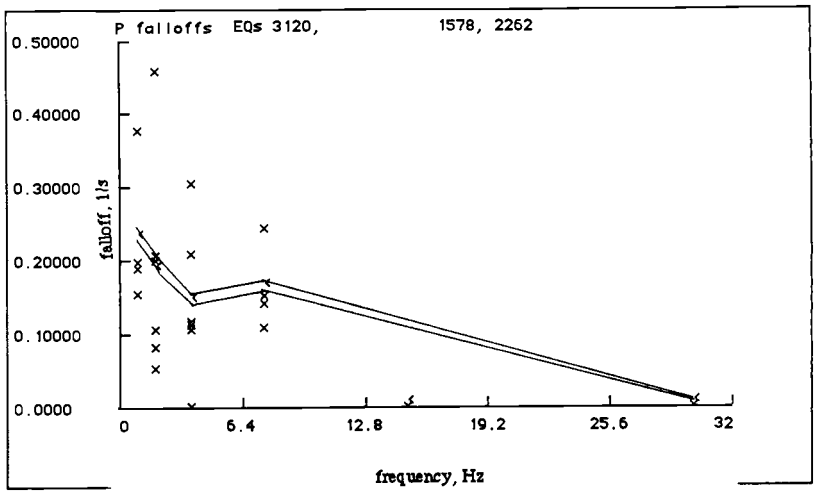

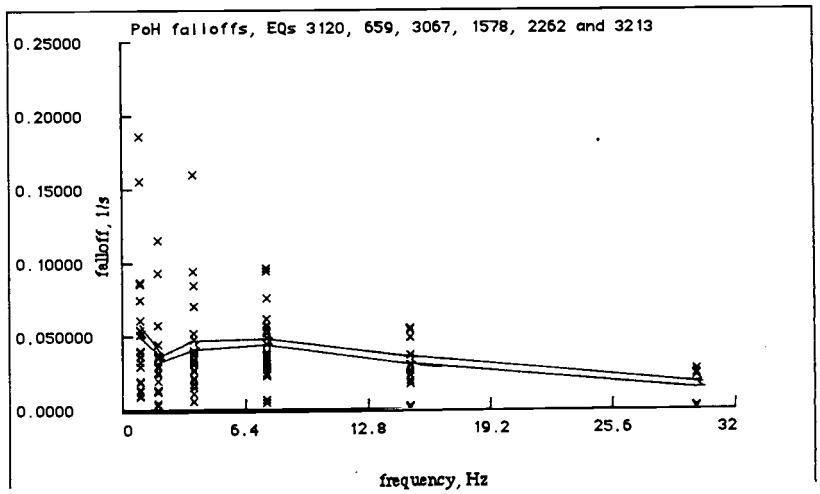

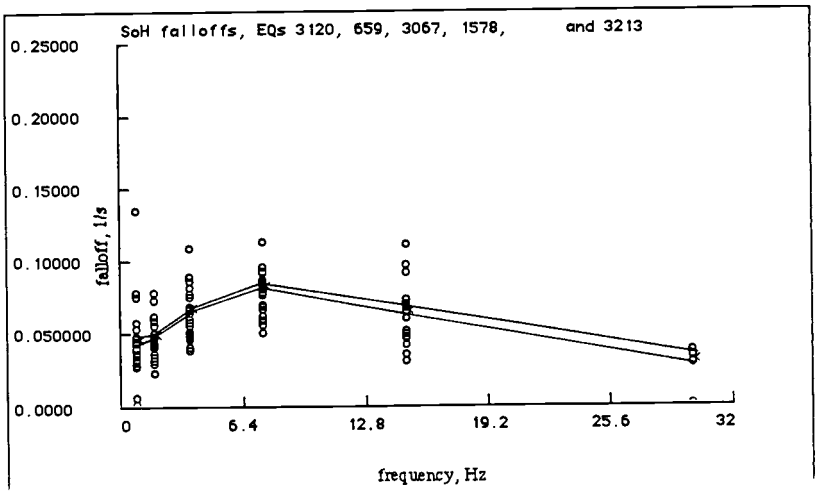

Figure 46. Falloff rate versus frequency for the sea floor hydrophones of the Wake array (inner trench Mariana and Bonin earthquakes). Top) P phases (crosses). Middle) P_{oH} phases (crossses). Bottom) S_{oH} phases (circles). The standard error of the mean are denoted with solid lines.

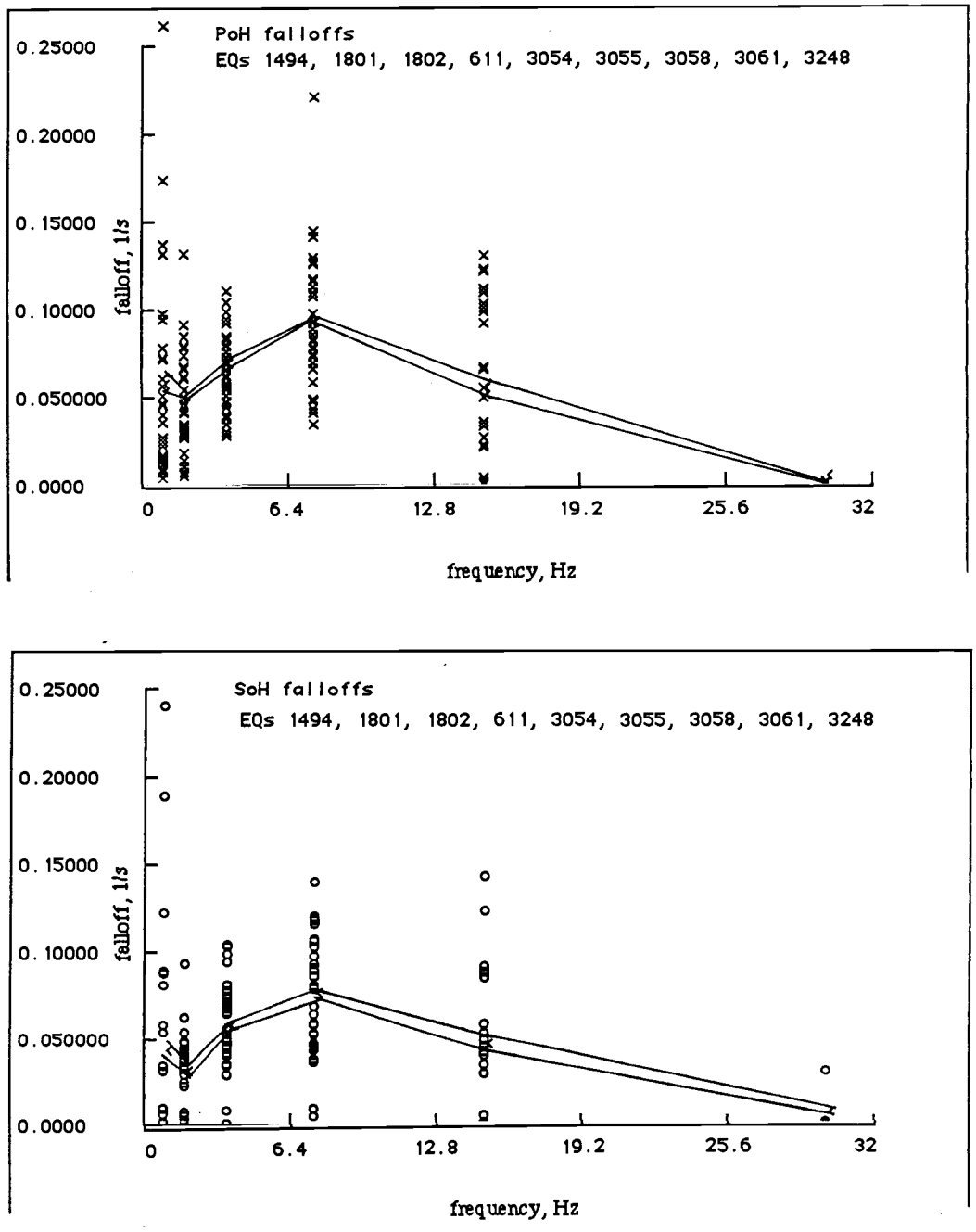

Figure 47. Falloff rate versus frequency for the sea floor hydrophones of the Wake array (outer trench Izu earthquakes). Top) P_{oH} phases (crosses). Bottom) S_{oH} phases (circles). The standard error of the mean are denoted with solid lines.

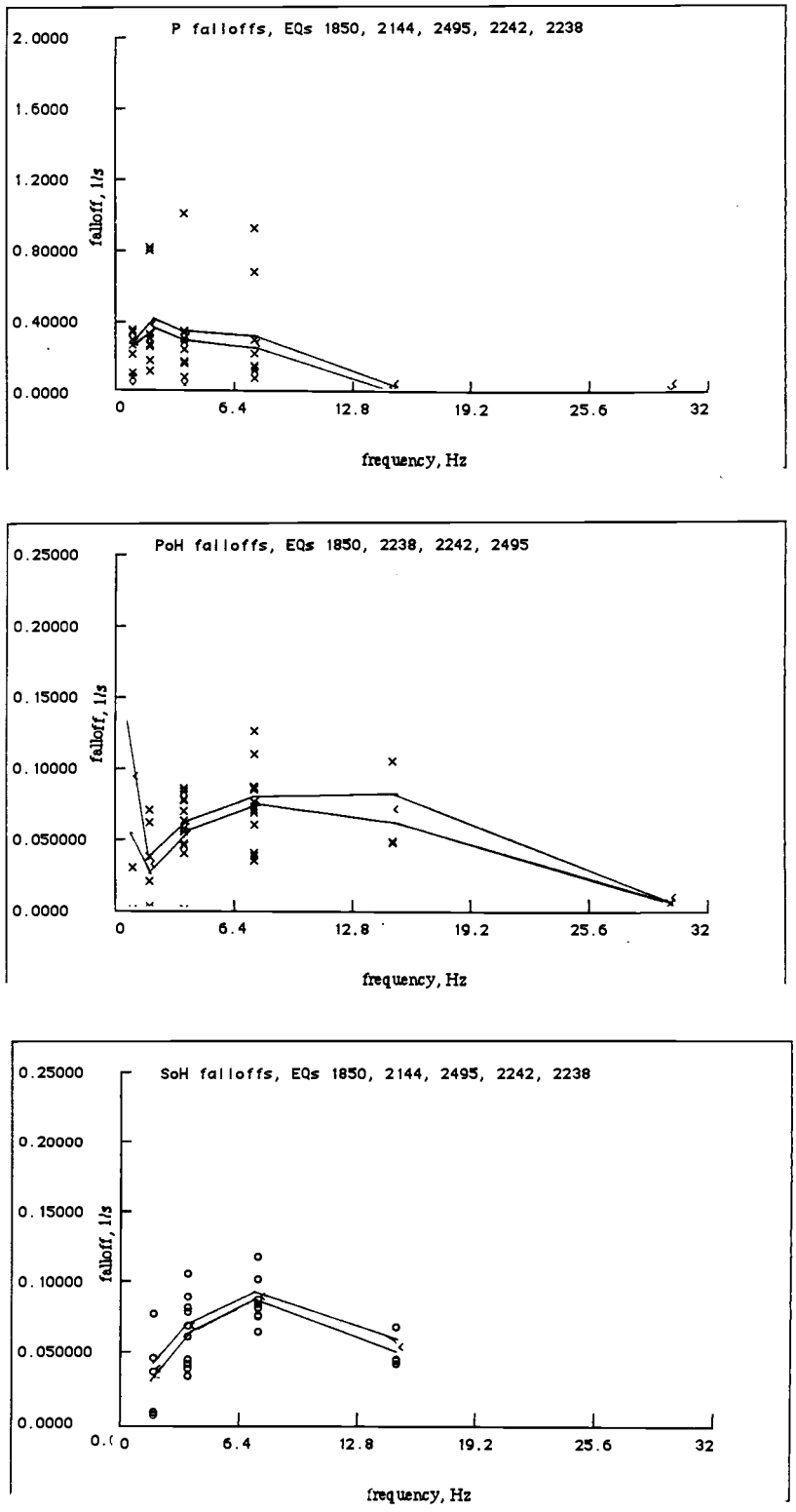

Figure 48. Falloff rate versus frequency for the sea floor hydrophones of the Wake array (inner trench Izu earthquakes). Top) P phases (crosses). Middle) P_{oH} phases (crosses). Bottom) S_{oH} phases (circles). The standard error of the mean are denoted with solid lines.

phases are still merged for these EQs. The inner trench EQs have higher average P and P_{oL} APVELs of 10.89 ±0.16 km/s and 9.13 ± 0.03 km/s whereas their P_{oH} and S_{oH} APVELs are 8.15 ± 0.05 km/s and 4.65 ± 0.01 km/s. These inner trench P_{oH} and S_{oH} APVEL values are significiantly lower than the outer trench values.

The P_{oH} average falloffs for the Izu outer trench are considerably lower than those found on the Mariana outer trench. Also, the inner Izu trench P_{oH} falloff values are higher than the Mariana and Bonin inner trench values. Average S_{oH} falloff values for both the inner and outer trench are similar to those found for the Mariana and Bonin trenches. The Izu inner trench P_{oH} and S_{oH} falloff values have a greater standard deviations from the mean than the inner Mariana and Bonin values. The Izu inner trench S_{oH} phases recorded at Wake are smaller than those from the Mariana and Bonin trenches, indicating a greater absorption along their raypaths.

Japan trench:

This dataset includes EQs 1451, 715, 1272, and 1806, all shallow EQs, located at the outer strike of the Japan trench. It also includes one deep EQ with an epicenter in the Japan Sea and EQs 1518 and 2911, with epicenters on the western coast of Kyushu. Only the P phases were detected from EQs 1518 and 2911.

Average P, P_{oL}, P_{oH}, and S_{oH} APVELs of the four outer trench EQs are 9.29 ± 0.11 km/s, 9.12 ± 0.04 km/s, 8.20 ± 0.03 km/s, and 4.69 ± 0.01 km/s, respectively. Figure 49 shows the P falloffs for EQs 2911 and 1518 (Kyushu EQs), as well as the P_{oH} and S_{oH} falloffs for the Japan outer trench EQs (1451, 715, 1272, and 1806). The P_{oH} falloff values for EQ 2261 are lower (Figure 50) than for the outer trench EQs. Overall, the P_{oH} falloff values for the Japan outer trench are lower than those for the Mariana trench but are similar to the Izu outer trench falloffs. The S_{oH} falloffs for the Japan outer trench EQs are higher in the highest four frequency bands than both the Mariana and Izu outer trench falloffs.

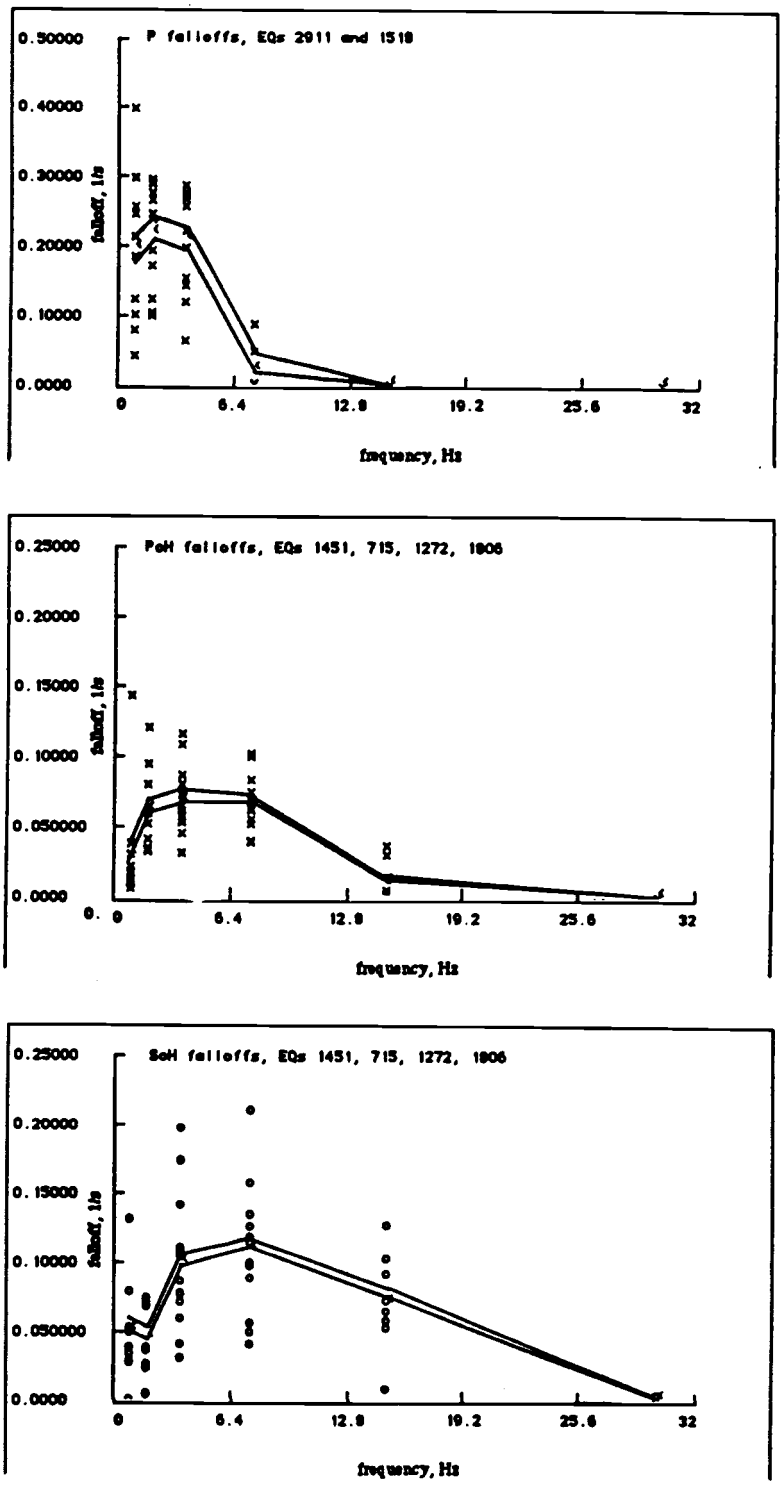

Figure 49. Falloff rate versus frequency for the sea floor hydrophones of the Wake array (outer trench Japan earthquakes). Top) P wave (crosses). Middle) P_{oH} phases (crosses). Bottom) S_{oH} phases (circles). The standard error of the mean are denoted with solid lines.

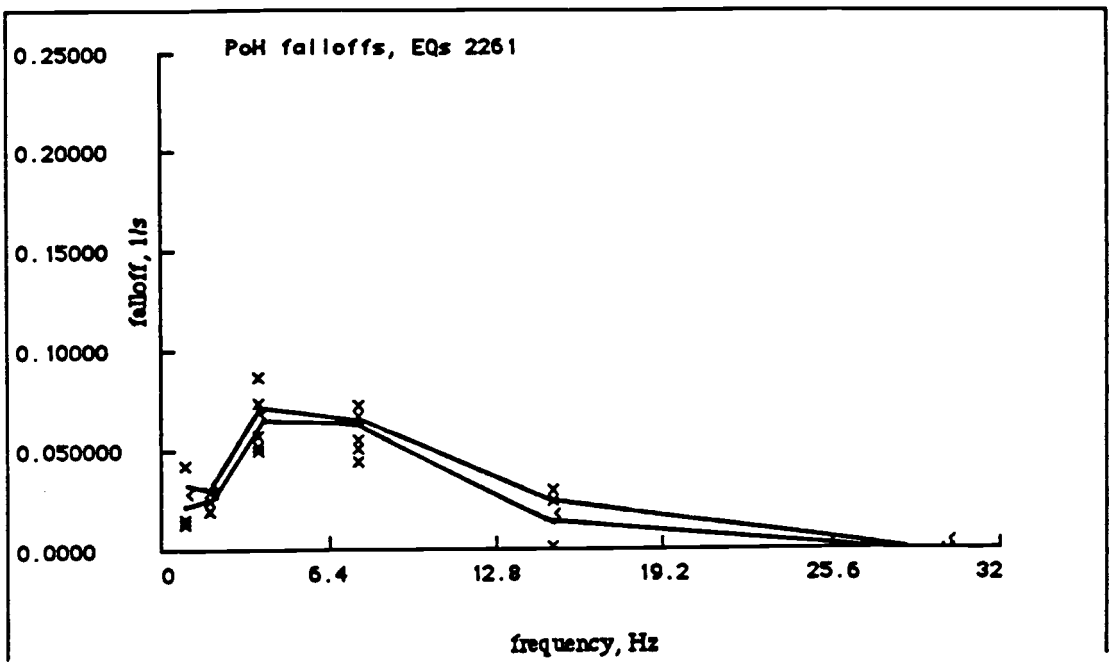

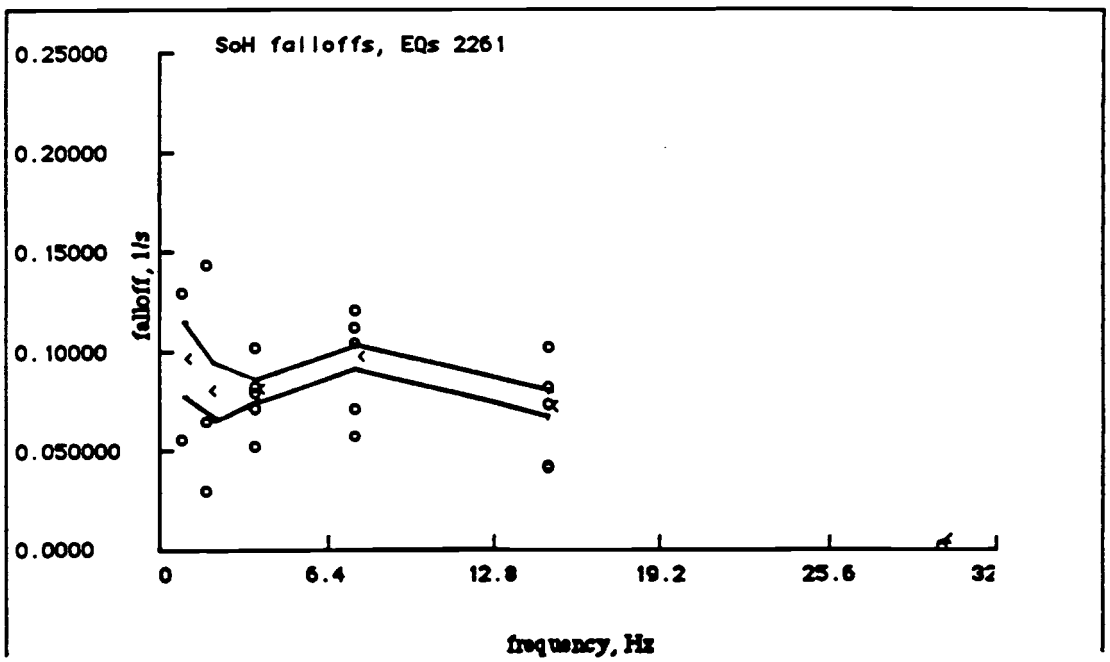

Figure 50. Falloff rate versus frequency for the sea floor hydrophones of the Wake array (inner trench Japan earthquake). Top) P phases (crosses). Middle) P_{oH} phases (crosses). Bottom) S_{oH} phases (circles). The standard error of the mean are denoted with solid lines.

Kuril trench:

Average apparent P, P_{oL}, P_{oH}, and S_{oH} velocities for all Kuril EQs (all EQs on Figure 10) recorded by the Wake ocean bottom hydrophones were found to be 9.68 ± 0.09 km/s, 8.62 ± 0.09 km/s, 8.13 ± 0.02 km/s, and 4.85 ± 0.03 km/s, respectivly (Figure 51). These P_{oL} and P_{oH} APVELs are significiantly lower than for the entire Wake data set, but the S_{oH} APVEL is higher. Average APVELs for all Kuril EQs with epicentral depths less than 100 km are not significiantly different from the average of all Kuril EQs. EQs 993, 2001, 2246, and 319 have lower than average P_{oL} and P_{oH} APVELs. EQs 2001, 2321, and 2246 have lower than average S_{oH} APVELs, but EQs 3237, 2283, 2884, and 2340 have unusually high S_{oH} APVELs. APVELs are plotted against depth on Figure 52. Again, there are large variations at the normal (fixed) depth of about 30 km.

Falloffs for all Kuril EQs are shown in Figure 53. The P_{oH} average falloff values for the Kuril EQs are higher than those of the entire Wake data set, but the S_{oH} falloff averages are about the same. Figures 54 - 58 are falloff plots for all Kuril EQs with depths less than 100 km. Average falloffs for both P_{oH} and S_{oH} phases from the Hokkaido EQs (Figure 54), at the junction between the Japan and Kuril trenches, are lower and more diffuse than the average falloffs for EQs north of Hokkaido (Figures 55 and 57). Average P_{oH} APVELs and average falloffs are similar for all EQs in frequency bands 2 - 6 (excluding EQs 993 and 2001, Figure 57) along the Kuril trench (Figures 55 and 56). For Kamchatka they are slightly higher (Figure 58). However, S_{oH} APVELs and average S_{oH} falloff values are more variable. The average falloff values in frequency band one (0.78 - 1.56 Hz) and five (12.5 - 20 Hz) have the greatest variability. Higher average falloff values in the lowest frequency band are most likely due to contamination by the P and P_{oL} phases whose coda often stretch into the P_{oH} coda in the lowest frequency bands. EQs 993 and 2001 have anomalously low P_{oH} and S_{oH} APVELs. Their P_{oH} falloff average (Figure 57) is higher than that of the other shallow Kuril EQs. EQs 2001, 993, and 1201 are the only shallow Kuril EQs which have clear P phases. P phase contamination is clearly seen in the lowest band of the P_{oH} falloff for EQs 993 and 2001, and these EQs have

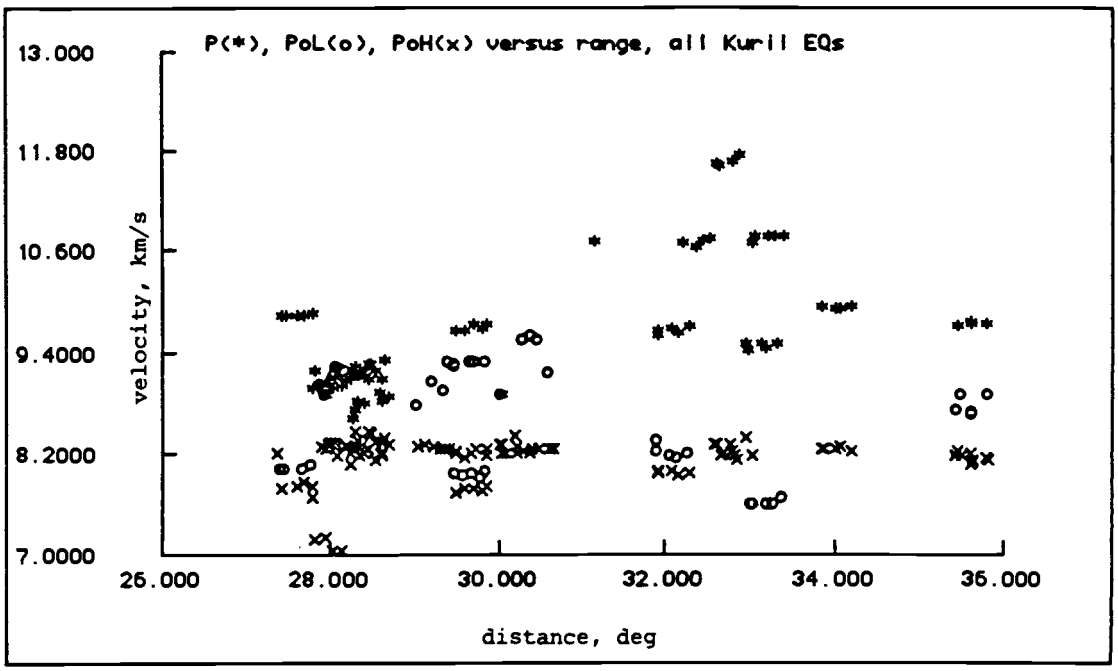

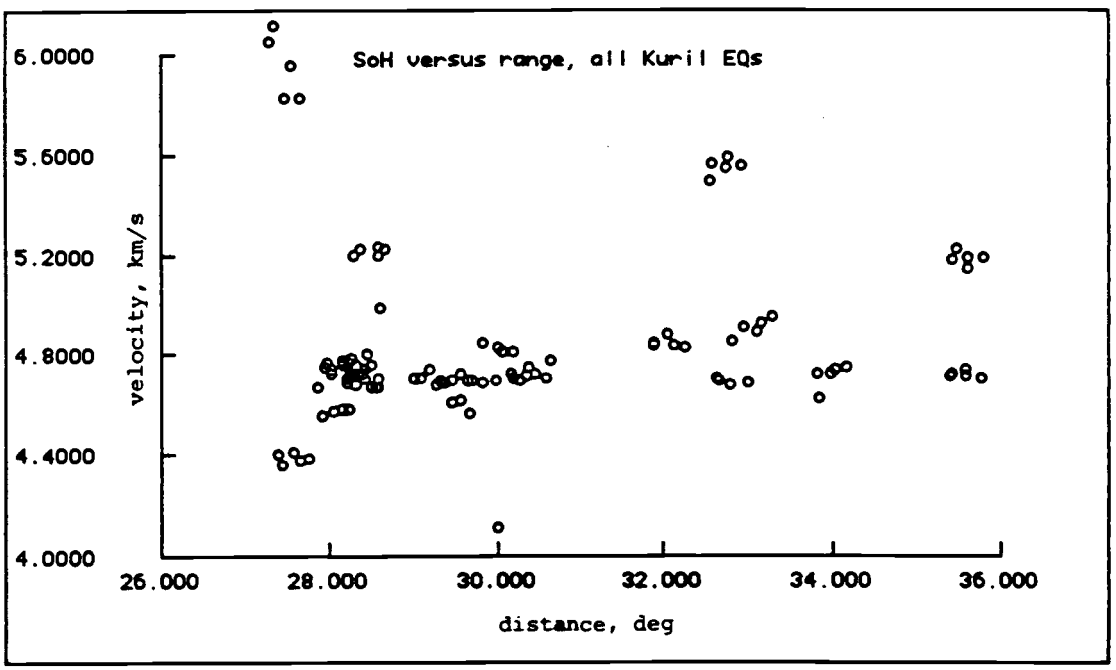

Figure 51. Apparent velocity versus range for all Kuril earthquakes recorded by the sea floor hydrophones of the Wake array. Top) P phases (stars), P_{oL} phases (circles), P_{oH} phases (crosses). Bottom) S_{oH} phases (circles).

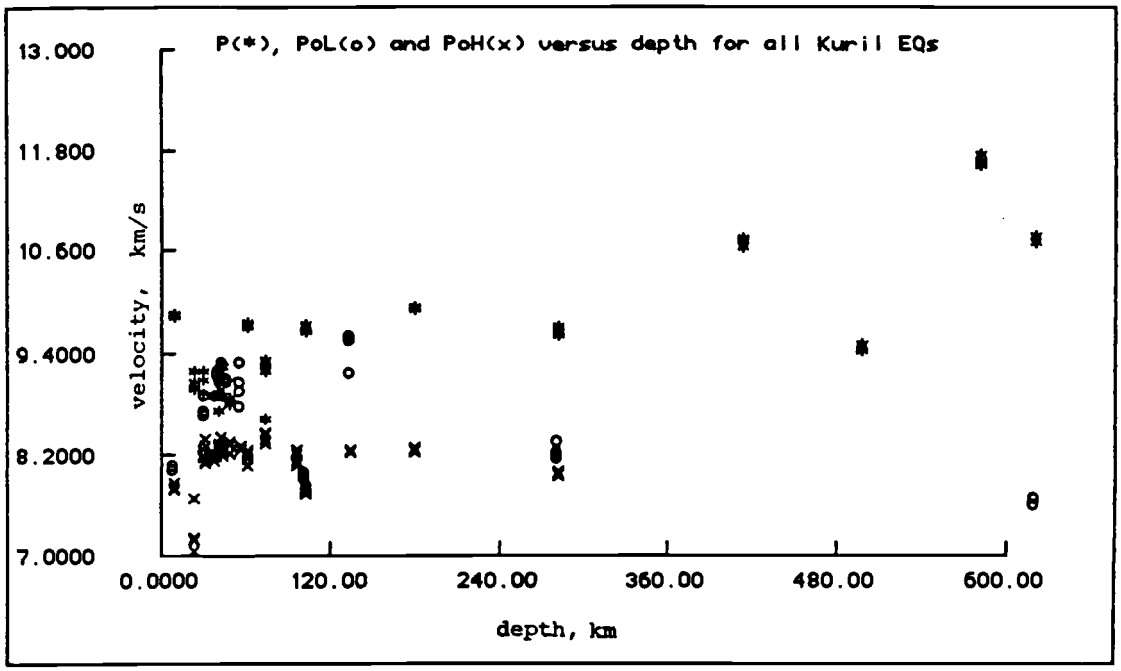

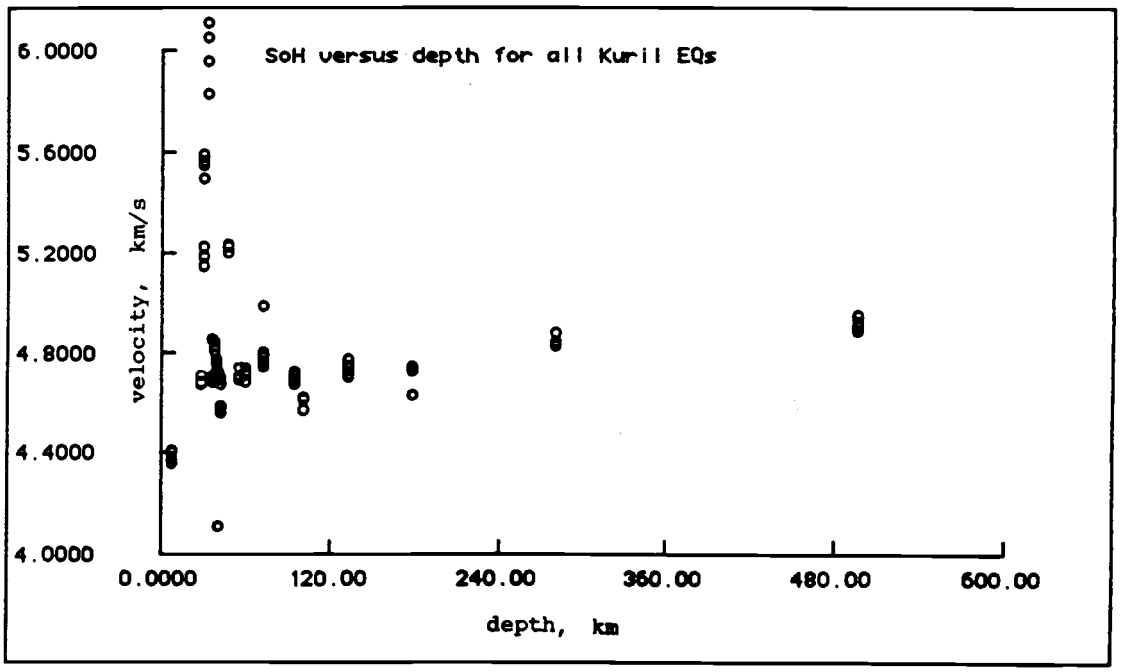

Figure 52. Apparent velocity versus depth for all Kuril earthquakes recorded by the sea floor hydrophones of the Wake array. Top) P phases (stars), P_{oL} phases (circles), P_{oH} phases (crosses). Bottom) SoH phases (circles).

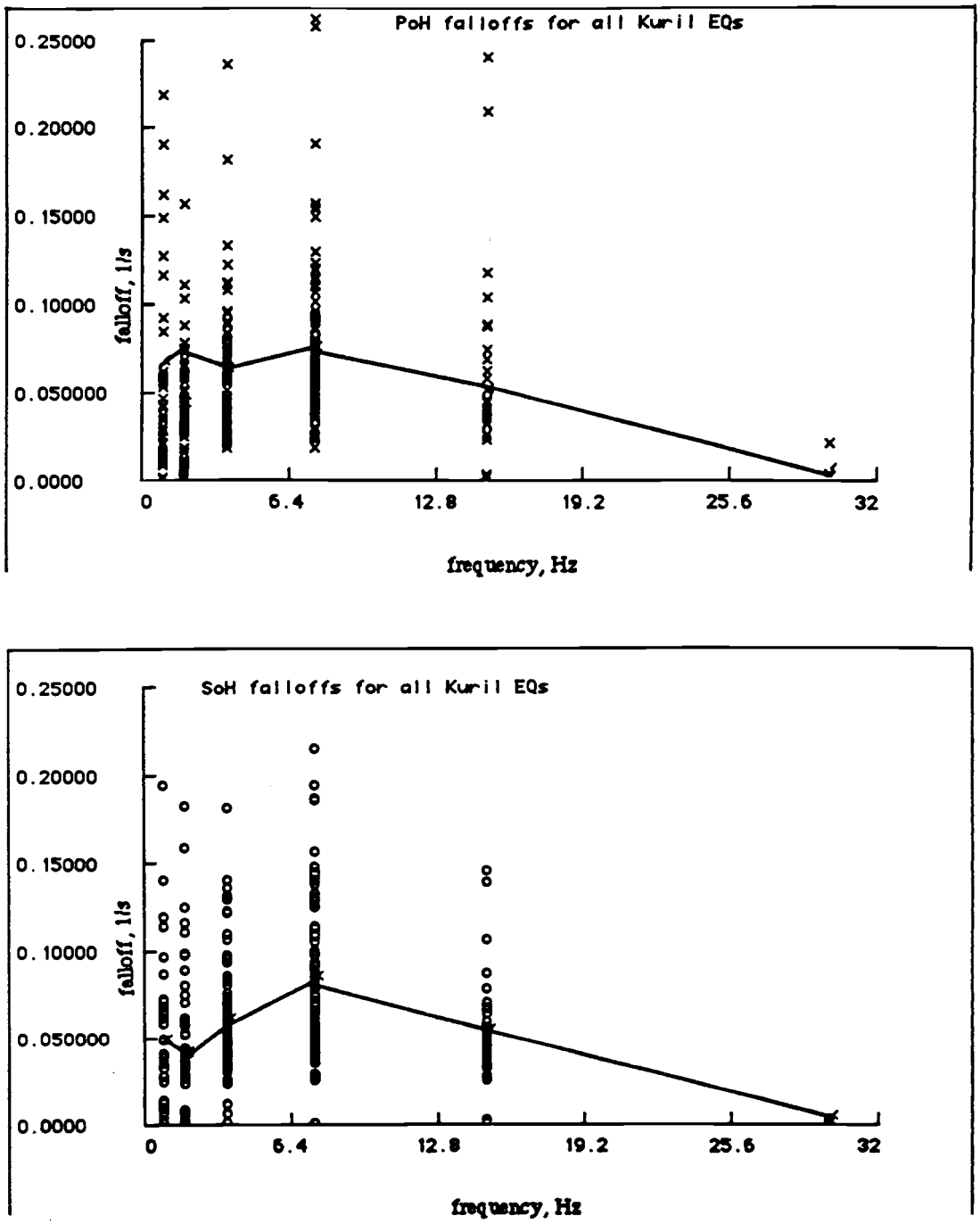

Figure 53. Falloff rate versus frequency for all Kuril earthquakes recorded by the sea floor hydrophones of the Wake array. Top) P_{oH} phases (crosses). Bottom) S_{oH} phases (circles). The standard error of the mean are denoted with solid lines.

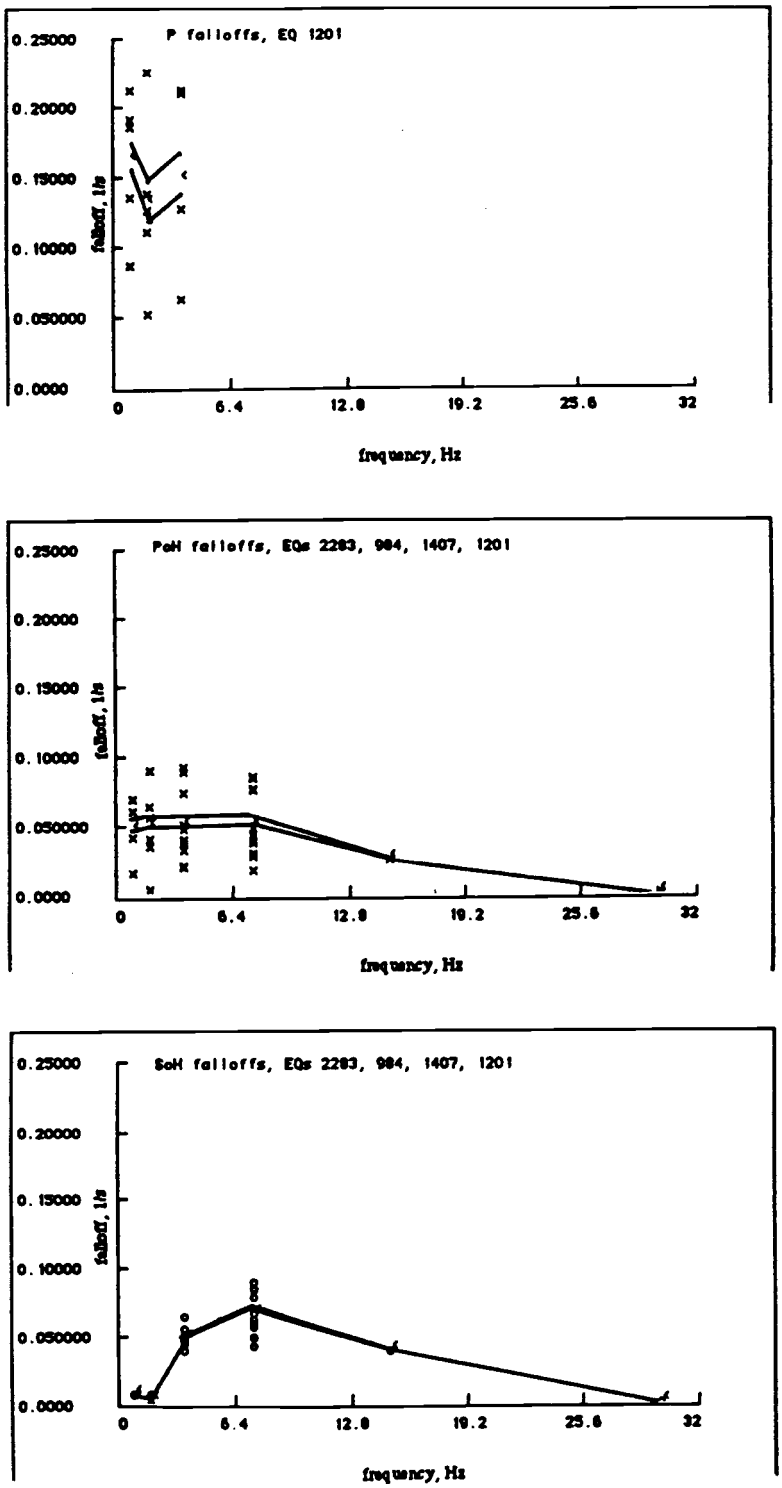

Figure 54. Falloff rate vs. frequency for shallow Hokkaido earthquakes at the junction of the Japan and Kuril trenches recorded by the sea floor hydrophones of the Wake array. Top) P wave (crosses). Middle) P_{oH} wave (crosses). Bottom) S_{oH} (circles). The standard error of the mean are denoted with solid lines.

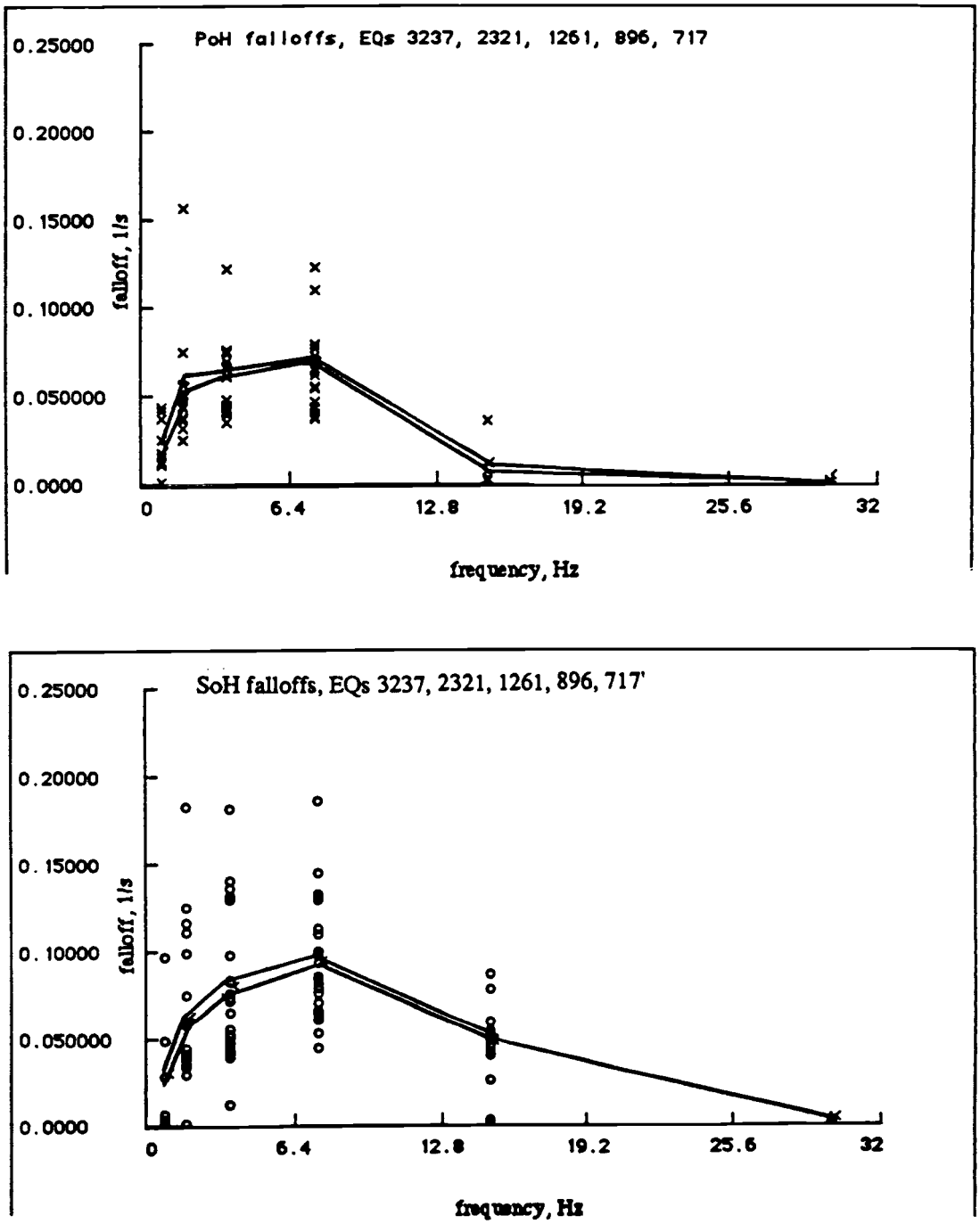

Figure 55. Falloff rate vs. frequency for south Kuril trench earthquakes recorded by the sea floor hydrophones of the Wake array. Top) P_{oH} wave (crosses). Bottom) S_{oH} (circles). The standard error of the mean are denoted with solid lines.

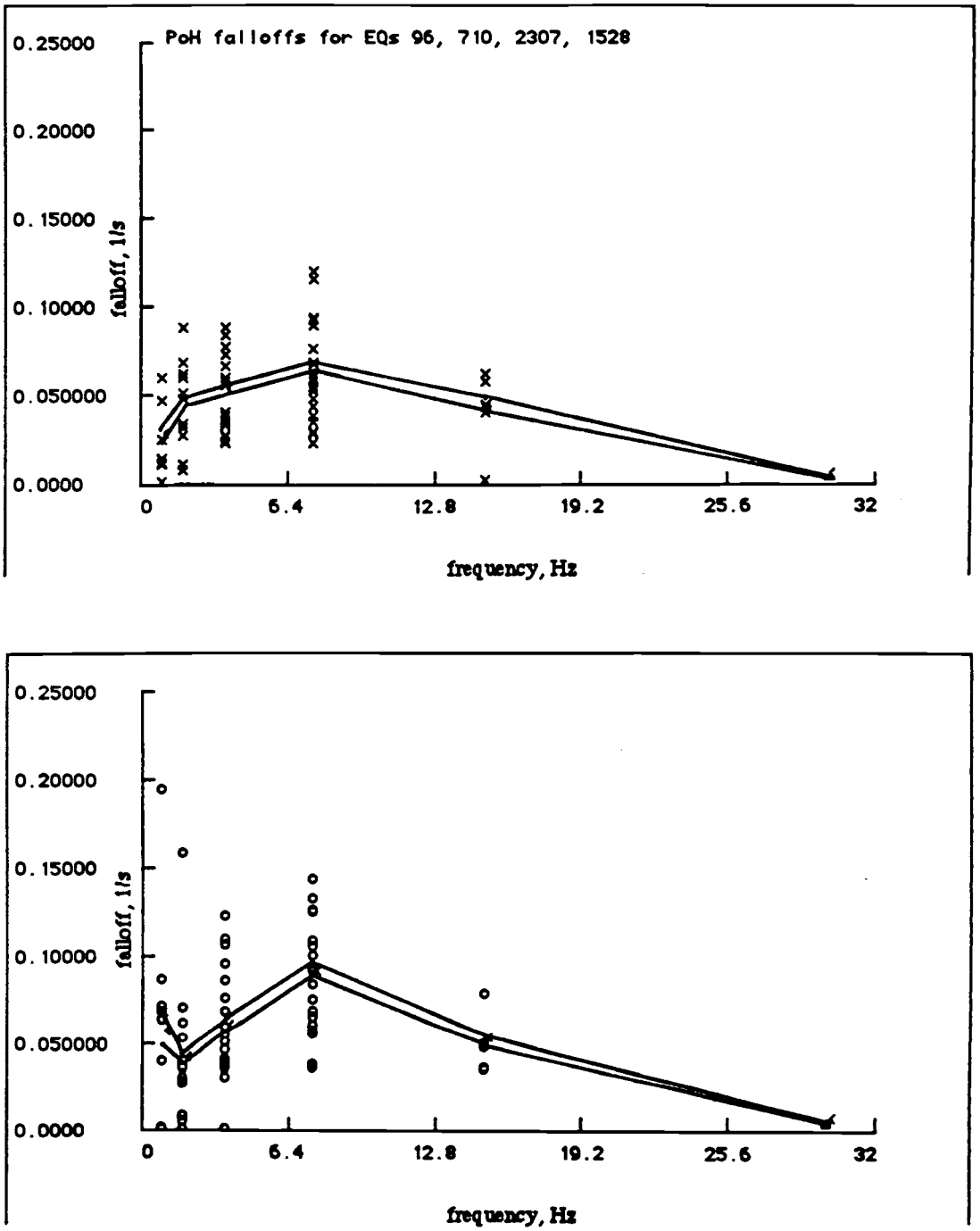

Figure 56. Falloff rate versus frequency for north Kuril trench earthquakes recorded by the sea floor hydrophones of the Wake array. Top) P_{oH} phases (crosses). Bottom) S_{oH} phases (circles). The standard error of the mean are denoted with solid lines.

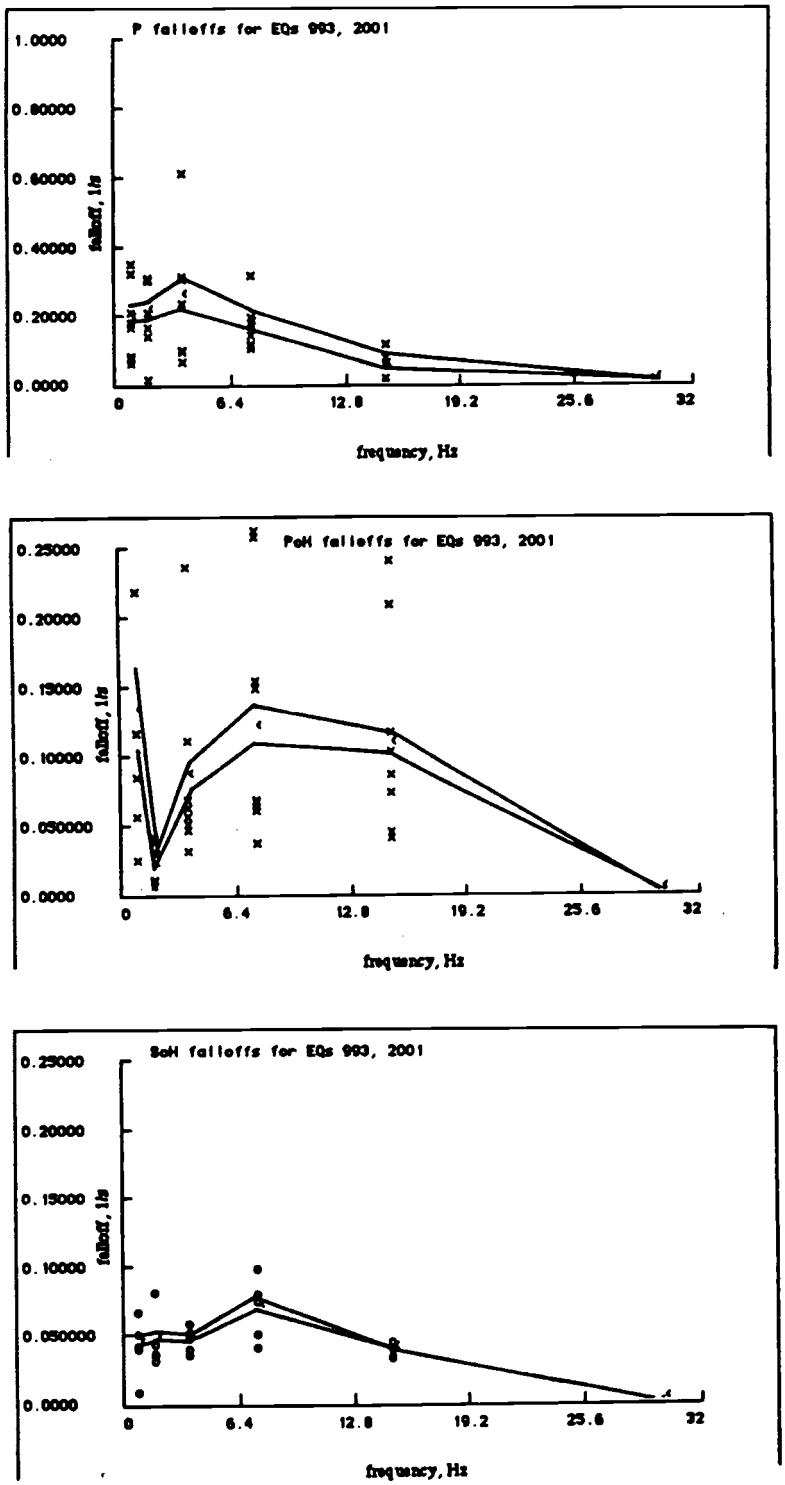

Figure 57. Palloff rate versus frequency for two middle Kuril trench earthquakes recorded by the sea floor hydrophones of the Wake array. Top) P phases (crosses). Middle) P_{oH} phases (crosses). Bottom) S_{oH} phases (circles). The standard error of the mean are denoted with solid lines.

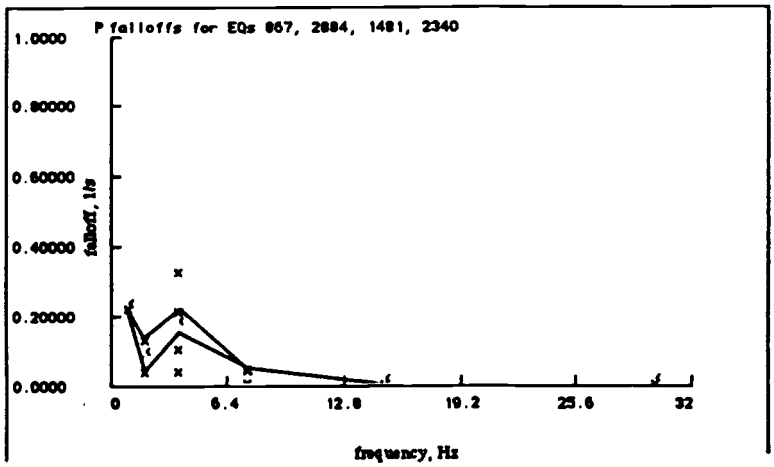

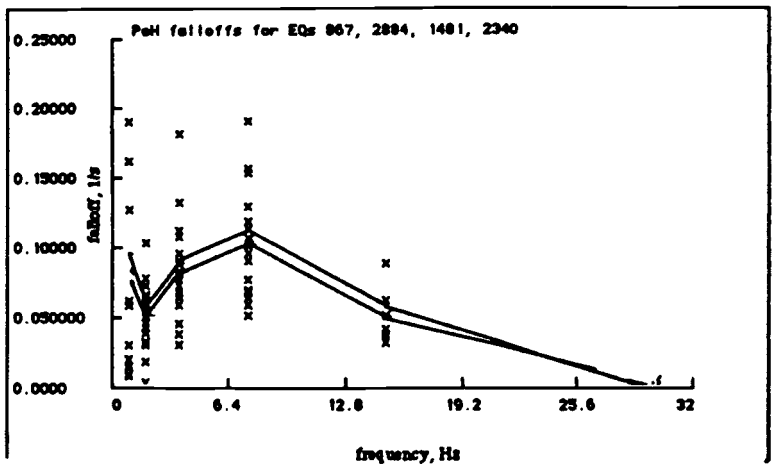

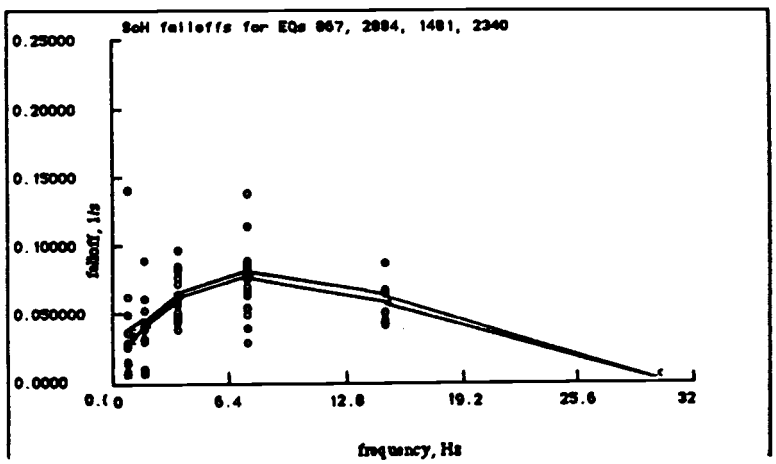

Figure 58. Falloff rate versus frequency for Kuril to Kamchatka earthquakes recorded by the sea floor hydrophones of the Wake array. Top) P phases (crosses). Middle) P_{oH} phases (crosses). Bottom) S_{oH} phases (circles). The standard error of the mean are denoted with solid lines.

falloff value characteristics more related to deeper (inner trench, Figures 59 and 60) EQs. Because they both have normal (fixed) depths, it is likely that they have deeper origins, as indicated by their falloff values. Thus the falloff values indicate the the epicenters for these EQs were inaccurately determined.

Five EQs with epicenters in the Sea of Okhotsk (2492, 319, 2477, 2645, and 2566) were recorded. Each of these EQs has different P, P_{oL}, P_{oH}, and S_{oH} APVEL characteristics. They all had clear P phases and two (319 and 2566) had P_{oL} phases as well. These P_{oL} average APVELs were abnormally low, 7.6 ± 0.01 km/s (319) and 8.21 ± 0.04 km/s (2566). Only one (2566) had a clear P_{oH} phase with a low phase APVEL of 7.96 ± 0.01 km/s. Two (EQs 2566 and 2654) had visible S_{oH} phases, both with a high S_{oH} APVEL average of 4.88 ± 0.01 km/s. The average falloff values for the Okhotsk EQs are shown in Figure 60. Their average falloff values are lower and more constant between frequency bands than those of the shallower (outer trench) EQs.

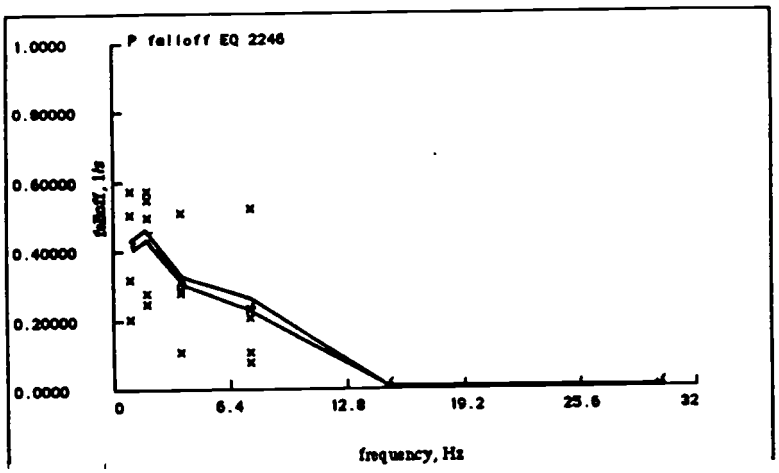

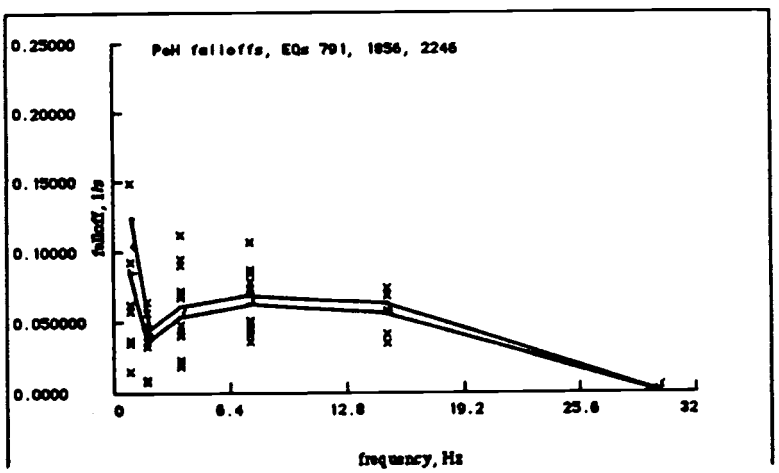

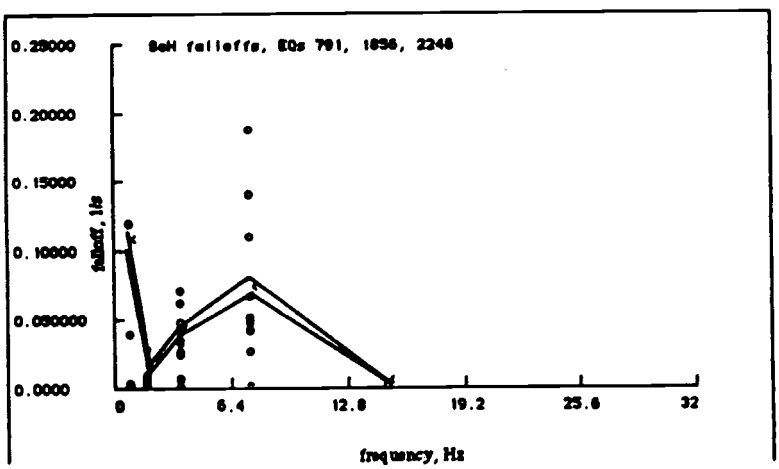

Figure 39. Falloff rate versus frequency for deeper Hokkaido earthquakes at the junction of the Japan and Kuril trenches recorded by the sea floor hydrophones of the Wake array. Top) P phases (crosses). Middle) P_{oH} phases (crosses). Bottom) S_{oH} phases (circles). The standard error of the mean are denoted with solid lines.

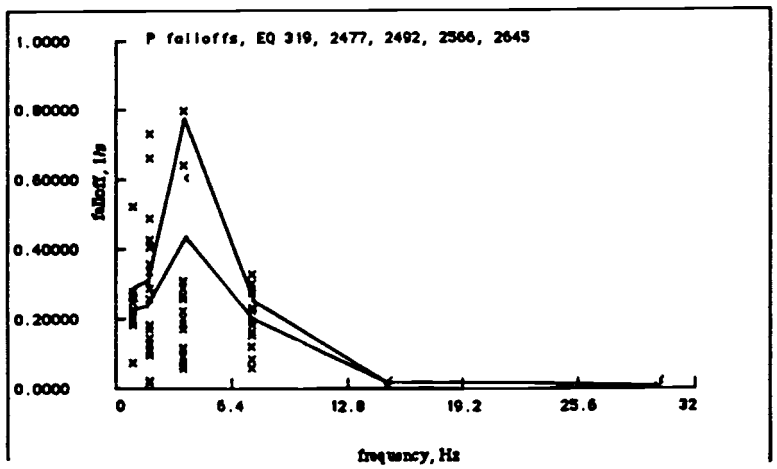

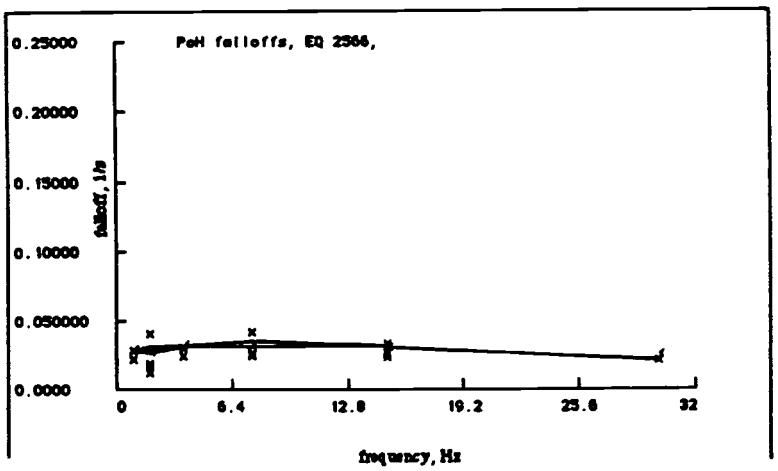

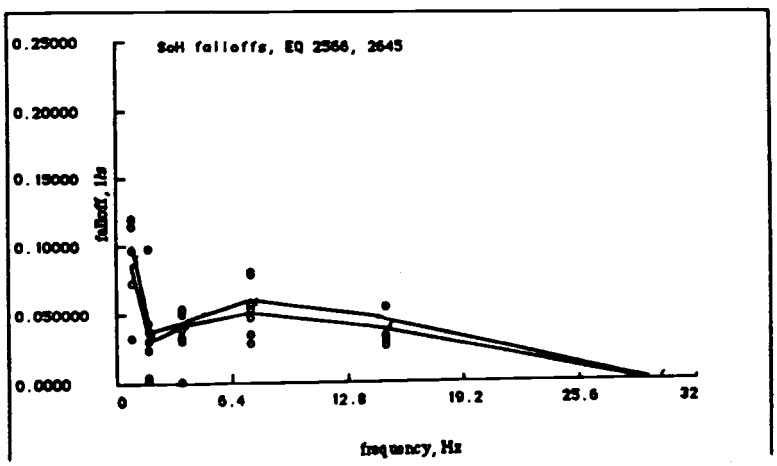

Figure 60. Falloff rate versus frequency for Sea of Okhotsk earthquakes recorded by the sea floor hydrophones of the Wake array. Top) P phases (crosses). Middle) P_{oH} phases (crosses). Bottom) S_{oH} phases (circles). The standard error of the mean are denoted with solid lines.

PACIFIC NORTHWEST BASIN FALLOFF MEASUREMENTS:

Twelve EQs, with epicentral range 8 - 22°, were recorded at the Pacific Northwest Basin seismic array by two OSU OBS's (Figures 10 and 12). Their average P_o and S_o APVELs, on the vertical component, are 8.35 ± 0.06 km/s and 4.69 ± 0.04 km/s respectively (Figure 61). This average P_o APVEL is higher than for both other data sets whereas the average S_o APVEL is equal to that found for the Philippine Sea data set.

Average P_o falloffs, as measured by the vertical geophone and hydrophone, are similar to one another (Figures 62 and 63, top), but the average S_o falloffs for the Pacific Northwest Basin data are significiantly higher on the vertical component than on the hydrophone (Figures 62 and 63, bottom). The average hydrophone P_o falloffs (Figure 63) are similar to the average Wake P_o falloffs (Figure 44) in the first four bands (up to about 15 Hz) and slightly higher than the Wake P_o falloffs in the highest two bands. Average S_o falloffs are significiantly higher on the Pacific Northwest Basin hydrophones than the Wake hydrophones.

EQs 7, 9, 10, 11, and 13 all occurred within the same area in the southern part of the Kurile trench at epicentral distance of about 8°. The S_o/P_oratios, for these EQs, on the hydrophone and vertical component at station 3, are 1.3 - 1.4 and 1.5 - 2.2 respectively, in the two middle frequencies. Their average P_o and S_o falloffs are lower than for Philippine EQs at the same range (Figures 64 and 65) and their falloff average ratios between the vertical component and the hydrophone (Figures 66 and 67) on station 3 ($P_o v/P_o hy$ and $S_o v/S_o hy$) in the two middle frequencies are 1.4 - 1.5 and 1.6 - 2.5 respectively.

EQ 27 (Figure 3) has the greatest epicentral distance (21°) and depth of EQs recorded at the Pacific Northwest Basin array. Its hypocenter is at a depth of 155 km in the Izu subduction zone. The $P_o v/P_o hy$ and $S_o v/S_o hy$ ratios for EQ 27 are 2.1 - 2.8 and 1.4 - 1.6 in the middle two frequencies. Its vertical component falloff values are exceptionally low (Figure 68) which can best be seen by comparing it to the average falloff rate of Wake recorded EQs at epicentral distances of 20 - 22° (Figure 69). The $P_o v/P_o hy$ and $S_o v/S_o hy$ ratios for EQ 27 are 2.1 - 2.8 and 1.4 - 1.6.

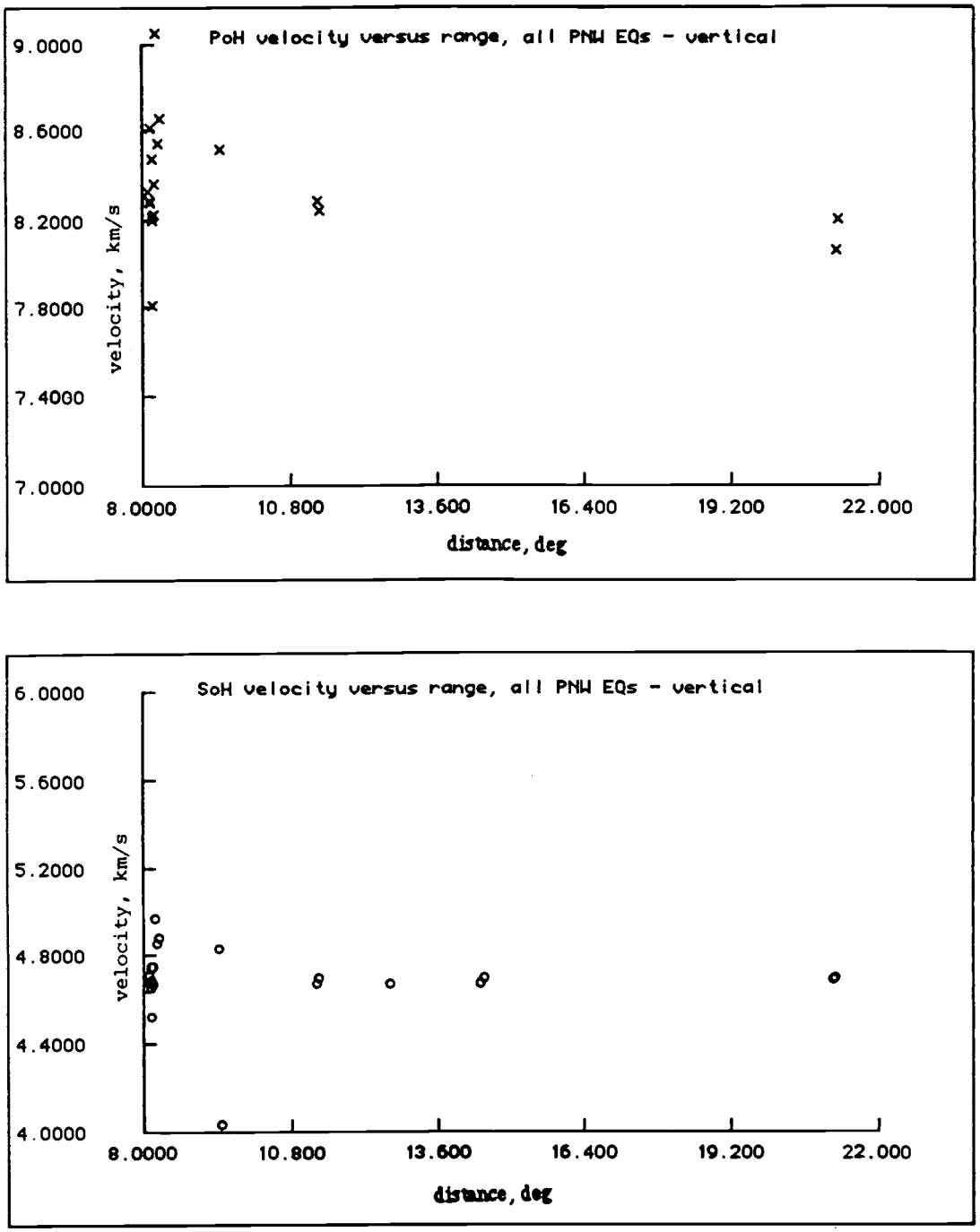

Figure 61. Apparent velocity of the P_0 phase and S_0 phase onset versus distance for the vertical component of the Northwest Pacific Basin data set. Top) P_0 phases. Bottom) S_0 phases.

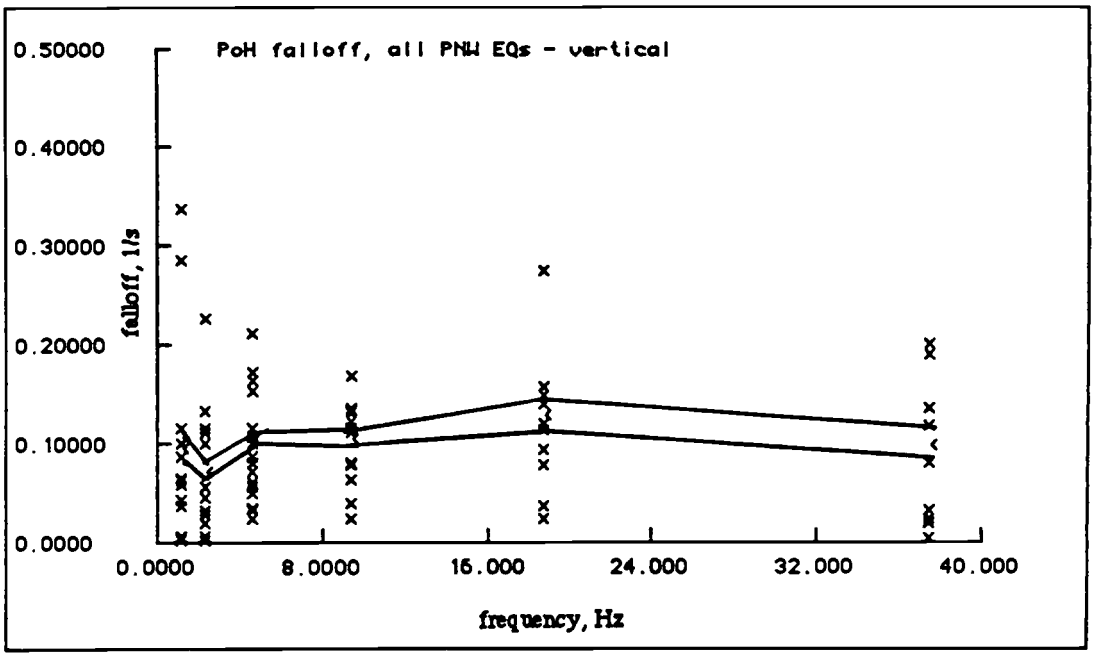

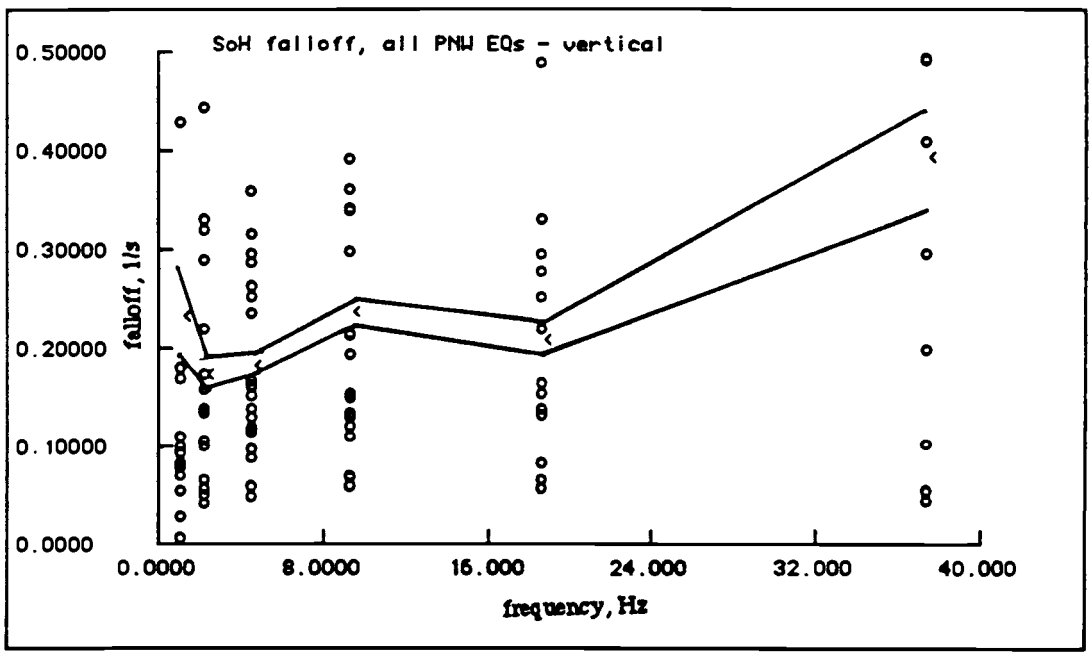

Figure 62. Falloff rate versus frequency for all Northwest Pacific Basin earthquakes recorded by the vertical geophone component. Top) P_0 phases (crosses). Bottom) S_0 phases (circles). The standard error of the mean are denoted with solid lines.

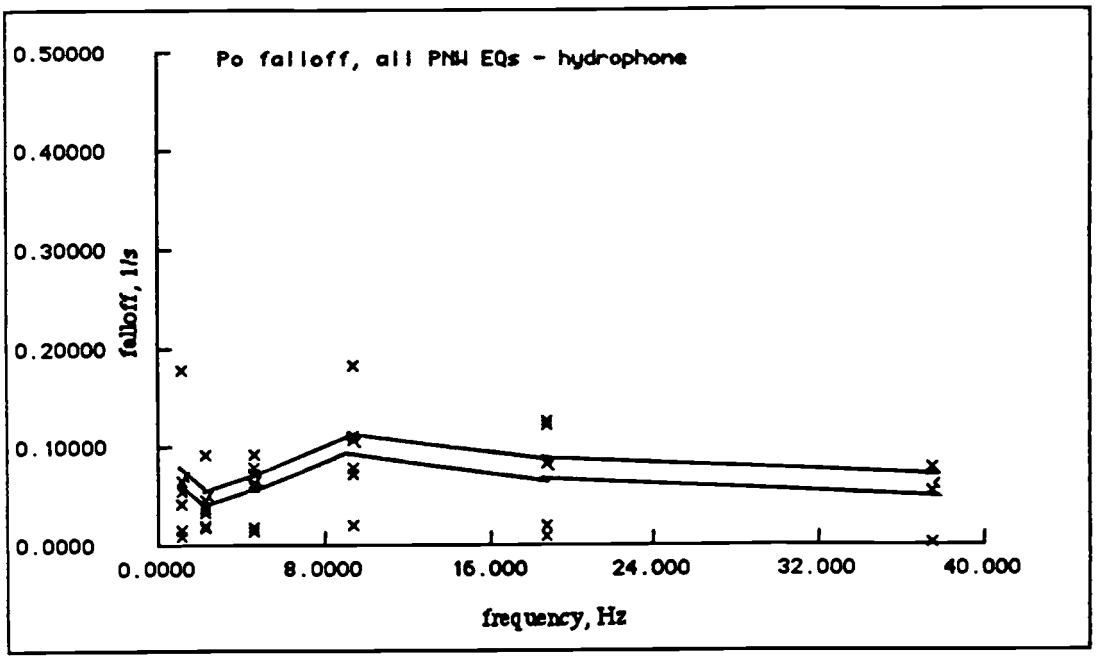

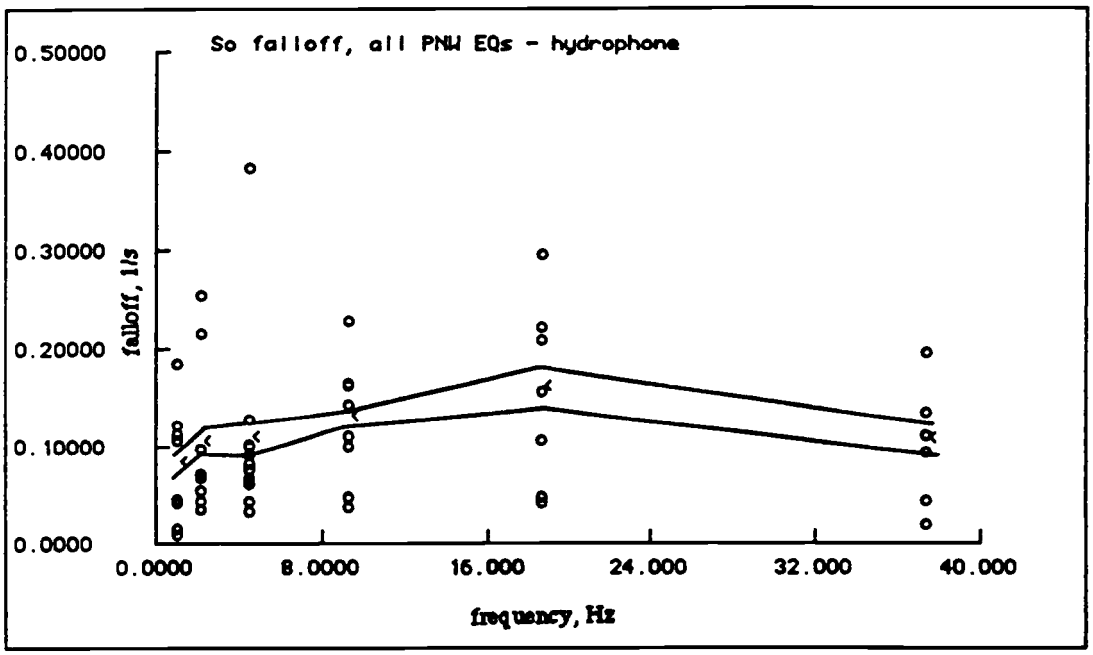

Figure 63. Falloff rate versus frequency for all Northwest Pacific Basin earthquakes recorded by hydrophones. Top) P_O phases (crosses). Bottom) S_O phases (circles). The standard error of the mean are denoted with solid lines.

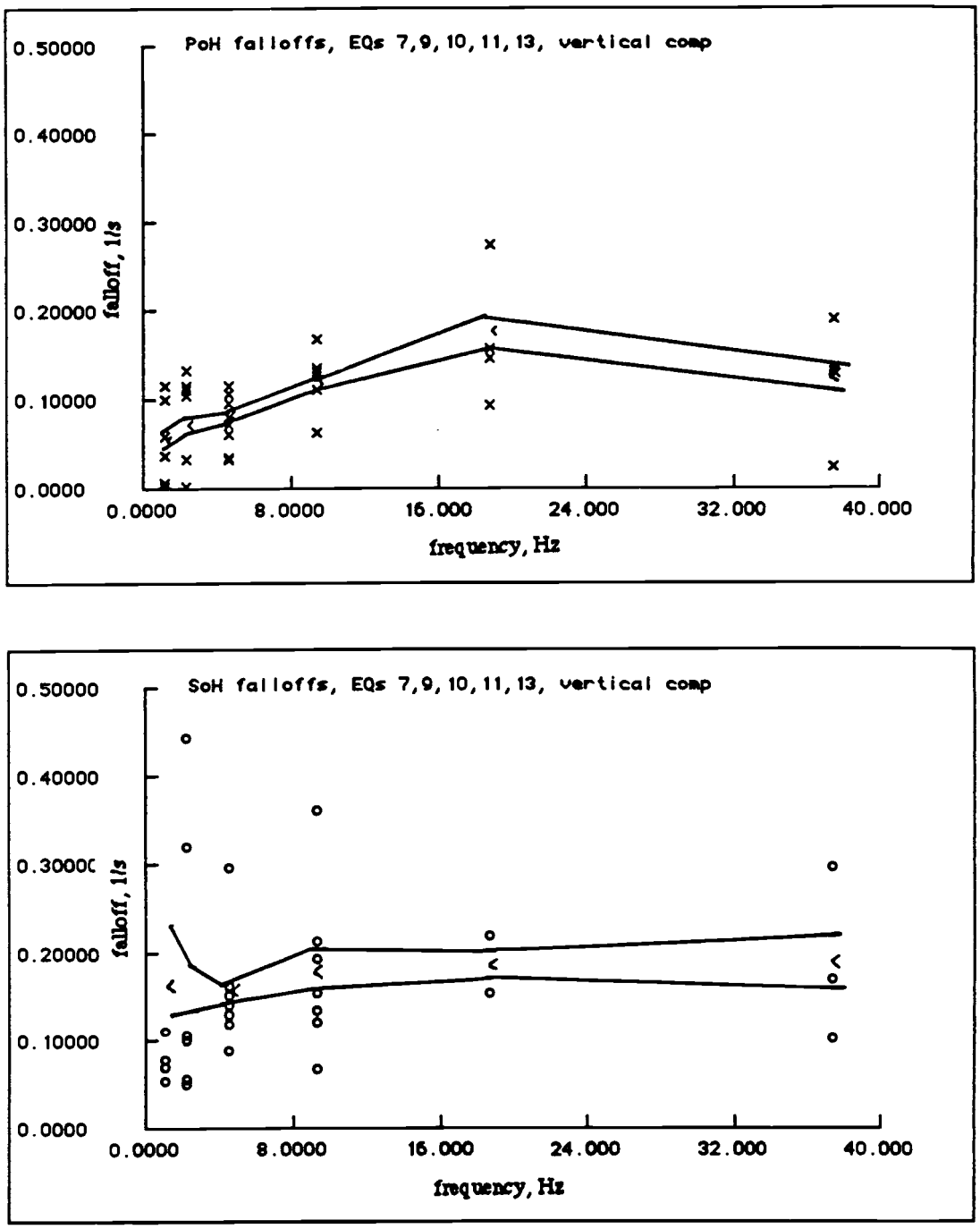

Figure 64. Falloff rate versus frequency for Northwest Pacific Basin earthquakes 7, 9, 10, 11, and 13, recorded by the vertical geophone component. Top) P_0 phases (crosses). Bottom) S_0 phases (circles). The standard error of the mean are denoted with solid lines.

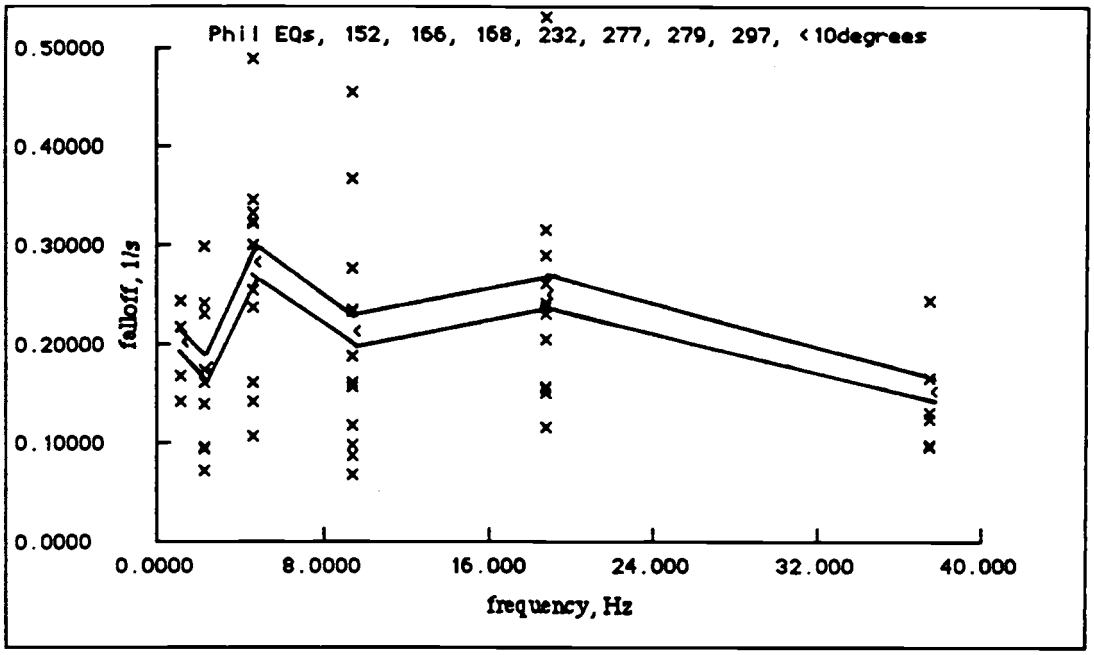

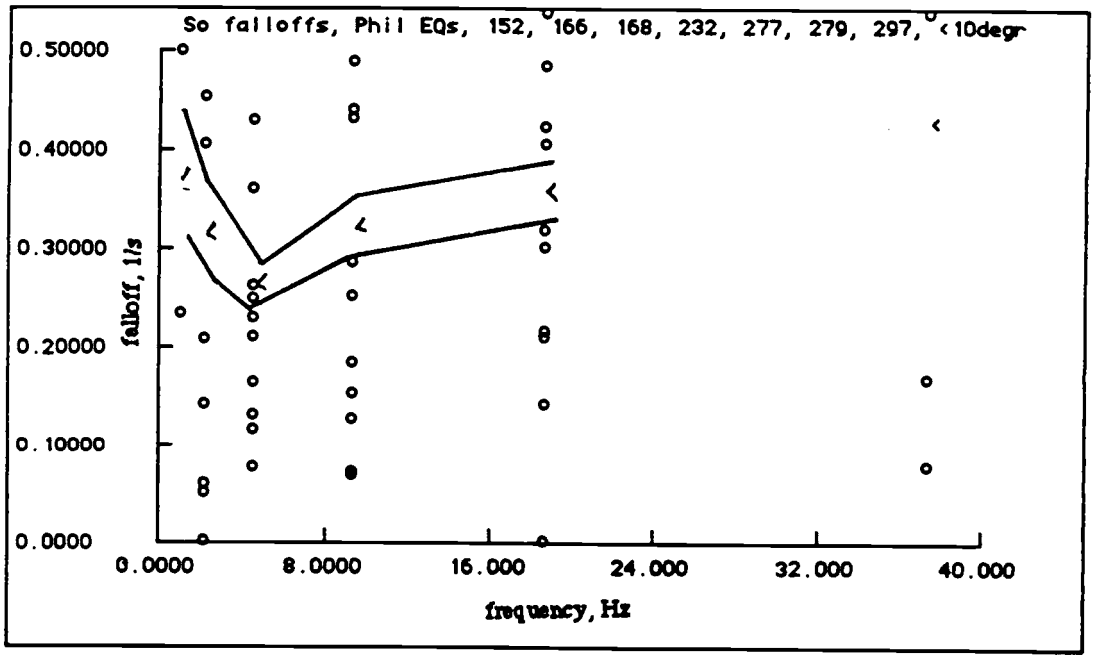

Figure 65. Falloff rate versus frequency for all Philippine Sea earthquakes that have epicentral distance less than 10°, recorded by the vertical geophone component. Top) P_0 phases (crosses). Bottom) S_0 phases (circles). The standard error of the mean are denoted with solid lines.

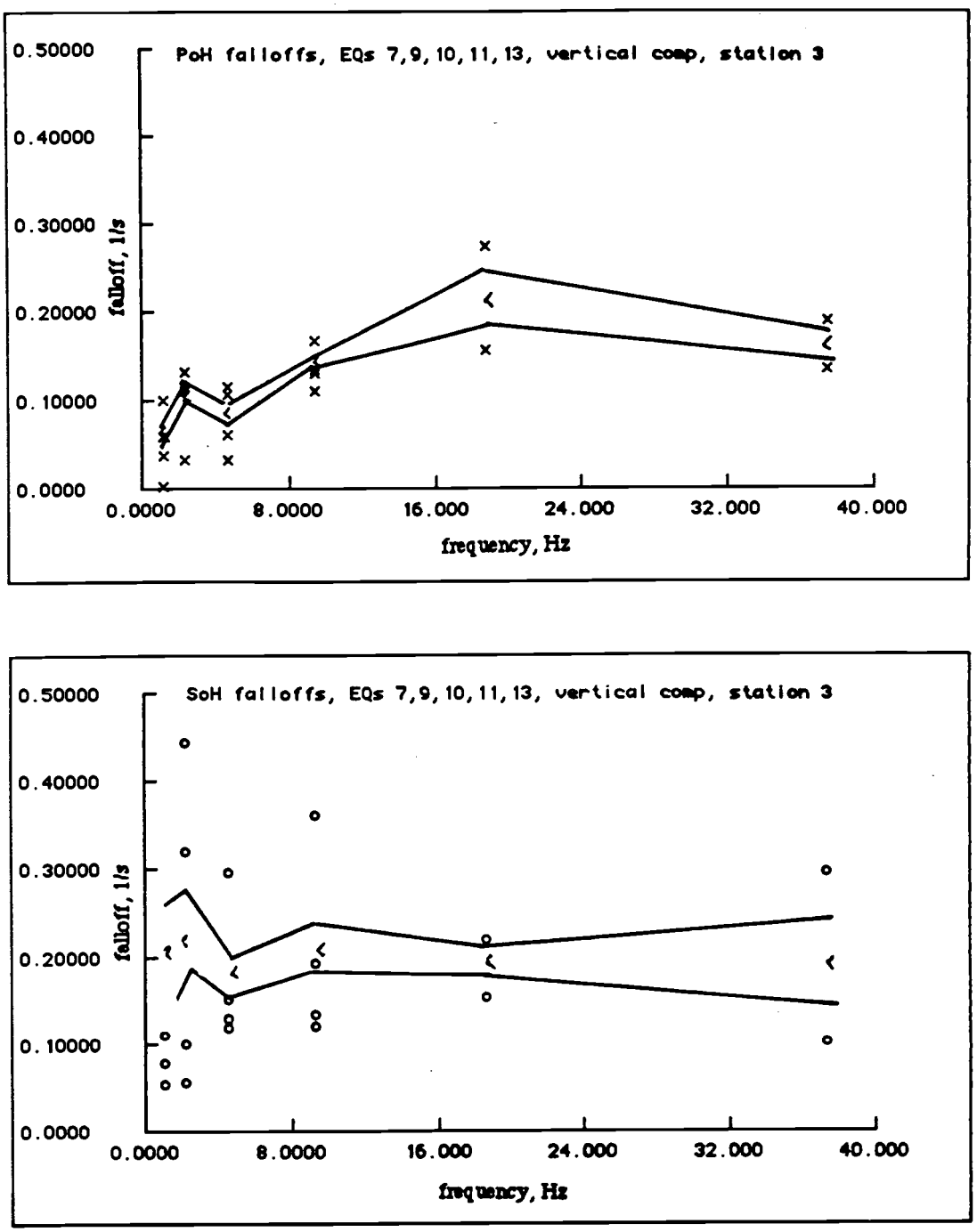

Figure 66. Falloff rate versus frequency for Northwest Pacific Basin earthquakes 7, 9, 10, 11, and 13, recorded by the vertical geophone component at station 3. Top) P_0 phases (crosses). Bottom) S_0 phases (circles). The standard error of the mean are denoted with solid lines.

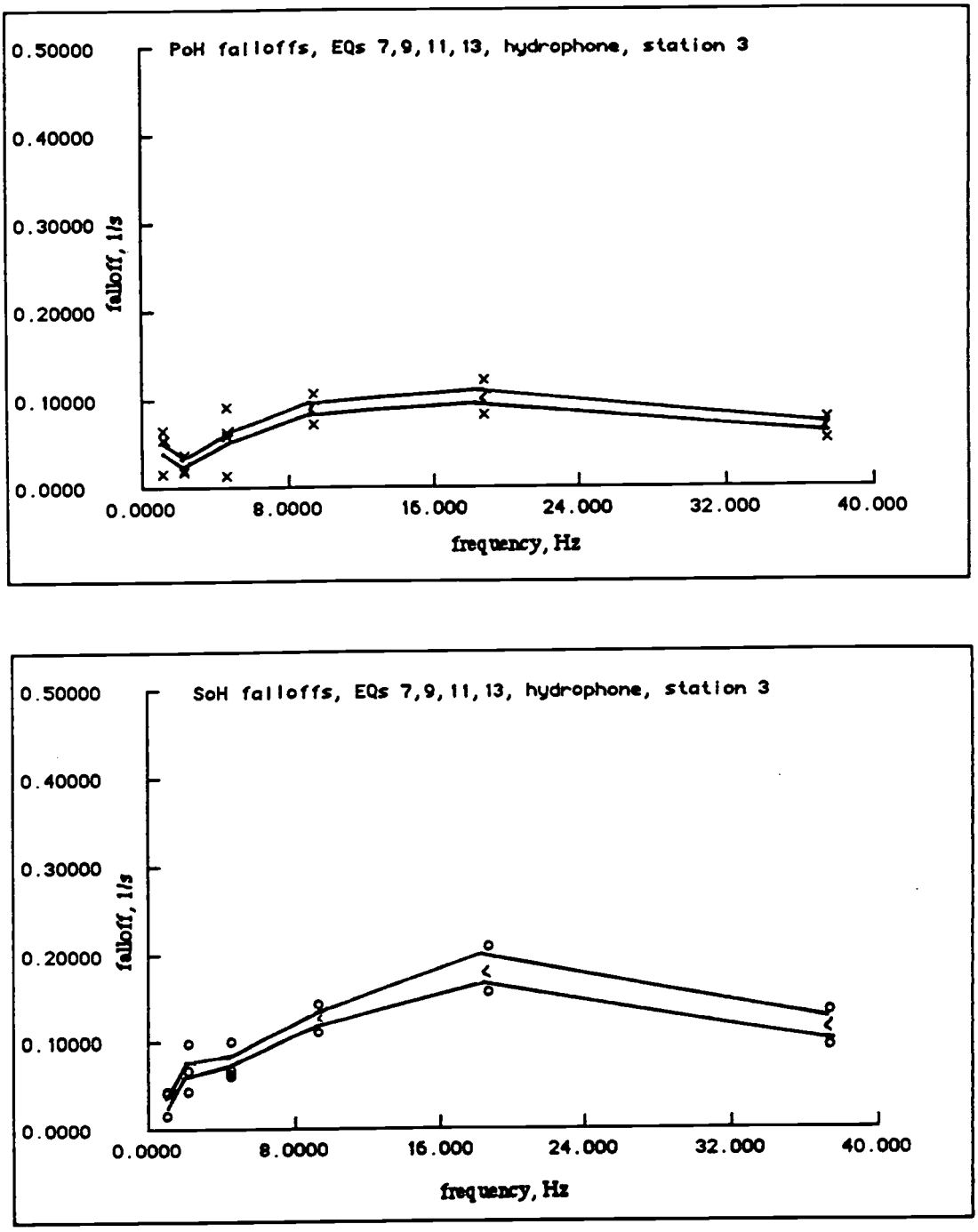

Figure 67. Falloff rate versus frequency for Northwest Pacific Basin earthquakes 7, 9, 10, 11, and 13, recorded by the hydrophone at station 3. Top) P_O phases (crosses). Bottom) S_O phases (circles). The standard error of the mean are denoted with solid lines.

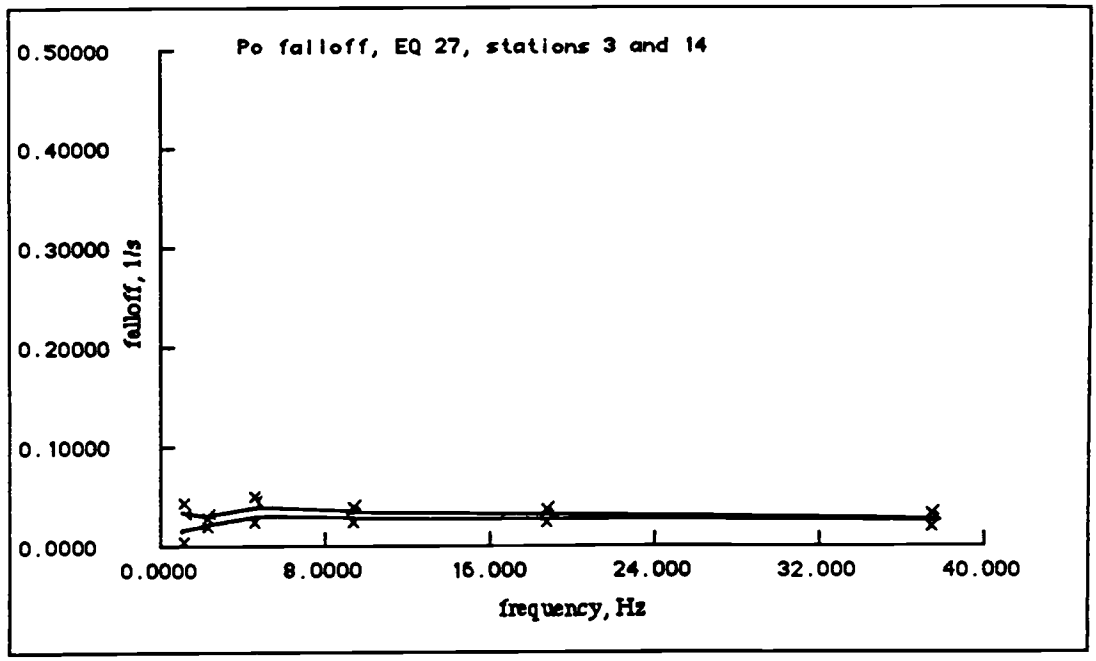

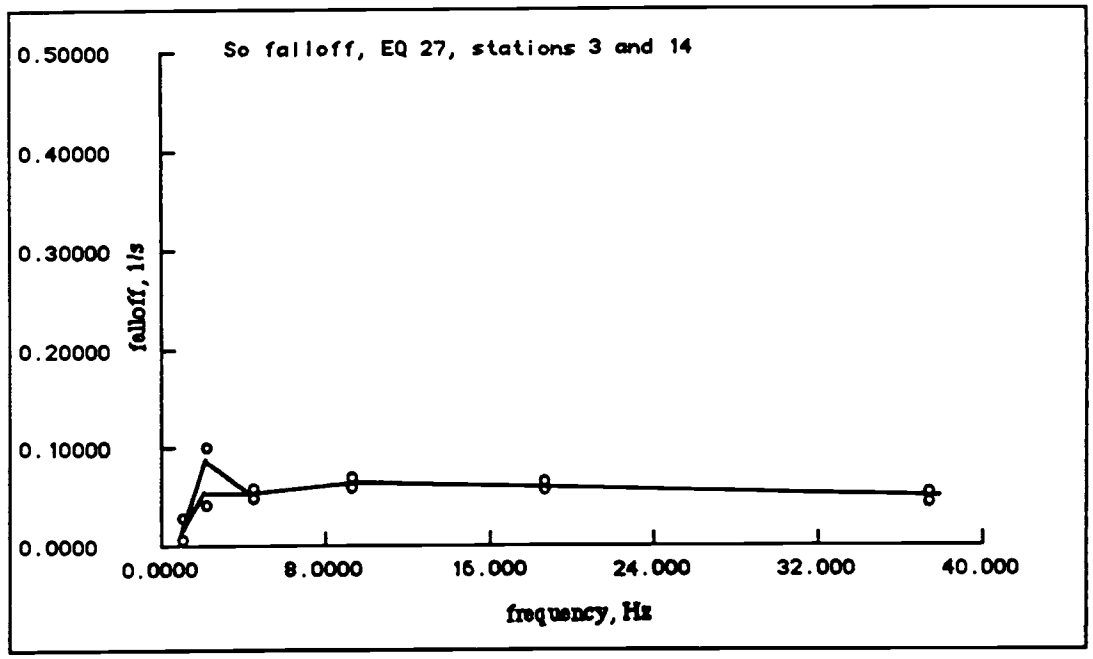

Figure 68. Falloff rate versus frequency for Northwest Pacific Basin earthquake 27 (Figure 3) recorded at stations 3 and 14. Top) P_0 phases (crosses). Bottom) S_0 phases (circles). The standard error of the mean are denoted with solid lines.

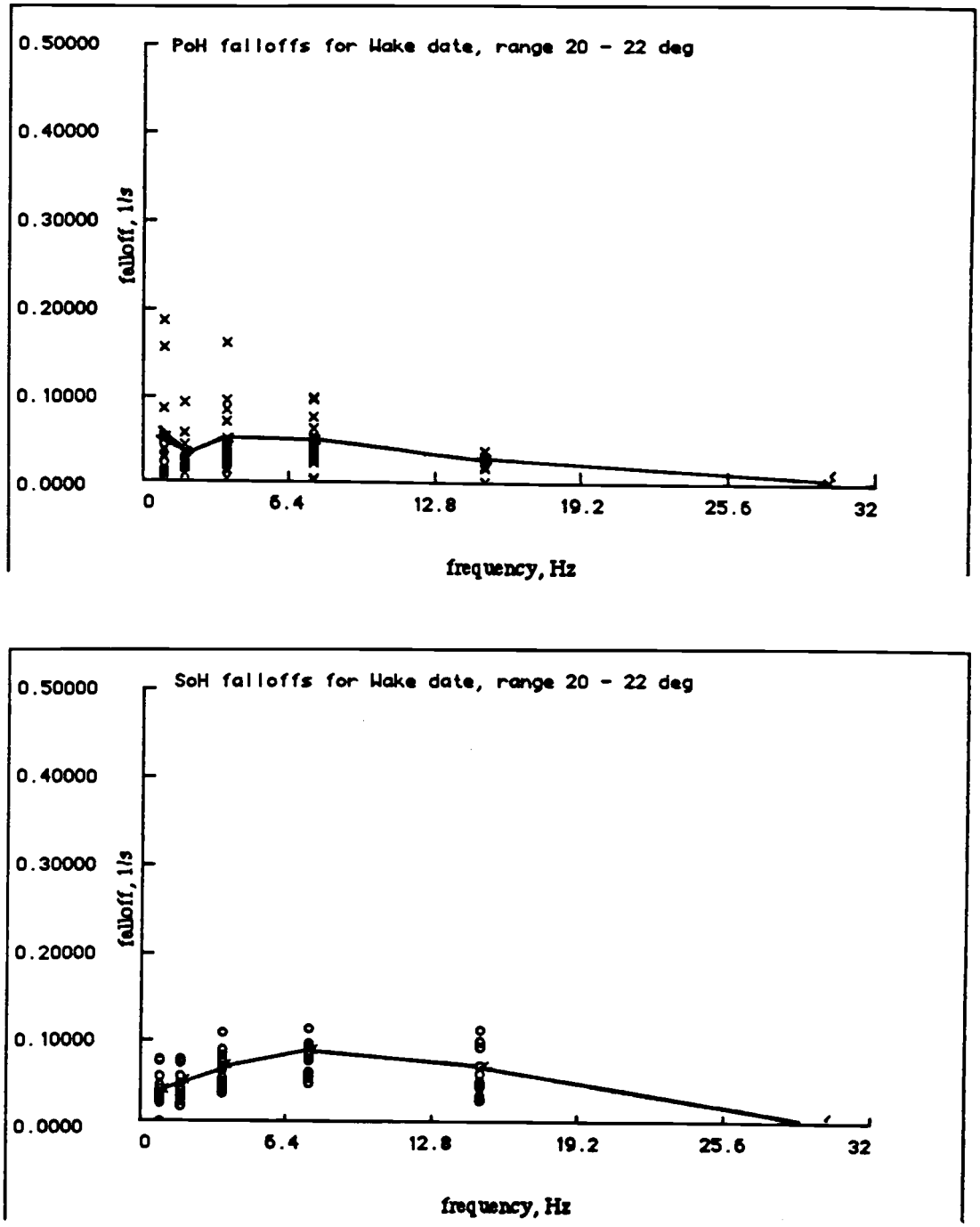

Figure 69. Falloff rate versus frequency for Wake earthquakes with epicentral distance from 20 to 22°. Top) P_0 phases (crosses). Bottom) S_0 phases (circles). The standard error of the mean are denoted with solid lines.

CONCLUSIONS:

We undertook a study of coda falloff rates of 93 Northwest Pacific Basin and Philippine Sea earthquakes recorded on analog and digital instruments. The P, P_O and S_O coda falloff rates exhibit a systematic pattern, dependent on frequency, epicentral range, depth of focus, and age of raypath.

1. The P_O and S_O falloff rates are significantly lower than that of the P wave. The P/P_{OH} falloff ratio for earthquakes recorded by the Wake hydrophone array is approximately 4.0. This high ratio emphasizes the different propagation nature of these two phases.

2. Both the P_O and S_O falloff rates vary systematically with frequency. The lowest frequencies (0.8 - 3.1 Hz) have the minimum decay rate for both the P_O and S_O phases (unless they are contaminated by low frequency P and S phases which can occur over shorter ranges). The highest P_O average falloff rates occur in the mid-frequency range, 3.1 - 12.5 Hz, with the position of the maximum varying somewhat from earthquake to earthquake. Average falloff rates are most difficult to measure in the highest frequency bands (12.5 - 50 Hz) because the signal/noise ratio is lowest there. Where measurable, they give average falloff rates that are intermediate between those of the lowest and middle frequencies. The variation in falloff between earthquakes is very large, with the trends only becoming apparent after averaging many measurements. The strong increase in falloff rates at about 3 Hz may be associated with a decrease in the number of scatterers having scale lengths of about one half the wavelength of a 3 Hz compressional wave, that is, about 1.3 km.

3. There is a significant difference in falloff rates of P_O and S_O in measurements made with geophones. The S_O/P_O falloff ratio for earthquakes recorded by geophones is 1.7 - 2.0. This falloff ratio is consistent with the rate of falloff of the coda being

dominated by frictional attenuation. An attenuating medium that has all its losses confined to shear and none to pure compression - as is typically the case for rocks - has higher shear wave attenuation than compressional wave attenuation, with the ratio of quality factors being $Q_S^{-1}/Q_P^{-1} = 3\alpha^2/4\beta^2$ (Aki and Richards, 1980). Here α and β are the two wave speeds and the quality factor, Q, is the fractional loss of energy per wavelength. Average apparent velocities (X/T) for the P_o and S_o waves are 8.1 km/s and 4.7 km/s, respectively. Therefore, $3\alpha^2/4\beta^2 = 2.23$, predicting a falloff rate of 2.23, close to the observed amount.

If we ascribe all the coda decay to attenuation, then we can estimate the amount of attenuation using the rule $\exp(-\gamma t) = \exp(-2\pi f t/Q)$. For our Wake data the average falloff (γ) for P_o phases is approximately 0.05 1/s, at f= 10 Hz. Substituting this information into the attenuation formula we get $Q \approx 1250$, which is a reasonable number for the compressional wave quality factor in rocks. However, the fact that the falloff rate is fairly constant in the frequency range 5 - 30 Hz but varies strongly with propagation distance, both of which contradict the rule $\exp(-2\pi f t/Q)$, suggests that attenuation cannot be the only phenomenon determining the falloff rate of the coda. A completely different explanation for the observed S_o/P_o falloff ratio involves the presence of the water column. Since only compressional waves propagate in liquids, it is possible that the lower P_o falloff rates are caused by reverberations of compressional waves in the relatively low velocity (1.5 km/s) water column.

4. There are low falloff rates for S_o in measurements made with hydrophones.

The S_{oH}/P_{oH} falloff ratio for earthquakes recorded by the Wake hydrophone array is 0.8 - 1.1, a factor of two lower than the geophone measurements. Average apparent velocities for P_o and S_o phases recorded by the Wake array are 8.2 km/s and 4.8 km/s, respectively. Thus $3\alpha^2/4\beta^2 = 2.19$, so the difference cannot be ascribed to a different Q_S^{-1}/Q_P^{-1}. The difference in ratios is most likely due to differences in the manner in which geophones and hydrophones record the S_o phase. Hydrophones are pressure sensitive devices located in the water column a few meters above the ocean bottom so, unlike the geophones, they do not measure shear waves directly. Instead hydrophones measure compressional waves in the water that result from conversion of

shear waves at or below the sea-floor. This conversion process is complex, and depends upon the angle of incidence of the rays that comprise the S_0 phase. The angle of incidence probably decreases with time into the coda, leading to different falloff rates as measured by the different types of instruments. This conclusion is indirectly supported by the observation that the amplitude of the S_0 phase observed with hydrophones often increases with frequency more strongly than the amplitude of P_0 (see, for instance, Figures 39 and 40), which is also most easily explained by (in this case) a frequency-dependent wave-conversion process.

5. P_0 falloff rates decrease with epicentral range. The average falloff rates of the Northwest Pacific Basin data set, with ranges of 8 - 21°, are 20 - 30% higher than those of the Wake data set, with ranges of 20 - 35°. The fact that both the data sets have raypaths trough the Cretaceous and Jurassic Northwest Pacific lithosphere indicates that the difference in observed falloff rates may be due to increased scattering with length of propagation path. The scattering that produces the coda is thus not concentrated in the source region but distributed along the propagation path. A decrease in falloff with range has also been noted by Menke and Chen (1984), who studied forward scattering in plane layers and found $\gamma \propto x^{-3/2}$, where x is epicentral range. The $x^{-3/2}$ dependence would imply a ratio of about 4 for the Pacific Northwest Basin and Wake data sets, higher than what is observed.

6. Earthquakes with 100 - 300 km deep hypocenters have systematically lower P_0 falloff values than shallow (< 100 km deep) earthquakes. The effect is seen in outer trench/inner trench EQs recorded by the Wake array, where the inner trench (deeper) EQ have lower falloff values than the outer (shallower) EQs. This difference indicates that significant scattering is occuring within (or near) the deeply buried part of the subducting plate. There is some indication (though it is not statistically significant because of uncertainties in earthquake location) that rays that travel obliquely up the slap have lower falloff than those that travel straight up the slab.

7. The falloff rates of both P_0 and S_0 measured in the Philippine Sea and Pacific Northwest Basin (both with epicentral ranges of about 8 - 12 deg) are significantly different. The P_0 falloff rate for Band 4 (10 Hz) is 0.143 ± 0.013 1/s for the Philippine Sea, whereas it is 0.096 ± 0.011 1/s for the Pacific Northwest Basin. Likewise the S_0 falloff rate for Band 4 (10 Hz) is 0.302 ± 0.033 1/s for the Philippine Sea, whereas it is 0.220 ± 0.035 1/s for the Pacific Northwest Basin. The difference may be due to the different average ages of the lithospheres in these two geographical areas. The Pacific Northwest Basin crust is of Cretaceous and Jurassic age whereas the Philippine crust is of Tertiary age. Average apparent P_0 velocities recorded by the Northwest Pacific Basin and Wake arrays are higher than recorded from the Philippine Sea. Oceanic crust thickens with age, and presuming that thinner (younger) crust has less heterogeneities than thicker (more hydothermally altered?) crust we can explain the higher falloff values in the Philippine Sea as due to fewer heterogeneities and less scattering.

8. There is a systematic variation in the position of the maximum of the coda with frequency for the Philippine Sea events. The peak in the low-frequency (0.8 - 3.1 Hz) coda occurs 60 - 100 s after the peak of the high-frequency (50 - 100 Hz) coda. This 'reverse-dispersion' may be due to a correlation between attenuation and velocity in the lithosphere (that is, a high-attenuation, low-velocity crust and a low-attenuation, high-velocity mantle). The low-frequency coda will then contain mostly crustal rays, which have propagated at lower speeds.

BIBLIOGRAPHY:

Aki, K., and B. Chouet, Origin of coda waves: Source, attenuation, and scattering effects, *J. Geophys. Res.*, 80, 3322 - 3342, 1975.

Aki, K., and P. G. Richards, *Quantitative Seismology: Theory and results, Volume 1,* 557pp, 1980.

Asada, T., and H. Shimamura, Observation of earthquakes and explosions at the bottom of the western Pacific: Structure of oceanic lithosphere revealed by Longshot experiment, in; *The geophysics of the Pacific Ocean Basin; Geophys. Monogr. Ser.*, 19, 135 - 153, 1976

Båth, M., Propagation of S_n and P_n to teleseismic distances, *P. and Appl. Geophysics,* 64, 19 - 30, 1966.

Bée, M., A comparison of seismic properties of young and mature oceanic crust, *Ph.D. Thesis, Oregon State University,* 183 pp, 1984.

Black, P.R., and L.W. Braile, P_n velocity and cooling of the continental lithosphere, *J. Geophys. Res.*, 87, 10.557 - 10.568, 1982.

Butler, R., Anisotropic propagation of P and S waves in the western Pacific lithosphere, *J. Geophys. J. R. astr. Soc.*, 81, 89 - 101, 1985.

Creager, K. C. and T. H. Jordan, Slab penetration into the lower mantle beneath the Mariana and other island arcs of the Northwest Pacific, *J. Geophys. Res.*, 91, 3573 - 3589, 1986.

Fedotov, S. A., The absorption of transverse seismic waves in the upper mantle and energy classification of near earthquakes of intermediate focal depth , *IZV. Geophys. Ser.*, 829 - 849, 1963.

Fedotov, S. A., and L. B. Slavina, An estimate of the longitudinal-wave velocities in the upper mantle under the northwestern part of the Pacific Ocean and Kamchatka, *IZV. Earth Physics,* 2, 8 - 31, 1968.

Fuchs, K., and K. Schulz, Tunneling of low-frequency waves through the subcrustal lithosphere, *J. Geophys.*, 42, 175 - 190, 1976.

Gettrust, J. F., and L.N. Frazer, A computer model study of the propagation of the long-range Pn phase, *Geophys. Res. Lett.*, 8, 749 - 752, 1981.

Goodman, D., Seismic refraction survey of crustal and upper mantle structures in the west Philippine basin, *M.S. Thesis, Oregon State University,* 122pp, 1983.

Hamilton, W., Tectonics of the Indonesian region, *U. S. Geol.Surve.Prof. Pap.,* 1078, 345 pp, 1979.

Hart, R.S., and F. Press, S_n velocities and the composition of the lithosphere in the regionalized Atlantic, *J. Geoph. Res.,* 78, 407 - 411, 1973.

Hatherton, T., and W. R. Dickinson, The relationship between andesitic volcanism and seismicity in Indonesia, the Lesser Antilles, and other island arcs, *J. Geoph. Res.,* 74, 5301 - 5310, 1969.

Herrin, E., and J. Taggart, Regional variations in P_n velocity and their effect on the location of epicenters, *Bull. Seism. Soc. of Am.,* 52, 1037 - 1046, 1962.

Huestis, S., P. Molnar, and J. Oliver, Regional S_n velocities and shear velocity in the upper mantle, *Bull. Seism. Soc. Am.,* 63, 469 - 475, 1973.

Kanamori, H., Seismic and aseismic slip along subduction zones and their tectonic implications, in; *Island arcs, deep sea trenches and back-arc basins, Maurice Ewing Ser.,* 1, 163 - 174, 1977.

Karig, D. E., Origin and development of marginal basins in the western Pacific, *J. Geoph. Res.,* 76, 2542 - 2561, 1971.

Katsumata, M., and L.R. Sykes, Seismicity and tectonics of the western Pacific: Izu - Mariana - Caroline and Ryukyu - Taiwan regions, *J. Geoph. Res.,* 75, 5923 - 5948, 1969.

LaTraille, S.L., J.F. Gettrust, and M.E. Simpson, The ROSE seismic data storage and exchange facility, *J. Geoph. Res.,* 87, 8359 - 8363, 1982.

Lee, C. S., G. G. Shor, Jr., L. D. Bibee, R. S. Lu, and T. W. C. Hilde, Okinawa trough: Origin of a back-arc basin, *Marine Geology,* 35, 219 - 241, 1980.

Linehan, D., Earthquakes in the West Indian Region, *Trans. Am. Geophys. Union,* 21, 229 - 232, 1940.

Louden, K. E., Magnetic anomalies in the West Philippine Basin, in; *The geophysics of the Pacific Ocean Basin and its Margin, Geophys. Monogr. Ser.,* 19, 253 - 267, 1976.

Mantovani, E., F. Schwab, H. Liao, and L. Knopff, Teleseismic S_n: a guided wave in the mantle, *Geophys. J. R. Astr. Soc.,* 51, 709 - 726, 1977.

McCreery, C.S., High-frequency P_n, S_n phases recorded by ocean bottom seismometers on the Cocos plate, *Geophys. Res. Lett.,* 8, 489 - 492, 1981.

McCreery, C.S., The continuous digital data collection system for the Wake Island hydrophones, *HIG report,* 25 pp, no date.

Menke, W.H., and P.G. Richards, Crust mantle whispering gallery phases: A deterministic model of teleseismic P_n wave propagation, *J. Geophys. Res.,* 85, 5416 - 5422, 1980.

Menke, W.H., and P.G. Richards, The horizontal propagation of P waves through scattering media: analog model studies relevant to long range P_n propagation, *Bull. Seism. Soc. Am.,* 73, 125 - 142, 1983.

Menke, W. H., and R. Chen, Numerical studies of the coda falloff rate of multiply-scattered waves in randomly layered media, *Bull. Seism. Soc. Am.,* 74, 1605 - 1621, 1984.

Menke, W. H., *Geophysical data analyses: Discrete inverse theory,* 260 pp, 1984.

Mitronovas, W., B. Isacks, and W. Seeber, Earthquake locations and seismic wave propagation in the upper 250 km of the Tonga island arc, *Bull. Seism. Soc. Am.,* 59, 1115 - 1135, 1969.

Molnar, P., and J. Oliver, Lateral variations of attenuation in the upper mantle and discontinuities in the lithosphere, *J. Geophys. Res.,* 74, 2648 - 2682, 1969.

Novelo-Casanova, D. A., and R. Butler, High-frequency seismic coda and scattering in the northwest Pacific, *Bull. Seism. Soc. Am.,* 76, 617 - 626, 1986.

Oliver, J., and B. Isacks, Deep earthquake zones: Anomalous structures in the upper mantle, and the lithosphere, *J. Geophys, Res.,* 72, 4259 - 4275, 1967.

Ouchi, J., Spectral studies of high frequency P and S phases observed by OBS's in the Mariana Basin, *J. Phys. Earth,* 29, 305 - 326, 1981.

Ouchi, T., S. Nagumo, J. Kasahara, and S. Koresawa, Separation of high-frequency P_n phases and mantle refracted P phases at distances between 6° and 18° in the western Pacific by ocean bottom seismograph array, *Geoph. Res. Lett.*, 10, 1069 - 1072, 1983.

Press, F., and M.Ewing, Waves with P_n and S_n velocity at great distances, *Proc. Natl. Acad. Sci. U.S.*, 41, 24 - 27, 1955.

Richards, P. G., and W. H. Menke, The apparent attenuation of a scattering medium, *Bull. Seism. Soc. Am.*, 73, 1005 - 1021, 1983.

Roecker, S. W., Velocity structure in the Izu-Bonin seismic zone and the depth of the Olivine-Spinel transition in the slab, *J. Geophys. Res.*, 90, 7771 - 7794, 1985.

Samowitz, I. R., and D. W. Forsyth, Double seismic zone in the Mariana island arc, *J. Geophys. Res.*, 86, 7013 - 7021, 1981.

Sato, H., Attenuation and envelope formation of three-component seismograms of small local earthquakes in randomly inhomogeneous lithosphere *J. Geophys. Res.*, 89, 1221 - 1241, 1984.

Sereno, T.J., and J.A. Orcutt, Synthesis of realistic oceanic P_n wave trains, *J. Geophys. Res.*, 90, 12.755 - 12.776, 1985.

Shimamura, H., Anisotropy in the oceanic lithosphere of the northwestern Pacific Basin, *Geophys. J. R. astr. Soc.*, 76, 253 - 260, 1984.

Shurbet, D.H., The high frequency P and S phases from the West Indies, *Bull. Seism. Soc Am.*, 52, 957 - 962, 1962.

Shurbet, D. H., The high frequency S phase and the structure of the upper mantle, *J. Geophys. Res.*, 69, 2065 - 2070, 1964.

Silver, E. A., and J. C. Moore, The Molucca Sea collision zone, Indonesia, *J. Geophys. Res.*, 83, 1681 - 1691, 1978.

Solano-Borrego, A.E., Crustal structure and seismicity of the Gorda Ridge, *Ph.D. thesis, Oregon State University,* 185 pp, 1984.

Stephens, C., and B.L. Isacks, Toward an understanding of S_n: Normal modes of Love waves in an oceanic structure, *Bull. Seism. Soc. Am.*, 67, 69 - 78, 1977.

Sutton , G.H., and D.A. Walker, Oceanic mantle phases recorded on seismographs in the northwestern Pacific at distances between 7° and 40°, Bull. Seism. Soc. *Am.*, 62, 631 - 655, 1972.

Sutton, G.H., C.S. McCreery, F.K. Duennebier, and D.A. Walker, Spectral analysis of high frequency P_n, S_n phases recorded on ocean bottom seismographs, *Geophys. Res. Lett.*, 5, 745 - 747, 1978.

Talandier, J., and M. Bouchon, Propagation of high frequency P_n waves at great distances in the central and south Pacific and its implications for the structure of the lower lithosphere, *J. Geophys. Res.*, 84, 5613 - 5619, 1979.

Toksöz, M.N., A.M. Dainty, S.C. Solomon, and K.R. Anderson, Structure of the moon, *Reviews of Geophysics and Space Physics,* 12, 539 - 567, 1974.

Utsu, T., and H. Okada, Anomalies in seismic wave velocity and attenuation associated with a deep earthquake zone (II), *J. Fac. Sci. Hokkaido Univ. Japan Ser.*, VII, Vol. III, 65 - 84, 1968.

Uyeda, S., and Z. Ben-Avraham, Origin and development of the Philippine Sea, *Nature,* 240, 176 - 178, 1972.

Walker, D.A., A study of the northwestern Pacific upper mantle, *Bull. Seism. Soc. Am.*, 55, 925 - 939, 1965.

Walker, D.A., and G.H. Sutton, Oceanic mantle phases recorded on hydrophones in the northwestern Pacific at distances between 9° and 40°, *Bull. Seism. Soc. Am.*, 61, 65-78, 1971.

Walker, D.A., High-frequency P_n and S_n phases recorded in the Western Pacific, *J. Geophys. Res.*, 82, 3350 - 3360, 1977a.

Walker, D.A., High-frequency P_n phases observed in the Pacific at great distances, *Science,* 197, 257 - 259, 1977b.

Walker, D.A., C.S. McCreery, G.H. Sutton, and F.K. Duennebier, Spectral analysis of high-frequency P_n and S_n phases observed at great distances in the western Pacific, *Science,* 199, 1333 - 1335, 1978.

Walker, D.A., High-frequency P_n, S_n velocities: some comparisons for the western, central, and south Pacific, *Geophys. Res. Lett.*, 8, 207 - 209, 1981.

Walker, D. A., C. S. McCreery, and G.H. Sutton, Spectral characteristics of high-frequency P_n, S_n phases in the western Pacific, *J. Geophys. Res.*, 88, 4289 - 4298, 1983.

Webb, S.C., and C.S. Cox, Observations and modeling of seafloor microseisms, *J. Geophys. Res.*, 91, 7343 - 7358, 1986.

APPENDICES

APPENDIX 1

PHILIPPINE SEA STATIONS

station id name	number	position lat, deg	long, deg
A	12	16.945	133.454
B	14	16.964	133.397
D	13	17.550	131.463
E	01	17.939	130.136
G	03	18.240	129.083
AA	14	17.333	131.917
BB	12	17.567	131.450
EE	03	16.927	132.233
BBB	05	16.655	133.262
DDD	03	17.395	132.057
EEE	12	17.767	130.875
FFF	14	18.017	130.127

PACIFIC NW BASIN STATIONS

station id number	position lat, deg	long, deg
03	43.894	159.809
14	43.931	159.864

WAKE ARRAY STATIONS

station id number	position lat, deg	long, deg
71	20.4123	166.4298
72	20.3162	166.2620
73	20.5416	166.2555
74	20.6010	166.5051
75	20.4104	166.6428
76	20.2305	166.4711
10	19.2702	166.6185
11	19.2687	166.6173
20	17.9275	167.4993
21	17.9275	167.4993
40	19.4105	165.8559
41	19.4105	165.8559

PHILIPPINE EARTHQUAKE LOCATIONS

EQ #	date	time		position		depth,	magnitude
	yr day mon	hr min	sec	lat, deg	long, deg	km	
35	810207	0350	19.59	22.144	127.128	033.0	5.3
126	810209	1906	54.00	05.681	125.232	230.1	4.7
152	810210	1511	23.09	23.889	123.386	041.3	5.2
166	810212	2333	37.46	19.162	121.206	046.0	4.7
168	810213	1108	34.39	09.563	126.588	045.0	5.6
191	810214	041	03.75	02.564	125.815	140.5	5.1
194	810214	0731	33.69	03.333	128.128	154.9	5.6
232	810217	2033	25.31	09.686	126.272	063.0	0.00
239	810218	1548	10.69	29.328	130.216	034.0	5.4
243	810219	1333	23.32	00.759	127.400	153.4	4.7
249	810220	2009	09.92	22.918	121.448	026.0	5.4
266	810224	0645	09.67	28.314	129.410	043.0	5.6
277	810225	1619	03.75	11.280	140.291	027.0	5.4
278	810225	1626	13.85	28.333	130.804	033.0	5.3
279	810225	1841	26.62	11.198	140.352	093.4	4.6
282	810227	0227	33.30	24.608	121.848	070.6	4.7
293	810302	1213	45.34	22.894	121.453	023.5	5.5
297	810305	0636	36.77	09.399	126.357	051.1	4.5
334	810316	1228	29.62	29.333	129.358	033.0	5.1
338	810316	1755	28.24	01.985	129.488	033.5	5.4
428	810320	2331	43.20	00.453	126.185	033.6	4.6

PACIFIC NW BASIN EARTHQUAKES

EQ #	date	time		position		depth,	magnitude
	yr day mon	hr min	sec	lat, deg	long, deg	km	
7	820903	0132	04.80	43.710	148.920	010.1	6.0
9	820903	0340	15.10	43.700	148.750	010.1	5.8
10	820903	0411	57.64	43.774	148.471	033.0	5.4
11	820903	0806	41.24	43.724	148.479	033.0	5.1
12	820903	0828	39.40	43.480	148.560	016.3	5.7
13	820903	1004	43.72	43.743	148.558	033.0	5.0
25	820906	0037	59.22	44.020	148.283	033.0	4.9
27	820906	0147	06.70	29.180	140.650	155.6	6.5
34	820907	1551	23.94	41.827	142.707	057.5	4.9
42	820909	1249	09.22	43.314	146.738	051.6	4.6
43	820909	1425	36.29	38.567	141.910	067.9	0.0
47	820910	1020	37.65	55.178	161.698	033.0	5.0

WAKE ARRAY EARTHQUAKE LOCATIONS

EQ #	date	time		position		depth,	magnitude
	yr day mon	hr min	sec	lat, deg	long, deg	km	
96	820926	0109	28.51	50.053	158.798	044.0	5.5
319	821127	0955	38.94	50.205	147.727	622.0	5.6
443	821227	0132	57.68	19.013	144.995	600.0	5.3
611	830130	2245	41.56	33.407	140.812	063.1	5.7
659	830213	0635	30.00	13.837	144.935	105.0	5.7
663	830214	0023	19.42	10.504	140.924	039.0	5.8
710	830226	0711	01.9	48.87	155.73	045.4	6.0
715	830227	1214	20.77	35.869	139.916	078.3	5.9
717	830228	0544	24.45	44.161	148.058	042.0	5.8
791	830317	1959	28.83	41.817	140.650	134.4	5.4
867	830404	1904	20.64	52.931	159.858	038.0	6.0
896	830411	1534	55.49	44.290	147.751	097.0	5.1
984	830430	1403	49.23	41.473	143.764	030.4	6.5
993	830501	1810	40.39	46.353	153.453	024.0	6.1
1201	830621	0625	27.35	41.346	139.099	009.9	6.7
1261	830630	1339	04.04	44.043	147.837	042.4	5.6
1272	830701	2203	42.10	36.935	141.115	051.7	5.5
1398	830724	2307	30.97	53.930	158.372	180.4	6.1
1407	830728	1506	44.76	41.970	142.654	062.8	5.5
1451	830808	0347	57.10	35.498	139.069	024.8	5.9
1481	830817	1055	54.13	55.867	161.287	062.6	6.6
1494	830820	1308	32.56	27.904	141.793	040.8	5.7
1518	830825	2023	33.32	33.509	131.484	126.4	6.1
1528	830828	1130	14.59	46.177	151.514	074.9	5.5
1578	830914	1125	00.90	18.104	145.770	158.5	6.0
1801	831115	1735	08.4	31.11	142.09	017.4	5.6
1802	831115	1803	58.77	31.196	141.809	025.8	5.5
1806	831116	1044	06.54	37.353	141.618	042.7	5.5
1850	831129	2059	50.85	32.598	140.003	136.7	5.6
1856	831130	0256	47.28	41.790	142.772	056.9	5.8
1886	831208	1318	00.2	03.50	149.16	023.9	5.9
1893	831211	0913	49.23	08.137	137.239	023.9	6.2
2001	840104	2240	44.2	45.27	151.67	010.8	6.2
2144	840213	0940	26.10	34.275	139.998	115.0	5.2
2238	840305	1100	59.88	28.726	139.252	460.4	5.1
2242	840306	0217	21.26	29.384	138.935	457.4	6.2
2246	840306	1455	16.55	42.570	142.840	103.3	5.5
2261	840311	2222	25.75	38.392	135.482	351.0	5.3
2262	840312	0234	17.99	22.286	143.110	187.5	5.2
2283	840316	1710	46.57	42.931	145.484	049.1	5.5
2307	840321	0244	24.35	49.176	155.385	040.5	6.0
2321	840324	0944	02.60	44.117	148.192	044.4	6.1
2340	840326	2312	35.23	56.012	163.019	031.6	5.6
2477	840420	0631	10.63	50.120	148.745	582.0	6.0
2492	840423	2140	35.51	47.450	146.692	414.1	6.0
2495	840424	0411	35.2	30.81	138.46	394.8	6.1
2566	840515	1515	53.35	50.982	153.735	281.8	4.9
2645	840604	1836	05.80	51.244	150.770	498.9	5.2
2884	840727	1251	10.50	52.997	161.257	033.0	5.7
2911	840806	1906	38.36	32.386	131.945	046.2	6.3
3054	840918	1702	46.5	34.11	141.37	035.0	6.6
3055	840919	0120	55.86	33.933	141.333	043.2	5.7
3057	840920	1919	23.04	16.784	147.166	044.6	5.7
3058	840920	2153	55.25	33.975	141.554	032.7	5.7
3061	840921	0929	53.48	34.003	141.507	040.2	5.9
3067	840922	1810	35.54	13.822	145.378	098.0	5.9
3120	841023	2228	59.86	13.714	144.917	122.7	5.4
3213	841204	0743	23.16	22.609	143.334	121.5	5.8
3237	841217	2357	01.2	44.17	149.63	035.8	5.9
3248	841228	1037	59.3	56.24	163.8	021.5	6.2

APPENDIX 2

```
      PROGRAM WAKEROSEBD

      INTEGER ITM(7), LUN(1)
      CHARACTER*1 Q, PASS
      CHARACTER*80  FOUT

      COMMON/ARRAYS/ Y(70000), H(70000), K(70000)

      REAL Y /* THE TIME SERIES
      REAL H  /* COPY OF TIME SERIES OVERLAIN WITH ITS FOURIER
            /*  TRANSFORM
      COMPLEX CH(35000)
      EQUIVALENCE (H(1),CH(1))

      REAL K  /* COPY OF THE TIME SERIES OVERLAIN WITH ITS FOURIER
            /* TRANSFORM
      COMPLEX CK(35000)
      EQUIVALENCE (K(1),CK(1))

      INTEGER F1(10), F2(10), F3(10)  /* FREQUENCY CUTOFFS
      REAL CUTOFF, SIGMA2

$INSERT MENKE>REGTAB>HEAD.F77
$INSERT MENKE>REGTAB>IOCOM.F77
$INSERT MENKE>REGTAB>TABLE.F77

      WRITE(1,'("GAUSSIAN BANDPASS")')

      CALL OPENFL( 5 )

      WRITE(1,'("OUTPUT FILE")')
      READ(1,'(A80)') FOUT

      CALL OPNDAT( 6, FOUT, 1, IERR )
      IF( IERR.NE.0 ) THEN
            WRITE(1,'("CANT OPEN REGTAB FILE")')
            STOP
            END IF

      WRITE(1, '("INSTRUMENT?")')
      READ(1,'(I10)') INST

      WRITE(1,'("EVENT?")')
      READ(1,'(I10)') IEVT

      WRITE(1,'("CHANNEL?")')
      READ(1,'(I10)') ICH

      WRITE(1,'("YR, MON, DAY, HR, MIN, SEC, MILLISECOND?")')
      READ(1,'(7I10)') (ITM(I),I=1,7)

      NSAMP = 65536

      N=70000
      N0=1
      NUN = 1
      LUN(1) = 5

      CALL RSEIS( INST, IEVT, ICH, ITM, NSAMP, Y, N, N0, NUN,
     & LUN, NST, NTRAN, IER)  /* READ DATA TO ARRAY Y

      WRITE(1,'("LENGTH OF DATA: ",I10)') NTRAN
      WRITE(1,'("STARTING INDEX ",I10)') NST
      WRITE(1,'("STATUS = ",I10," PROCEED? Y OR N")') IER
      READ(1,'(A1)') Q
      IF( Q.EQ.'N' ) STOP
```

```
      N=NTRAN

      DO 1 I=1, NST-1  /* ZERO BEGINNING OF DATA
                  Y(I)=0.0
1                 CONTINUE

      DO 3 I=N+1, 65536
                  Y(I)=0.0  /* ZERO END OF DATA
3                 CONTINUE

      DO 5453 I=1, 65536  /* COPY DATA TO H
                  H(I) = Y(I)
5453          CONTINUE

      CALL RFFT (H, 65536) /* FOURIER TRANSFORM
      WRITE (1, '(" RFFT CALLED")')

      F1(1)=8193*2-1
      F2(1)=16385*2-1
      F3(1)=8192*3+1

      F1(2)=4097*2-1
      F2(2)=8193*2-1
      F3(2)=4096*3+1

      F1(3)=2049*2-1
      F2(3)=4097*2-1
      F3(3)=2048*3+1

      F1(4)=1025*2-1
      F2(4)=2049*2-1
      F3(4)=1024*3+1

      F1(5)=513*2-1
      F2(5)=1025*2-1
      F3(5)=512*3+1

      F1(6)=257*2-1
      F2(6)=513*2-1
      F3(6)=256*3-1

      WRITE(1, '("WHAT DO YOU WANT THE CUTOFF LEVEL TO BE?")')
      READ(1, *) CUTOFF
      WRITE(1,'("CUTOFF = ",E13.5)') CUTOFF

      DO 1101 J=1, 6  /*LOOP OVER BANDS


            /* STANDARD DEVIATION OF GAUSSIAN
            SIGMA2 = -0.5 * (FLOAT(F1(J)-F3(J))**2)  / ALOG(CUTOFF)

            WRITE(1,'("ITERATION ",I4)') J
            WRITE(1,'("FREQUENCY CUTOFFS ",3I10)') F1(J),F2(J),F3(J)
            WRITE(1,'("SIGMA ",E13.5)') SQRT(SIGMA2)

            DO 41 I=1, 32769  /* COPY FOURIER TRANSFORM TO H
                  CK(I) = CH(I)
41                CONTINUE

            DO 51 I=1, F1(J)  /* ZERO OUT TO START OF BAND
                  CK(I)=0.0
51                CONTINUE

            /* APPLY GAUSSIAN TAPER
            KKK = F2(J)
```

```
                DO 61 I=F1(J), F3(J)
                    TEMP = EXP(-0.5*FLOAT(I-F3(J))**2/SIGMA2)
                    CK(I) = TEMP*CK(I)
                    CK(KKK) = CK(KKK)*TEMP
                    KKK = KKK -1
61                  CONTINUE

                DO 81 I=F2(J), 32769 /* ZERO PAST END OF BAND
                    CK(I)=0.0
81                  CONTINUE

                CALL RFFTI( K, 65536 ) /* INVERSE FOURIER TRANSFORM

                DO 91 I=1, 65536 /* NORMALIZATION OF DOUBLE FFT
                    K(I) = K(I) / 32768.
91                  CONTINUE

                /* CORRECT BECAUSE OF DIGITATION RATE 80 (WAKE)
                /* ROSE DATA HAS DIGITATION RATE 100
                /* WE WANT THE SAME SAMPLING RATE FOR BOTH
                /* DATASETS FOR EASIER COMPARISON

                NSUM = 102

                DO 99 I=1,639
                    IF(NSUM.EQ.102)THEN
                    NSUM = 103
                    ELSE IF(NSUM.EQ.103)THEN
                    NSUM = 102
                    END IF

                /* COMPUTE POWER IN BAND
                IC=1
                DO 101 I=1, 65536-NSUM, NSUM
                    SUM = 0.0
                    DO 111 L=1, NSUM
                        SUM = SUM+K(I+L-1)**2
111                 CONTINUE
                    TABLE(IC,8-J)=SUM
                    IC=IC+1
101                 CONTINUE
 99                 CONTINUE

1101    CONTINUE /*END DO FOR GAUSSIAN BANDPASSER

        ITYPE=1 /* INTERPOLATED DATASET
        SAMP = 1.28
        DMIN = 0.0
        NROW = 639
        NCOL = 7
        WRITE(TITLE,'("ROSEBD: INST ",I5," EVT ",I5," ICH ",I5)')
       & INST,IEVT,ICH

        COLNAM(1)='TIME'
        COLNAM(2)='BAND 1'
        COLNAM(3)='BAND 2'
        COLNAM(4)='BAND 3'
        COLNAM(5)='BAND 4'
        COLNAM(6)='BAND 5'
        COLNAM(7)='BAND 6'

        CALL PUTDAT( 6, HEAD, TABLE, MROW, MCOL, IERR )
        CALL CLSDAT( 6 )
        CLOSE(UNIT=5)
        STOP
        END
```

```
            PROGRAM WAKEFALLOFF

          COMMON/ARRAYS/ DAT(639,10), X(639), Y(639,7)
          COMMON/ARRAYS/ E(639,7), NN(7), A(7), GAMMA(7), ERR(7)
          COMMON/KLUGE/ LASTN, LASTCOL, IPS, ERRPLOT(2,0:10,7)
          DIMENSION YMIN(12), YMAX(12), MAXROW(12), MINROW(12)
          DIMENSION APVEL(639),SIGMAA(7), SIGMAG(7)
          INTEGER IX, IY, NN
          INTEGER MAXROW, MINROW, X, Y
          INTEGER  POA, POB, SOA, SOB, SAROW, SBROW, PAROW, PBROW
          REAL RANGE, APVEL, SIGMAA, SIGMAG
          REAL DAT, TABLE, YMIN, YMAX, XMIN, XMAX, NENTRY
          REAL E, A, GAMMA, ERR
          character*80 fin, fout, STRING, STRIN, OLDTITLE, EQ
          INTEGER ISTA, IEQ, IBP
          CHARACTER*1 Q, C
$insert Menke>regtab>head.f77
          DATA NENTRY/0.0/, MROW/639/, MCOL/10/

          CALL PAGE
          CALL SETDIA( 20, 80, 3500, 1 )
          CALL DIAENA( .TRUE. )
          CALL DIAVIS( .TRUE. )
          CALL DIACLE

          write(1, '("ENTER STATION NUMBER")')
          read(1,'(I5)') ISTA

          IBP = 9

          write(1, '("ENTER EVENT NUMBER")')
          read(1, '(I5)') IEQ

          WRITE(FIN, '("W",I5,"Q",I4,"G",I2".REG")')
         &        ISTA, IEQ, IBP

          CALL DEBLANK(FIN)

          WRITE(FOUT, '("W",I5,"Q",I4,"G",I2".OUT")')
         &        ISTA, IEQ, IBP

          CALL DEBLANK(FOUT)

          /* OPEN INPUT FILE, READ DAT, CLOSE INPUT FILE
          call opndat( 5, fin, 0, ierr )
          if (ierr.ne.0) then
                          write(1,'("cant open"/A80)') fin
                          stop
                          end if
          call getdat( 5, head, DAT, mrow, mcol, ierr )
          if (ierr.ne.0) then
                         write(1, '("cant read input")')
                         stop
                         end if
               OLDTITLE = TITLE
          call clsdat( 5 )

          /* OPEN OUTPUT FILE
          call opndat( 6, fout, 1, ierr )
          if (ierr.ne.0) then
                          write(1,'("cant open"/A80)') fout
                          stop
                          end if
```

```
      /* GET THE STATION COORDINATES

       CALL GETSTA(ISTA, STLAT, STLON)

       /* GET THE EARTHQUAKE LOCATION

       CALL GETEQLOC(IEQ,IDATE,IHRMN,SEC,ELAT,
      & ELONG,DEP,MAG,JHRMN,TSEC)

      /* FIND THE RANGE

       CALL DISTAZ(ELAT,ELONG, STLAT, STLON, XDEG, AZ, AZINV)

      /* TRANSFER RANGE IN DEG TO KM
      /* FIND TRAVEL TIME

       RANGE = XDEG * 111.2
       TTSEC = TSEC - SEC
       TTMIN = JHRMN-IHRMN
       TT = (TTMIN*60) + TTSEC

       /* DAT IN ARRAY DAT(I,J)
       /* DAT(I,1) = TIME
       /* DAT(I,2) = BAND 1, ETC.
       /* APPARENT VELOCITY IN ARREY APVEL()

       DO 19 I=1,NROW
            APVEL(I) = 0.0
19  CONTINUE

      /* COLUMN ONE IS INTERPOLATED AND CONTAINS CUM SAMPL
      /* INTERVAL
      /* TRANSLATE SAMPL INTERVAL TO TIME
      DO 20 I=1,NROW
            APVEL(I) = RANGE/(TT+DAT(I,1))
20  CONTINUE

      /* FIND MIN AND MAX VALUE FOR EACH FREQ BAND

           XMIN=DAT(1,1)
      XMAX=DAT(NROW,1)

      ISTART=1
      IFINISH=NROW

      DO 21 J=2, NCOL
            YMIN(J)=DAT(ISTART,J)
            YMAX(J)=DAT(ISTART,J)

            MAXROW(J)=ISTART
            MINROW(J)=ISTART

            DO 22 I=ISTART,IFINISH
                  IF (DAT(I,J).GT.YMAX(J))THEN
                   YMAX(J)=DAT(I,J)
                   MAXROW(J)=I
                  ELSEIF (DAT(I,J).LT.YMIN(J))THEN
                   YMIN(J)=DAT(I,J)
                   MINROW(J)=I
                   END IF
22       CONTINUE
21  CONTINUE
```

```
/* BUILD X(I) AND Y(I,J) BEFORE PLOTTING ON TECTRONICS

      DO 30 I=1,NROW
            XVAL=(DAT(I,1)-XMIN)/(XMAX-XMIN)
            X(I)=4096*XVAL
30  CONTINUE

      DO 31 J=2,NCOL
            DO 32 I=1,NROW
                  YVAL=(DAT(I,J)-YMIN(J))/(YMAX(J)-YMIN(J))-0.5
                  Y(I,J) = (1000*YVAL) + (370*J)
32      CONTINUE
31  CONTINUE

      /* PLOTTING LOOP
      /* PROGRAM PLOTS BANDPASSED, SQUARED, EQ.TIME SERIES
      /* FROM REGTAB FILES
      /* LOWEST COLUMN NO = LOWEST FREQ. BAND

            CALL PAGE

      DO 40 J=2,NCOL
            CALL DRAWXY(X,Y(1,J),NROW,0,0)
40  CONTINUE

      /* DETERMINE VELOCITY LOCATIONS
      /* V = 7.6, 5.0, 4.5, 3.0

      DO 531 I=1,NROW
          IF (APVEL(I).LE.7.6)THEN
           POA = I
      WRITE( STRING, '(F5.2)' ) APVEL(I)
      WRITE( STRIN, '(I4)' ) POA
            GOTO 532 /* BREAK LOOP
          END IF
531  CONTINUE
532  CONTINUE
      IX = IFIX(FLOAT(POA)*4096.0/NROW)
      CALL LINESEG( IX, 1, IX, 3000)
      CALL ANOTAT( IX-30, 3050, STRING, 2, 0.0, 0.0 )
      CALL ANOTAT( IX-30, 3000, STRIN, 2, 0.0, 0.0 )

      DO 535 I=1,NROW
          IF (APVEL(I).LE.5.0)THEN
           POB = I
      WRITE( STRIN, '(I4)' ) POB
      WRITE( STRING, '(F5.2)' ) APVEL(I)
            GOTO 536 /* BREAK LOOP
          END IF
535  CONTINUE
536  CONTINUE
      IX = IFIX(FLOAT(POB)*4096.0/NROW)
      CALL LINESEG( IX, 1, IX, 3000)
      CALL ANOTAT( IX-30, 3000, STRIN, 2, 0.0, 0.0 )
      CALL ANOTAT( IX-30, 3050, STRING, 2, 0.0, 0.0 )

      DO 537 I=1,NROW
          IF (APVEL(I).LE.4.5)THEN
           SOA = I
      WRITE( STRING, '(F5.2)' ) APVEL(I)
      WRITE( STRIN, '(I4)' ) SOA
            GOTO 538 /* BREAK LOOP
          END IF
537  CONTINUE
538  CONTINUE
```

```
      IX = IFIX(FLOAT(SOA)*4096.0/NROW)
      CALL LINESEG( IX, 1, IX, 3000)
      CALL ANOTAT( IX-30, 3050, STRING, 2, 0.0, 0.0 )
      CALL ANOTAT( IX-30, 3000, STRIN, 2, 0.0, 0.0 )

      DO 539 I=1,NROW
      IF (APVEL(I).LE.3.0)THEN
            SOB = I
      WRITE( STRING, '(F5.2)' ) APVEL(I)
      WRITE( STRIN, '(I4)' ) SOB
            GOTO 540 /* BREAK LOOP
      END IF
539  CONTINUE
540  CONTINUE
     IX = IFIX(FLOAT(SOB)*4096.0/NROW)
      CALL LINESEG( IX, 1, IX, 3000)
      CALL ANOTAT( IX-30, 3050, STRING, 2, 0.0, 0.0 )
      CALL ANOTAT( IX-30, 3000, STRIN, 2, 0.0, 0.0 )

      WRITE(1,'("PICK START OF P")')
      CALL PICKXY( C, IX, IY, 0 )
            PROW = IFIX( FLOAT(NROW)*FLOAT(IX)/4096.0)
            WRITE( STRING, '(F5.2)' ) APVEL(PROW)
            WRITE( STRIN, '(I4)' ) PROW
            CALL LINESEG(IX, 1, IX, 3000)
            CALL ANOTAT( IX-30, 3050, STRING, 2, 0.0, 0.0 )
            CALL ANOTAT( IX-30, 3000, STRIN, 2, 0.0, 0.0 )

      WRITE(1,'("PICK START OF PO")')
      CALL PICKXY( C, IX, IY, 0 )
      PAROW = IFIX( FLOAT(NROW)*FLOAT(IX)/4096.0 )
      WRITE( STRING, '(F5.2)' ) APVEL(PAROW)
      WRITE( STRIN, '(I4)' ) PAROW
      CALL LINESEG( IX, 1, IX, 3000)
      CALL ANOTAT( IX-30, 3050, STRING, 2, 0.0, 0.0 )
      CALL ANOTAT( IX-30, 3000, STRIN, 2, 0.0, 0.0 )

      WRITE(1,'("PICK END OF PO")')
      CALL PICKXY( C, IX, IY, 0 )
      PBROW = IFIX( FLOAT(NROW)*FLOAT(IX)/4096.0 )
      WRITE( STRING, '(F5.2)' ) APVEL(PBROW)
      WRITE( STRIN, '(I4)' ) PBROW
      CALL LINESEG( IX, 1, IX, 3000)
      CALL ANOTAT( IX-30, 3050, STRING, 2, 0.0, 0.0 )
      CALL ANOTAT( IX-30, 3000, STRIN, 2, 0.0, 0.0 )

      WRITE(1,'("PICK START OF SO")')
      CALL PICKXY( C, IX, IY, 0 )
      SAROW = IFIX( FLOAT(NROW)*FLOAT(IX)/4096.0 )
      WRITE( STRING, '(F5.2)' ) APVEL(SAROW)
      WRITE( STRIN, '(I4)' ) SAROW
      CALL LINESEG( IX, 1, IX, 3000)
      CALL ANOTAT( IX-30, 3050, STRING, 2, 0.0, 0.0 )
      CALL ANOTAT( IX-30, 3000, STRIN, 2, 0.0, 0.0 )

      WRITE(1,'("PICK END OF SO")')
      CALL PICKXY( C, IX, IY, 0 )
      SBROW = IFIX( FLOAT(NROW)*FLOAT(IX)/4096.0 )
      WRITE( STRING, '(F5.2)' ) APVEL(SBROW)
      WRITE( STRIN, '(I4)' ) SBROW
      CALL LINESEG( IX, 1, IX, 3000)
      CALL ANOTAT( IX-30, 3050, STRING, 2, 0.0, 0.0 )
      CALL ANOTAT( IX-30, 3000, STRIN, 2, 0.0, 0.0 )


      CALL DIAENA( .TRUE. )
```

```
      TSAMP = 1.28

      /* COPY DATA INTO E ARREY

            DO 60 I=1,NROW
                  DO 61 J=1,NCOL
                        E(I,J) = DAT(I,J)
61                CONTINUE
60    CONTINUE

      /* LOOP OVER SPARKER DATA

           WRITE(1,'("PICK NEXT SPARKER OR HIT Q TO EXIT")')
           DO 667 IPICK=1,1000
                 CALL PICKXY( C, IX, IY, 0 )
                 IS = IFIX( FLOAT(NROW)*FLOAT(IX)/4096.0 )
                 IF(C.EQ.'Q')THEN
                       GOTO 67        /*BREAK LOOP
                 ELSE
                       IE = IS+6

DO 666 L=IS,IE
                                 E(L,5) = NENTRY
                                 E(L,6) = NENTRY
                                 E(L,7) = NENTRY
666                    CONTINUE
                       END IF
667     CONTINUE
67    CONTINUE

      WRITE(1,'("XDEG",F8.3,X1,"AZ",F8.3,X1,"AZINV"F8.3)')
     & XDEG, AZ, AZINV
      WRITE(1,'("ELAT",F8.3,X1,"ELONG",F8.3,X1,"STLAT",
     & F8.3,X1,"STLON",F8.3)') ELAT, ELONG, STLAT, STLON

      DO 555 K=1,2
           IF(K.EQ.1)THEN
                 WRITE(1,'("STARTING P WAVE")')
            NS = PAROW
            NE = PBROW
           ELSEIF(K.EQ.2)THEN
                 WRITE(1,'("STARTING S WAVE")')
            NS = SAROW
            NE = SBROW
           ENDIF

      INROW = NROW
      INCOL = NCOL
      IPS = K
      LASTCOL = NCOL

      CALL FIT(E,INROW,NS,NE,INCOL,TSAMP,NN,A,SIGMAA,GAMMA,
     & SIGMAG,ERR,IERROR)
      WRITE(1,'("BACK FROM FIT")')


      DO 931 J=2,NCOL
           DO 932 I=NS,NE
                 YVAL=(E(I,J)-YMIN(J))/(YMAX(J)-YMIN(J))-0.5
                 Y(I,J) = (1000*YVAL) + (370*J)
932     CONTINUE
           CALL DRAWXY(X(NS),Y(NS,J),(NE-NS+1),0,1)
931   CONTINUE
```

```
      NROWSAVE = NROW
      NCOLSAVE = NCOL

      /* PUT DECAY RATES INTO  FOUR TABLES
      /* EACH TABLE CONTAINS ONE SLOPE INTERVAL
      /* COLUMN 1: CENTER FREQUENCY OF BAND
      /* COLUMN 2: NN
      /* COLUMN 3: AREA
      /* COLUMN 4: SIGMAA
      /* COLUMN 5: GAMMA
      /* COLUMN 6: SIGMAG
      /* COLUMN 7: ERROR

      IF (K.EQ.1) THEN  /* PO CASE */

      /* SET UP THE HEADER OF THE FIRST OUTPUT TABLE
      nrow = 6
      ncol = 7
      itype = 0 /* OR 1 FOR INTERPOLATED TABLE
      TITLE = OLDTITLE(1:60)//' PO PHASE'
      EXTRA(1) = PAROW
      EXTRA(2) = APVEL(PAROW)
      EXTRA(3) = PBROW
      EXTRA(4) = APVEL(PBROW)
      COLNAM(1) = 'FREQ'
      COLNAM(2) = 'NN'
      COLNAM(3) = 'A'
      COLNAM(4) = 'SIGMAA'
      COLNAM(5) = 'GAMMA'
      COLNAM(6) = 'SIGMAG'
      COLNAM(7) = 'ERR'

      /* SET UP THE FIRST OUTPUT TABLE
      /* OVERWRITE THE DAT ARREY
      DAT(6,1) = 30.0
      DAT(5,1) = 15.0
      DAT(4,1) = 07.5
      DAT(3,1) = 03.75
      DAT(2,1) = 01.87
      DAT(1,1) = 00.93

      DO 100 I=1,NROW
            DAT(I,2) = NN(I+1)
            DAT(I,3) = A(I+1)
            DAT(I,4) = SIGMAA(I+1)
            DAT(I,5) = GAMMA(I+1)
            DAT(I,6) = SIGMAG(I+1)
            DAT(I,7) = ERR(I+1)
100   CONTINUE

      /* WRITE THE FIRST OUTPUT TABLE
      call putdat( 6, head, DAT, mrow, mcol, ierr )
      if(ierr.ne.0) then
                  write(1,'("cant write 1st table")')
                  stop
                  END IF

     ELSEIF(K.EQ.2)THEN

      /* SET UP THE HEADER OF THE SECOND OUTPUT TABLE
      nrow = 6
      ncol = 7
      itype = 0 /* OR 1 FOR INTERPOLATED TABLE
      TITLE = OLDTITLE(1:60)//'SO PHASE'
```

```
      EXTRA(1) = SAROW
      EXTRA(2) = APVEL(SAROW)
      EXTRA(3) = SBROW
      EXTRA(4) = APVEL(SBROW)

      COLNAM(1) = 'FREQ'
      COLNAM(2) = 'NN'
      COLNAM(3) = 'A'
      COLNAM(4) = 'SIGMAA'
      COLNAM(5) = 'GAMMA'
      COLNAM(6) = 'SIGMAG'
      COLNAM(7) = 'ERR'

      /* SET UP THE SECOND OUTPUT TABLE
      DAT(6,1) = 30.0
      DAT(5,1) = 15.0
      DAT(4,1) = 07.5
      DAT(3,1) = 03.75
      DAT(2,1) = 01.87
      DAT(1,1) = 00.93

      DO 101 I=1,NROW
            DAT(I,2) = NN(I+1)
            DAT(I,3) = A(I+1)
            DAT(I,4) = SIGMAA(I+1)
            DAT(I,5) = GAMMA(I+1)
            DAT(I,6) = SIGMAG(I+1)
            DAT(I,7) = ERR(I+1)
101   CONTINUE

      /* WRITE THE SECOND OUTPUT TABLE
      call putdat( 6, head, DAT, mrow, mcol, ierr )
      if(ierr.ne.0) then
                  write(1,'("cant write 1st table")')
                  stop
                  END IF

    END IF
    NROW = NROWSAVE
    NCOL = NCOLSAVE

555       CONTINUE
      CALL CLSDAT(6)
      CLOSE (UNIT=9)
      CLOSE (UNIT=10)

    WRITE(1,'(" THIS IS",X2,A80)')FIN
    WRITE(1,'("MAKE A HARD COPY AND HIT RETURN")')
    READ(1,'(A1)') Q

    CALL PAGE
    CALL PLOTERROR

      stop
      end
```

```
      SUBROUTINE LINESEG(X1,Y1,X2,Y2)
            INTEGER X1,Y1,X2,Y2

            DIMENSION IX(2), IY(2)

            IX(1) = X1
            IX(2) = X2

            IY(1) = Y1
            IY(2) = Y2

            CALL DRAWXY( IX, IY, 2, 0, 0 )

            RETURN
            END

            SUBROUTINE DEBLANK(S)
            CHARACTER*80 S,T
                  J=0
                  T=S
                  S=''
                        DO 111 I=1,80
                        IF( T(I:I).NE.' ') THEN
                          J=J+1
                          S(J:J)=T(I:I)
                          END IF
      111           CONTINUE

            RETURN
            END

            SUBROUTINE GETSTA(ISTA, STLAT, STLON)
            INTEGER ISTA
            REAL STLAT, STLON

            OPEN(UNIT=9, FILE='STATIONS')
            REWIND(UNIT=9)
                  DO 1 I=1,90
                  READ(9, '(I5,2F10.5)', ERR=100, END=102)
            &     KSTA,STLAT,STLON
                    IF (KSTA .EQ. ISTA)THEN
                          RETURN
                    END IF
      1     CONTINUE

      CALL DIAVIS( .FALSE. )
                  CALL DIAENA( .FALSE. )
       100  WRITE (1,'("READ ERROR IN STATION FILE, LINE",I5)')I
            STOP
       102  WRITE (1,'("CANT FIND STATION")')
            STOP
            END
```

```
      SUBROUTINE GETEQLOC(IEQ,IDATE,IHRMN,SEC,ELAT,
     & ELONG,DEP,MAG,JHRMN,TSEC)
      INTEGER ISTA, IEQ, IDATE, JHRMN, JHRMN
      REAL SEC, ELAT, ELONG, DEP, MAG, TSEC
      CHARACTER*80 EQ

      OPEN(UNIT=10, FILE='EQLOC')
      REWIND(UNIT=10)
            DO 2 I=1,110
            READ(10,'(I5,I8,I5,F7.3,2F9.4,F6.2,F4.2,I4,F7.3)',
     &  ERR=100, END=102)KEQ,IDATE,IHRMN,SEC,
     &  ELAT,ELONG,DEP,MAG,JHRMN,TSEC
               IF (KEQ .EQ. IEQ)THEN
                     RETURN
               END IF
2     CONTINUE
100  WRITE (1,'("READ ERROR IN EARTHQUAKE FILE, LINE",I5)')I
      STOP
102  WRITE (1,'("CANT FIND EARTHQUAKE")')
      STOP
      END




      SUBROUTINE FIT (E,NR,NS,NE,NCOL,TSAMP,NN,A,SIGMAA,
     & GAMMA,SIGMAG,ERR,IERROR)

      /* SUBROUTINE TO DO A LEAST SQUARE FIT TO A SEISMOGRAM
      /* THE SUBROUTINE CALLS HOUSE
      /* E=SEISMOGRAM AMPLITUDE DAT(I,J)
      /* NR=NROW
      /* NS=BEGINNING ROW
      /* NE=LAST ROW
      /* TSAMP=SAMPLING INTERVAL
      /* NN=VALUE OF N (FROM 1 TO 6) RETURNED
      /* A = AREA UNDER CURVE DELTAM(1) RETURNED
      /* SIGMAA = VARIANCE IN A, RETURNED
      /* GAMMA = DELTAM(2), EXPONENT VALUE RETURNED
      /* SIGMAG = VARIANCE IN GAMMA, RETURNED
      /* ERR =  ROOT MEAN SQ ERROR, RETURNED
      /* IERROR = ERRORCODE, RETURNED

      DIMENSION G(639,2), EMINP(639)
      DIMENSION E(639,7), AP(0:10), GAMMAP(0:10), ERROR(0:10)
      DIMENSION EP(639), TP(639)
      DIMENSION SIGMAA(7), SIGMAG(7), GP(639,2)
      DIMENSION A(7), NN(7), GAMMA(7), ERR(7)
      COMMON/KLUGE/ LASTN, LASTCOL, IPS, ERRPLOT(2,0:10,7)

      REAL TMINTS, EMINP, G, EX, PO, E, EP, AP, TSAMP, TP
      REAL GAMMAP, A, GAMMA, ERR, ERROR, EMIN, NFACT
      REAL GP, SIGMAA, SIGMAG
      REAL NENTRY
      INTEGER NR, NS, NE, ND, NN, IERROR

      MAXN = 6
      LASTN = MAXN
      NENTRY = 0.0
      WRITE(1,'("IN FIT",4I5)') NR,NS,NE,NCOL
      ND = NE-NS+1 /* NUMBER OF DATAPOINTS IN G
```

```
 DO 100 ICOL=2,NCOL  /* LOOP OVER COLUMNS (BANDS)

            DO 101 IN=0,MAXN    /* LOOP OVER VALUES OF N

        /* SET SPARKER DATA TO NENTRY = 0.0
        /* ARREY EP(NP) EXCLUDES SPARKER DATA

              NP = 0
              DO 102 IROW=NS,NE
                    IF( E(IROW,ICOL).NE.NENTRY ) THEN
                     NP=NP+1
                     TP(NP)=TSAMP*FLOAT(IROW-NS)
                     EP(NP)=E(IROW,ICOL)
                    END IF
 102    CONTINUE

            ETOTAL=0.0
            GAMPP = 0.1
            APP=0.0
            DO 15 IROW=NS,NE  /* ESTIM. AREA UNDER CURVE
                  APP = APP+TSAMP*E(IROW,ICOL)
                  ETOTAL = ETOTAL + E(IROW,ICOL)**2
 15          CONTINUE
            ETOTAL = SQRT( ETOTAL / FLOAT(NE-NS+1-2) )

            AP(IN) = APP
            GAMMAP(IN)=GAMPP

            NFACT = FACTORIAL(IN)

            DO 16 IT=1,100 /* ITERATIONS USING NONLIN. L.SQ.

                  DO 17 I=1,NP

                   TMINTS = TP(I)
                   IF( (IN.EQ.0) .AND. (I.EQ.1) ) THEN
                                POWER = 1
                   ELSE
                                POWER = TMINTS**IN
                                END IF

                   EX=EXP(-GAMMAP(IN)*TMINTS)

                   PO = AP(IN)*GAMMAP(IN)**(IN+1)
      &                    /NFACT*POWER*EX

                   EMINP(I)=EP(I)-PO
                   G(I,1)=PO/AP(IN)
                   G(I,2)=AP(IN)*POWER/NFACT*((IN+1)
      &
*GAMMAP(IN)**IN+(-TMINTS)*GAMMAP(IN)**(IN+1))*EX

                        GP(I,1) = G(I,1)
                        GP(I,2) = G(I,2)
 17           CONTINUE

            ITRIAG = 0

CALLHOUSE(G,EMINP,NP,639,2,2,ERROR(IN),1.0E-6,IERROR,ITRIAG)


            /* EMINP IS DESTROYED DURING THE HOUSE CALL AND
            /* REPLACED BY THE SOLUTION VECTOR (2)
            /* HOUSE RETURNES RMS ERROR
```

```
              DELA = EMINP(1)
              DELG = EMINP(2)

              SIZE = SQRT( (DELA/APP)**2 + (DELG/GAMPP)**2 )
              IF( IT.LT.30 ) THEN
                    TVALUE = 0.15
              ELSE
                    TVALUE = 0.30
                    END IF
              IF( SIZE.GT. TVALUE ) THEN
                    SCALE = TVALUE / SIZE
                    DELA = DELA * SCALE
                    DELG = DELG * SCALE
                    END IF

              AP(IN)=AP(IN) + DELA
              GAMMAP(IN)=GAMMAP(IN) + DELG

              IF( GAMMAP(IN).LT.0.0 ) GAMMAP(IN)=0.0


              IF( SIZE .LT. 1.E-4 ) GOTO 301 /*BREAK LOOP*/

 16       CONTINUE  /*END ITERATION LOOP*/
301             CONTINUE

              /* DETERMINE THE EXP AND AREA OF WITH SMALLEST ERROR
              /* FOR EACH IN
              ERRPLOT( IPS, IN, ICOL ) = ERROR(IN) / ETOTAL

101   CONTINUE  /*END OF N LOOP*/

             EMIN = ERROR(0)
             NN(ICOL) = 0
             A(ICOL) = AP(0)
             GAMMA(ICOL) = GAMMAP(0)
             ERR(ICOL) = ERROR(0)

             DO 21 J=1,MAXN
                   IF( EMIN.GT.ERROR(J) )THEN
                     NN(ICOL) = J
                     A(ICOL) = AP(J)
                     GAMMA(ICOL) = GAMMAP(J)
                     ERR(ICOL) = ERROR(J)
                     EMIN = ERROR(J)
                     END IF
 21          CONTINUE
```

```
            /* OVERWRITE DATA WITH CURVE FOR BEST N
          /* THE CURVE IS THEN SUMPERIMPOSED ON THE DATA PLOT

               DO 25 I=1,ND
                    IF( E(I+NS-1,ICOL) .NE. 0.0 ) THEN
                         IN = NN(ICOL)
                         NFACT = FACTORIAL(IN)
                         TMINTS = TSAMP * FLOAT( I-1 )
                         IF( (IN.EQ.0) .AND. (I.EQ.1) ) THEN
                              POWER = 1
                         ELSE
                              POWER = TMINTS**IN
                              END IF

                         EX=EXP(-GAMMA(ICOL)*TMINTS)

          E(I+NS-1,ICOL) = A(ICOL)*GAMMA(ICOL)**(IN+1)
          &                    /NFACT*POWER*EX
                         END IF
25                  CONTINUE

          /*GPTGP IS A 2*2 MATRIX, CONTAINING SUMS
          /* SUMA = GPTGP(1,1)
          /* SUMB = GPTGP(1,2) = GPTGP(2,1)
          /* SUMD = GPTGP(2,2)

          SUMA = 0.0
          SUMB = 0.0
          SUMD = 0.0

          DO 255 I=1,ND
               SUMA = SUMA +GP(I,1)**2
               SUMB = SUMB +GP(I,1)*GP(I,2)
               SUMD = SUMD +GP(I,2)**2
255  CONTINUE

          /* COV(MODEL PARAM) = (COV(DATA)**2)*(GPTGPI)

          DETER = 1/((SUMA*SUMD)-(SUMB**2))
          SIGMAA(ICOL) = SQRT(DETER*SUMD)*ERR(ICOL)
          SIGMAG(ICOL) = SQRT(DETER*SUMA)*ERR(ICOL)

          ERR(ICOL) = ERR(ICOL)/ETOTAL

100  CONTINUE /*END OF COLUMN LOOP*/
          RETURN
          END

          REAL FUNCTION FACTORIAL(I)
          IF( I .EQ. 0 ) THEN
                    FACTORIAL = 1.0
          ELSE IF( I.EQ.1 ) THEN
                    FACTORIAL = 1.0
          ELSE
                    FACTORIAL=I
                    DO 20 K=1,I-1
                              FACTORIAL=FACTORIAL*FLOAT(I-K)
20                       CONTINUE
                    END IF
          RETURN
          END
```

```
      SUBROUTINE PLOTERROR

      /* THIS SUBROUTINE PLOTS ERROR AGAINST N FOR EACH BAND

      COMMON/KLUGE/ LASTN, LASTCOL, IPS, ERRPLOT(2,0:10,7)
      DIMENSION X(0:10), Y(0:10)
      INTEGER X, Y, XO, YO

      LENGTH = 400.0
      LTICK = 400.0 / (LASTN+1)

      CALL PAGE

      DO 500 K=1, 2 /* LOOP OVER P AND S
      DO 300 ICOL=2, LASTCOL /* LOOP OVER COLUMNS

            XO = 100 + 500 * (ICOL-2)
            YO = 100 + 1000 * (K-1)

            CALL LINESEG( 0+XO, 0+YO, 400+XO, 0+YO )
            CALL LINESEG( 0+XO, 0+YO, 0+XO, 400+YO )

            DO 200 I=0, LASTN
                  X(I) = IFIX(I * 400.0/(LASTN+1)) + XO
                  Y(I) = IFIX( 400.0 * ERRPLOT(K,I,ICOL) ) + YO
200         CONTINUE
            CALL DRAWXY(X,Y,LASTN+1,0,0)

300   CONTINUE
500   CONTINUE

      RETURN
      END
```

APPENDIX 3

APPENDIX 3A:

PHILIPPINE SEA and PACIFIC NW BASIN DATA

Tables of measured apparent velocities and falloff values.

Explanation of columns:

column 1-EQNO	Earthquake number
column 2-STA	Station number
column 3-DIST	Epicentral distance, deg
column 4-DEPTH	Hypocenter depth, km
column 5-PoH/SoH	ratio of PoH to SoH apparent velocities
column 6-PoL-arr	apparent velocity of oneset of PoL, km/s
column 7-PoH-arr	apparent velocity of oneset of PoH, km/s
column 8-SoH-arr	apparent velocity of oneset of SoH, km/s
column 9-PoH-1.17	PoH Falloff rates, 1/s for band 1, 1.17 Hz
column 10-PoH2.34	PoH Falloff rates, 1/s for band 2, 2.34 Hz
column 11-PoH4.68	PoH Falloff rates, 1/s for band 3, 4.68 Hz
column 12-PoH9.37	PoH Falloff rates, 1/s for band 4, 9.37 Hz
column 13-PoH18.7	PoH Falloff rates, 1/s for band 5, 18.7 Hz
column 14-PoH37.5	PoH Falloff rates, 1/s for band 6, 37.5 Hz
column 15-SoH1.17	SoH Falloff rates, 1/s for band 1, 1.17 Hz
column 16-SoH2.34	SoH Falloff rates, 1/s for band 2, 2.34 Hz
column 17-SoH4.68	SoH Falloff rates, 1/s for band 3, 4.68 Hz
column 18-SoH9.37	SoH Falloff rates, 1/s for band 4, 9.37 Hz
column 19-SoH18.7	SoH Falloff rates, 1/s for band 5, 18.7 Hz
column 20-SoH37.5	SoH Falloff rates, 1/s for band 6, 37.5 Hz

1-EQNO	2-STA	3-DIST	4-DEPTH	5-PoH/SoH	6-PoL-arr	7-PoH-arr	8-SoH-arr	9-PoH-1.17	10-PoH2.34	11-PoH4.68	12-PoH9.37	13-PoH18.7	14-PoH37.5	15-SoH1.17	16-SoH2.34	17-SoH4.68	18-SoH9.37	19-SoH18.7	20-SoH37.5
35	121	7.893	33	1.8029		8.6	4.77		0.0323		0.0397	0.037	0.0094			0.0599	0.0079	0.0144	0.0221
35	122	7.893	33	1.7672		8.5	4.81	0.012	0.0341	0.029	0.0682	0.0637	0.0005	0.0352	0.0633	0.4302	0.5365	0.3763	0.068
35	123	7.893	33	1.6692		8.83	5.29	0.0132	0.0414	0.0343	0.0346	0.0402	0.0005		0.0345	0.0636	0.0352	0.0433	0.0468
35	131	6.126	33			8.35			0.1883										
35	132	6.126	33			8.22			0.0456										
35	141	7.84	33	1.7817		8.57	4.81	0.1479	0.0826	0.0976	0.103	0.0592	0.0069	0.0375	0.0806	0.0587	0.098	0.094	0.1105
35	142	7.84	33	1.7929		8.57	4.78		0.1882	0.1014	0.0654	0.0612	0.001		0.1414	0.1574	0.236	0.1775	0.3437
35	11	5.049	33	1.7813		8.55	4.8												
35	12	5.049	33				4.86							0.3845	0.5094	0.2888	0.8104	1.1676	1.0059
35	13	5.049	33			8.72													
152	31	7.738	41.3			8.25	4.78	0.2418	0.0926	0.1065	0.0975	0.1545	0.1238		0.4523	0.4292	0.2512	0.794	0.885
152	32	7.738	41.3			8.25	4.75		0.0937	0.1312	0.1704	0.1411			0.5398	0.275	0.6808	1.075	
152	121	9.821	41.3			8.23	4.69			0.2988	0.1863	0.2396			0.6818	0.5777	0.7384	0.4219	
152	122	9.821	41.3				4.67									0.6624	0.6744		
152	141	10.31	41.3			8.35	4.73			0.0723	0.202	0.3548				0.1059	0.359	0.348	
152	142	13.31	41.3			8.35	4.71			0.068						0.0932	0.0952		
166	31	10.72	46			8.03	4.61	0.0754	0.1882	0.0911	0.1614	0.1889			0.7261	0.4871	0.2254	0.1339	
166	121	9.856	46			7.98	4.55			0.3211	0.1606	0.1534			0.7924	0.2096	0.1845		
166	141	10.338	46			8.08	4.56		0.0801	0.0727	0.0757	0.0724			0.0041	0.1337	0.0829	0.0308	
168	31	9.151	45			8.12	4.97	0.2164	0.241	0.3317	0.1558	0.2883	0.2434	0.2338	0.2082	0.2619	0.0676	0.1432	0.0794
168	32	9.151	45			8.12	4.79		0.101	0.2435	0.4113	0.1751			0.0121	0.0848	0.0923	0.1061	
168	121	9.253	45			7.88	4.7	0.1411	0.2288	0.1407	0.1164	0.2597					0.4871	0.2106	
168	122	9.253	45			7.88	4.67			0.2343	0.1167						0.0912		
168	141	9.3	45			7.95	4.97		0.1723	0.3238	0.367	0.5308			0.0521	0.1155	0.0724	0.4843	
168	142	9.3	45			7.95	4.79			0.3246	0.2833	0.1606				0.12123	0.1228		
193	31	15.609	140.5			8.03	4.66		0.1037	0.1612	0.073	0.0544			0.2389	0.2748	0.1601	0.6294	
193	121	15.903	140.5				4.64								0.0688	0.0891	0.0918	0.0233	
193	141	15.853	140.5			8.03	4.66		0.1117	0.1587	0.0439	0.0484				0.2669	0.1909	0.0688	
194	31	14.098	154.9			7.65	4.5	0.0677	0.0926	0.1496	0.1299	0.1572	0.0655	0.1136	0.1036	0.1524	0.1802	0.1112	
194	32	14.098	154.9			7.6			0.0311	0.0929	0.0993								
194	121	14.516	154.9			7.61	4.49	0.024	0.0371	0.0985	0.1234	0.0974			0.0141	0.0825	0.0801	0.3331	
194	122	14.516	154.9			7.47				0.062	0.0383								
194	141	14.401	154.9			7.68	4.58	0.0149	0.0543	0.0842	0.1048	0.198			0.001	0.0727	0.1317	0.0687	
194	142	14.401	154.9			7.37				0.0339	0.0478								
232	31	9.243	63			7.92	4.77		0.0707	0.4878	0.0866	0.2362	0.0978		0.0587	0.2481	0.1539	0.3019	
232	32	9.243	63			8	4.58			0.4161	0.068								
232	121	9.309	63			7.73	4.71				0.0667	0.1495				0.3596	0.1281	0.4061	
232	141	9.374	63			7.82	4.72		0.2965	0.2364	0.4536	0.3139			0.0014	0.0776	0.285	0.3189	
232	142	9.374	63			7.75	4.68			0.1468	0.1645						0.1848		
239	31	12.482	34			8.12	4.74			0.0406	0.0588	0.0448			0.1021	0.1724	0.2386	0.319	
239	121	11.762	34			7.83	4.57	0.1946	0.2005	0.1463	0.1233	0.0579			0.3749	0.3306	0.4208	0.2301	
239	141	12.041	34			8.1	4.75		0.0703	0.1159	0.0536	0.0459			0.0528	0.5852	0.7157	0.14	
243	31	16.576	153.4			8.06		0.0874	0.0593	0.1306	0.0999								
243	32	16.576	153.4			8.01				0.4689									
243	121	17.171	153.4			8.09			0.0562	0.1214	0.0405								
243	141	17.059	153.4			8.17			0.0675	0.0937	0.0387	0.0256							
249	31	11.761	26			8.14	4.68	0.0363	0.1492	0.0899	0.1658	0.0982		0.2401	0.4449	0.4734	0.5032	0.6982	0.1053
249	32	11.761	26			8.14	4.68			0.1682	0.0796					0.5025	0.0637		
249	121	10.79	26			8.06	4.64		0.2936	0.1747	0.1489	0.204			0.0721	0.3782	0.2834	0.2711	
266	31	11.628	43			8.04	4.73	0.1694	0.0732	0.1871	0.1071	0.0872	0.0615	0.0314	0.2484	0.1833	0.5727	0.4836	0.4472
266	32	11.628	43			7.97	4.73			0.3289	0.1327	0.0027			0.1506	0.4814	0.6755	0.6994	
266	121	10.86	43			7.9	4.71	0.0441	0.101	0.193	0.1929	0.1095	0.0179	0.0008	0.1386	0.1622	0.5088	0.243	0.541
266	122	10.86	43			7.9	4.6			0.1454	0.3509					0.1956	0.6095		
277	31	9.621	27			7.98	4.62	0.1661	0.0938	0.1608	0.2316	0.1152	0.0944	0.4979	0.1421	0.164	0.4406	0.2171	0.1688
277	32	9.621	27			7.9	4.62			0.0781	0.4117	0.0097				0.7382	0.4417	0.0015	
277	33	9.621	27			7.9			0.3233	0.2576	0.1091	0.0219							

1-EQNO	2-STA	3-DIST	4-DEPTH	5-PoH/SoH	6-PoL-arr	7-PoH-arr	8-SoH-arr	9-PoH-1.17	10-PoH2.34	11-PoH4.68	12-PoH9.37	13-PoH18.7	14-PoH37.5	15-SoH1.17	16-SoH2.34	17-SoH4.68	18-SoH9.37	19-SoH18.7	20-SoH37.5
278	31	11.428	33			8.07	4.75		0.3092	0.0738	0.0671	0.2376			0.101	0.2501	0.1306	0.5999	0.0965
278	32	11.428	33				4.75									0.2113	0.1149	0.1045	
279	31	9.718	93.4			8.51	4.79		0.1374	0.3453	0.2342	0.2042	0.1298			0.1321	0.4314	0.0015	
279	32	9.718	93.4			8.34				0.189	0.1644								
279	33	9.718	93.4			8.42				0.1401	0.1223								
282	31	12.354	70.6			8.28	4.69		0.253	0.0881	0.1591	0.1101	0.0782		0.0825	0.9202	0.3321	0.383	0.242
282	32	12.354	70.6				4.67									0.4732	0.6875		
293	31	11.746	23.5			8.06	4.67	0.0703		0.1171	0.0788	0.1093	0.0743	0.3479	0.2188	0.5836	0.6009	0.6531	0.4257
293	32	11.746	23.5			8.08	4.67			0.0533	0.0015					0.2363	0.4684	0.1189	
297	31	9.418	51.1			8.15	4.74		0.1587	0.2529	0.2746	0.2286	0.1642		0.4046	0.2304	0.5508	0.5372	0.5373
297	32	9.418	51.1			8.07	4.69			0.4176	0.2871						0.6866		
297	33	9.418	51.1				4.59								0.1362	0.2206	0.5435	0.3944	0.3895
334	31	12.627	33			8.31	4.9			0.1982	0.1219					0.233	0.3459		
334	51	13.119	33			8.13	4.69			0.0779	0.1126					0.3236	0.1775		
338	31	15.091	33.5			7.65	4.42	0.1131	0.0795	0.1861	0.2174	0.1549			0.0055	0.6472	0.6111	0.2829	
338	32	15.091	33.5			7.65	4.39			0.1455	0.1208						0.1256		
338	33	15.091	33.5			7.69	4.29	0.0626	0.1102	0.0781	0.0942	0.0949							
338	51	15.043	33.5			8.04	4.58		0.1461	0.0908	0.1212	0.1169			0.5164	0.4649	0.3191		
428	31	17.42	33.6			7.8			0.0649	0.2447	0.1443	0.0522							
428	32	17.42	33.6			7.76				0.1761	0.052								
428	33	17.42	33.6			7.93		0.0938	0.1214	0.1194	0.1009	0.0016							
428	51	15.545	33.6			8.07			0.1963	0.2131	0.2051								
428	121	17.778	33.6			7.88		0.0004	0.0638	0.2395	0.2687								

1-EQNO	2-STA	3-DIST	4-DEPTH	5-PoH/SoH	6-PoL-arr	7-PoH-arr	8-SoH-arr	9-PoH-1.17	10-PoH2.34	11-PoH4.68	12-PoH9.37	13-PoH18.7	14-PoH37.5	15-SoH1.17	16-SoH2.34	17-SoH4.68	18-SoH9.37	19-SoH18.7	20-SoH37.5
7	31	8.184	10.1	1.758		8.28	4.71	0.0984	0.0307	0.1064	0.1304	0.155	0.1333	0.0525	0.0556	0.1186	0.1215	0.2178	0.1019
7	32	8.184	10.1	1.6827		8.38	4.98												
7	33	8.184	10.1	1.7853		8.48	4.75	0.0526	0.0351	0.0571	0.1058	0.1202	0.0529	0.0143	0.067	0.0628	0.1419	0.2066	0.1335
7	141	8.221	10.1	1.7832		8.47	4.75	0.1131	0.1026	0.0956	0.1256	0.1444	0.1302		0.0545	0.1413	0.1531		0.1681
7	142	8.221	10.1	1.7221		8.18	4.75			0.2104						0.1139	0.2959	0.1631	
9	31	8.223	10.1	1.76		8.36	4.75	0.0363	0.1142	0.1151	0.11	0.2739	0.189	0.11	0.3175	0.1304	0.1915	0.1525	0.294
9	33	8.223	10.1	1.76		8.36	4.75	0.0636	0.0187	0.0895	0.0713	0.0807	0.0763	0.0393	0.0422	0.0589	0.109	0.1561	0.093
9	141	8.271	10.1	1.8209		9.05	4.97	0.0006	0.0007	0.071	0.062	0.0931	0.0232	0.0689	0.1048	0.087	0.212		
9	142	8.271	10.1				4.97									0.1588	0.093		
9	143	8.271	10.1				4.91									0.382			
10	31	8.2	33	1.7484		8.2	4.69												
10	32	8.2	33	1.7484		8.2	4.69		0.1214						0.2071				
11	31	8.198	33	1.7618		8.21	4.66	0.0577	0.11	0.0587	0.1336			0.5645	0.099	0.2938	0.1344		
11	32	8.198	33	1.7292		8.11	4.69												
11	33	8.198	33	1.7394		8.21	4.72			0.0609						0.0656			
11	141	8.236	33	1.7602		8.22	4.67		0.0005	0.079	0.0624				0.049	0.0875	0.067		
12	31	8.165	16.3	1.8242		8.61	4.72	0.1149	0.0557	0.1502	0.0613	0.1182		0.0987	0.1739	0.1291	0.34	0.1378	
12	32	8.165	16.3			8.31													
12	33	8.165	16.3	1.7803		8.51	4.78	0.0397	0.0445	0.0715	0.078			0.1205	0.0542	0.0892	0.1642		
12	141	8.204	16.3	1.7241		7.81	4.53	0.2835	0.005	0.1149	0.077			0.1677	0.1336	0.0969	0.1104		
12	142	8.204	16.3				4.5									0.8959	0.3986		
13	31	8.139	33	1.7876		8.33	4.66	0.0009	0.1322	0.0323	0.1662			0.0781	0.443	0.1507	0.3597		
13	32	8.139	33	1.7326		8.23	4.75	0.0705	0.0768	0.0715	0.0774	0.175	0.0006	0.0119	0.0456	0.0492	0.0715	0.1295	0.0665
13	33	8.139	33	1.7974		8.43	4.69	0.015	0.0169	0.0109				0.0421	0.0966	0.0981			
13	141	8.177	33	1.7671		8.27	4.68	0.0061	0.0008	0.0327					0.0998	0.1628			
13	142	8.177	33				4.68									0.1622			
25	31	8.318	33	1.7572		8.54	4.86	0.3356	0.0443	0.1616	0.0798	0.1126	0.1998	0.428	0.1585	0.2514	0.6608	0.2521	0.7271
25	32	8.318	33	1.7572		8.54	4.86	0.1355	0.01	0.0426	0.0652	0.3131	0.0014	0.0533		0.0437		0.0832	
25	33	8.318	33				4.9									0.0808			
25	141	8.355	33	1.7746		8.66	4.88			0.1708						0.2866			
27	31	21.201	155.6	1.7186	8.9	8.06	4.69	0.0433	0.0277	0.0479	0.0389	0.0349	0.0319	0.0063	0.0411	0.0465	0.0576	0.0564	0.0531
27	32	21.201	155.6		8.9	8.21													
27	33	21.201	155.6	1.7113		8.06	4.71	0.0086	0.0326	0.0171	0.0187	0.0184		0.0078	0.0331	0.0326	0.0351	0.0412	
27	141	21.255	155.6	1.7447		8.2	4.7	0.0028	0.0174	0.022	0.0231	0.0238	0.0189	0.0265	0.0997	0.0584	0.0692	0.0646	0.0415
27	142	21.255	155.6				4.69									0.0826			
27	143	21.255	155.6				4.66							0.0449	0.0423	0.043	0.0474	0.0471	0.0417
34	31	12.72	57.5				4.67									0.1373	0.1528	0.0824	
34	32	12.72	57.5				4.67								0.0177	0.0219	0.1181	0.9166	
42	31	9.503	51.6	1.764		8.52	4.83	0.0649	0.2258	0.056	0.1322	0.0768	0.0024	0.0922	0.1328	0.1607	0.2147	0.3285	1.0368
42	32	9.503	51.6	1.5349		8.35	5.44	0.0601	0.0778	0.0449	0.0791	0.1045	0.0431	0.0339	0.1032			0.0799	0.0519
42	33	9.503	51.6	1.7826		8.61	4.83			0.0605	0.1819	0.0084	0.0008	0.1116	0.0713	0.127	0.163	0.2955	0.1097
42	141	9.542	51.6				4.03							1.1775	0.0645	0.3141	0.3376	0.2942	0.4901
42	142	9.542	51.6				4.03							0.192	0.2469	0.2268	0.1437	0.2669	0.2177
42	143	9.542	51.6				4.05							0.1841	0.2543	0.1009	0.2269	0.2208	0.1951
43	31	14.475	67.9				4.67							0.1785	0.33	0.3575	0.3374	0.1318	0.492
43	32	14.475	67.9				4.69							0.3864	0.3526	0.0863	0.0634	0.3004	0.0693
43	141	14.523	67.9				4.7								0.1387	0.1673	0.391	0.4887	
43	142	14.523	67.9				4.69								0.1039	0.0839	0.0766	0.0656	0.0632
47	31	11.361	33	1.7532		8.24	4.7	0.0861		0.0981	0.1199	0.1475	0.1156	0.0812	0.2174	0.2618	0.129	0.2777	0.4072
47	32	11.361	33	1.7457		8.17	4.68												
47	33	11.361	33	1.7421		8.24	4.73	0.1764	0.0906	0.0774	0.109	0.1257	0.0778	0.1047	0.2135	0.0751	0.0988	0.1047	0.0184
47	141	11.321	33	1.773		8.28	4.67	0.0622	0.0991	0.0851	0.1146	0.1388	0.0795		0.2889	0.2343	0.1497	0.1371	0.1961
47	142	11.321	33	1.7228		8.08	4.69			0.4673	0.0873				0.1153	0.3589	0.1454		

APPENDIX 3B:

WAKE DATA

Tables of measured apparent velocities and falloff values.

Explanation of columns:

column 1- EQNO	Earthquake number
column 2-STA	Station number
column 3-DIST	epicentral distance, deg
column 4-DEPTH	hypocentral depth, km
column 5-Parr	P wave apparent velocity, km/s
column 6-PoL-arr	PoL wave apparent velocity, km/s
column 7-PoH-arr	PoH wave apparent velocity, km/s
column 8-SoL-arr	SoL wave apparent velocity, km/s
column 9-SoH-arr	SoH wave apparent velocity, km/s
column 10-P0.93	P wave Falloff, 1/s, for band 1, 0.93 Hz
column 11-P1.87	P wave Falloff, 1/s, for band 2, 1.87 Hz
column 12-P3.75	P wave Falloff, 1/s, for band 3, 3.75 Hz
column 13-P7.5	P wave Falloff, 1/s, for band 4, 7.5 Hz
column 14-P15	P wave Falloff, 1/s, for band 5, 15 Hz
column 15-P30	P wave Falloff, 1/s, for band 6, 30 Hz
column 16-PoL0.93	PoL wave Falloff, 1/s, for band 1, 0.93 Hz
column 17-PoL1.87	PoL wave Falloff, 1/s, for band 2, 1.87 Hz
column 18-PoL3.75	PoL wave Falloff, 1/s, for band 3, 3.75 Hz
column 19-PoH0.93	PoH wave Falloff, 1/s, for band 1, 0.93 Hz
column 20-PoH1.87	PoH wave Falloff, 1/s, for band 2, 1.87 Hz
column 21-PoH3.75	PoH wave Falloff, 1/s, for band 3, 3.75 Hz
column 22-PoH7.5	PoH wave Falloff, 1/s, for band 4, 7.5 Hz
column 23-PoH15	PoH wave Falloff, 1/s, for band 5, 15 Hz
column 24-PoH30	PoH wave Falloff, 1/s, for band 6, 30 Hz
column 25-SoL0.93	SoL wave Falloff, 1/s, for band 1, 0.93 Hz
column 26-SoL1.87	SoL wave Falloff, 1/s, for band 2, 1.87 Hz
column 27-SoH0.93	SoH wave Falloff, 1/s, for band 1, 0.93 Hz
column 28-SoH1.87	SoH wave Falloff, 1/s, for band 2, 1.87 Hz
column 29-SoH3.75	SoH wave Falloff, 1/s, for band 3, 3.75 Hz
column 30-SoH7.5	SoH wave Falloff, 1/s, for band 4, 7.5 Hz
column 31-SoH15	SoH wave Falloff, 1/s, for band 5, 15 Hz
column 32-SoH30	SoH wave Falloff, 1/s, for band 6, 30 Hz

1- EQNO	2-STA	3-DIST	4-DEPTH	5-Parr	6-PoL-arr	7-PoH-arr	8-SoL-arr	9-SoH-arr	10-P0.93	11-P1.87	12-P3.75	13-P7.5	14-P15	15-P30	16-PoL0.93
96	74	30.019	44			8.28		4.7							
96	73	30.038	44			8.29		4.11							
96	71	30.192	44			8.39		4.73							
96	75	30.229	44			8.26		4.71							
96	76	30.377	44			8.2		4.72							
319	73	33.041	622	10.68	7.6		5.68				0.1106				
319	74	33.074	622	10.77	7.59		5.67		0.223	0.4831	0.197	0.1589	0.0024	0.0036	
319	71	33.222	622	10.78	7.58		5.68		0.0718	0.401	0.0619	0.0526			
319	75	33.299	622	10.77	7.6				0.191	0.0915	0.261	0.3258			
319	76	33.404	622	10.76	7.66					0.0162	0.0697	0.15		0.0011	
319	20	35.892	622	10.95	7.59		6.03		0.5771	0.6635	0.581				
443	73	20.066	600	9.74		7			0.2278	0.5365	0.2041	0.2216			
443	71	20.228	600	9.76	7.67				0.0998	0.0816	0.257				
443	76	20.267	600	9.75		7.17			0.289	0.2825	0.0803	0.068			
443	74	20.3	600	9.63	8.58				0.2474	0.2615	0.1421	0.1117			
443	75	20.428	600	9.72		7.07			0.1722	0.1139	0.1921	0.1651			
611	73	25.966	63.1			8.35		4.75							
611	74	26.124	63.1			8.3		4.73							
611	71	26.173	63.1			8.32		4.73							
611	76	26.309	63.1			8.3		4.72							
611	75	26.338	63.1			8.31		4.72							
611	10	26.982	63.1			8.27									
611	20	28.455	63.1			8.23									
659	40	20.791	105			8.23		4.69							
659	73	21.419	105			8.18		4.69							
659	10	21.467	105			8.24		4.7							
659	76	21.539	105			8.26		4.67							
659	71	21.545	105			8.27		4.67							
659	74	21.66	105			8.17		4.69							
659	75	21.738	105			8.2		4.69							
659	20	22.075	105			8.22		4.67							
663	73	26.331	39			8.18		4.72							
663	76	26.428	39		9.01	8.21		4.69							
663	71	26.446	39		9.02	8.24		4.67							
663	74	26.572	39			8.22		4.69							
663	75	26.636	39		9.02	8.21		4.68							
663	20	26.774	39		8.96	8.17		4.68							
710	74	29.499	45.4		9.23	8.19		4.7							
710	73	29.499	45.4		9.26	8.22		4.7							
710	71	29.664	45.4		9.28	8.19		4.7							
710	75	29.715	45.4		9.29	8.25		4.7							
710	76	29.848	45.4		9.27	8.24		4.69							
715	73	27.667	78.3		9.06	8.25		4.72							
715	74	27.811	78.3		9.14	8.3		4.71							

17-PoL1.87	18-PoL3.75	19-PoH0.93	20-PoH1.87	21-PoH3.75	22-PoH7.5	23-PoH15	24-PoH30	25-SoL0.93	26-SoL1.87	27-SoH0.93	28-SoH1.87	29-SoH3.75	30-SoH7.5	31-SoH15	32-SoH30
				0.0328	0.1142	0.044	0.0006					0.0544	0.0605	0.0473	0.0005
				0.0567	0.0538	0.0568						0.0755			
				0.0257	0.0276							0.0378			
			0.0308	0.0351	0.0588	0.0431						0.059	0.0682		
				0.0344	0.0576	0.0615						0.0506	0.0571		
								0.218							
								0.5847							
								0.2215							
								0.2709							
								0.07					0.09		
								0.3147							
		0.0975	0.0407	0.0478	0.085	0.0327				0.0806	0.0445	0.0456	0.0972	0.0018	0.0005
		0.0721	0.0837	0.0571	0.0921	0.1005				0.0005	0.0482	0.065	0.1032	0.0536	
		0.0393	0.0911	0.098	0.093	0.0988				0.1218	0.0005	0.0937	0.1398	0.0491	
		0.0167		0.0783	0.1266	0.1303				0.0005	0.0007	0.0465	0.0854	0.0915	
		0.2613	0.073	0.1108	0.1165	0.1117					0.0345	0.1042	0.0592	0.0595	
			0.0385	0.0519	0.0609										
			0.0737	0.0796	0.0729	0.0003									
		0.0028	0.04	0.0244	0.0004					0.0768	0.0548	0.0397	0.0503		
		0.0289		0.0256	0.0064					0.0424	0.0418	0.0681	0.0862		
			0.0451	0.0637	0.0708					0.1106	0.2276	0.1652	0.1276	0.0756	
				0.0263	0.0347	0.0186				0.0469	0.0435	0.0471	0.0549	0.0479	
		0.04	0.0288	0.0359	0.0314					0.046	0.0718	0.0762	0.085	0.0449	
		0.0289	0.0361	0.0048	0.0384					0.0469	0.0335	0.0806	0.0868		
		0.0138	0.0116	0.0301	0.0295					0.0775	0.0351	0.0673	0.0833		
		0.1298	0.0566	0.0446	0.0429	0.0048				0.0725	0.0562	0.0654	0.08	0.0146	
				0.0753	0.055							0.1077	0.0358		
		0.0205	0.151	0.1062	0.0996					0.0675	0.0457	0.0767	0.0579	0.0359	
		0.0308	0.0559	0.1001	0.0925					0.0635	0.0357	0.079	0.0607		
		0.0798	0.077	0.0562	0.0933					0.1168	0.0354	0.0843	0.0537		
				0.0445	0.0908							0.0375	0.0457		
		0.0383	0.0165	0.0829	0.0552					0.1167	0.1207	0.0482	0.0514		
			0.0509	0.0767	0.1194					0.086	0.1586	0.1093	0.1256		
		0.0116	0.0261	0.0402	0.0891					0.1935	0.0368	0.1218	0.1052		
		0.014	0.0681	0.0722	0.052					0.068	0.005	0.106	0.0933		
		0.0099	0.0595	0.0653	0.0932					0.0397	0.028	0.0857	0.0993		
		0.0458	0.0476	0.0876	0.0919					0.064	0.0609	0.0947	0.1317		
			0.0407	0.0688	0.0655						0.0749	0.1061	0.0885		
		0.1432	0.1205	0.0532	0.1					0.1305	0.068	0.1035	0.0996		

1- EQNO	2-STA	3-DIST	4-DEPTH	5-Parr	6-PoL-arr	7-PoH-arr	8-SoL-arr	9-SoH-arr	10-P0.93	11-P1.87	12-P3.75	13-P7.5	14-P15	15-P30	16-PoL0.93
715	71	27.875	78.3		9.2	8.26		4.72							
715	76	28.019	78.3		9.21	8.27		4.72							
715	75	28.031	78.3		8.98	8.28		4.72							
715	20	30.248	78.3		9.34	8.1									0.0515
717	73	27.999	42			8.3		4.75							
717	74	28.06	42		9.12	8.26		4.74							
717	71	28.19	42		9.17	8.27		4.77							
717	75	28.288	42		9.13	8.24		4.72							
717	76	28.368	42		9.12	8.26		4.76							
791	73	30.293	134.4		9.55	8.21		4.7							
791	74	30.398	134.4		9.59	8.24		4.75							
791	71	30.496	134.4		9.55	8.24		4.73							
791	75	30.626	134.4		9.16	8.23		4.71							
791	76	30.66	134.4			8.24		4.78							
867	74	32.678	38			8.17		4.71							
867	73	32.707	38			8.18		4.7							
867	71	32.855	38			8.1		4.86							
867	75	32.833	38			8.15		4.68							
867	76	33.039	38			8.17		4.69							
896	73	28.238	97			8.05		4.69							
896	74	28.299	97			8.23		4.72							
896	71	28.429	97			8.24		4.73							
896	75	28.528	97			8.11		4.67							
896	76	28.606	97			8.19		4.71							
984	73	28.256	30.4			8.19		4.71							
984	74	28.351	30.4	9.17		8.17		4.68							
984	71	28.457	30.4	9.07		8.25		4.71							
984	75	28.58	30.4	8.91		8.18		4.67							
984	76	28.624	30.4			8.16		4.67							
993	73	27.798	24	8.98		7.67									
993	74	27.82	24	9.18		7.18			0.0806						
993	71	27.973	24	9.04		7.19			0.1638	0.2048					
993	75	28.042	24	8.96		7.05			0.0588		0.0932	0.1095	0.0004		
993	76	28.157	24	9		7.05			0.0725	0.0107	0.0973	0.1026	0.0003		
993	40	28.744	24			6.83									
993	10	29.105	24			6.29									
993	20	30.64	24	9.28		5.41			0.0558	0.0041					
1201	73	30.973	9.9	9.27		8.4			0.1907	0.0517	0.2109				
1201	74	31.085	9.9	9.24		8.32			0.2118	0.2247	0.1264				
1201	71	31.178	9.9	9.26					0.1338	0.11	0.0621				
1201	75	31.313	9.9	9.27		8.76			0.0865	0.1252	0.2088				
1201	76	31.338	9.9	9.28		7.95			0.1852	0.137	0.1267				
1201	20	33.706	9.9	9.43					0.1181	0.3818	0.4351	0.0042	0.0034	0.0005	
1261	73	28.007	42.4			8.31		4.77							

17-PoL1.87	18-PoL3.75	19-PoH0.93	20-PoH1.87	21-PoH3.75	22-PoH7.5	23-PoH15	24-PoH30	25-SoL0.93	26-SoL1.87	27-SoH0.93	28-SoH1.87	29-SoH3.75	30-SoH7.5	31-SoH15	32-SoH30
		0.0209	0.0587	0.1083	0.0626	0.0028	0.0003			0.0279	0.039	0.0776	0.1257	0.0079	0.0009
		0.0179	0.033	0.0643	0.0828	0.0003	0.0003			0.0496	0.0367	0.1101	0.1573		0.0044
		0.0301	0.0515	0.1161	0.0683	0.0003				0.0337	0.0715	0.0712	0.1183		
0.1015		0.02	0.1064	0.0759											
		0.0004	0.0518	0.0615	0.0646							0.082	0.0444	0.0032	0.0032
		0.0164	0.0314	0.0746	0.0662					0.0279	0.0395	0.0544	0.0852	0.0416	0.0004
		0.0112	0.0355	0.0346	0.0374	0.0011	0.0011			0.0483	0.0567	0.0723	0.0819	0.0255	0.0004
		0.0002	0.0597	0.0395	0.043	0.0003	0.0002				0.0371	0.0409	0.0995	0.0419	0.0005
		0.0105	0.0565	0.0672	0.066	0.0025				0.096	0.0335	0.0735	0.1283	0.0005	0.0003
				0.0427								0.0617			
			0.0316	0.0941	0.0453							0.0317	0.1093		
				0.0473	0.0861							0.0704	0.1397		
				0.0895	0.0773							0.0468	0.0658		
				0.0689	0.106							0.0256	0.1861		
			0.1022	0.0451	0.0954						0.0005	0.0562	0.053	0.0435	
				0.0644	0.0503							0.0006	0.0688		
			0.0381	0.0375									0.0277		
				0.0718	0.0896								0.076		
				0.0676	0.1175								0.0654		
													0.0638		
				0.0417	0.0632							0.0486	0.0839	0.0398	
					0.0631								0.0836		
				0.0391	0.0393							0.0114	0.0628		
				0.0385	0.0722							0.0514	0.0654	0.0542	
				0.0378	0.0371							0.0452	0.0555		
			0.0564	0.0471	0.0769							0.0545	0.0579		
				0.04	0.04							0.0507	0.0418		
			0.0345	0.0883	0.0847						0.0006	0.0455	0.0654		
		0.0403	0.04	0.0735	0.085						0.0006	0.0473	0.0653		
				0.0562	0.0631										
		0.0242		0.2358	0.2609	0.2396									
		0.0019	0.002		0.1538	0.0859									
					0.2569	0.2082									
		0.0005	0.0053	0.1104	0.1479	0.1027									
			0.2295	0.2203	0.2643										
				0.1092	0.117	0.043	0.0005								
				0.0647	0.2502	0.2454									
		0.0694	0.0631	0.0506											
				0.0922											
		0.0598	0.0896												
			0.038	0.0404	0.0551	0.0006	0.0006				0.0442	0.0651	0.0704		

1- EQNO	2-STA	3-DIST	4-DEPTH	5-Parr	6-PoL-arr	7-PoH-arr	8-SoL-arr	9-SoH-arr	10-P0.93	11-P1.87	12-P3.75	13-P7.5	14-P15	15-P30	16-PoL0.93
1261	74	28.069	42.4	9.1		8.33		4.73							
1261	72	28.206	42.4	9.08		8.28		4.76							
1261	71	28.199	42.4	9.04		8.28		4.78							
1261	75	28.298	42.4	8.72		8.28		4.73							
1261	76	28.376	42.4	9.14		8.28		4.73							
1272	73	27.315	51.7	9.07		8.22		4.69							
1272	74	27.449	51.7	8.94		8.17		4.67							
1272	72	27.747	51.7	8.95		8.12		4.67							
1272	71	27.552	51.7	9.13		8.14		4.68							
1272	75	27.672	51.7	9.14		8.1		4.68							
1272	76	27.673	51.7	9.11		8.18		4.68							
1272	20	29.954	51.7	9.24		8.14		4.63							
1272	21	29.954	51.7	9.28		8.19		4.65							
1398	73	33.873	180.4			8.25		4.63	0.2241	0.2796	0.0976	0.0088	0.0029		
1398	74	33.849	180.4	9.94		8.24		4.73	0.1054	0.0711	0.1147	0.0048	0.0006		
1398	71	34.024	180.4	9.92		8.24		4.73	0.1502	0.5158	0.1583	0.1519	0.0013		
1398	75	34.056	180.4	9.9		8.27		4.74	0.1311	0.1901	0.198	0.0884	0.0009		
1398	76	34.209	180.4	9.94		8.21		4.75	0.3491	0.2568	0.158	0.2992	0.001		
1407	74	29.308	62.8			8.24		4.68							
1407	76	29.579	62.8			8.13		4.73							
1451	74	28.278	24.8			8.07		4.62							
1451	76	28.479	24.8			8		4.67							
1481	74	35.43	62.6			8.15		4.72							
1481	73	35.469	62.6	9.69		8.22		4.73			0.1017	0.0447			
1481	71	35.611	62.6	9.73		8.06		4.72	0.2191	0.1277	0.323	0.0073			
1481	75	35.631	62.6	9.74		8.19		4.74			0.0362	0.0005			
1481	76	35.795	62.6	9.72		8.14		4.71		0.0353	0.2127	0.0395	0.0023	0.0008	
1494	73	23.455	40.8	8.7		8.28		4.7							
1494	74	23.648	40.8	8.73		8.28		4.74							
1494	71	23.656	40.8	8.74		8.25		4.69							
1494	76	23.763	40.8	8.78		8.25		4.68							
1494	75	23.84	40.8	8.77		8.24		4.7							
1494	10	24.285	40.8	8.75		8.27		4.69							
1494	20	25.627	40.8	8.76		8.18		4.63							
1518	73	33.397	126.4	9.74					0.3977	0.2871	0.2751	0.001		0.001	
1518	72	33.515	126.4	9.74					0.1833	0.2895	0.2863	0.0885			
1518	74	33.57	126.4	9.72					0.0423	0.1934	0.2716	0.0006	0.0007	0.0006	
1518	71	33.603	126.4	9.73					0.1012	0.2758	0.2664	0.0016	0.0007	0.0014	
1518	76	33.728	126.4	9.73					0.2442	0.2642	0.1423	0.003	0.0017	0.0006	
1518	75	33.777	126.4	9.72					0.1235	0.1026	0.2557	0.0008		0.0007	
1528	73	28.281	74.9	8.61				4.77							
1528	74	28.315	74.9	9.24		8.44		4.79							
1528	71	28.462	74.9	9.25		8.46		4.74							
1528	72	28.492	74.9	9.26		8.41		4.8							

17-PoL1.87	18-PoL3.75	19-PoH0.93	20-PoH1.87	21-PoH3.75	22-PoH7.5	23-PoH15	24-PoH30	25-SoL0.93	26-SoL1.87	27-SoH0.93	28-SoH1.87	29-SoH3.75	30-SoH7.5	31-SoH15	32-SoH30
		0.024	0.0359	0.0443	0.0537	0.0004				0.0011	0.0338	0.048	0.0793	0.0454	
			0.0745	0.0758	0.109						0.0293	0.0428	0.0754		
		0.0144	0.0309	0.0652	0.036					0.003	0.0745	0.0758	0.109		
		0.0112	0.0457	0.0654	0.0617					0.0015	0.0405	0.0382	0.0524	0.0452	
		0.0409	0.0425	0.0729	0.0701	0.0352					0.0404	0.0394	0.0827	0.0483	0.0004
		0.0124	0.0611	0.0449	0.0517	0.0004				0.0523	0.0693	0.1066	0.099	0.1032	
		0.0155	0.0799	0.0534	0.0651	0.0296				0.0511	0.0052	0.0596	0.1132	0.0727	
		0.0059		0.0556	0.0389	0.0049				0.0787	0.027	0.1403	0.0973	0.0647	
		0.0065	0.0594	0.08	0.069	0.0004				0.0286	0.0239	0.173	0.1137	0.0586	
		0.0376	0.0937	0.0617	0.0748	0.0369				0.0386	0.0359	0.0862	0.1134	0.1261	
		0.0094	0.0326	0.0861	0.0551	0.036					0.0701	0.197	0.2104	0.0921	
		0.023	0.0441	0.0666	0.0317	0.0006	0.0003					0.0618	0.0619	0.0005	0.0009
		0.0183	0.0428	0.0611	0.0303	0.0004					0.0488	0.0601			
		0.0531	0.0004	0.0417	0.0443	0.0011				0.0024	0.0022	0.0522	0.1272	0.0698	
		0.0547	0.1108	0.0433	0.0422	0.0017				0.0281	0.0702	0.0674	0.156	0.1064	
		0.0158	0.0405	0.0688	0.0452	0.0011				0.0582	0.0391	0.0931	0.1468	0.0543	
		0.0422	0.0078	0.0445	0.0449	0.0307				0.0094	0.0324	0.1209	0.2142	0.1448	
			0.0016	0.0895	0.0795	0.0407				0.0005	0.006	0.093	0.1936	0.1385	
				0.0323	0.0424							0.0636	0.0577		
				0.037	0.0758								0.0845		
				0.0723	0.0398							0.0407	0.0493		
				0.0583	0.0396							0.0309	0.0408		
		0.0203	0.0325	0.0947	0.1006	0.0407				0.0245	0.0885	0.0797	0.1139	0.0861	
		0.0091	0.0037	0.0872	0.0766	0.0356				0.014	0.0605	0.0847	0.0887	0.0491	
		0.015	0.0317	0.0885	0.1526					0.1399	0.0291	0.0754	0.0819		
		0.0082	0.0724	0.1814	0.1062	0.0873				0.0124	0.0082	0.0641	0.1371	0.0409	
		0.0154	0.0181	0.0819	0.1892	0.0379	0.0004			0.061	0.038	0.0822	0.0536	0.05	0.0005
		0.0159	0.034	0.0383	0.0434	0.0356	0.0003			0.009	0.0934	0.04	0.0426	0.0458	0.0005
		0.1735	0.0655	0.0549	0.0653	0.0916	0.0004			0.0536	0.0541	0.0404	0.0649	0.0404	0.0004
		0.0558	0.0407	0.0797	0.2197	0.0492	0.0004			0.0061	0.0283	0.0399	0.0367	0.0452	0.0005
			0.0106	0.0402	0.0743	0.0655	0.0004				0.0071	0.0337	0.0452	0.043	0.0014
		0.0246	0.0135	0.0437	0.0885	0.0547	0.0013			0.0004	0.041	0.0348	0.039	0.0504	0.0004
			0.0509	0.055	0.0583		0.0003			0.0378		0.0522	0.0546	0.0041	0.0004
		0.0191		0.0823	0.0637	0.0033	0.0005			0.028	0.0389	0.0502	0.0577	0.0005	
		0.0003		0.0219	0.022					0.0007	0.0392	0.0413	0.0908	0.0348	
		0.0242	0.0101	0.0331	0.0616	0.0017				0.0712	0.0525	0.036	0.0836	0.0346	
		0.0592	0.0069	0.0761	0.0289					0.0004	0.0348	0.0392	0.0642		
				0.0592	0.0373					0.0011	0.027	0.0354	0.1077		

1- EQNO	2-STA	3-DIST	4-DEPTH	5-Parr	6-PoL-arr	7-PoH-arr	8-SoL-arr	9-SoH-arr	10-P0.93	11-P1.87	12-P3.75	13-P7.5	14-P15	15-P30	16-PoL0.93
1528	75	28.539	74.9	9.17		8.31		4.76							
1528	76	28.644	74.9	9.31		8.37		4.99							
1578	73	19.484	158.5	8.65		8.23		4.71	0.1538	0.458	0.0013				
1578	71	19.639	158.5			8.26		4.7							
1578	76	19.669	158.5			8.23		4.69							
1578	74	19.721	158.5	8.71		8.21		4.62							
1578	10	19.785	158.5	8.7		8.28		4.71	0.6782	0.613	0.509	0.0019	0.0022	0.0023	
1578	75	19.839	158.5			8.26		4.74							
1578	20	20.666	158.5	8.69		8.25		4.73	0.7041	0.7443	0.6802				
1801	73	24.114	17.4	8.68		8.17		4.67							
1801	74	24.285	17.4	8.43		8.17		4.63							
1801	71	24.32	17.4	8.75		8.18		4.57							
1801	76	24.447	17.4	8.73		8.19		4.58							
1801	75	24.493	17.4	8.71		8.24		4.68							
1801	20	26.506	17.4	8.81		8.13									
1802	74	24.541	25.8	9.07		8.2		4.82							
1806	74	27.31	42.7	8.75		8.15		4.69							
1806	76	27.54	42.7			8.14		4.69							
1886	20	22.988	23.9		9.83	9.15									0.7635
1886	10	23.164	23.9			9.18									
1886	76	23.692	23.9			9.22		4.92							
1886	73	23.754	23.9			9.12		4.91							
1886	71	23.785	23.9		9.89	9.26		4.94							0.2101
1886	75	23.931	23.9			9.19		4.91							
1886	74	23.965	23.9			9.21		4.92							
1893	10	30.558	23.9		8.62	8.27		5.13							
1893	73	30.632	23.9		8.58	8.11		5.09							
1893	76	30.721	23.9		8.69	8.19		5.12							0.4782
1893	71	30.743	23.9		8.56	8.17		5.14							0.2054
1893	74	30.872	23.9		8.62	8.16		5.05							0.3899
1893	75	30.932	23.9		8.58	8.19		5.13							
1893	20	30.999	23.9		8.74	8.39		4.81							0.4192
2001	73	27.444	10.8	9.82	8	7.77		4.4	0.3482	0.1628	0.2323	0.1137			
2001	74	27.481	10.8	9.83	8.01			4.36		0.3085	0.3012	0.316	0.1163	0.0131	
2001	71	27.626	10.8	9.84		7.79		4.41	0.2068	0.2983	0.6103	0.1952	0.075	0.0009	
2001	75	27.706	10.8	9.83	8	7.84		4.38	0.1748	0.1355	0.3088	0.1427	0.0172	0.0037	0.2174
2001	76	27.808	10.8	9.86	8.06	7.8		4.39	0.3216	0.3008	0.0627	0.178	0.0548	0.0006	
2001	10	28.744	10.8	10.03	8.19	7.93			0.328	0.0852	0.3893		0.0184	0.0008	
2001	20	30.297	10.8	10.09	8.28				1.1805	1.2498	0.6501	0.2293	0.0012	0.0012	
2144	73	26.931	115	11.61					0.3565	0.3062	1.0011	0.9187			
2144	74	27.086	115	11.56					0.339	0.7962	0.3328	0.6774			
2144	71	27.139	115	11.53					0.2926	0.3032	0.2783	0.1326			
2144	76	27.277	115	11.53		7.42			0.3424	0.2752	0.1621	0.1136			
2144	75	27.302	115	11.54					0.348	0.1746	0.241	0.2105			

17-PoL1.87	18-PoL3.75	19-PoH0.93	20-PoH1.87	21-PoH3.75	22-PoH7.5	23-PoH15	24-PoH30	25-SoL0.93	26-SoL1.87	27-SoH0.93	28-SoH1.87	29-SoH3.75	30-SoH7.5	31-SoH15	32-SoH30
			0.0336	0.0399	0.0468					0.0004	0.0083	0.0381	0.1434	0.0495	
				0.032	0.0428	0.0392	0.0027				0.0302	0.068	0.1245	0.0778	0.0031
		0.0601	0.0246	0.0325	0.0541	0.0479	0.0014			0.0392	0.0614	0.0854	0.0684	0.0673	0.0282
		0.0349	0.1145	0.0314	0.0575	0.0552	0.0241			0.1344	0.0551	0.0587	0.0695	0.0639	0.0325
		0.0363		0.0342	0.0369	0.0554	0.0231			0.0401	0.029	0.0574	0.0779	0.0722	0.0364
		0.0863		0.0341	0.0564	0.0544	0.0218			0.053	0.0352	0.0479	0.0615	0.0503	
		0.0852	0.0326	0.0333	0.0447	0.0406	0.0004			0.0412	0.0813	0.0919	0.0607	0.0909	0.0394
		0.0747		0.0102	0.0314	0.0536	0.0265			0.0445	0.0474	0.0749	0.066	0.0407	0.0328
		0.035	0.0136	0.045	0.0456	0.0416	0.0011			0.0505	0.0459	0.0794	0.088	0.0956	0.0029
		0.0505	0.0311	0.0274	0.0408	0.0017	0.0003			0.0005		0.0005	0.0432	0.0005	0.0005
		0.1307	0.0309	0.0646	0.0807	0.0043	0.0003				0.0006	0.0525	0.0525	0.0006	
		0.0151	0.0282	0.058	0.0469						0.0005	0.0496	0.0051		
		0.0067	0.0174	0.0816	0.1123	0.0209	0.0008				0.0409		0.0648		
		0.0227	0.0498	0.0501	0.1255	0.0227	0.0003			0.0006	0.005	0.0342	0.0374		
			0.0282	0.0406											
		0.06	0.0673	0.0923	0.0975	0.0004				0.0016	0.0005	0.0006	0.0581	0.0058	
		0.0208	0.034	0.0535	0.1018	0.0021				0.0005	0.004	0.0762	0.0557	0.0527	
				0.0314	0.0613	0.0004	0.0006						0.1347	0.0522	0.0004
			0.0342	0.276	0.2854										
			0.1026	0.0956	0.1889	0.0005									
			0.0408	0.1998	0.1643	0.1728	0.0003					0.0442	0.0442	0.0444	
		0.0576	0.0227	0.1267	0.1791	0.0608	0.0004			0.0075		0.0402	0.0579		
				0.156	0.1783	0.0658	0.0017					0.0398	0.0461		
		0.0132	0.0398	0.137	0.1617	0.1509	0.0003			0.0007	0.0008	0.0491	0.0531	0.065	0.0008
		0.0646		0.1386	0.1869	0.1442	0.0003			0.0006	0.0006	0.0853	0.0478	0.0007	0.0007
			0.123	0.0971	0.2142	0.0005									
		0.0522	0.0214	0.1401	0.1924	0.0776	0.0006			0.0049		0.0431	0.0612		
0.197		0.0379	0.039	0.1926	0.1594	0.167	0.0004			0.0007	0.0007	0.0431	0.0451	0.0447	0.0081
				0.1548	0.1768	0.0653						0.0398	0.0446		
		0.0537	0.0283	0.0809	0.1464	0.0731						0.0663	0.0683		
		0.0122	0.0082	0.136	0.1604	0.1283	0.0003			0.0006	0.0017	0.0471	0.0447	0.0537	
			0.0381	0.2767	0.3175					0.0006	0.0005	0.0268	0.0006		
		0.0561	0.0405	0.0464	0.0641	0.0413	0.0016			0.0386	0.0422	0.0566	0.0394	0.0335	0.0005
		0.0842	0.0309	0.0682	0.0669	0.0738	0.0017			0.0657	0.0352	0.0467	0.0491	0.0441	
		0.1154	0.01	0.0315	0.0361	0.0409	0.0003			0.0409	0.0347	0.0506	0.0975	0.0323	
		0.2174	0.0376	0.0627	0.0683	0.1166	0.003			0.0076	0.0797	0.039	0.0729	0.0384	
		0.54	0.0094	0.0502	0.0605	0.0455	0.002			0.049	0.03	0.0338	0.0784	0.0383	0.0009
		0.0402	0.0322	0.1125	0.0785	0.0303									
		0.1191	0.0364	0.0717	0.0689	0.0003	0.0003								
		0.3294	0.2353	0.7221	0.1205										

1- EQNO	2-STA	3-DIST	4-DEPTH	5-Parr	6-PoL-arr	7-PoH-arr	8-SoL-arr	9-SoH-arr	10-P0.93	11-P1.87	12-P3.75	13-P7.5	14-P15	15-P30	16-PoL0.93
2144	10	27.964	115	11.49					0.0872						
2144	20	29.447	115	11.55					0.0807	1.0827	0.9015	0.8796			
2238	73	25.82	460.4			8.22		4.65							
2238	74	26.011	460.4			8.22		4.64							
2238	71	26.022	460.4			8.29		4.63							
2238	76	26.131	460.4			8.23		4.65							
2238	75	26.285	460.4			8.23		4.63							
2238	20	28.009	460.4			8.14									
2242	73	26.236	457.4	10.1						0.2728			0.0014	0.0014	
2242	40	26.395	457.4	10.03					0.1629	0.2357	0.345	0.1593	0.0073	0.0014	
2242	74	26.424	457.4	10.09					0.2629	0.2964	0.2991	0.1411	0.0013	0.0011	
2242	71	26.439	457.4	10.05					0.211	0.3236	0.3307	0.116	0.0012	0.0046	
2242	76	26.551	457.4	10.09					0.0803	0.1205	0.0832	0.0767	0.0009	0.0008	
2242	75	26.621	457.4	10.03						0.3003			0.0082	0.0043	
2242	10	27.099	457.4	10.34						0.2718				0.0122	
2242	20	28.464	457.4	10.15					0.3303	1.3764	1.3375			0.0017	
2246	73	29.493	103.3	9.65	7.94	7.73		4.61	0.3143	0.5714	0.2837	0.2071		0.0011	0.0917
2246	74	29.586	103.3	9.64	7.92	7.78		4.62		0.5466	0.2757	0.5185	0.0011		0.1361
2246	71	29.694	103.3	9.72	7.95	7.76		4.57	0.5027	0.4935	0.3091	0.1072	0.0063	0.0005	0.0917
2246	75	29.815	103.3	9.68	7.91	7.74			0.2022	0.2459	0.5085	0.234		0.0085	0.3507
2246	76	29.862	103.3	9.73	7.97	7.79			0.5718	0.2776	0.1083	0.074			0.1484
2246	40	30.186	103.3	9.84	8.08	7.91			0.3846	0.5462	0.2775	0.4633	0.0009		0.1357
2246	10	30.716	103.3	10.05	8.27	8			0.1903	0.5672	0.2809	0.1292			
2246	20	32.289	103.3	10.04	8.12	7.91			0.6079	0.2394	0.6341	0.4079	0.0011	0.0011	0.5029
2261	73	31.952	351	9.72		8.15		4.87							
2261	74	32.092	351	9.25		8.14		4.84							
2261	71	32.16	351	9.24		8.16		4.86							
2261	76	32.307	351	9.25		8.15		4.87							
2261	75	32.313	351	9.83		8.08		4.88							
2261	40	32.413	351	9.34		8.25		4.9							
2261	10	33.042	351	10.06		8.19		5.03							
2261	20	34.559	351	9.37		8		4.78							
2262	40	21.445	187.5	11.48		8.16			0.2829	0.0531	0.1401	0.1372			
2262	73	21.616	187.5	11.71		8.33				0.1052	0.1126				
2262	71	21.797	187.5	11.74		8.29			0.1974	0.2055	0.2075	0.1076			
2262	74	21.838	187.5	11.69		8.34			0.187	0.0543	0.1156	0.1398	0.0008		
2262	76	21.865	187.5	11.7		8.36			0.3745	0.1983	0.1048	0.2425			
2262	75	21.995	187.5	11.7		8.3				0.0806	0.3034	0.1516	0.0011	0.0011	
2262	10	22.179	187.5	11.94		8.44									
2283	73	28.32	49.1	8.82		8.34		5.2							
2283	74	28.399	49.1	8.78		8.2		5.22							
2283	71	28.617	49.1	8.82		8.32		5.23							
2283	75	28.629	49.1	9.08		8.21		5.2							
2283	76	28.689	49.1	8.87		8.28		5.22							

17-PoL1.87	18-PoL3.75	19-PoH0.93	20-PoH1.87	21-PoH3.75	22-PoH7.5	23-PoH15	24-PoH30	25-SoL0.93	26-SoL1.87	27-SoH0.93	28-SoH1.87	29-SoH3.75	30-SoH7.5	31-SoH15	32-SoH30
				0.0547	0.0702							0.0681	0.0757		
				0.0773	0.109							0.0806	0.0831	0.0667	
				0.0567	0.0723							0.089	0.0745		
				0.063	0.0684							0.0601	0.101		
				0.0692	0.086							0.1047	0.1173	0.0431	
				0.0484	0.0472										
		0.0347	0.0358	0.0212	0.0405	0.0411	0.0013			0.1187	0.0068	0.0234	0.0254		
		0.0367	0.0082	0.0213	0.0493	0.0338	0.0005			0.3559	0.006	0.0056	0.0005		
		0.0917	0.0077	0.0218	0.0838	0.0739	0.0009			0.039	0.0084	0.0005	0.041	0.0005	
		0.3507	0.0068	0.0178	0.0426	0.057	0.0016								
		0.1484	0.032	0.0197	0.035	0.0674	0.0003								
		0.1357	0.0059	0.0179	0.0602	0.049	0.0003								
		0.0335	0.0298	0.0209	0.0407	0.0393	0.0002								
		0.5029	0.0479	0.0209	0.0584	0.0268	0.0003								
				0.0574	0.0443	0.0014	0.0009				0.0283	0.0816	0.0712	0.0409	0.0006
		0.0123	0.029	0.0866	0.0721	0.0242	0.0003			0.0549	0.0647	0.0514	0.0566	0.1011	0.0004
		0.0149	0.0241	0.0514	0.0509	0.0012	0.0003				0.1424	0.0717	0.1203	0.0418	0.0006
		0.0414	0.0193	0.049	0.0669		0.0003			0.1289	0.0649	0.1017	0.1111	0.0738	0.0003
				0.0734	0.0544	0.0294	0.0003					0.0784	0.1035	0.0825	0.0014
		0.0121	0.0274	0.0848	0.0712	0.0253	0.0003				0.0852	0.0471	0.0867	0.1326	0.0004
				0.0288	0.0332	0.0006	0.0011				0.0301	0.0589	0.0747	0.0787	0.0006
				0.0498	0.211	0.2342						0.0484		0.0006	
		0.0531	0.0332	0.0734	0.0717										
			0.0289	0.0327											
		0.0189	0.0022	0.1594	0.076										
		0.0504	0.0575	0.0704	0.0965	0.0016	0.0012								
		0.0126	0.0346	0.0941	0.0617										
			0.0926	0.0842	0.0379	0.0004	0.0018								
				0.0371											
					0.0183							0.0381	0.048		
		0.0154	0.0034	0.0209	0.0482	0.0251	0.0003			0.0071	0.0076	0.0441	0.0834	0.039	0.0006
					0.0436							0.0473	0.0889		
					0.0278							0.0381	0.078		
				0.0205	0.0296		0.0023					0.0467	0.0618		0.0004

1- EQNO	2-STA	3-DIST	4-DEPTH	5-Parr	6-PoL-arr	7-PoH-arr	8-SoL-arr	9-SoH-arr	10-P0.93	11-P1.87	12-P3.75	13-P7.5	14-P15	15-P30	16-PoL0.93
2283	40	29.066	49.1	8.99		8.39		5.34							
2283	10	29.567	49.1	9.21		8.68		5.43							
2307	73	29.865	40.5			8.15									
2307	74	29.867	40.5			8.15		4.85							
2307	71	30.031	40.5	8.9	8.9	8.2		4.83							
2307	75	30.083	40.5			8.19		4.81							
2307	76	30.215	40.5			8.2		4.81							
2307	40	30.867	40.5			8.43		4.9							
2321	73	27.905	44.4	9.01	9.01	8.27		4.67							
2321	74	27.965	44.4	8.9	8.9	8.23		4.56							
2321	71	28.096	44.4	9.24	9.24	8.16		4.58							
2321	75	28.193	44.4			8.3		4.59							
2321	76	28.273	44.4	9.13	9.13	8.24		4.59							
2321	40	28.725	44.4	9.1	9.1	8.46		4.69							
2321	10	29.181	44.4			8.62		4.77							
2340	74	35.455	31.6		8.7			5.18							
2340	73	35.501	31.6		8.89	8.16		5.22							
2340	71	35.638	31.6		8.67	8.1		5.19							
2340	75	35.652	31.6		8.65	8.09		5.14							
2340	76	35.821	31.6		8.89	8.12		5.19							
2340	40	36.605	31.6		9.19	8.46		5.38							
2340	10	36.783	31.6		9.13			5.4							
2477	73	32.619	582	11.64						0.1046	1.5867				
2477	74	32.649	582	11.6						0.1253	1.8916				
2477	71	32.798	582	11.65						0.143	0.1794				
2477	75	32.872	582	11.73						0.1658	0.3037				
2447	76	32.981	582	11.67						0.203	0.1357				
2447	40	33.541	582	11.92						0.1259	1.8937				
2447	10	33.923	582	12.01						0.1082	1.5797				
2492	73	31.182	414.1	10.71					0.2215	0.0925	0.0561	0.2292			
2492	74	32.232	414.1	10.69					0.2119	0.3545	2.0122	0.2981	0.0059	0.0012	
2492	71	32.369	414.1	10.65					0.181	0.1041	1.5359	0.1899			
2492	75	32.459	414.1	10.72					0.2678	0.6606	0.2535	0.2825			
2492	76	32.548	414.1	10.75					0.2757	0.2866	0.1167	0.1804	0.0083		
2492	40	32.036	414.1	10.96					0.2101	0.3511	2.0112	0.826		0.0016	
2492	10	32.469	414.1	11.16					0.2224	0.1164	0.0608	0.2348		0.0011	
2492	20	34.034	414.1	10.88					1.1149	1.2073	1.1388	0.9257	0.0085	0.0009	
2495	73	26.991	394.8	11.1		8.13			0.0391		0.039				
2495	74	27.17	394.8	11.07		8.19			0.2998	0.8127	0.3405	0.2921			
2495	71	27.195	394.8	11.02		8.25			0.1086	0.2648	0.084	0.006			
2495	40	27.206	394.8	11.08		8.2			0.2956	0.8098	0.3421	0.6854	0.0015	0.0037	
2495	76	27.315	394.8	11.02		8.17			0.3019	0.2535	0.1684	0.118	0.0037	0.0009	
2495	75	27.373	394.8	11.04		8.22					0.1721	0.0724			
2495	10	27.9	394.8	10.62		8.41					0.0805				

17-PoL1.87	18-PoL3.75	19-PoH0.93	20-PoH1.87	21-PoH3.75	22-PoH7.5	23-PoH15	24-PoH30	25-SoL0.93	26-SoL1.87	27-SoH0.93	28-SoH1.87	29-SoH3.75	30-SoH7.5	31-SoH15	32-SoH30
		0.0179	0.0037	0.0197	0.0481	0.0246	0.0004			0.0052	0.0077	0.0451	0.0846	0.0422	0.0007
				0.0176	0.0205		0.0003					0.0374	0.0491		0.0023
				0.0238	0.0338										
			0.0329	0.0372	0.068		0.0003				0.0004	0.0459	0.0548		0.0006
			0.0328	0.0271	0.0378						0.0082	0.0005	0.0353		
			0.0875	0.0836	0.0668						0.07	0.0004	0.0373		
			0.0617	0.0553	0.0755						0.0004	0.0304	0.0746		
			0.0326	0.0376	0.068						0.0005	0.0386	0.0502		
			0.0247	0.0604	0.0458						0.0595	0.0972	0.0606		
		0.0363	0.0361	0.0476	0.0765		0.0003				0.0367	0.0712	0.0653		0.0006
		0.043	0.0505	0.0738	0.0785					0.0061	0.0005	0.0441	0.0436		
			0.1565	0.1217	0.0686						0.0005	0.0831	0.0934		
		0.012	0.0443	0.0694	0.1227		0.0004			0.048	0.0005	0.0458	0.0972		0.0013
		0.0359	0.0365	0.0475	0.0785						0.0006	0.0669	0.108		
				0.0329								0.0553			
		0.03	0.0493	0.132	0.1286	0.0617				0.0273	0.0512	0.0577	0.0622	0.0668	
		0.0582	0.0298	0.0297	0.0581	0.0307				0.0003	0.0515	0.0624	0.0891	0.064	
		0.0144		0.1068	0.0684	0.0351				0.0003	0.0315	0.0964	0.074	0.0431	
		0.0303	0.0655	0.1115	0.1556	0.0504				0.0024	0.0314	0.0709	0.087	0.0503	
		0.0619	0.0654	0.0891	0.1286		0.0007				0.0607	0.0639	0.0862	0.0441	
		0.0417	0.0429	0.1271	0.1245	0.1321				0.0261	0.0669	0.0526	0.0804	0.0616	
		0.0571	0.0299	0.0298	0.0582	0.0313					0.0523	0.0644	0.0919	0.0695	

				0.0343			
		0.0003	0.0003	0.0003	0.0392		
		0.0003	0.0003	0.0003	0.0596		
		0.0003	0.0003	0.0003	0.0392	0.0324	0.0004
		0.0294	0.0203	0.0398	0.0752	0.0459	0.0035
					0.037		
					0.0343		

1- EQNO	2-STA	3-DIST	4-DEPTH	5-Parr	6-PoL-arr	7-PoH-arr	8-SoL-arr	9-SoH-arr	10-P0.93	11-P1.87	12-P3.75	13-P7.5	14-P15	15-P30	16-PoL0.93
2495	20	29.299	394.8	10.91					0.8901	1.4351	1.1139	0.0013	0.0013		
2566	73	31.938	281.8	9.65	8.35	7.99		4.84	0.262	0.178		0.0795			0.249
2566	74	31.942	281.8	9.59	8.22	7.94		4.85	0.5186	0.7261	0.2852	0.2984	0.0025		0.1268
2566	71	32.105	281.8	9.67	8.17	7.98		4.88	0.2463	0.4254	0.3063	0.2701	0.002		0.1757
2566	75	32.159	281.8	9.62	8.13	7.93		4.84	0.1989	0.1291	0.6355	0.2196	0.0008		0.0496
2566	76	32.29	281.8	9.69	8.19	7.94		4.83	0.26	0.3327	0.2205	0.2978	0.0012	0.0011	0.2993
2566	40	32.933	281.8	9.88	9.04	8.19		5	0.5161	0.7257	0.2849	0.2939	0.0049	0.001	0.4054
2566	10	33.248	281.8	10.05	8.71	8.31		5.03	0.3426	0.2832	0.2886	0.379	0.0011		0.274
2566	20	34.755	281.8	9.85		8.15			0.6886	0.9226	1.1631	0.3202	0.0046	0.0011	
2645	73	32.965	498.9	9.48											
2645	74	32.982	498.9	9.42				4.91		0.2527	0.1689	0.1166			
2645	71	33.138	498.9	9.5				4.89		0.3341	1.7398				
2645	75	33.202	498.9	9.45				4.93		0.1787	0.7952				
2645	76	33.322	498.9	9.49				4.95		0.0196	0.0873				
2645	40	33.926	498.9	9.69				5.05		0.2512	0.1687	0.121			
2645	10	34.274	498.9												
2884	74	32.59	33			8.28		5.49							
2884	73	32.626	33			8.28		5.56							
2884	71	32.77	33			8.29		5.54							
2884	75	32.792	33			8.22		5.59							
2884	76	32.954	33			8.36		5.55							
2884	40	33.711	33			8.4		5.68							
2884	10	33.918	33			8.6		5.81							
2884	20	35.336	33			8.76									
2911	73	32.764	46.2	9.64					0.2109	0.2945	0.1963	0.0499	0.0008	0.0006	
2911	74	32.943	46.2	9.63					0.2974	0.1224	0.2203				
2911	71	32.969	46.2	9.64					0.1845	0.2446	0.153				
2911	40	32.982	46.2	9.64					0.2341	0.123	0.218				
2911	76	33.089	46.2	9.64					0.2565	0.1714	0.1181				
2911	75	33.146	46.2	9.86		8.49			0.0803	0.0985	0.0633				
2911	10	33.676	46.2	9.91					0.211	0.2942	0.1982	0.0007	0.0038	0.0008	
2911	20	35.073	46.2	9.73					0.3511	0.3109	0.0792	0.0045	0.0008	0.0007	
3054	73	25.828	35		8.99	8.26		4.74							
3054	74	25.981	35		9.01	8.28		4.75							
3054	71	26.036	35		9.03	8.3		4.75							
3054	76	26.176	35		9.04	8.31		4.73							0.3161
3054	75	26.197	35		9.05	8.32		4.75							
3054	40	26.221	35		9.02	8.24		4.73							
3054	10	26.87	35		9.06	8.26		4.75							
3054	20	28.361	35		9.17	8.22		4.68							0.4602
3055	73	25.781	43.2		8.7	8.32		4.8							
3055	74	25.935	43.2		8.87	8.25		4.74							
3055	71	25.989	43.2		8.71	8.24		4.7							
3055	76	26.128	43.2		8.93	8.28		4.7							

17-PoL1.87	18-PoL3.75	19-PoH0.93	20-PoH1.87	21-PoH3.75	22-PoH7.5	23-PoH15	24-PoH30	25-SoL0.93	26-SoL1.87	27-SoH0.93	28-SoH1.87	29-SoH3.75	30-SoH7.5	31-SoH15	32-SoH30
0.0644			0.0162	0.0233	0.0231	0.0323				0.072	0.0428	0.0301	0.0355	0.0323	
			0.0401	0.0285	0.0404	0.0218				0.1134	0.0378	0.0539	0.0534	0.0555	
0.2194			0.0274		0.026	0.0228				0.0959		0.0498	0.0475	0.0274	
0.0727		0.0212	0.018	0.0283	0.025	0.0259				0.1185	0.0969	0.0496	0.0284	0.0355	
		0.0279	0.011	0.0301	0.0235	0.0241	0.0203			0.0323	0.0232	0.0523	0.081	0.0351	0.0013
			0.0401	0.0285	0.0404	0.0218				0.1134	0.0384	0.0536	0.0527	0.0561	
			0.0163	0.0235	0.0236	0.0336				0.0796	0.0075	0.0312	0.0365	0.0346	
				0.0302	0.0327	0.0003	0.0002								
											0.0005	0.0387	0.0793		
											0.0042	0.0006	0.0571		
											0.0296	0.033			
											0.0031	0.0313			
											0.0005	0.0403	0.0805	0.0386	
		0.1615	0.0646	0.0765	0.1126					0.0487	0.0393	0.0454	0.0858		
		0.1619	0.0463	0.0637	0.0665					0.0021		0.0374	0.0388		
		0.1896	0.0578	0.0673	0.1059					0.0063		0.0475	0.0483		
		0.1269	0.0415	0.058	0.069					0.0356	0.0287	0.0504	0.0648		
		0.2827	0.0778	0.0804	0.0638					0.0279	0.0051	0.0425	0.0622		
		0.162	0.0646	0.0766	0.1115					0.0491	0.04	0.0429	0.0842		
		0.1615	0.0454	0.0627	0.0646					0.0004		0.0349	0.0357		
		0.0428	0.0429	0.0908	0.0068	0.0029									
		0.0787	0.0421	0.0125											
		0.0137	0.0261	0.1036	0.0659	0.0668	0.0014			0.2395	0.0421	0.0809	0.0859	0.0883	0.0318
		0.0453	0.0616	0.0701	0.0768	0.1211	0.0012			0.0881	0.0414	0.0565	0.1186	0.085	0.0012
		0.0134	0.0462	0.0923	0.1087	0.1091	0.0004			0.0312	0.0388	0.1031	0.118	0.1232	0.0004
0.2046	0.1653	0.0227	0.0436	0.0785	0.1283	0.103	0.0004			0.0338	0.0472	0.0717	0.0902	0.1431	0.0027
		0.0465	0.0779	0.0538	0.0737	0.1221	0.0008			0.0871	0.0626	0.0982	0.1061	0.089	0.0023
		0.064	0.0532	0.0348	0.0734	0.0359	0.0197			0.0616	0.0373	0.0347	0.0386	0.0328	0.0004
		0.0205	0.0604	0.1015	0.0945	0.0987				0.0303	0.1472	0.0816	0.0749	0.0492	0.0351
0.7902	0.692	0.079	0.0489	0.0541	0.0946	0.1064	0.0014				0.0484	0.0558	0.0647		
		0.0139	0.0298	0.0297	0.0342					0.0003	0.0031	0.0292	0.0647		
		0.1369	0.0536	0.0645	0.1153	0.0003				0.1881	0.0049	0.0781	0.0857	0.0006	
		0.0711	0.0436	0.0686	0.0485	0.0004				0.058	0.003	0.0445	0.0475	0.0006	
		0.0266	0.0045	0.0461	0.1158	0.0003				0.054	0.0028	0.0416	0.0588	0.0294	

1- EQNO	2-STA	3-DIST	4-DEPTH	5-Parr	6-PoL-arr	7-PoH-arr	8-SoL-arr	9-SoH-arr	10-P0.93	11-P1.87	12-P3.75	13-P7.5	14-P15	15-P30	16-PoL0.93
3055	75	26.151	43.2		8.54			4.67							
3055	10	26.818	43.2		9.03	8.35		4.74							
3057	40	17.958	44.6			8.34		4.73							
3057	73	18.467	44.6			8.35		4.72							
3057	71	18.611	44.6			8.37		4.73							
3057	76	18.625	44.6			8.38		4.74							
3057	10	18.644	44.6			8.35		4.75							
3057	74	18.707	44.6			8.33		4.72							
3057	75	18.808	44.6			8.37		4.73							
3057	20	19.443	44.6			8.36		4.76							
3058	73	25.633	32.7		8.82	8.2		4.72							
3058	74	25.786	32.7		8.8	8.22		4.72							
3058	71	25.84	32.7		8.89	8.24		4.7							
3058	76	25.98	32.7		8.9	8.22		4.69							
3058	75	26.002	32.7		8.87	8.23		4.69							
3058	10	26.673	32.7		8.93	8.09		4.7							
3058	20	28.163	32.7		9.04	8.09									
3061	73	25.68	40.2		8.96	8.23		4.72							
3061	74	25.833	40.2		8.9	8.25		4.73							
3061	71	25.888	40.2		8.96	8.27		4.71							
3061	76	26.027	40.2		8.94	8.28		4.71							
3061	75	26.049	40.2		8.98	8.26		4.7							
3067	40	20.387	98		8.54	8.18		4.7							
3067	73	21.029	98		8.6	8.21		4.7							
3067	10	21.062	98		8.69	8.19		4.69							
3067	76	21.14	98		8.64	8.07		4.7							
3067	71	21.148	98		8.65	8.26		4.7							
3067	74	21.265	98		8.68	8.09		4.7							
3067	75	21.341	98		8.61	8.07		4.72							
3067	20	21.661	98		8.57	8.24		4.73							
3120	73	21.48	122.7		8.76	8.26		4.72							
3120	76	21.598	122.7		8.73	8.23		4.75							
3120	10	21.521	122.7		8.54	8.31		4.73							
3120	71	21.605	122.7		8.73	8.31		4.72							
3120	74	21.721	122.7		8.74	8.28		4.72							
3120	75	21.798	122.7		8.73	8.27		4.75							
3120	20	22.121	122.7		8.78	8.25		4.71							
3213	73	21.413	121.5		8.6	8.29		4.72							0.4256
3213	72	21.458	121.5		8.74	8.35		4.69							
3213	71	21.596	121.5		8.75	8.33		4.73							
3213	74	21.634	121.5		8.65	8.27		4.71							
3213	76	21.666	121.5		8.73	8.21		4.73							
3213	75	21.793	121.5		8.63	8.26		4.69							
3213	11	21.993	121.5		8.71	8.3		4.75							

17-PoL1.87	18-PoL3.75	19-PoH0.93	20-PoH1.87	21-PoH3.75	22-PoH7.5	23-PoH15	24-PoH30	25-SoL0.93	26-SoL1.87	27-SoH0.93	28-SoH1.87	29-SoH3.75	30-SoH7.5	31-SoH15	32-SoH30
		0.0779	0.1305	0.0677	0.1066	0.0003				0.0005	0.00459	0.0416	0.0088	0.0006	
				0.0559		0.0004	0.0004					0.0456		0.0006	0.0017
		0.0785	0.0986	0.1734	0.292	0.0722				0.0504	0.1672	0.2188	0.0792	0.0625	
		0.0369	0.0345	0.0566	0.0591	0.0604					0.1152	0.0927	0.0533	0.0968	
		0.2173	0.0438	0.1703	0.149	0.13	0.0004			0.1015	0.0362	0.0832	0.0961	0.057	0.0005
		0.0982	0.0597	0.0759	0.1181	0.1166				0.0583	0.0408	0.0801	0.082	0.1322	
		0.0372	0.0456	0.1048	0.384	0.2284	0.0793			0.0548	0.2722	0.1758	0.2379	0.1267	0.0461
		0.0428	0.0641	0.1016	0.1752	0.1063				0.0389	0.0822	0.0883	0.1235	0.0914	
		0.0528	0.1074	0.0586	0.1195	0.0638				0.0476	0.0381	0.0409	0.0871	0.1009	0.001
		0.0355	0.2974	0.612	0.1663	0.3851	0.0015			0.1138	0.1919	0.1179	0.1278	0.181	0.0006
			0.0598	0.037	0.0827	0.0265				0.0004	0.0316	0.0702	0.1159		
		0.035	0.0325	0.0751	0.0782	0.0003				0.0005	0.0346	0.0742	0.0806	0.0005	
			0.0616	0.094	0.079						0.0243	0.0346	0.0854	0.0005	
		0.0116	0.0344	0.056	0.0929					0.0004	0.0417	0.075	0.0926	0.0351	
		0.0079	0.0317	0.0601	0.141	0.0003					0.0015	0.044	0.0896		
			0.0536	0.0618	0.069	0.0043						0.0464	0.039	0.001	0.0035
		0.0241	0.0154	0.066	0.0683	0.0007									
		0.0078	0.0287	0.0609	0.0721					0.0004	0.0374	0.0499	0.0791		
		0.0942	0.0332	0.0845	0.0819					0.0005	0.0222	0.0451	0.1205		
			0.042	0.0655	0.0685							0.0701	0.0803		
		0.0092	0.0075	0.0565	0.1438					0.0097	0.0011	0.0657	0.0903		
		0.004	0.0792	0.0832	0.1088					0.0004	0.048	0.0736	0.1069		
		0.0109	0.026	0.0003	0.0003	0.0003				0.031	0.0434	0.0393	0.0388	0.0351	
		0.0318	0.0038	0.0152	0.0241	0.0359				0.0321	0.0497	0.0395	0.0756	0.0907	
		0.0381	0.0212	0.0164	0.0041	0.0044	0.0003				0.0437	0.066	0.1197	0.095	0.0733
		0.0389	0.0256	0.021	0.0233	0.0259				0.031	0.0394	0.0374	0.0947	0.0966	
		0.0851	0.0236	0.0169	0.0227	0.0254	0.0002			0.0575	0.0225	0.0669	0.0866	0.1108	0.0003
		0.0402	0.0188	0.0205	0.0268	0.0233				0.0749	0.0315	0.0466	0.0806	0.0505	
		0.0543	0.0019	0.0212	0.004	0.0297				0.0276	0.043	0.0667	0.0768	0.0589	
		0.0312	0.027	0.0243	0.0281	0.0271				0.0382	0.1059	0.0887	0.0962	0.098	
		0.0396		0.0401	0.038	0.0003				0.0317	0.0287	0.0661	0.0814	0.0297	
		0.1544	0.0114	0.0344	0.0521	0.017				0.0063	0.0578	0.108	0.1129	0.069	
		0.0036	0.0014	0.0404	0.0563	0.002	0.0005				0.1023	0.2243	0.113	0.0608	0.0013
		0.0088	0.0337	0.0391	0.0935						0.0773	0.0447	0.0834	0.0341	
			0.0439	0.0469	0.0441						0.0328	0.0545	0.0844		
		0.0086	0.0119	0.0343	0.0356					0.0064	0.0499	0.0641	0.0903		
		0.0863	0.0685	0.0918	0.2049	0.0004	0.0013			0.0402	0.0944	0.1181	0.0676	0.0078	0.0004
			0.0355	0.052	0.0489	0.0222				0.0357	0.049	0.0502	0.0492	0.048	
		0.0182	0.0247	0.0326	0.0319					0.03	0.0425	0.0466	0.0617		
		0.012	0.0259	0.0334	0.0291					0.0011	0.0328	0.0663	0.049		
		0.1849	0.0298	0.0371	0.0541					0.0384	0.0455	0.089	0.092		
			0.0124	0.0365	0.037	0.0284				0.0261	0.044	0.0744	0.0905	0.0464	
		0.0111	0.0282	0.032	0.0329					0.0011	0.0412	0.0494	0.0582		
		0.0643	0.0678	0.0806	0.1413	0.0037	0.0009			0.0348	0.0899	0.179	0.0599	0.0051	

1- EQNO	2-STA	3-DIST	4-DEPTH	5-Parr	6-PoL-arr	7-PoH-arr	8-SoL-arr	9-SoH-arr	10-P0.93	11-P1.87	12-P3.75	13-P7.5	14-P15	15-P30	16-PoL0.93
3213	10	21.993	121.5		8.71	8.33		4.74							
3213	20	23.132	121.5		8.4	8.38		4.7							
3213	21	23.132	121.5		8.4	8.4		4.72							
3237	73	27.323	35.8					6.05							
3237	74	27.378	35.8			8.19		6.11							
3237	71	27.511	35.8					5.82							
3237	75	27.603	35.8					5.95							
3237	76	27.69	35.8					5.82							
3237	40	28.17	35.8					5.61							
3237	10	28.608	35.8					5.41							
3237	20	30.174	35.8					4.71							
3248	73	25.688	41.1			8.28		4.67							
3248	74	25.841	41.1			8.26		4.73							
3248	71	25.895	41.1			8.25		4.71							
3248	75	26.057	41.1			8.3		4.67							
3248	76	26.085	41.1			8.21		4.72							
3248	20	28.217	41.1			8.15									
1850	73	26.296	136.7		9.22	8.16		4.63							
1850	74	26.461	136.7		9.05	8.15		4.69							
1850	71	26.503	136.7		9.18	8.17		4.68							
1850	76	26.683	136.7		9.15	8.18		4.64							
1850	75	26.672	136.7		9.09	8.16		4.67							
1850	20	28.73	136.7		9.32	8.16									
1856	73	29.028	56.9		8.76	8.27		4.71							
1856	74	29.126	56.9			8.3		4.71							
1856	71	29.23	56.9		9.04	8.27		4.74							
1856	75	29.354	56.9		8.95	8.23		4.7							
1856	76	29.397	56.9		9.29	8.24		4.69							

17-PoL1.87	18-PoL3.75	19-PoH0.93	20-PoH1.87	21-PoH3.75	22-PoH7.5	23-PoH15	24-PoH30	25-SoL0.93	26-SoL1.87	27-SoH0.93	28-SoH1.87	29-SoH3.75	30-SoH7.5	31-SoH15	32-SoH30
		0.0141	0.0488	0.008						0.0686	0.1086	0.1259	0.1358	0.0067	
		0.0087	0.2397	0.0564	0.045	0.0094					0.0991	0.1112	0.0535	0.0035	
		0.0732	0.1533	0.0532	0.0076	0.0135				0.0427	0.0851	0.0922	0.0487	0.0005	
											0.098	0.129	0.1126	0.0782	
											0.1247	0.1309	0.1436	0.0863	
											0.1819	0.1813	0.185		0.0004
										0.0004	0.1153	0.1402	0.1318	0.0512	0.0004
											0.1098	0.1348	0.1294	0.0596	
										0.2427	0.2267	0.1073	0.0264	0.2366	0.2396
												0.1091	0.1325	0.0378	0.0004
											0.2049	0.2293	0.2259	0.1232	
				0.0622	0.0581							0.0482	0.0537		
				0.0723	0.0727							0.0674	0.0444		
				0.0718	0.0434							0.0392	0.0462		
				0.0345	0.0723							0.0085	0.0694		
				0.0391	0.0749							0.0654	0.0469		
				0.0532											
				0.0451	0.0754						0.0447	0.0438	0.0632		
			0.07	0.0768	0.0853						0.0348	0.0324			
			0.0024	0.0834	0.0843						0.077	0.0773	0.0799		
			0.0377	0.0467	0.0676	0.1043					0.007	0.0412	0.0868	0.0445	
			0.0615	0.0856	0.1254	0.0471					0.0049	0.0378	0.0811	0.0404	
			0.0661	0.0765	0.0587	0.0005	0.002								
		0.0616	0.0398	0.1117	0.0358							0.0421	0.0474		
			0.0556	0.071	0.0733						0.0039	0.0406	0.0508		
		0.0575	0.0444	0.0396	0.0403					0.0028	0.0282	0.0339	0.0423		
		0.015	0.0638	0.0406	0.0508					0.0005	0.0005	0.07	0.0504		
			0.0459	0.0665	0.0719						0.0005	0.0424	0.0654		